Kyoko Ohno-Matsui
Editor

Atlas of Pathologic Myopia

Springer

MOREMEDIA

Atlas of Pathologic Myopia

Kyoko Ohno-Matsui
Editor

Atlas of Pathologic Myopia

Springer

Editor
Kyoko Ohno-Matsui
Department of Ophthalmology and Visual Science
Tokyo Medical and Dental University
Tokyo
Japan

ISBN 978-981-15-4260-2 ISBN 978-981-15-4261-9 (eBook)
https://doi.org/10.1007/978-981-15-4261-9

This Springer imprint is published by the registered company Springer Nature Singapore Pte Ltd.
The registered company address is: 152 Beach Road, #21-01/04 Gateway East, Singapore 189721, Singapore

Foreword

The great Takashi Tokoro, MD, was Professor and Chairman of the Department of Ophthalmology at the Tokyo Medical and Dental University School of Medicine. He produced the first atlas of myopia, entitled Atlas of Posterior Fundus Changes in Myopia that was published in 1998. This set of insights into myopia was established through careful clinical examination and documented by fundus photography and angiography. The book was a milestone, as was the 1985 book, The Myopias, by Dr. Brian Curtin. These two volumes influenced generations of ophthalmologists concerning a disease that is one of the leading causes of vision loss and blindness around the world.

Ophthalmology is a curious subject. It is a study of the eye and its diseases that uses written or spoken words for basic communication but relies on visual imagery to communicate much more profound insights. Even the words we chose to explain understanding, such as insight, reveal how imagery, visual or mental, are fundamental to human understanding. To expand our insight into the pathologic processes of the eye, we employ an increasing array of imaging instruments. Wide-field imaging helped in our understanding of the elemental changes throughout the fundus in myopia, and augmented by fluorescein and indocyanine green angiography, many pathological changes in the retina and choroid have been elucidated. Cross-sectional images of the posterior portion of the eye became possible with optical coherence tomography (OCT) and advances in this form of imaging led to wide-field OCT and OCT angiography, which does not require dye injection that has refined older ideas and expanded possibilities beyond anything imaginable with ophthalmoscopy or fundus photography. Each of these modalities examines part of the eye; 3D magnetic resonance imaging gets a more global look.

Each of these imaging modalities multiplies the amount of data available, and the interactions among these pieces of information increases geometrically. It is easy to generate mountains of images, but to understand the meaning of the images requires a visionary (another vision-related word) such as Dr. Kyoko Ohno-Matsui, the present Professor and Chairman of the Department of Ophthalmology at the Tokyo Medical and Dental University School of Medicine, She started as a star pupil of Dr. Tokoro and has continued the tradition of diligence and innovative work. She has taken the abundance of interconnected imagery and data and synthesized new classification systems and novel ways to look at pathologic myopia. This has been distilled with singular clarity into this Atlas of Pathologic Myopia. This atlas will educate clinicians, scientists, students, and patients with memorable, archetypical representations of the ocular changes in pathologic myopia. With this book, we all can learn the wisdom from generations of masters at Tokyo Medical and Dental University.

New York, NY — Richard F. Spaide

Preface

A rapid increase in the prevalence of myopia is of great concern worldwide. According to Holden et al., about 50% of the global population will be myopic by 2050, and about 10% will be highly myopic. Although myopia has mainly been regarded as an "East Asian" problem, these data suggest that myopia is now a global issue.

In most cases of physiologic myopia, good "corrected visual acuity" can be obtained under proper optical correction; the only exception to this is "pathologic myopia." Pathologic myopia involves various myopia-related fundus changes in the macular retina and optic nerve, which result in visual impairments. Actually, myopic maculopathy in eyes with pathologic myopia has been reported to be a major cause of irreversible vision impairment and blindness in many East Asian countries.

The Meta-analysis of Pathologic Myopia (META-PM) study group categorized various myopic maculopathy lesions (categories 1-4) and "plus lesions" based on color fundus photos. Pathologic myopia is defined as the eyes having myopic maculopathy equal to or more serious than diffuse atrophy (category 2) or posterior staphylomas. Recently, Fang and others established an optical coherence tomography (OCT)-based classification of myopic maculopathy for the objective and quantitative classification of myopic maculopathy.

It is sometimes challenging to diagnose each myopic maculopathy lesion accurately because various lesions tend to coexist, and each lesion tends to show different progression patterns. In addition, how each lesion progresses with time and what kinds of lesions are the main risk factors of developing visual impairment are not widely known.

Posterior staphyloma is a posterior outpouching of the limited area of the posterior sclera and is an important landmark of pathologic myopia. Posterior staphylomas can also occur in non-highly myopic eyes. Curtin reported that the presence of staphylomas was the most reliable indicator for the presence of pathologic myopia, as opposed to the refractive error or axial length. Despite its importance, diagnosing posterior staphylomas based on conventional fundus photos or OCT remains difficult because staphylomas span wider areas than those shown by these conventional tools. Therefore, special imaging modalities capable of visualizing a wide area of the eye, such as three-dimensional magnetic resonance imaging (3D-MRI) of the eye or ultra-wide-field OCT, are necessary.

The High Myopia Clinic at Tokyo Medical and Dental University was established in 1974 by Honorary Professor Takashi Tokoro and coworkers. Based on their long-term experience, the *Atlas of Posterior Fundus Changes of Pathologic Myopia* was published by Springer in 1998. This atlas contains numerous remarkable images of eyes with pathologic myopia and has been a valuable resource for many eye care professionals around the world.

It has been 22 years since the publication of Professor Tokoro's wonderful *atlas*. During this period, ocular imaging has greatly improved, as represented by OCT, OCT angiography, ultra-wide-field imaging, and 3D-MRI of the eye. In addition, the High Myopia Clinic has now expanded to become the "Advanced Clinical Center for Myopia," which is composed of three sectors: the "myopia prevention sector," the "refractive surgery sector," and the "pathologic myopia sector." Nonetheless, the pathologic myopia sector remains the core of this center and has had more than 6000 registered patients from all over the world with a long history spanning more than 46 years.

Therefore, based on the long-term experience of the pathologic myopia specialists at the Advanced Clinical Center for Myopia and the great improvements achieved in ocular imaging, we have decided to publish a new and revised version of the *atlas* for pathologic myopia. We hope that this updated *atlas* will help enable a better understanding of the pathology of pathologic myopia and provide useful knowledge on the proper diagnosis and ideal management of affected patients in order to prevent myopia-related blindness.

Finally, I would like to express my sincere appreciation to all members (current and previous) for their great effort in caring for patients with pathologic myopia through their professional knowledge of this specific disease. I would especially like to thank the founder of the High Myopia Clinic, Honorary Professor Takashi Tokoro.

Tokyo, Japan Kyoko Ohno-Matsui

Contents

Part I

Definition

Definition of Pathologic Myopia (PM)

1

Kyoko Ohno-Matsui

Abstract

The definition of pathologic myopia had not been standardized for a long time, and pathologic myopia was often confused with high myopia. These two are distinctly different; "high myopia" is defined as an eye with a high degree of myopic refractive error, and "pathologic myopia" is defined as myopic eyes with the presence of pathologic lesions in the posterior fundus. The changes are the presence of myopic maculopathy equal to or more serious than diffuse chorioretinal atrophy and/or the presence of a posterior staphyloma.

Keywords

Pathologic myopia · High myopia · Posterior staphyloma
Diffuse atrophy · Axial length

1.1 Importance of Myopia and Pathologic Myopia

Myopia is defined as a refractive condition of the eye in which parallel rays of light entering the eye are brought to a focus in front of the retina when the ocular accommodation is relaxed [1]. This refractive status is dependent on the axial length, and a disproportionate increase of the axial length of the eye can lead to myopia, called axial myopia, or a disproportionate increase in the refractive power of the eye can also lead to myopia, called refractive myopia. The WHO Report defines myopia as "a condition in which the refractive error (spherical equivalent) is ≤ -0.50 diopter (D) in either eye" [2].

Myopia is a significant public health concern worldwide [2–4], and the rapid increase in the prevalence of myopia is of considerable concern to health care personnel and governments [5, 6]. It is estimated that by 2050, there will be 4.8 billion people with myopia which is approximately one-half (49.8%) of the world population. Of these, 938 million individuals will have high myopia which is 9.8% of the world population [5]. This is important because even mild myopia can be a risk factor for other ocular disorders [3, 7, 8]. However, it is uncertain whether the prevalence of pathologic myopia increases in parallel with an increase of myopia or high myopia.

Eyes with pathologic myopia have different types of lesions in the posterior fundus, called myopic maculopathy, which can lead to a significant reduction of central vision [9, 10]. In fact, myopic maculopathy in eyes with pathologic myopia is a major cause of blindness worldwide and especially in east Asian countries [11–15].

The definitions of myopia and pathologic myopia had not been standardized, and the term "pathologic myopia" was often confused with "high myopia." These two are distinctly different pathologies; "high myopia" is defined as an eye with a high degree of myopic refractive error, and "pathologic myopia" is defined as myopic eyes with the presence of pathologic lesions in the posterior fundus. Duke-Elder defined "pathologic myopia" although he used the term "degenerative myopia" as "the type of myopia which is accompanied by degenerative changes occurring especially in the posterior pole of the globe" [16].

K. Ohno-Matsui (✉)
Department of Ophthalmology and Visual Science, Tokyo Medical and Dental University, Tokyo, Japan
e-mail: k.ohno.oph@tmd.ac.jp

K. Ohno-Matsui (ed.), *Atlas of Pathologic Myopia*, https://doi.org/10.1007/978-981-15-4261-9_1

Curtin [17, 18] showed that the refractive error and axial length in eyes with the same type of staphylomas varied considerably and suggested that these measurements were unreliable indicators of pathologic myopia. He suggested that the morphology of the posterior staphyloma would be a much more reliable measure for diagnosing pathologic myopia.

1.2 Classification of Myopia According to Refractive Error (Spherical Equivalent) (Table 1.1)

Myopia is classified into low myopia, moderate myopia, and high myopia. The cut-off values for the different degrees have not been consistent among studies. The WHO Report defined "high myopia" as "a condition in which the objective refractive error (spherical equivalent) is ≤ −5.00 D in either eye" [3]. Very recently, Flitcroft on behalf of the International Myopia Institute (IMI) proposed a set of standards to define and classify myopia [1]. Low myopia is defined as a refractive error of ≤ −0.50 and > −6.00, and high myopia is defined as refractive error of ≤ −6.00 D [1]. The Japan Myopia Society proposed a category of "moderate myopia" between "low myopia" and "high myopia" (http://www.myopiasociety.jp/member/guideline/index.html). According to this society, low myopia is defined as a refractive error of ≤ −0.50 and > −3.00 D, moderate myopia is ≤ −3.00 and > −6.00 D, and high myopia is ≤ −6.00 D. A summary of the modified definition is presented in Table 1.1.

1.3 Classification of Pathologic Myopia (Table 1.1)

Pathologic myopia is classified as being present when myopic eyes have characteristic lesions in the posterior fundus. The changes are the presence of myopic maculopathy equal to or more serious than diffuse choroidal atrophy (equal to Category 2 in the META-PM classification [9]) and/or the presence of a posterior staphyloma [19]. The cut-off values of the myopic refractive error and axial length are not set for the definition of pathologic myopia because a posterior staphyloma has been reported to occur even in eyes with normal axial length (Fig. 1.1) [20] or in eyes with axial lengths <26.5 mm [21]. This suggested that pathologic myopia is considered an independent pathology of the axial elongation of the eye. Although an axial elongation mainly occurs in the equatorial region of the eye, pathologic myopia is characterized by a formation of posterior staphyloma as suggested by Spaide [22]. Thus, the mainly affected area is different between high myopia and pathologic myopia.

Optical coherence tomographic evaluations showed that the progressive choroidal thinning and a formation of Bruch's membrane defects in the macular region were key phenomena associated with myopic maculopathy, the lesions of myopic maculopathy are better classified by their appearance in the OCT images (see Chap. 4 for OCT-based classification) [23].

Table 1.1 Summary of definitions of various types of myopia (modified from Flitcroft et al. [1])

Term	Definition
Myopia	A condition in which the spherical equivalent refractive error of an eye is ≤ −0.50 D when ocular accommodation is relaxed.
Low myopia	A condition in which the spherical equivalent refractive error of an eye is ≤ −0.50 D and > −3.00 D when ocular accommodation is relaxed.
Moderate myopia	A condition in which the spherical equivalent refractive error of an eye is ≤ −3.000 D and > −6.00 D when ocular accommodation is relaxed.
High myopia	A condition in which the spherical equivalent refractive error of an eye is ≤ −6.000 D when ocular accommodation is relaxed.
Pathologic myopia	Myopia that accompanies characteristic myopic fundus changes (the presence of myopic maculopathy equal to or more serious than diffuse choroidal atrophy or the presence of posterior staphyloma)

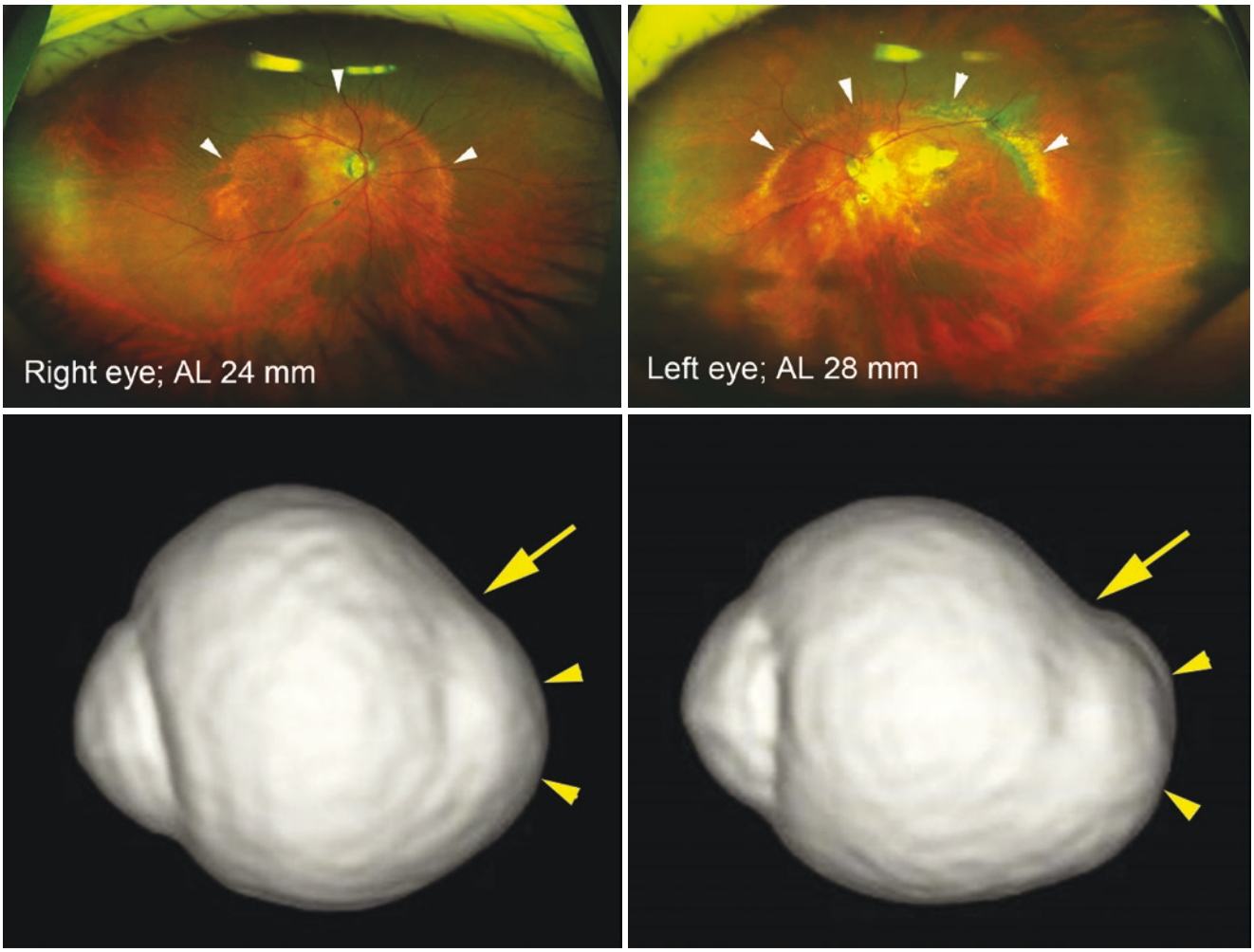

Fig. 1.1 Posterior staphyloma seen in an emmetropic fellow eye of the patient with unilateral high myopia (modified with permission from [20]). Top Row: Wide-field fundus imaging shows upper margin of wide macular staphyloma (arrowheads) both in the highly myopic left eye (axial length; 28 mm) as well as non-myopic right eye (axial length; 24 mm). Please note that the posterior fundus of the right eye is almost normal and the staphyloma edge is outside the conventional 50 degree fundus photo. Bottom Row: Three-dimensional magnetic resonance imaging (3D MRI) of both eyes. Left eye (right image) shows a clear posterior staphyloma as posterior outpouching (arrowheads). The upper margin of staphyloma is seen (arrow). The right eye also shows a similar staphyloma with the upper edge of staphyloma, although the degree of staphyloma is milder

References

1. Flitcroft DI, He M, Jonas JB, et al. IMI - defining and classifying myopia: a proposed set of standards for clinical and epidemiologic studies. Invest Ophthalmol Vis Sci. 2019;60(3):M20–m30.
2. Institute WHO-BHV. The impact of myopia and high myopia report of the joint World Health Organization - Brien Holden Vision Institute Global Scientific Meeting on Myopia. https://www.visionuk.org.uk/download/WHO_Report_Myopia_2016.pdf.2016.
3. Morgan IG, Ohno-Matsui K, Saw SM. Myopia. Lancet. 2012;379(9827):1739–48.
4. Resnikoff S, Jonas JB, Friedman D, et al. Myopia - A 21st century public health issue. Invest Ophthalmol Vis Sci. 2019;60(3):Mi–Mii.
5. Holden BA, Fricke TR, Wilson DA, et al. Global prevalence of myopia and high myopia and temporal trends from 2000 through 2050. Ophthalmology. 2016;123(5):1036–42.
6. Rudnicka AR, Kapetanakis VV, Wathern AK, et al. Global variations and time trends in the prevalence of childhood myopia, a systematic review and quantitative meta-analysis: implications for aetiology and early prevention. Br J Ophthalmol. 2016;100(7):882–90.
7. Suzuki Y, Iwase A, Araie M, et al. Risk factors for open-angle glaucoma in a Japanese population: the Tajimi study. Ophthalmology. 2006;113(9):1613–7.
8. Marcus MW, de Vries MM, Montolio FG, Jansonius NM. Myopia as a risk factor for open-angle Glaucoma: a systematic review and meta-analysis. Ophthalmology. 2011;118(10):1989–1994.e2.
9. Ohno-Matsui K, Kawasaki R, Jonas JB, et al. International photographic classification and grading system for myopic maculopathy. Am J Ophthalmol. 2015;159(5):877–83. e7
10. Fang Y, Yokoi T, Nagaoka N, et al. Progression of myopic maculopathy during 18-year follow-up. Ophthalmology. 2018;125(6):863–77.

11. Iwase A, Araie M, Tomidokoro A, et al. Prevalence and causes of low vision and blindness in a Japanese adult population: the Tajimi study. Ophthalmology. 2006;113(8):1354–62.
12. Xu L, Wang Y, Li Y, et al. Causes of blindness and visual impairment in urban and rural areas in Beijing: the Beijing eye study. Ophthalmology. 2006;113(7):1134.e1–11.
13. Buch H, Vinding T, La Cour M, et al. Prevalence and causes of visual impairment and blindness among 9980 Scandinavian adults: the Copenhagen City eye study. Ophthalmology. 2004;111(1): 53–61.
14. Cotter SA, Varma R, Ying-Lai M, et al. Causes of low vision and blindness in adult Latinos: the Los Angeles Latino eye study. Ophthalmology. 2006;113(9):1574–82.
15. Varma R, Kim JS, Burkemper BS, et al. Prevalence and causes of visual impairment and blindness in Chinese American adults: the Chinese American eye study. JAMA Ophthalmol. 2016;134(7):785–93.
16. Duke-Elder S, editor. Pathological refractive errors. St. Louis: Mosby; 1970.
17. Curtin BJ. Ocular findings and complications. In: Curtin BJ, editor. The myopias. New York: Harper and Row; 1985.
18. Curtin BJ. The posterior staphyloma of pathologic myopia. Trans Am Ophthalmol Soc. 1977;75:67–86.
19. Ohno-Matsui K, Lai TYY, Cheung CMG, Lai CC. Updates of pathologic myopia. Prog Retin Eye Res. 2016;52(5):156–87.
20. Moriyama M, Ohno-Matsui K, Hayashi K, et al. Topographical analyses of shape of eyes with pathologic myopia by high-resolution three dimensional magnetic resonance imaging. Ophthalmology. 2011;118(8):1626–37.
21. Wang NK, Wu YM, Wang JP, et al. Clinical characteristics of posterior staphylomas in myopic eyes with axial length shorter than 26.5 mm. Am J Ophthalmol. 2016;162:180–90.
22. Spaide RF. Staphyloma: part 1. In: Spaide RF, Ohno-Matsui K, Yannuzzi LA, editors. Pathologic myopia. New York: Springer-Verlag; 2014.
23. Fang Y, Du R, Nagaoka N, et al. OCT-based diagnostic criteria for different stages of myopic maculopathy. Ophthalmology. 2019;126(7):1018–32.

Part II

Overview

Overview of Fundus Lesions Associated with Pathologic Myopia

2

Kyoko Ohno-Matsui

Abstract

Various kinds of lesions of myopic maculopathy occur in the posterior fundus of the eyes with pathologic myopia (PM), which could impair the vision. In addition to META-PM classification, the recent OCT-based classification clearly showed that the lesions of myopic maculopathy were characterized by "extreme thinning of the choroid," "macular Bruch's membrane defects," "macular retinoschisis and tractional lesions," and "dome-shaped macula." The underlying cause of developing these lesions is a deformity of the eye represented by posterior staphylomas. In this chapter, an overview of posterior staphyloma and each lesion of myopic maculopathy will be presented.

Keywords

Pathologic myopia · Posterior staphyloma · Myopic maculopathy · 3D MRI · Optical coherence tomography

2.1 Introduction

In eyes with pathologic myopia (PM), various kinds of lesions are present in different regions of the fundus, e.g., in the macula, mid-periphery, periphery, and on the optic disc (Fig. 2.1). The different kinds of lesions often coexist which makes an accurate diagnosis of each type of lesion difficult. In this Atlas, morphological features of each lesion associated with PM are presented based on recent multimodal imaging technology. First, an important cause of developing these lesions, posterior staphylomas, is described.

K. Ohno-Matsui (✉)
Department of Ophthalmology and Visual Science, Tokyo Medical and Dental University, Tokyo, Japan
e-mail: k.ohno.oph@tmd.ac.jp

2.2 Posterior Staphylomas: A Cause of Developing Myopic Maculopathy

A posterior staphyloma is a posterior outpouching of the posterior segment of the eye (Fig. 2.2). Posterior staphylomas are a hallmark of pathologic myopia and are one of the major causes of the development of myopic maculopathy [1–6].

In spite of its importance, there was no standardized definition of posterior staphylomas. Posterior staphylomas were occasionally confused with a simple backward bowing of the sclera which was commonly seen in the OCT images of highly myopic eyes.

Spaide [7] presented a comprehensive definition of posterior staphylomas in which he stated that a posterior staphyloma was an outpouching of a circumscribed region of the posterior pole of the eye that had a radius of curvature that was shorter than the radius of curvature of the adjacent eye wall (Fig. 2.3). The important point is that the formation of a staphyloma is an independent phenomenon that can develop from the continuous elongation of the axial length. Supporting this, staphylomas can also occur in non-axially elongated eyes [8] (Fig. 2.3d).

The importance of staphylomas is in its affected area of the eye. In the process of axial elongation, the equatorial region is mainly expanded while the posterior aspect of the eye is relatively unaffected (Fig. 2.3b). However, a staphyloma causes a deformity of the posterior pole of the eye where the visually important tissues, such as the macula and optic nerve head, are situated. It can easily be imagined that staphylomas can mechanically damage these tissues which can then lead to an impairment of vision. Supporting this, highly myopic eyes with staphylomas have poorer vision, and more commonly have myopic macular pathological lesions [2].

Curtin [9] examined staphylomas by ophthalmoscopic observations and chart drawings, and he classified them into 10 different types. Later, Ohno-Matsui [2] made a simpler

K. Ohno-Matsui (ed.), *Atlas of Pathologic Myopia*, https://doi.org/10.1007/978-981-15-4261-9_2

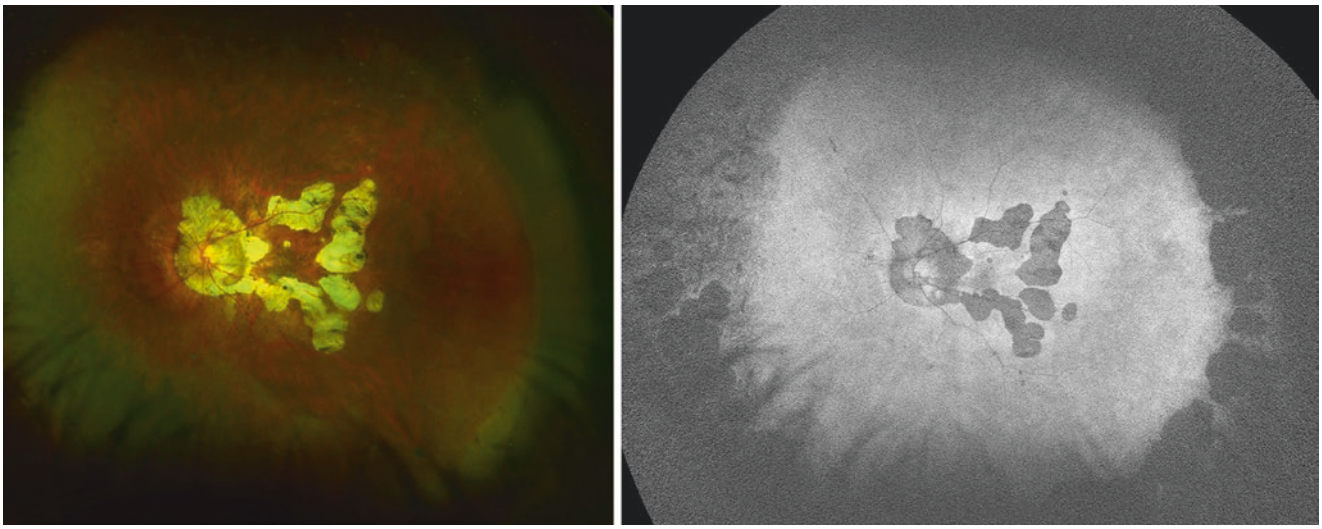

Fig. 2.1 Different types of fundus lesions can be seen in an eye with pathologic myopia in fundus photo (left) and in fundus autofluorescence image (right). Left fundus of a 67-year-old woman with an axial length of 34.9 mm. Ultra-widefield fundus image shows multiple lesions of patchy atrophy in and around the macula. A very large peripapillary atrophy is observed. Yellowish diffuse atrophy is seen around the peripapillary atrophy. Multiple cobblestone lesions are seen in the periphery

Fig. 2.2 Macroscopic images of staphylomas (modified with permission from the textbook *Pathologic Myopia*, Courtesy of Professor Emeritus Shigekuni Okisaka of the National Defense Medical College, Saitama, Japan). (left) A highly myopic eye with a narrow, macular staphyloma. The macular area is protruded posteriorly, and the sclera is extremely thinned in the protruded area. The axial length of the globe is 29 mm. (right) A highly myopic eye with large, multiple protrusions in a wide, macular staphyloma. Both, the peripapillary and macular regions, are protruded posteriorly. A large chorioretinal atrophy is seen extending over the entire posterior fundus. Axial length of the globe is 37 mm

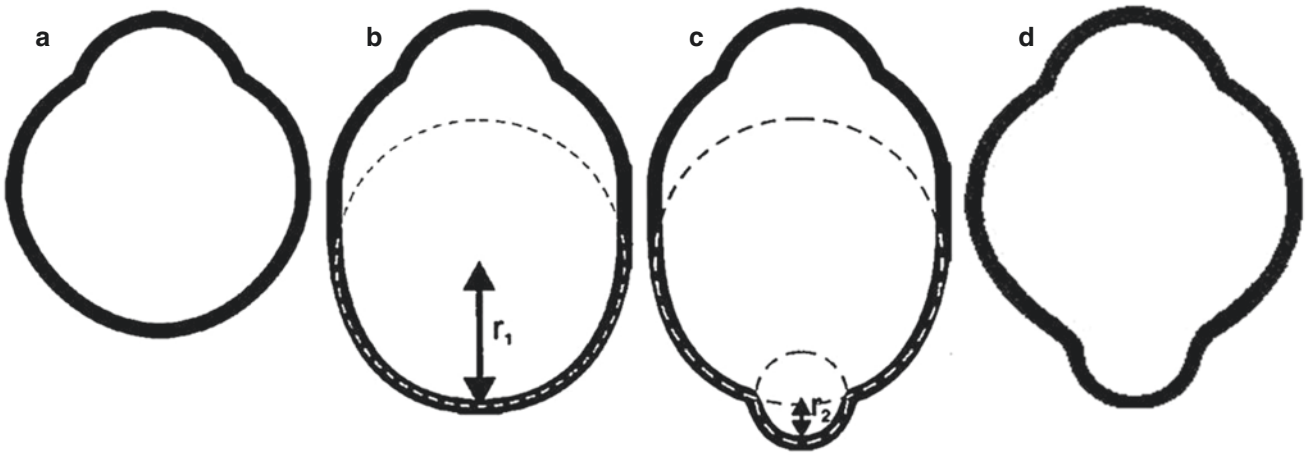

Fig. 2.3 Definition of posterior staphyloma (modified with permission from the Spaide [7]). (**a**) Emmetropic eye. (**b**) Axial myopia without posterior staphyloma. Axial elongation is present mainly in the equatorial region that does not induce an altered curvature in the posterior aspect of the eye. (**c**) A second curvature occurs in the posterior portion of the eye, and this second curvature has a shorter radius of curvature (r_2) than the surrounding eye wall (r_1). This secondary curve is a staphyloma. (**d**) In some eyes, a staphyloma characterized by a secondary curvature (r_2) can occur without marked axial elongation

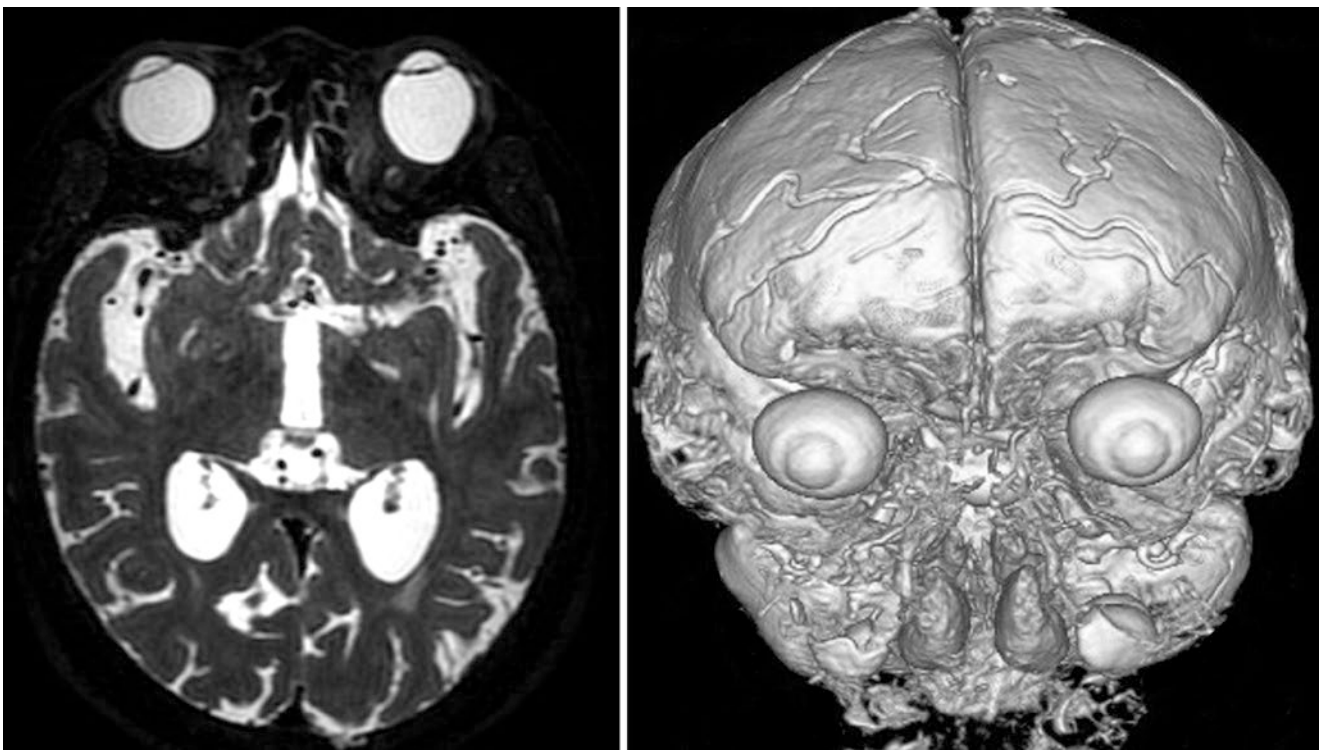

Fig. 2.4 Three-dimensional magnetic resonance imaging (3D MRI) of an eye. (left) 2D image of T2-weighed MRI shows unilateral high myopia. (right) Using volume rendering of T2-weighed MRI image, 3D view is created. Then the 3D image of the eye is extracted by trimming the surrounding tissue

classification and renamed staphylomas according to their size and location (see Chap. 3).

Most of the studies analyzing staphylomas used ophthalmoscopic observations and were subjective. Moriyama et al. [1] used modified 3D MRI technology to evaluate the entire shape of the eye (Fig. 2.4). This was a very powerful method, and it allowed them to classify the different shapes of eyes with staphylomas more extensively and accurately. However, 3D MRI is still not feasible as a screening technique. To overcome this deficit, we have turned to ultra-widefield OCT which had been recently introduced (Fig. 2.5) [10, 11]. The morphological shape of the staphylomas is clearly visible for their entire extent in the ultra-widefield OCT images. Different from 3D

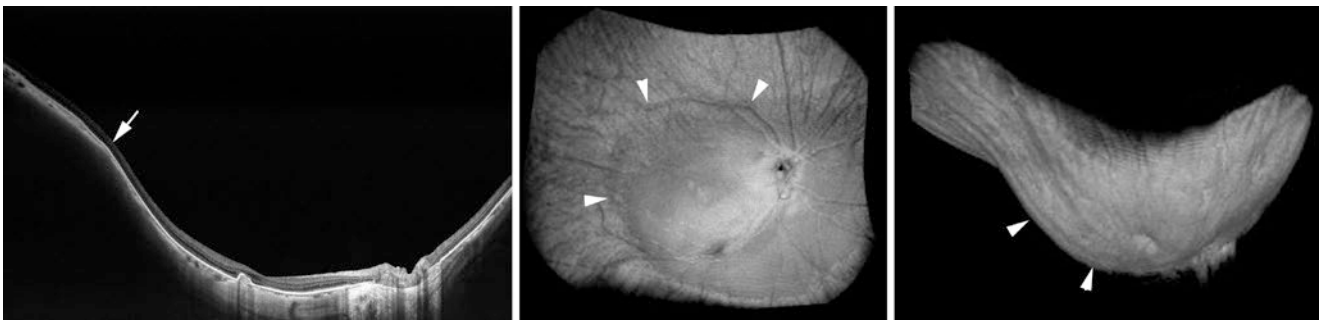

Fig. 2.5 Ultra-widefield OCT image of an eye with a posterior staphyloma. (left) B-scan shows a posterior displacement of the sclera in the area of a staphyloma. An arrow shows a staphyloma edge. (middle) 3D reconstructed image viewed from the front shows a staphyloma (outlined by arrowheads). (right) 3D reconstructed image viewed from the side shows a posterior protrusion due to staphyloma (arrowheads)

MRI, a detailed structure of the retina and the optic nerve are also visible, and these images show how eye deformities represented by staphylomas mechanically affect the visually important tissues.

Many of the fundus lesions associated with PM are difficult to cure; however, based on these imaging data, future treatments to prevent and treat staphylomas before blinding complications occur are expected.

2.3 Myopic Maculopathy: Diffuse Atrophy and Patchy Atrophy

In 2015, a consensus classification of myopic maculopathy was established based on fundus photographs by a group of retina experts. This group was named the Meta-analysis for Pathologic Myopia (META-PM) Study group [12]. In this META-PM classification, myopic maculopathy was classified into five categories; Category 0, "no maculopathy"; Category 1, "tessellated fundus"; Category 2, "diffuse choroidal atrophy"; Category 3, "patchy choroidal atrophy"; and Category 4, "macular atrophy." Three additional features to supplement these categories were defined as "plus" lesions; namely, lacquer cracks, myopic choroidal neovascularization (myopic CNV), and Fuchs' spot.

The META-PM classification is a well-established classification and has been widely used in many studies [5, 13, 14]. However, this classification is based on fundus photographs, and as is well known, the tone of the color of the fundus is affected by degree of fundus pigmentation which greatly differs among different ethnic groups. Thus, such photographical classification will depend on the ethnicity of the patient and will still be subjective. In addition, longitudinal studies with an 18 year follow-up period showed that most of the macular atrophy was CNV-related [5], i.e., the macular atrophy gradually developed around a CNV and did not develop without a preexisting myopic CNV. This indicated that a progression from Category 3 to Category 4 in the META-PM classification was very rare.

The imaging of the fundus of the eye has been greatly advanced especially for the OCT images. Earlier studies using enhanced depth imaging (EDI)-OCT and swept-source OCT showed a thinning of the choroid in myopic eyes [15, 16]. In eyes with PM, the choroid is extremely thin and is occasionally completely absent with large choroidal vessels remaining sporadically. Compared to retinal and scleral thinning, the choroidal thinning is disproportionately notable. Such extreme thinning of the choroid first develops temporal to the optic disc in childhood [17], and it expands and then involves the macular area. Choroidal thinning progresses from tessellation to diffuse choroidal atrophy [18]; however, no further thinning is noted from diffuse atrophy to patchy atrophy [18]. Recent swept-source OCT studies showed that patchy choroidal atrophies were not simply atrophic areas but were holes in Bruch's membrane (BM) [19]. These findings suggested a possibility that the lesions of myopic maculopathy can be categorized according to the degree and extent of the choroidal thinning as well as to the formation of BM holes [18].

Artificial intelligence (AI) is expected to become a powerful method to diagnose and evaluate the progression of myopic maculopathy. In addition, an OCT-based classification of myopic maculopathy is considered to best fit the AI diagnosis. Please see Chap. 4 for details of OCT-based classification (see Chap. 17).

2.4 Myopic Maculopathy; Myopic Macular Neovascularizations (MNV)

A myopic macular neovascularization (MNV) is also known as myopic CNV. However recent OCT studies revealed that at least some myopic CNVs were originated directly from intra-

scleral branches of short posterior ciliary arteries, myopic macular neovascularization (MNV) is considered a more accurate term. MNV is a major cause of a reduction of central vision in patients with PM, and it develops in 10% of highly myopic eyes [20]. When untreated, most of the patients with MNV have the best-corrected visual acuity (BCVA) of <0.1 at 5 years after the onset of the MNV [21]. The cause of a long-term vision reduction in eyes with PM is mainly due to the development of MNV-related macular atrophy rather than a recurrence or growth of the MNV [5, 6, 21].

A breakthrough in the prognosis of MNV was the application of anti-VEGF therapies [22–24]. The difference between anti-VEGF therapies and other therapies such as photodynamic therapy is that the former causes a marked shrinkage of the MNV. For small and non-subfoveal MNVs, it is quite common for them to completely disappear after the anti-VEGF therapy [25]. In the eyes whose MNV completely disappeared, the MNV-related macular atrophy, which is a long-term complication of MNV, does not develop. However, in the eyes whose MNV shrinks but does not disappear, MNV-related macular atrophy gradually develops and impairs the vision in the long-term. Swept-source OCT showed that the MNV-related macular atrophy was due to BM holes [26] similar to patchy atrophy, and thus it is different from the geographic atrophy present in age-related macular degeneration. To improve the long-term prognosis of MNV, it is necessary to prevent the formation and enlargement of BM holes around the MNV remnants.

In addition to the advancement of treatments, the improvements of imaging and diagnosing MNV have been made. The diagnosis of MNV was previously made with fundus observations and fluorescein angiograms. Besides OCT detection of MNVs, OCT angiography has been useful for detecting and analyzing vascular networks. However, a MNV is small and less active than the CNV associated with AMDs. It is sometimes difficult to obtain clear images with OCT angiography. Thus, for proper diagnosis of the presence and the activity of MNVs, multimodal imaging by OCT, OCT angiography, and fluorescein angiogram are recommended [25, 27, 28]. Functional analyses using fundus microperimetry, such as by MP3, are also useful.

2.5 Myopic Macular Retinoschisis and Tractional Lesions

The use of OCT has led to the identification of new pathologies associated with PM, e.g., myopic macular retinoschisis and dome-shaped macula (DSM). Takano and Kishi [29] first reported that patients with PM had macular retinoschisis before developing a macular hole retinal detachment. With the improved resolution of OCT instruments, other pathologies have been clarified, such as foveal retinal detachment, lamellar macular holes, retinal vascular microfolds, and paravascular lamellar holes [30–35]. Myopic macular retinoschisis was originally thought to always develop in eyes with a posterior staphyloma [29], but recent ultra-widefield OCT images showed that it was also present in eyes without a staphyloma [11]. Vitreous abnormalities in eyes with PM may play important roles in the development of myopic macular retinoschisis in eyes without an evident staphyloma [36, 37].

The usefulness of surgeries for myopic traction maculopathy is widely known [38, 39]. Modified surgical techniques such as fovea-sparing ILM peeling is now being widely used [40, 41]. The surgical indications for this procedure still need to be standardized. In addition, how the surgical outcome is quantified also needs to be determined. Besides the anatomical outcomes, functional outcomes by fundus microperimetry are recommended [42].

2.6 Dome-Shaped Macula (DSM)

A DSM is an inward protrusion of the macula area that can be identified by OCT [43, 44], and it is due to a local thickening of the sclera in the macular region [45]. The DSM is associated with various macular complications such as serous retinal detachment (RD) and MNV [46]. Although the mechanism(s) causing the formation of a DSM has not been definitively determined, the presence of macular BM defects may be one cause [47].

2.7 Conclusions

Various pathological lesions are present in wide areas of the fundus in eyes with PM, e.g., a peripheral avascular zone in 360 degrees [48], formation of a macular vortex vein [49], and radial tracts spreading from the staphyloma edge [50]. These pathological changes that develop in eyes with PM are probably related to the axial elongation and staphylomas present in eyes with PM.

The shape of the eye and ocular circulation, especially the choroidal circulation, are markedly altered in eyes with PM (Fig. 2.6, see Chap. 16) [49]. Such changes cause mechanical damage of the retina/choroid/sclera and the optic nerve. It is recommended that thorough examinations regarding a relationship between fundus pathologies and the eye shape should be conducted. It is important to clarify where the mechanical damage is loaded in the eyes with PM. Many pathologies in PM might be "mechanical."

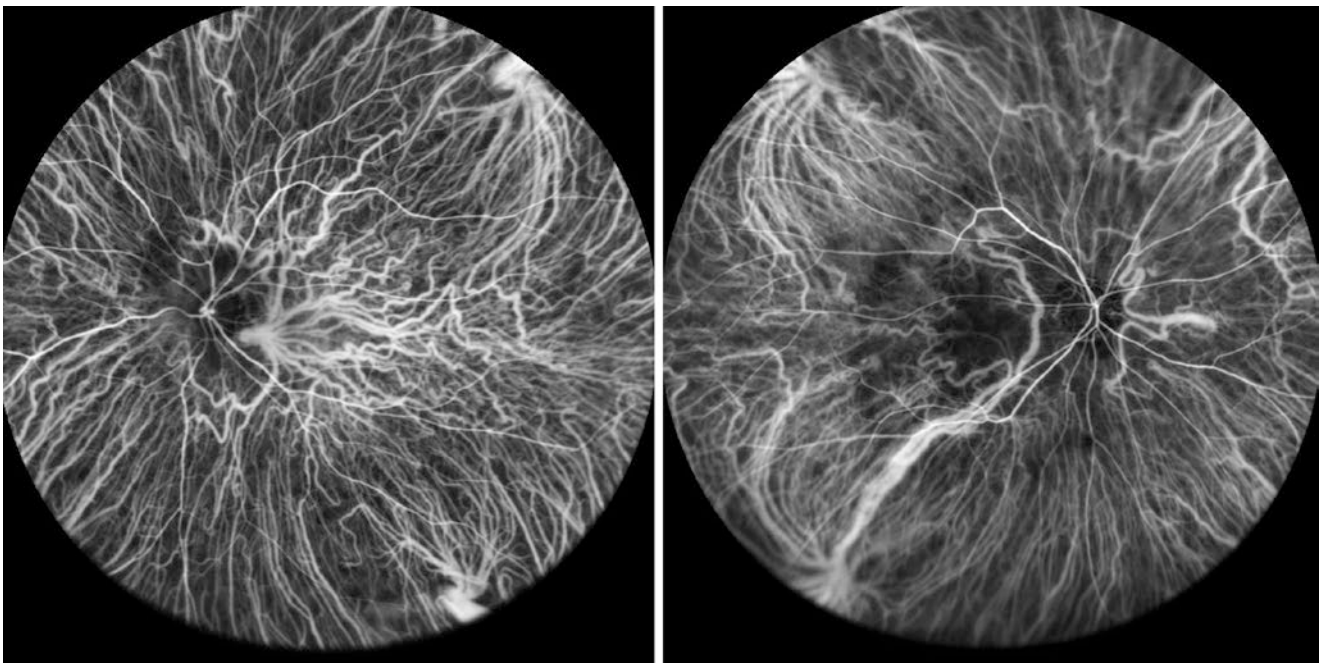

Fig. 2.6 Changes of choroidal vasculature shown by widefield indocyanine green angiography. (left) Macular vortex vein collects the choroidal venous blood and exits around the optic nerve after forming an ampulla. The choroidal venous flow is opposite within and outside the staphyloma. (right) Choroidal veins cannot go beyond the upper staphyloma edge and most of the macular choroidal venous blood drains to the lower temporal vortex vein through many collaterals

References

1. Moriyama M, Ohno-Matsui K, Hayashi K, et al. Topographical analyses of shape of eyes with pathologic myopia by high-resolution three dimensional magnetic resonance imaging. Ophthalmology. 2011;118(8):1626–37.
2. Ohno-Matsui K. Proposed classification of posterior staphylomas based on analyses of eye shape by three-dimensional magnetic resonance imaging. Ophthalmology. 2014;121(9):1798–809.
3. Vongphanit J, Mitchell P, Wang JJ. Prevalence and progression of myopic retinopathy in an older population. Ophthalmology. 2002;109(4):704–11.
4. Yan YN, Wang YX, Yang Y, et al. Ten-year progression of myopic maculopathy: The Beijing eye study 2001–2011. Ophthalmology. 2018;125:1253–63.
5. Fang Y, Yokoi T, Nagaoka N, et al. Progression of myopic maculopathy during 18-year follow-up. Ophthalmology. 2018;125(6):863–77.
6. Hayashi K, Ohno-Matsui K, Shimada N, et al. Long-term pattern of progression of myopic maculopathy: a natural history study. Ophthalmology. 2010;117(8):1595–611.
7. Spaide RF. Staphyloma: part 1. New York: Springer; 2013. p. 167–76.
8. Wang NK, Wu YM, Wang JP, et al. Clinical characteristics of posterior staphylomas in myopic eyes with axial length shorter than 26.5 mm. Am J Ophthalmol. 2016;162:180–90.
9. Curtin BJ. The posterior staphyloma of pathologic myopia. Trans Am Ophthalmol Soc. 1977;75:67–86.
10. Shinohara K, Shimada N, Moriyama M, et al. Posterior Staphylomas in pathologic myopia imaged by Widefield optical coherence tomography. Invest Ophthalmol Vis Sci. 2017;58(9):3750–8.
11. Shinohara K, Tanaka N, Jonas JB, et al. Ultra-widefield optical coherence tomography to investigate relationships between myopic macular retinoschisis and posterior staphyloma. Ophthalmology. 2018;125(10):1575–86.
12. Ohno-Matsui K, Kawasaki R, Jonas JB, et al. International photographic classification and grading system for myopic maculopathy. Am J Ophthalmol. 2015;159(5):877–83.e7.
13. Cheung CMG, Ohno-Matsui K, Wong TY, et al. Influence of myopic macular degeneration severity on treatment outcomes with intravitreal aflibercept in the MYRROR study. Acta Ophthalmol. 2019;97(5):e729–35.
14. Wong YL, Sabanayagam C, Ding Y, et al. Prevalence, risk factors, and impact of myopic macular degeneration on visual impairment and functioning among adults in Singapore. Invest Ophthalmol Vis Sci. 2018;59(11):4603–13.
15. Fujiwara T, Imamura Y, Margolis R, et al. Enhanced depth imaging optical coherence tomography of the choroid in highly myopic eyes. Am J Ophthalmol. 2009;148(3):445–50.
16. Ikuno Y, Tano Y. Retinal and choroidal biometry in highly myopic eyes with spectral-domain optical coherence tomography. Invest Ophthalmol Vis Sci. 2009;50(8):3876–80.
17. Yokoi T, Jonas JB, Shimada N, et al. Peripapillary diffuse Chorioretinal atrophy in children as a sign of eventual pathologic myopia in adults. Ophthalmology. 2016;123(8):1783–7.
18. Fang Y, Du R, Nagaoka N, et al. OCT-based diagnostic criteria for different stages of myopic maculopathy. Ophthalmology. 2019;126(7):1018–32.
19. Ohno-Matsui K, Jonas JB, Spaide RF. Macular Bruch membrane holes in highly myopic patchy Chorioretinal atrophy. Am J Ophthalmol. 2016;166:22–8.
20. Ohno-Matsui K, Yoshida T, Futagami S, et al. Patchy atrophy and lacquer cracks predispose to the development of choroi-

dal neovascularisation in pathological myopia. Br J Ophthalmol. 2003;87(5):570–3.
21. Yoshida T, Ohno-Matsui K, Yasuzumi K, et al. Myopic choroidal neovascularization: a 10-year follow-up. Ophthalmology. 2003;110(7):1297–305.
22. Wolf S, Balciuniene VJ, Laganovska G, et al. RADIANCE: a randomized controlled study of ranibizumab in patients with choroidal neovascularization secondary to pathologic myopia. Ophthalmology. 2014;121(3):682–92.e2.
23. Ikuno Y, Ohno-Matsui K, Wong TY, et al. Intravitreal Aflibercept injection in patients with myopic Choroidal neovascularization: the MYRROR study. Ophthalmology. 2015;122(6):1220–7.
24. Ruiz-Moreno JM, Montero JA, Araiz J, et al. Intravitreal antivascular endothelial growth factor therapy for choroidal neovascularization secondary to pathologic myopia: six years outcome. Retina. 2015;35(12):2450–6.
25. Ohno-Matsui K, Ikuno Y, Lai TYY, Gemmy Cheung CM. Diagnosis and treatment guideline for myopic choroidal neovascularization due to pathologic myopia. Prog Retin Eye Res. 2018;63:92–106.
26. Ohno-Matsui K, Jonas JB, Spaide RF. Macular Bruch membrane holes in choroidal neovascularization-related myopic macular atrophy by swept-source optical coherence tomography. Am J Ophthalmol. 2016;162:133–9.e1.
27. Cheung CMG, Arnold JJ, Holz FG, et al. Myopic choroidal neovascularization: review, guidance, and consensus statement on management. Ophthalmology. 2017;124(11):1690–711.
28. Lai TY, Cheung CM. Myopic choroidal neovascularization: diagnosis and treatment. Retina. 2016;36(9):1614–21.
29. Takano M, Kishi S. Foveal retinoschisis and retinal detachment in severely myopic eyes with posterior staphyloma. Am J Ophthalmol. 1999;128(4):472–6.
30. Ikuno Y, Sayanagi K, Soga K, et al. Foveal anatomical status and surgical results in vitrectomy for myopic foveoschisis. Jpn J Ophthalmol. 2008;52(4):269–76.
31. Shimada N, Ohno-Matsui K, Baba T, et al. Natural course of macular retinoschisis in highly myopic eyes without macular hole or retinal detachment. Am J Ophthalmol. 2006;142(3):497–500.
32. Gaucher D, Haouchine B, Tadayoni R, et al. Long-term follow-up of high myopic foveoschisis: natural course and surgical outcome. Am J Ophthalmol. 2007;143(3):455–62.
33. Ikuno Y, Gomi F, Tano Y. Potent retinal arteriolar traction as a possible cause of myopic foveoschisis. Am J Ophthalmol. 2005;139(3):462–7.
34. Panozzo G, Mercanti A. Optical coherence tomography findings in myopic traction maculopathy. Arch Ophthalmol. 2004;122(10):1455–60.
35. Baba T, Ohno-Matsui K, Futagami S, et al. Prevalence and characteristics of foveal retinal detachment without macular hole in high myopia. Am J Ophthalmol. 2003;135(3):338–42.
36. Takahashi H, Tanaka N, Shinohara K, et al. Ultra-widefield optical coherence tomographic imaging of posterior vitreous in eyes with high myopia. Am J Ophthalmol. 2019;206:102–12.
37. Itakura H, Kishi S, Li D, et al. Vitreous changes in high myopia observed by swept-source optical coherence tomography. Invest Ophthalmol Vis Sci. 2014;55(3):1447–52.
38. Kobayashi H, Kishi S. Vitreous surgery for highly myopic eyes with foveal detachment and retinoschisis. Ophthalmology. 2003;110(9):1702–7.
39. Ikuno Y, Sayanagi K, Ohji M, et al. Vitrectomy and internal limiting membrane peeling for myopic foveoschisis. Am J Ophthalmol. 2004;137(4):719–24.
40. Shimada N, Sugamoto Y, Ogawa M, et al. Fovea-sparing internal limiting membrane peeling for myopic traction Maculopathy. Am J Ophthalmol. 2012;24:24.
41. Ho TC, Chen MS, Huang JS, et al. Foveola nonpeeling technique in internal limiting membrane peeling of myopic foveoschisis surgery. Retina. 2012;32(3):631–4.
42. Shinohara K, Shimada N, Takase H, Ohno-Matsui K. Functional and structural outcomes after fovea-sparing internal limiting membrane peeling for myopic macular retinoschisis by microperimetry. Retina. 2019; https://doi.org/10.1097/IAE.0000000000002627.
43. Gaucher D, Erginay A, Lecleire-Collet A, et al. Dome-shaped macula in eyes with myopic posterior staphyloma. Am J Ophthalmol. 2008;145(5):909–14.
44. Caillaux V, Gaucher D, Gualino V, et al. Morphologic characterization of dome-shaped macula in myopic eyes with serous macular detachment. Am J Ophthalmol. 2013;156(5):958–67.
45. Imamura Y, Iida T, Maruko I, et al. Enhanced depth imaging optical coherence tomography of the sclera in dome-shaped macula. Am J Ophthalmol. 2011;151(2):297–302.
46. Ellabban AA, Tsujikawa A, Matsumoto A, et al. Three-dimensional tomographic features of dome-shaped macula by swept-source optical coherence tomography. Am J Ophthalmol. 2013;155(2):320–8.e2
47. Fang Y, Jonas JB, Yokoi T, et al. Macular Bruch's membrane defect and dome-shaped macula in high myopia. PLoS One. 2017;12(6):e0178998.
48. Kaneko Y, Moriyama M, Hirahara S, et al. Areas of nonperfusion in peripheral retina of eyes with pathologic myopia detected by ultra-widefield fluorescein angiography. Invest Ophthalmol Vis Sci. 2014;55(3):1432–9.
49. Moriyama M, Ohno-Matsui K, Futagami S, et al. Morphology and long-term changes of choroidal vascular structure in highly myopic eyes with and without posterior staphyloma. Ophthalmology. 2007;114(9):1755–62.
50. Ishida T, Moriyama M, Tanaka Y, et al. Radial tracts emanating from Staphyloma edge in eyes with pathologic myopia. Ophthalmology. 2014;122(1):215–6.

Part III

Posterior Staphyloma

TMDU Classification and Curtin's Classification

3

Noriko Tanaka

Abstract

A posterior staphyloma is a hallmark abnormality of the globe with pathologic myopia, in which a portion of the posterior pole protrudes posteriorly. It is highly characteristic and specific to pathologic myopia since it rarely occurs except for pathologic myopia. The most commonly used classification is the Curtin's classification, which was based on his observations of the fundi by an ophthalmoscope. Using Optos and 3D MRI, Ohno-Matsui proposed the TMDU classification that simplifies the Curtin's classification and makes it easier to use. In the TMDU classification, the range of the posterior staphyloma was evaluated by the range of the outermost edge.

Keywords

Pathologic myopia · Posterior staphyloma · Classification · Wide-field fundus imaging · 3D MRI

A posterior staphyloma is a hallmark abnormality of the eyes with pathologic myopia, in which a part of the posterior pole protrudes posteriorly, It is defined by Spaide [1] as "an outpouching of the wall of the eye that has a radius of curvature that is less than the surrounding curvature of the wall of the eye."

Since a posterior staphyloma rarely occurs except for pathologic myopia, it is very characteristic and specific to pathologic myopia.

3.1 Curtin's Classification

The most commonly used classification to date is the Curtin's classification [2]. This classification was based on his observations and chart drawing of the fundi by an ophthalmoscope.

The classification consists of 10 types from I to X. Types I to V are primary staphylomas and Types VI to X are compound staphylomas. Depending on the location of posterior staphylomas, those in the posterior pole are classified as Type I, in the macula as Type II, in the peripapillary region as Type III, in the nasal side of the optic disc as Type IV, and in the inferior side of the optic disc as Type V.

Compound staphylomas are a combination of some primary staphylomas. Type VI is a combination of Types I and II, and Type VII is the combination of Types I and III. Type VIII has tiers or steps across the wall of Type I staphyloma. Type XI has a vertical septum which passes from the upper to the lower border of the staphyloma through, or to either side of, the optic nerve. Type X has thin plicae which divide the staphyloma into several compartments and typically extend from the optic nerve to the margin of the staphyloma.

3.2 TMDU Classification

Using Optos and 3D MRI, Ohno-Matsui proposed TMDU classification, which simplified and made the Curtin's classification easier to use and renamed very rare types as 'others' (Fig. 3.1).

N. Tanaka (✉)
Department: Ophthalmology & Visual Science, Tokyo Medical and Dental University, Tokyo, Japan

K. Ohno-Matsui (ed.), *Atlas of Pathologic Myopia*, https://doi.org/10.1007/978-981-15-4261-9_3

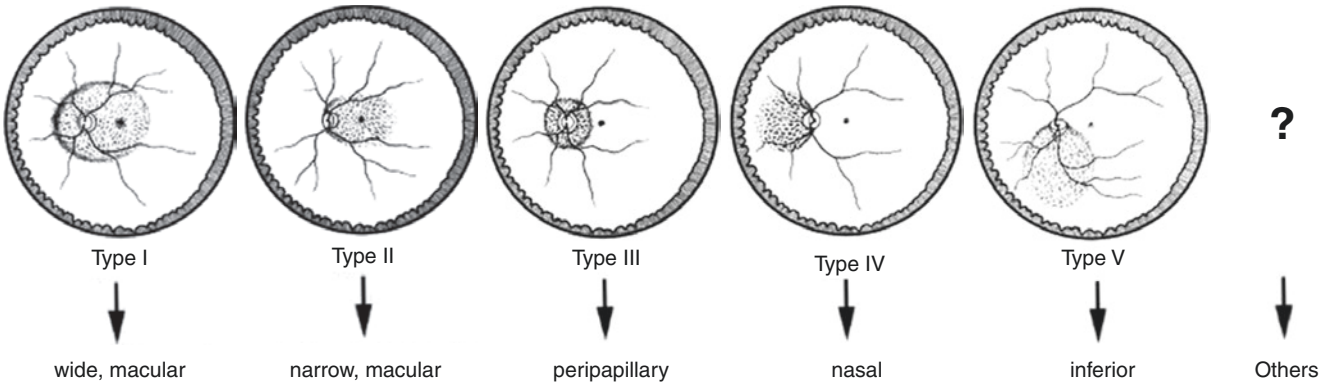

Fig. 3.1 TMDU classification, renaming of staphylomas according to their location ([3] cited with permission)

In this classification, the range of the posterior staphyloma was evaluated by the range of the outermost edge [4]. As a result, Types VI to X in the Curtin's classification are integrated into Type I. In addition, Types I to V were renamed according to the range of the staphyloma. Type I is wide, macular staphyloma, including the optic disc and macula. Type II is narrow, macular staphyloma, limited to a narrow area of the posterior pole. Type III is peripapillary staphyloma, protruding in a circle around the optic disc. Type IV is nasal staphyloma, extending to the nasal side of the optic disc. Type V is inferior staphyloma, protruding in the lower half of the eye. Staphylomas other than Types I to V are defined as others.

References

1. Spaide RF. Staphyloma: part 1. In: Spaide RF, Ohno-Matsui K, Yannuzzi LA, editors. Pathologic myopia. New York: Springer; 2014. p. 167–85.
2. Curtin BJ. The posterior staphyloma of pathologic myopia. Trans Am Ophthalmol Soc. 1977;75:67–86. [Published Online First: 1977/01/01]
3. Ohno-Matsui K. Proposed classification of posterior staphylomas based on analyses of eye shape by three-dimensional magnetic resonance imaging and wide-field fundus imaging. Ophthalmology. 2014;121(9):1798–809. https://doi.org/10.1016/j.ophtha.2014.03.035. [Published Online First: 2014/05/13]
4. Ohno-Matsui K, Alkabes M, Salinas C, et al. Features of posterior staphylomas analyzed in wide-field fundus images in patients with unilateral and bilateral pathologic myopia. Retina (Philadelphia, Pa). 2017;37(3):477–86. https://doi.org/10.1097/iae.0000000000001327. [Published Online First: 2016/08/25]

3D MRI of Posterior Staphyloma

4

Muka Moriyama

Abstract

Three-dimensional magnetic resonance imaging (3D MRI) of the eye is a powerful tool to visualize the entire shape of the eye. Using 3D MRI, posterior staphylomas can be observed in its full extent and how the entire eye shape changes in parallel. It has also been shown that some specific eye shape is related to poor visual outcome.

Keywords

Posterior staphyloma · Axial length · Three dimensional MRI

With the development of high-field MRI systems and newer designs of radio-frequency coils, the acquisition of volumetric ocular MRI data having high intrinsic resolution in three dimensions (3D), has become feasible [1]. 3D MRI images are obtained by volume rendering of fat-suppressed T_2-weighted images. The use of 3D MRI has advantages of visualizing the shape of the globe from any angle and to analyze the entire shape of the eye [2, 3].

3D MRI images showed that posterior segment of emmetropic eyes had an almost hemispherical shape (Fig. 4.1; Movie 4.1). In axial myopia, an equatorial region of the eye mainly elongates. Thus, highly myopic eyes without staphyloma show an elongated eye shape in anterior-posterior direction (Figs. 4.2 and 4.3). However, in axially myopic eyes without staphyloma, the curvature of the posterior eye segment is relatively well-maintained.

In contrast, the eyes with pathologic myopia is characterized by a deformity of the posterior eye segment represented by posterior staphylomas (Figs. 4.4, 4.5, and 4.6; Movie 4.2). In some cases, multiple staphylomas can be seen (Fig. 4.6). It is noted that the eye curvature peripheral to the staphylomas is sometimes flattened. This suggests that a formation of staphyloma may affect an entire shape of the eye.

The most protruded point exists along the midline of the eye in a shallow staphyloma. However, in deep staphylomas, the area below the midline tends to protrude most posteriorly.

Electronic Supplementary Material The online version of this chapter (https://doi.org/10.1007/978-981-15-4261-9_4) contains supplementary material, which is available to authorized users.

M. Moriyama (✉)
Ophthalmology and Visual Science Tokyo Medical and Dental University, Tokyo, Japan

K. Ohno-Matsui (ed.), *Atlas of Pathologic Myopia*, https://doi.org/10.1007/978-981-15-4261-9_4

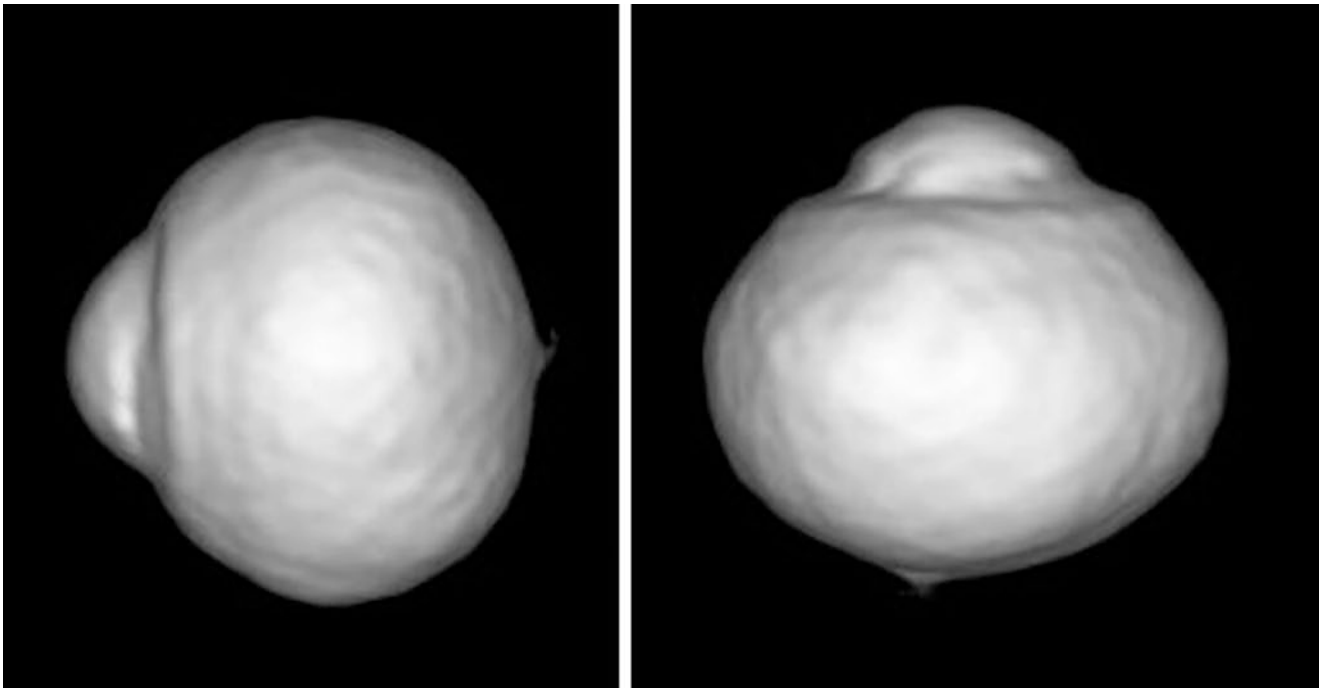

Fig. 4.1 3D MRI of an emmetropic eye viewed from temporally (left) and viewed from inferiorly (right). The left eye of a 70-year-old woman with an axial length of 23.3 mm. The eye is almost spherical

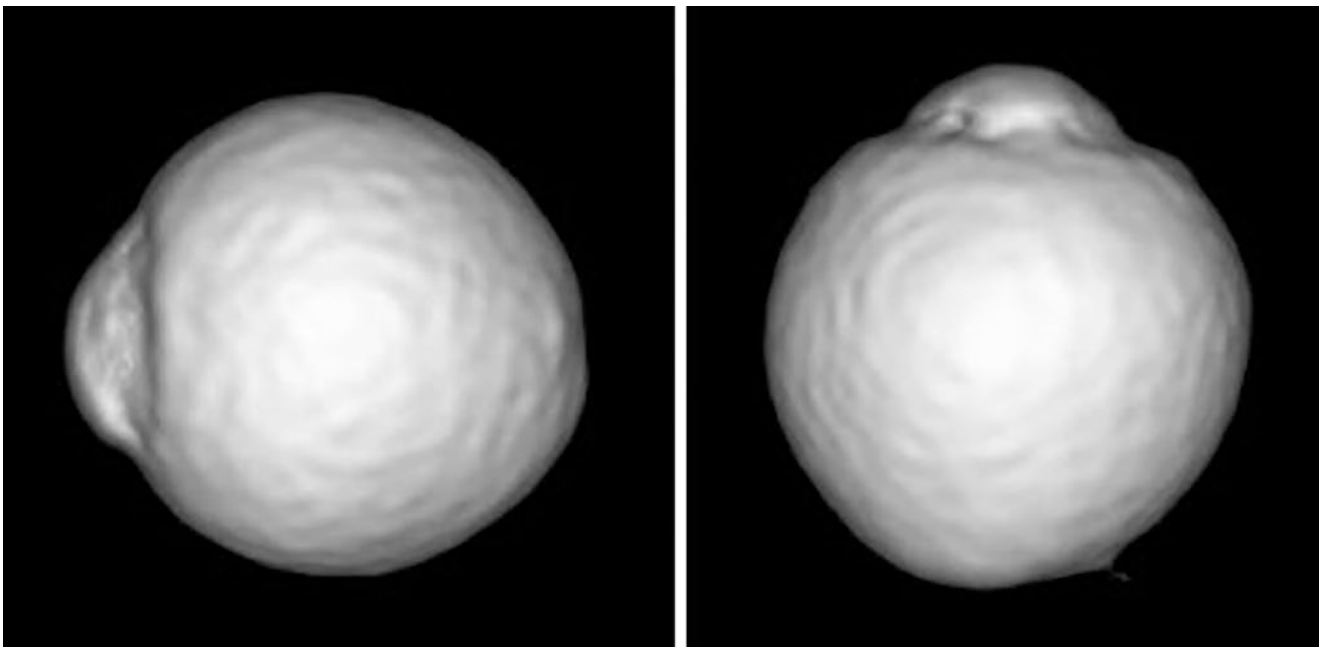

Fig. 4.2 3D MRI of a highly myopic eye without staphyloma viewed from nasally (left) and viewed from inferiorly (right). The right eye of a 61-year-old woman with an axial length of 28.4 mm. The eye is slightly elongated in antero-posterior direction. However, the curvature of the posterior eye cup is maintained

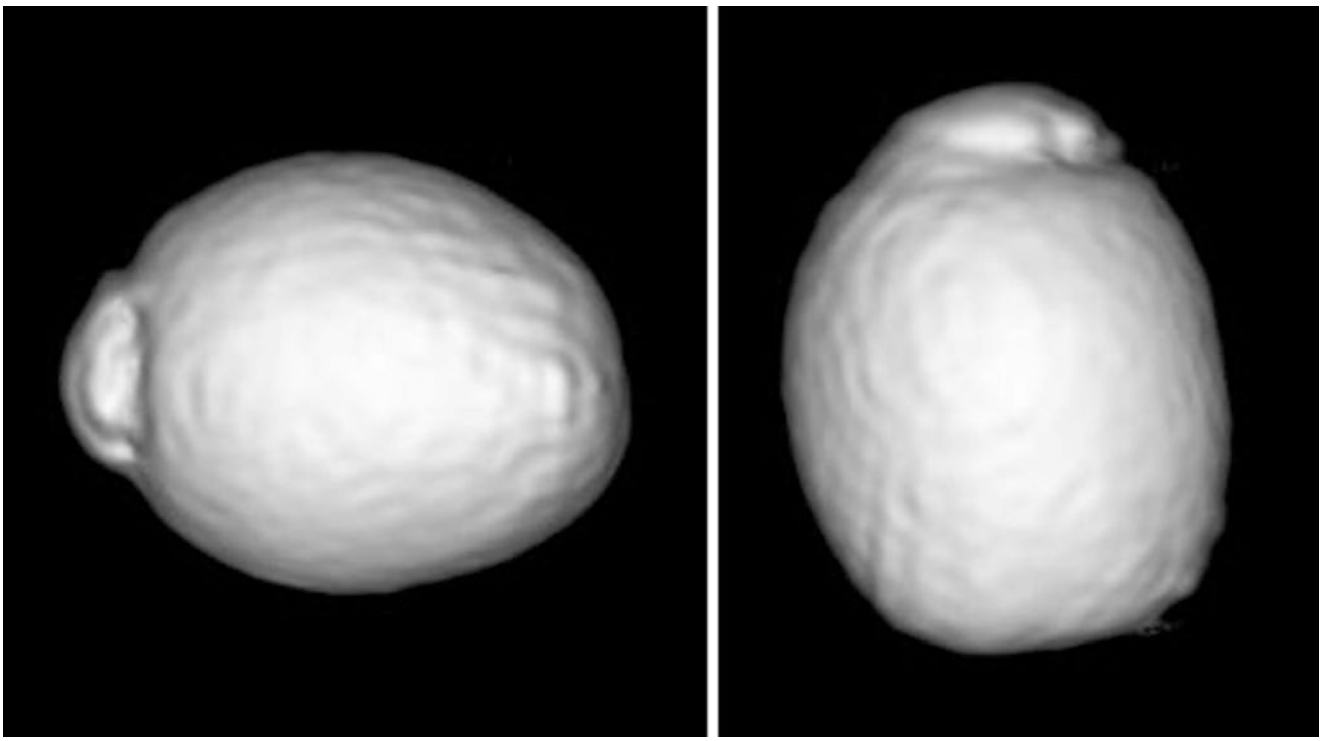

Fig. 4.3 3D MRI of an advanced highly myopic eye viewed from nasally (left) and viewed from inferiorly (right). The right eye of a 47-year-old woman with an axial length of 32.0 mm. The eye is severely elongated in antero-posterior direction. However, there is no posterior outpouching suggesting a staphyloma

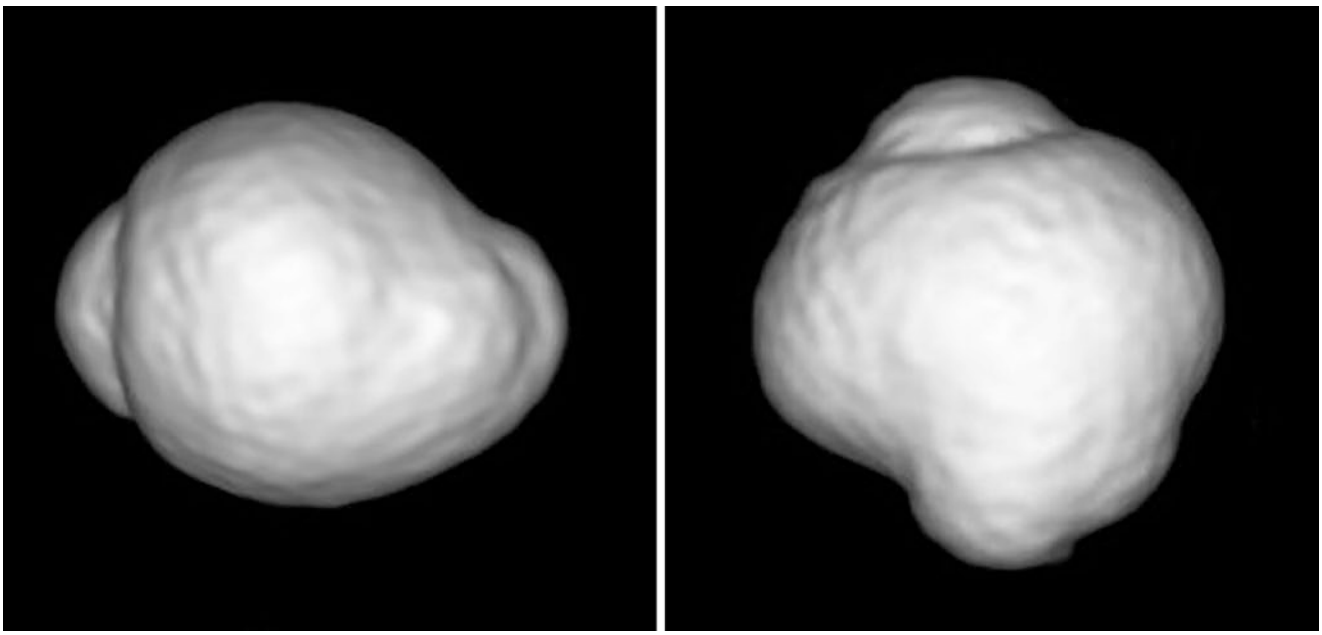

Fig. 4.4 3D MRI of an eye with pathologic myopia with staphyloma viewed from nasally (left) and viewed from inferiorly (right). The left eye of a 71-year-old woman with an axial length of 28.1 mm. There is an evident staphyloma. The upper edge and the temporal edge of the staphyloma are abrupt, seen as "notch." The eye curvature peripheral to the upper or temporal edge is flattened

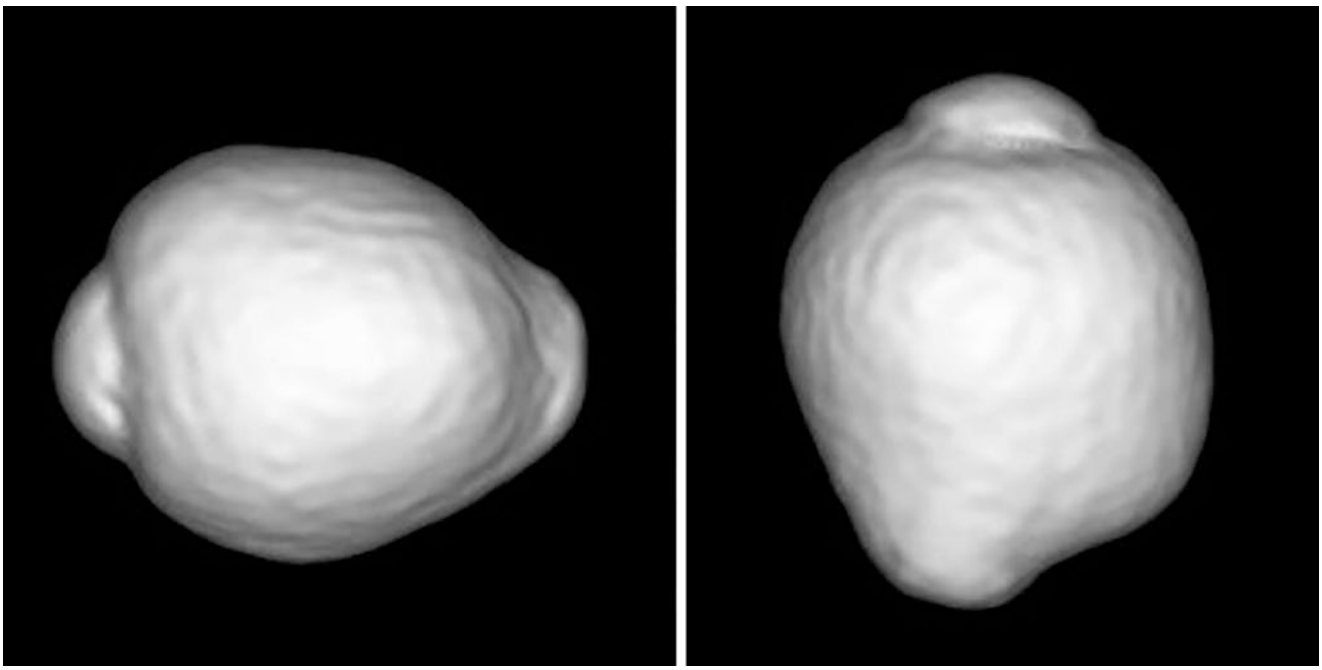

Fig. 4.5 3D MRI of an eye with pathologic myopia with staphyloma viewed from nasally (left) and viewed from inferiorly (right). The right eye of a 60-year-old woman with an axial length of 31.6 mm. There is an evident staphyloma. The upper edge and the nasal edge of the staphyloma are abrupt. The eye shows a temporal distorted shape

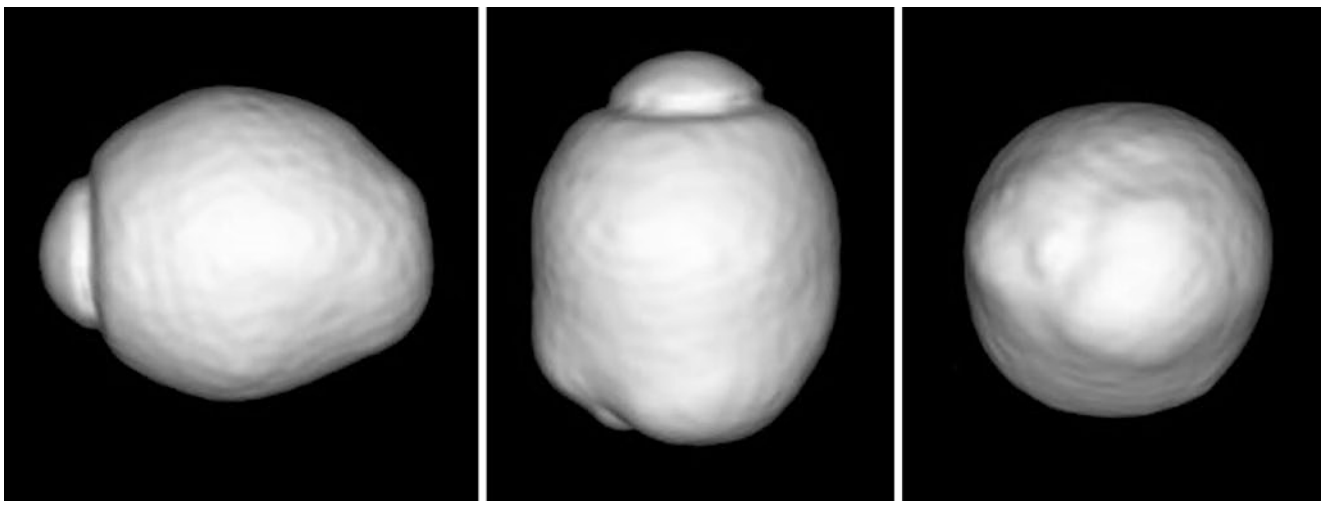

Fig. 4.6 3D MRI of an eye with pathologic myopia with multiple staphylomas viewed from nasally (left), viewed from inferiorly (center), and viewed from the back (right). The left eye of a 67-year-old woman with an axial length of 31.8 mm

References

1. Singh KD, Logan NS, et al. Three-dimensional modeling of the human eye based on magnetic resonance imaging. Invest Ophthalmol Vis Sci. 2006;47:2272–9.
2. Moriyama M, Ohno-Matsui K, et al. Topographic analyses of shape of eyes with pathologic myopia by high-resolution three-dimensional magnetic resonance imaging. Ophthalmology. 2011;118(8):1626–37.
3. Moriyama M, Ohno-Matsui K, et al. Quantitative analyses of high-resolution 3D MR images of highly myopic eyes to determine their shapes. Invest Ophthalmol Vis Sci. 2012;53(8):4510–8.

Ultra-Wide Field OCT of Posterior Staphyloma

5

Kosei Shinohara

Abstract

Ultra-wide field OCT (UWF-OCT) is a useful instrument for the detection and classification of posterior staphylomas. Morphological features of posterior staphylomas shown by UWF-OCT are gradual thinning of the choroid from the periphery toward the edge of the staphyloma and a gradual re-thickening of the choroid in the direction toward the posterior pole along with a posterior displacement of the sclera in the staphylomatous area. Also, there is a gradual thickening and inward protrusion of the sclera at the staphyloma edge. UWF-OCT will be a standard instrument for the detection of posterior staphylomas.

Keywords

Posterior staphyloma · Ultra-wide field OCT · Sclera · Choroid

It had long been difficult to visualize the entire extent of posterior staphylomas with conventional optical coherence tomography (OCT) because staphylomas are usually wider than the scanned area by OCT. Therefore, the usefulness of conventional OCT for the detection of staphylomas has been limited to peripapillary staphyloma [1]. As approaches to cover a large area by OCT, combining multiple scans at different locations or placing a +20 diopter lens between the eye and the OCT device were performed. In addition to the limited width of OCT images, the depth of images was not sufficient to accommodate a deep staphyloma [2, 3]. Recent advance in OCT technology has allowed clinicians to evaluate a much wider area than the posterior fundus. Morphological hallmarks of posterior staphylomas as examined by UWF-OCT are; a gradual thinning of the choroid from the periphery toward the staphyloma edges and a gradual re-thickening of the choroid in a direction toward the posterior pole along with a posterior displacement of the sclera in the staphylomatous area (Fig. 5.1). Additionally, there was a gradual thickening and inward protrusion of the sclera at the staphyloma edge (Figs. 5.1, 5.2, 5.3, and 5.4). These features should be used as the criteria of the diagnoses of a posterior staphyloma. Among these morphological changes, the choroidal thinning and the posterior displacement of the sclera are occasionally observed even in children with high myopia (Fig. 5.5), indicating these two features are the early change in the process of the development of staphylomas [4]. Shinohara et al. reported the usefulness of ultra-wide field OCT (UWF-OCT) for the detection of posterior staphylomas compared its usefulness with 3D MRI (Table 5.1) [5].

The advantages of UWF-OCT is that it enables to visualize different tissues such as vitreous, retina, choroid, and sclera in a high resolution. Especially, the spatial relationship between a posterior staphyloma and other tissues such as optic nerve, and retinal vasculature is clearly seen. Due to these advantages, UWF-OCT can detect and classify posterior staphylomas more accurately and objectively than conventional methods, and some subtle staphylomas which are difficult to be detected ophthalmoscopically or by 3D MRI can be detected by UWF-OCT (Fig. 5.6). It is expected that UWF-OCT will be a standard instrument for the detection of posterior staphylomas.

K. Shinohara (✉)
Department of Ophthalmology and Visual Science, Tokyo Medical and Dental University, Tokyo, Japan

Musashino Red-Cross Hospital, Tokyo, Japan

K. Ohno-Matsui (ed.), *Atlas of Pathologic Myopia*, https://doi.org/10.1007/978-981-15-4261-9_5

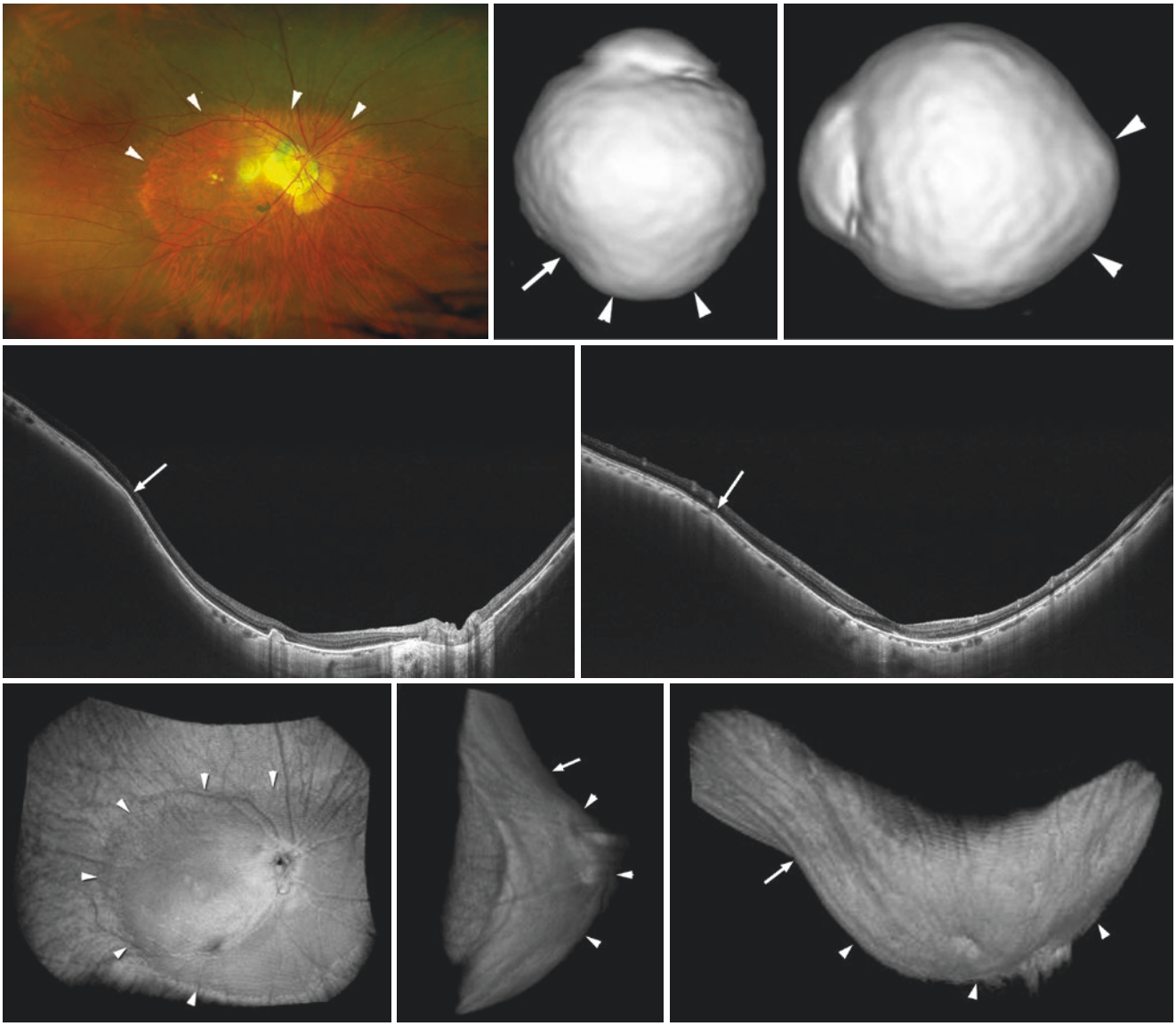

Fig. 5.1 Wide macular staphyloma as visualized by ultra-wide field optical coherence tomography (UWF-OCT) and three-dimensional magnetic resonance imaging (3D MRI). Cited with permission from [5]. Top left: Image of the right fundus of a 79-year-old woman (axial length: 26.6 mm) showing the border of a wide staphyloma as indicated by pigmentary abnormalities (arrowheads). Top middle and top right: 3D-MRI images viewed from the inferior (Middle) and from the nasal side (Right), showing a wide macular staphyloma (arrowheads) with a notch at the temporal border (arrow in Middle image). Middle row: Cross-sectional UWF-OCT images across the fovea. Left: horizontal scan. Right: vertical scan. An inward protrusion of the sclera and a thinning of the choroid are observed at the edge of the staphyloma in the horizontal section and in the vertical section (arrows). The staphylomatous region shows a posterior displacement of the sclera nasal to the staphyloma edge in the Left image and inferior to the staphyloma edge in the Right image. Bottom row: Three-dimensional UWF-OCT images viewed from the anterior (Left), the nasal (Middle), and from the inferior side (Right), show a scleral outpouching (arrowheads) due to a wide macular staphyloma. In the Left image, the staphyloma border is spatially associated with the optic nerve head and the retinal vessels

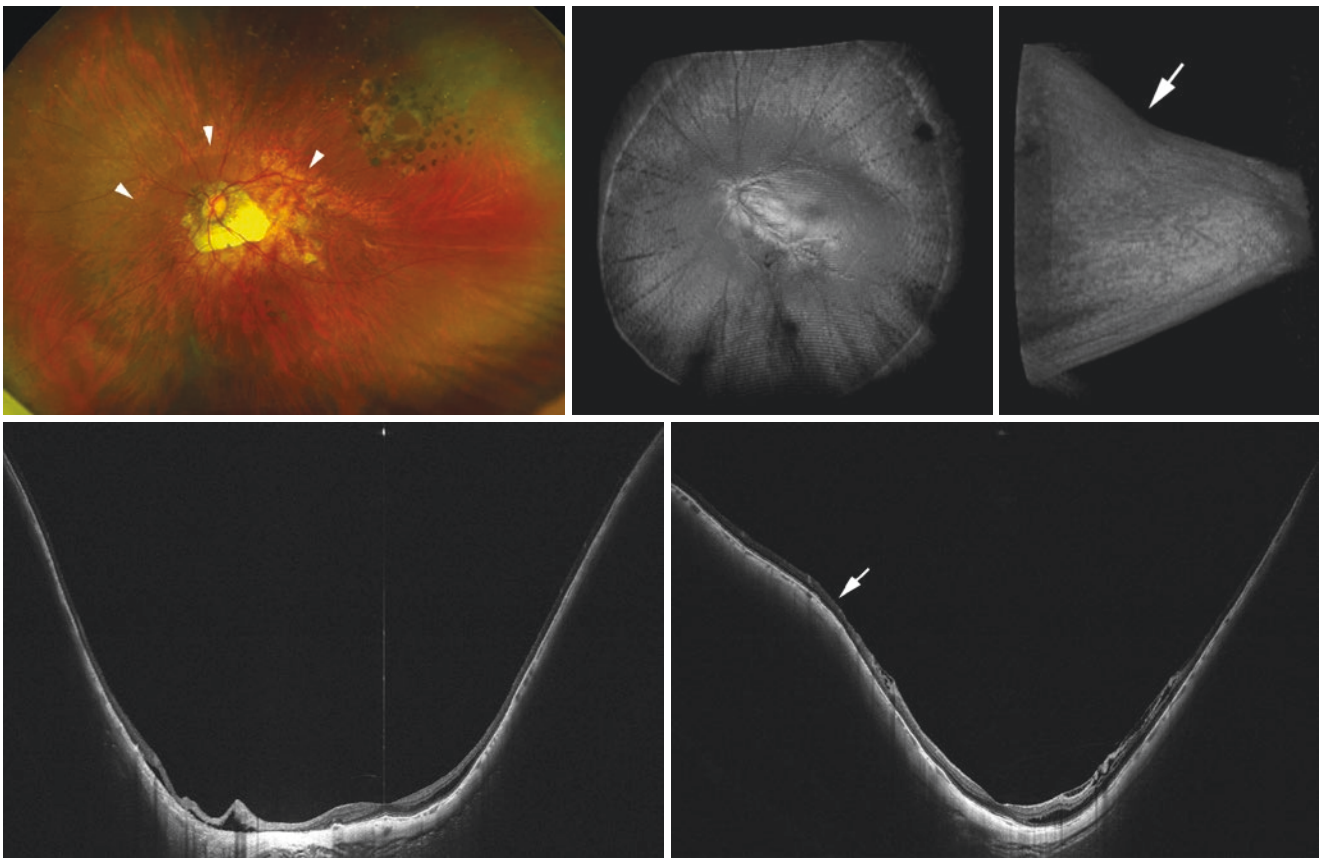

Fig. 5.2 Staphyloma classified as wide macular staphyloma by ultra-wide field optical coherence tomography (UWF-OCT). Top Left: Left fundus of a 56-year-old woman (length: 29.3 mm) showing the border of a wide macular staphyloma as indicated by pigmentary abnormalities (arrowheads). Top middle and Top right: 3D UWF-OCT images viewed from the anterior (Middle) and from the temporal side (Right) with a notch at the superior staphyloma edge (arrow). Bottom row: Cross-sectional UWF-OCT images across the fovea (Left: horizontal scan, Right: vertical scan) showing an inward protrusion of the sclera and a thinning of the choroid at the staphyloma edge in the vertical scan (Right image) (arrow). A posterior displacement of the sclera within the staphylomatous area inferior to the staphyloma edge in Right image is observed

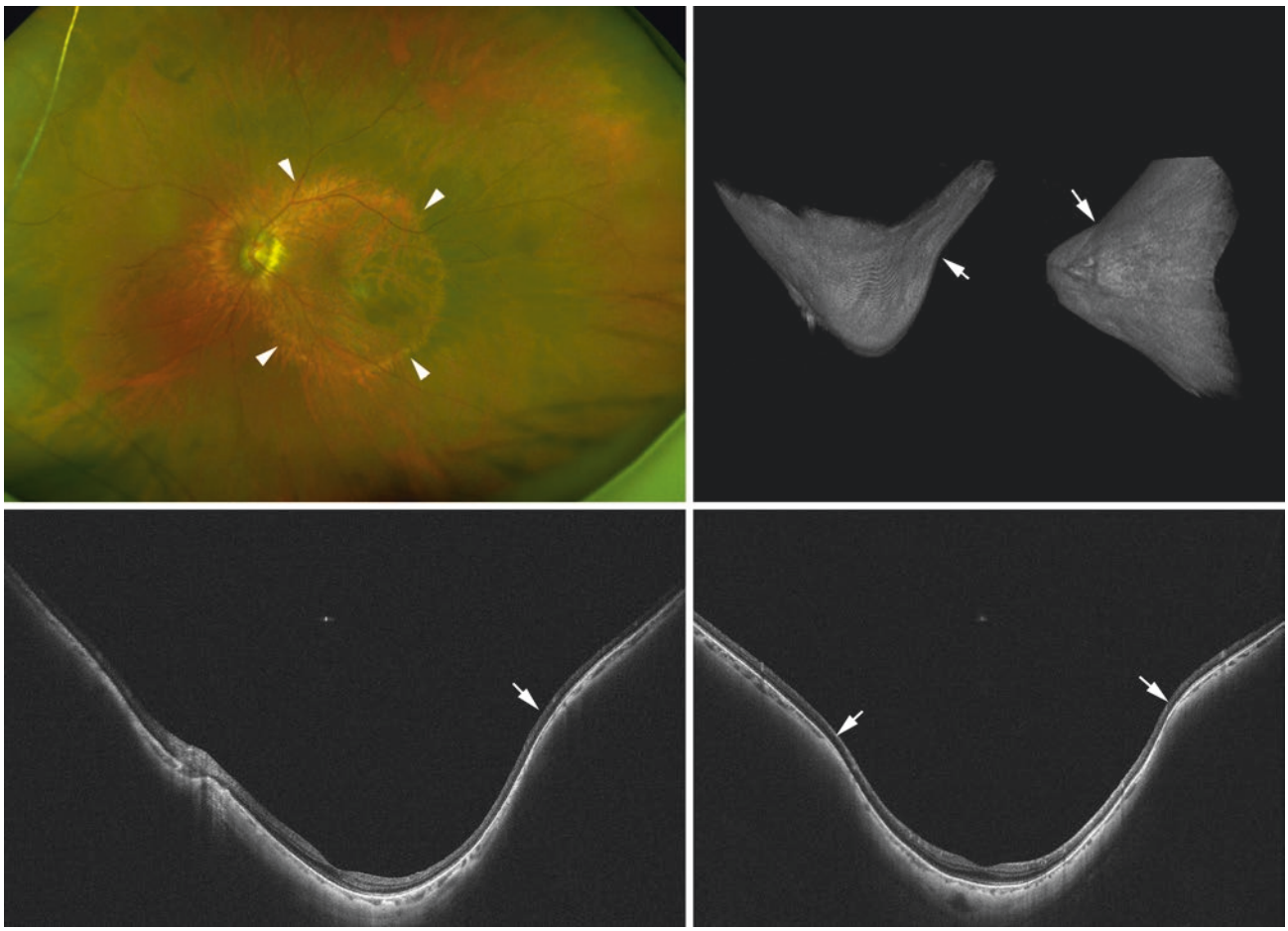

Fig. 5.3 Staphyloma classified as narrow macular staphyloma by ultra-wide field optical coherence tomography (UWF-OCT). Top Left: Left fundus of a 77-year-old woman (length: 26.6 mm) showing the border of a narrow macular staphyloma as indicated by pigmentary abnormalities (arrowheads). Top middle and Top right: 3D UWF-OCT images viewed from the inferior (Middle) and from the nasal side (Right) with a notch at the staphyloma edge (arrows). Bottom row: Cross-sectional UWF-OCT images across the fovea (Left: horizontal scan, Right: vertical scan) showing an inward protrusion of the sclera and a thinning of the choroid at the staphyloma edge (arrows). A posterior displacement of the sclera within the staphylomatous area is clearly observed

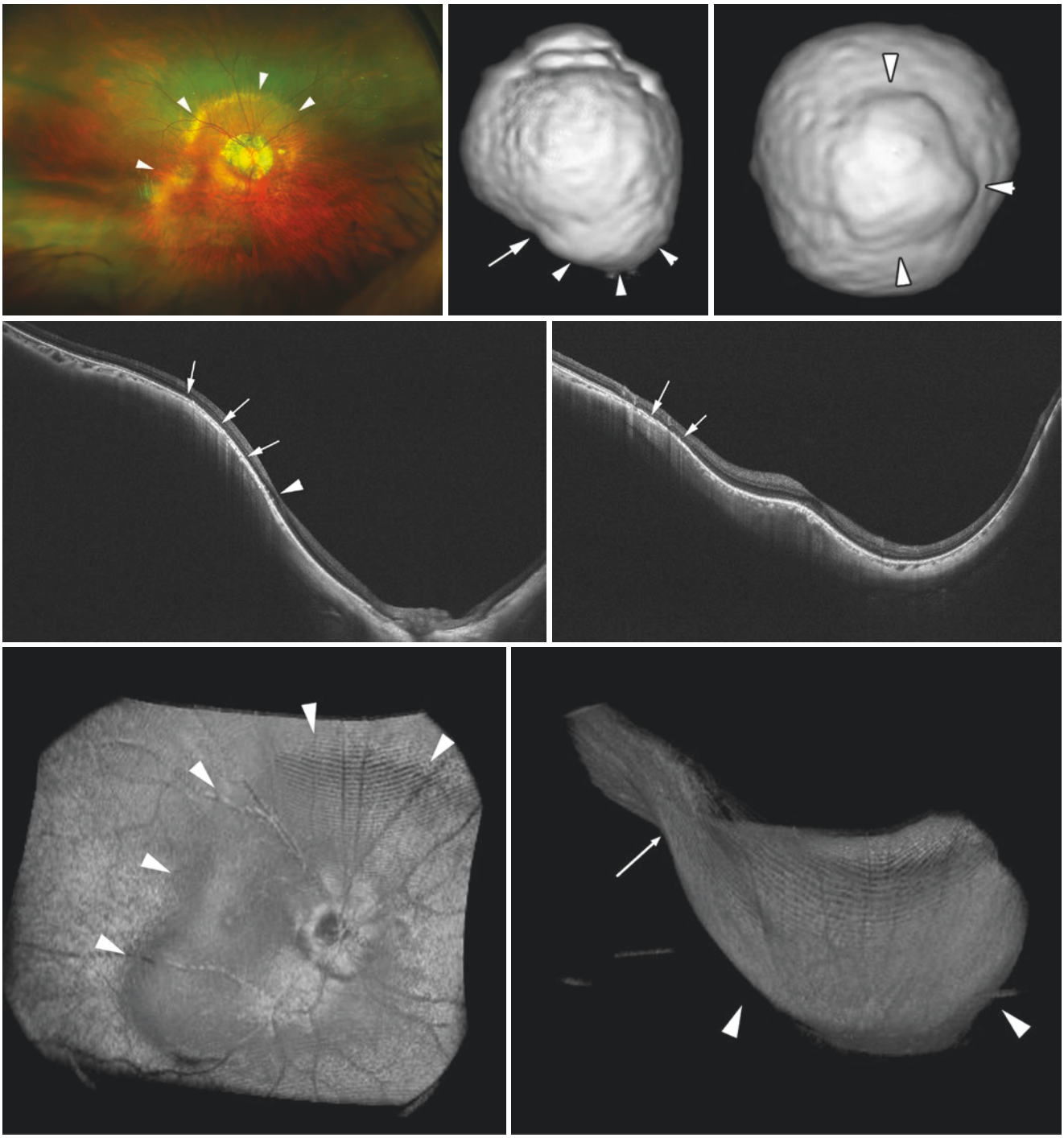

Fig. 5.4 Staphyloma classified as "others" (peripapillary and inferior type) both by three-dimensional magnetic resonance imaging (3D MRI) and ultra-wide field optical coherence tomography (UWF-OCT). Cited with permission from [5]. Top Left: Right fundus of a 68-year-old woman (axial length: 27.4 mm) with pigmentary abnormalities indicating the border of a staphyloma (arrowheads). Top Middle and Top Right: Three-dimensional magnetic resonance imaging (3D MRI) images viewed from the inferior (Middle) and from the posterior side (Right) showing a staphyloma (arrowheads). In the Middle image, the posterior outpouching is located mainly nasally; however, different from a peripapillary staphyloma, the outpouching has a wide opening angle. A notch is located at the temporal border of the staphyloma (arrow, Middle image). Due to the nasal dislocation of the wide scleral outpouching, this staphyloma type was classified as "others." Middle row: Cross-sectional UWF-OCT images across the fovea. Left: horizontal scan. Right: vertical scan. An inward protrusion of the sclera and a thinning of the choroid are located at the edge of the staphyloma both in the horizontal and vertical sections (arrows). A posterior displacement of the sclera is present in the staphylomatous area, nasal to the staphyloma edge in Left image and inferior to the staphyloma edge in Right image. The foveal region (arrowhead) is located on the slope of the staphyloma nasal to the staphyloma edge, and the optic nerve head is located at the bottom of the staphyloma in Left image. The Right image shows a posterior scleral displacement in the lower fundus with a dome-shaped appearance of the macula. This staphyloma was classified as "others" (peripapillary and inferior staphyloma type) by UWF-OCT. Bottom row: Three-dimensional UWF-OCT images viewed from the anterior (Left) and from the inferior side (Right) showing a peculiar shape of the staphyloma. The staphyloma is wider in the inferior fundus compared to the superior fundus. In the Left image, the spatial relationship between the optic nerve head and the retinal vessels is shown. The temporal border of the staphyloma is shown in the Right image (arrow)

Fig. 5.5 Early signs of posterior staphyloma in children. Cited with permission from [4]. Top Left: Left fundus of an 11-year-old girl with an axial length of 27.1 mm showing peripapillary diffuse atrophy. Top right: Horizontal ultra-wide field optical coherence tomography (UWF-OCT) image shows that the nasal choroid gradually thins toward the staphyloma edge (arrow) and gradually re-thickens toward the posterior pole (arrowheads). Inner scleral surface is posteriorly displaced in the area between the edge of the staphyloma (arrow) and nasal edge of the optic disc, compared to the curvature more nasal to the staphyloma edge. However, the scleral inward protrusion at staphyloma edge is not obvious. Bottom Left: Right fundus photograph of a 17-year-old young man with an axial length of 28.1 mm showing peripapillary diffuse chorioretinal atrophy (PDCA). Bottom right: Horizontal UWF-OCT image showing that the inner scleral surface is slightly displaced posteriorly nasal to the optic nerve. The choroid gradually thins toward the edge of the staphyloma (arrow) and re-thickens toward the posterior pole (yellow arrowheads). However, scleral inward protrusion at the staphyloma edge is not obvious. Choroidal thickening closer to the optic nerve appears to be similar to peripapillary intrachoroidal cavitation. In the area of the PDCA (blue arrowheads), the scleral curvature is also displaced posteriorly

Table 5.1 Correlation of types of posterior staphyloma identified by 3D MRI and wide-field OCT

OCT / 3D MRI	None	Wide macular	Narrow macular	Peripapillary	Nasal	Inferior	Others	Total
None	23	2	6	2	0	0	2	35
Wide macular	2	26	4	0	0	2	8	42
Narrow macular	0	0	17	0	0	0	0	17
Peripapillary	0	0	0	4	0	0	0	4
Nasal	0	0	0	0	0	0	0	0
Inferior	0	1	0	0	0	0	0	1
Others	0	0	0	0	0	0	1	1
Total	25	29	27	6	0	2	11	100

3D MRI three-dimensional magnetic resonance imaging, *OCT* optical coherence tomography
Number of observed agreements: 71 (71.0% of the observations)
Number of agreements expected by chance: 25.9 (25.89% of the observations)
Kappa = 0.609
SE of kappa = 0.058
95% confidence interval: From 0.496 to 0.722
The strength of agreement is considered to be "good"

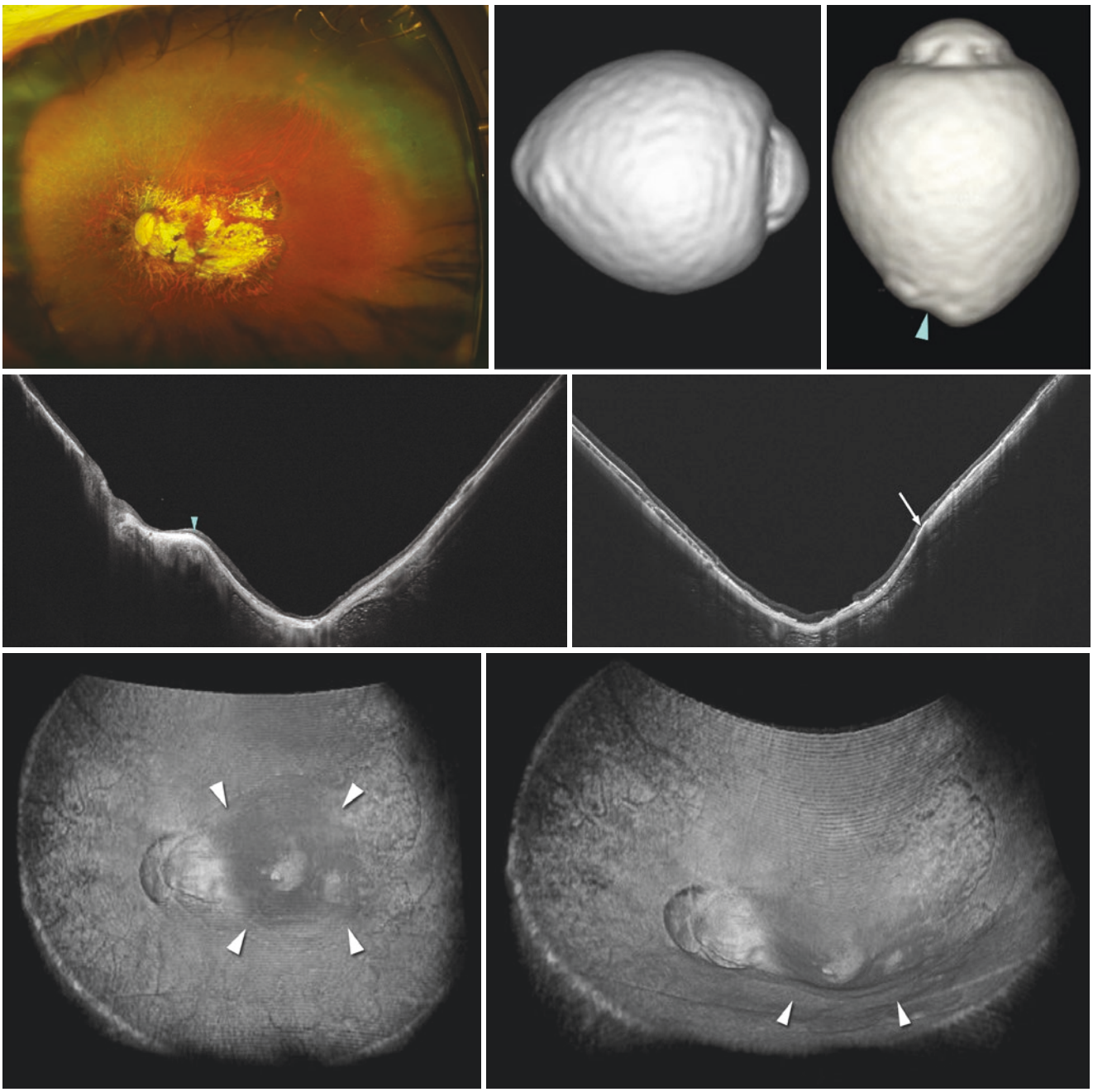

Fig. 5.6 An eye showing a narrow macular staphyloma by ultra-wide field optical coherence tomography (UWF-OCT) but no obvious protrusion by three-dimensional magnetic resonance imaging (3D MRI). Cited with permission from [5]. Top left: Left fundus of a 72-year-old woman (axial length: 31.6 mm) showing a severe chorioretinal atrophy and large parapapillary atrophy. Top Middle and Top Right: 3D-MRI images viewed from the nasal (Middle) and from the inferior side (Right). The eye is elongated without any obvious outpouching. A notch indicating the temporal ridge is observed (arrowhead in Right image). This case is classified as no staphyloma by 3D MRI. Middle row: Cross-sectional UWF-OCT images across the fovea. Left: horizontal scan. Right: vertical scan. An inward protrusion of the sclera and a thinning of the choroid are observed at the lower edge of the staphyloma in the vertical section (arrow, Right image). A posterior displacement of the sclera is shown within the staphylomatous area. The vertical ridge temporal to the optic nerve head is shown (arrowhead, Left image). Bottom row: Three-dimensional UWF-OCT images viewed from the anterior (Left) and from the anterior with slightly rotated angle (Right). The margin of the staphyloma is observed in both images (arrowheads). A spatial relationship between the staphylomatous area and the optic nerve head and the macula is demonstrated

References

1. Shinohara K, Moriyama M, Shimada N, Yoshida T, Ohno-Matsui K. Characteristics of Peripapillary Staphylomas associated with high myopia determined by swept-source optical coherence tomography. Am J Ophthalmol. 2016;169:138–44. https://doi.org/10.1016/j.ajo.2016.06.033.
2. Mori K, Kanno J, Gehlbach PL, Yoneya S. Montage images of spectral-domain optical coherence tomography in eyes with idiopathic macular holes. Ophthalmology. 2012;119(12):2600–8. https://doi.org/10.1016/j.ophtha.2012.06.027.
3. Uji A, Yoshimura N. Application of extended field imaging to optical coherence tomography. Ophthalmology. 2015;122(6):1272–4. https://doi.org/10.1016/j.ophtha.2014.12.035.
4. Tanaka N, Shinohara K, Yokoi T, Uramoto K, Takahashi H, Onishi Y, et al. Posterior staphylomas and scleral curvature in highly myopic children and adolescents investigated by ultra-widefield optical coherence tomography. PLoS One. 2019;14(6):e0218107. https://doi.org/10.1371/journal.pone.0218107.
5. Shinohara K, Shimada N, Moriyama M, Yoshida T, Jonas JB, Yoshimura N, et al. Posterior Staphylomas in pathologic myopia imaged by Widefield optical coherence tomography. Invest Ophthalmol Vis Sci. 2017;58(9):3750–8. https://doi.org/10.1167/iovs.17-22319.

Wide-Field Fundus Imaging of Posterior Staphyloma

6

Tomoka Ishida

Abstract

Posterior staphylomas involve a wider area than the area covered in 50 degree fundus photos. Wide-field fundus images can accommodate an entire extent of wide staphylomas. Although wide-field fundus images do not provide 3D information, the pigmentary alterations along the staphyloma edges may be a good indicator of staphylomas.

Keywords

Posterior staphyloma · Wide-field fundus imaging

It is difficult to show the entire extent of posterior staphylomas as well as staphyloma edges in the conventional 50 degree fundus photos, because the most common type of staphylomas involve a wider area. In this chapter, wide-field fundus images obtained with Optos® and Mirante® are shown to capture the entire extent of posterior staphylomas (findings along the staphyloma edges). Although wide-field fundus images do not provide three-dimensional information, pigmentary alterations along staphyloma edges may be a good indicator of staphyloma edges. In Optos images, a combination of pseudocolor images, red-free fundus images, and fundus autofluorescence images is reported to be useful to delineate the pigmentary alterations along staphyloma edges [1–3]. Different from Optos, Mirante® provides real color images (Figs. 6.1, 6.2, 6.3, and 6.4).

T. Ishida (✉)
Department of Ophthalmology and Visual Science, Tokyo Medical and Dental University, Tokyo, Japan

Department of Ophthalmology, Kyorin University, Tokyo, Japan
e-mail: tom-oph@ks.kyorin-u.ac.jp

K. Ohno-Matsui (ed.), *Atlas of Pathologic Myopia*, https://doi.org/10.1007/978-981-15-4261-9_6

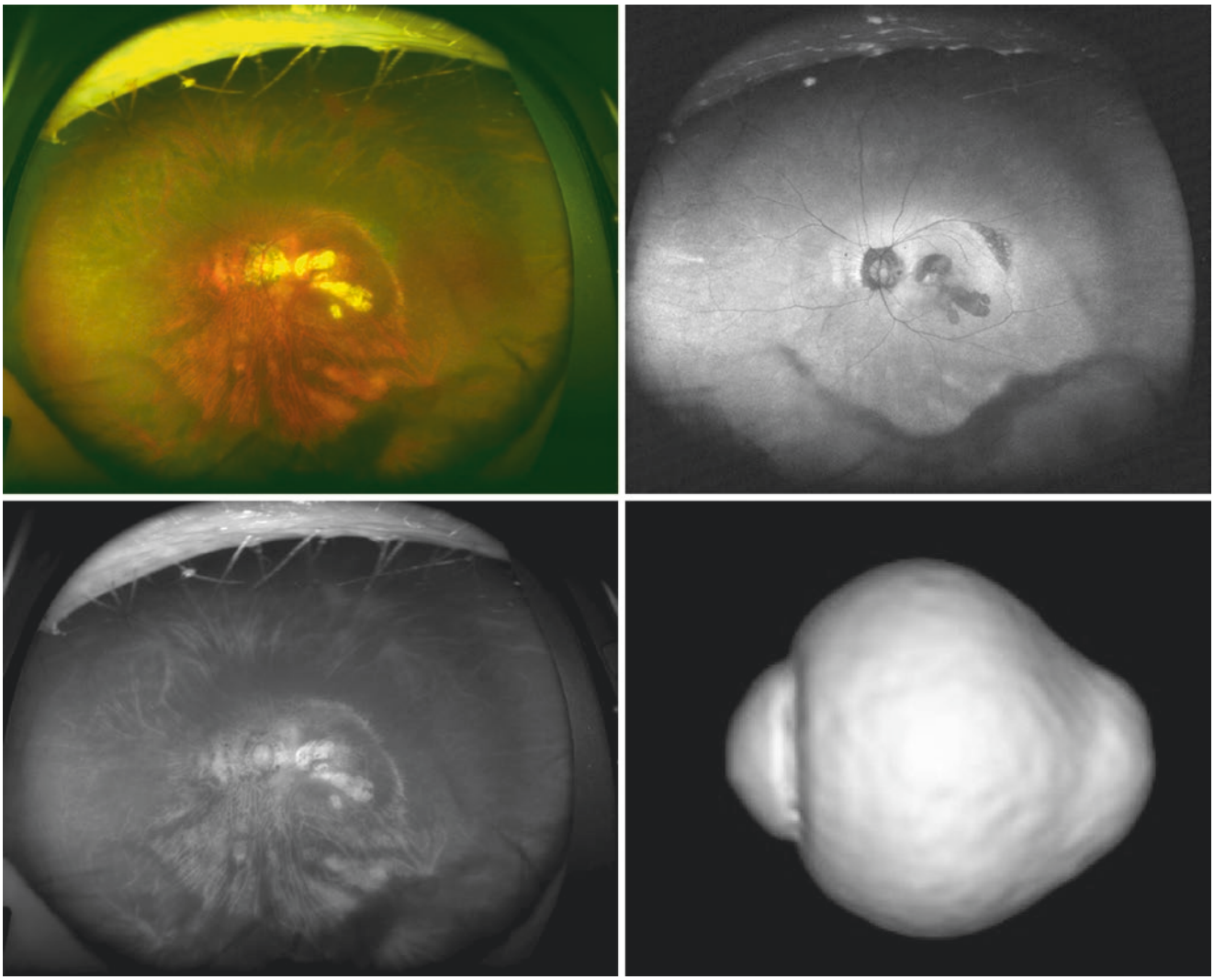

Fig. 6.1 Wide macular staphyloma in the left fundus of a 78-year-old woman with an axial length of 28.2 mm. (Top left) Pseudo-color fundus image shows depigmentation along the upper margin of wide macular staphyloma. (Top right) Fundus autofluorescence image shows hypofluorescence especially along the upper temporal border of staphyloma. (Bottom left) Red-free fundus image shows the hyper-reflectance along the upper margin of staphyloma. (Bottom right) Three-dimensional magnetic resonance imaging (3D MRI) of the left eye viewed from the side shows posterior outpouching of the posterior segment due to a wide macular staphyloma

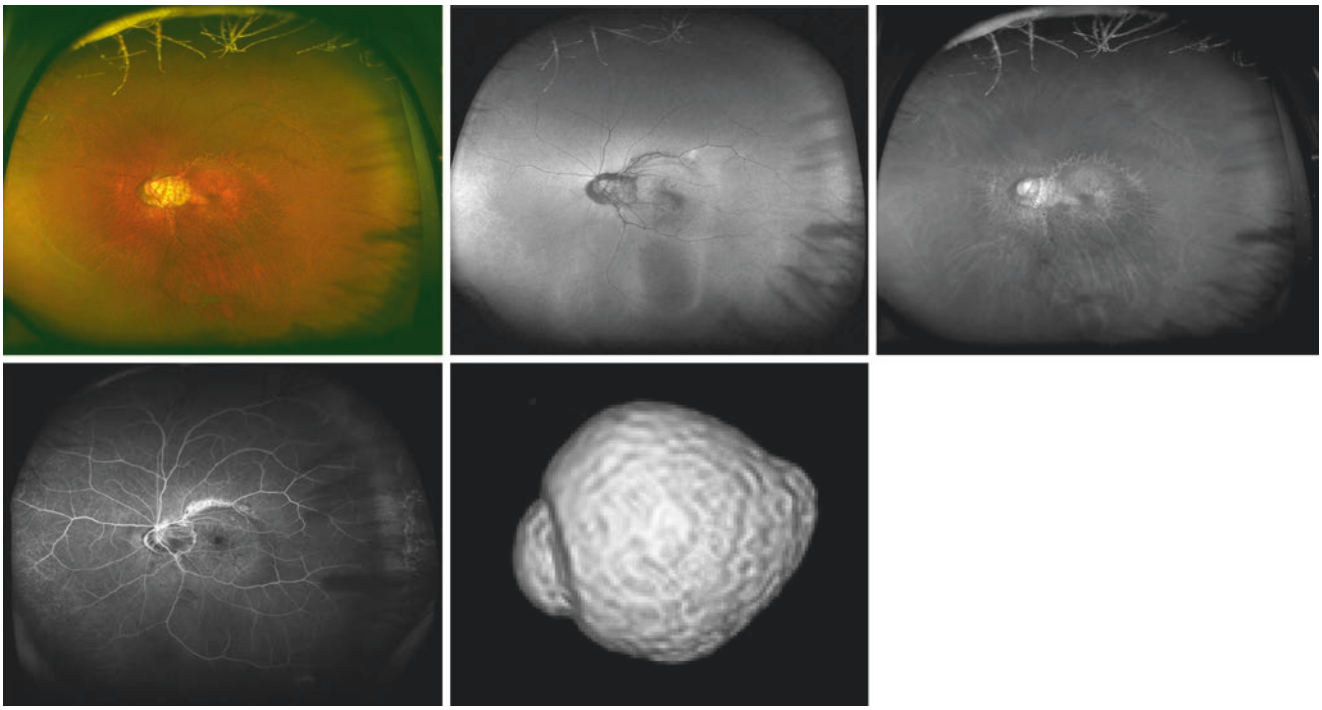

Fig. 6.2 Narrow macular staphyloma in the left fundus of a 64-year-old woman with an axial length of 30.2 mm. (Top left) Pseudo-color fundus image shows slight depigmentation along the upper and nasal border of the staphyloma. (Top middle) Fundus autofluorescence image shows slight hypo-autofluorescence along the upper edge of the staphyloma. (Top right) Red-free fundus image shows a slight hyper-reflectance along the upper margin of staphyloma. (Bottom left) Fluorescein angiographic image shows granular hyper-fluorescence along the upper staphyloma border. (Bottom right) Three-dimensional magnetic resonance imaging (3D MRI) of the left eye viewed from the side shows the posterior pole of the eye is pointed and the eye shows a cylinder shape

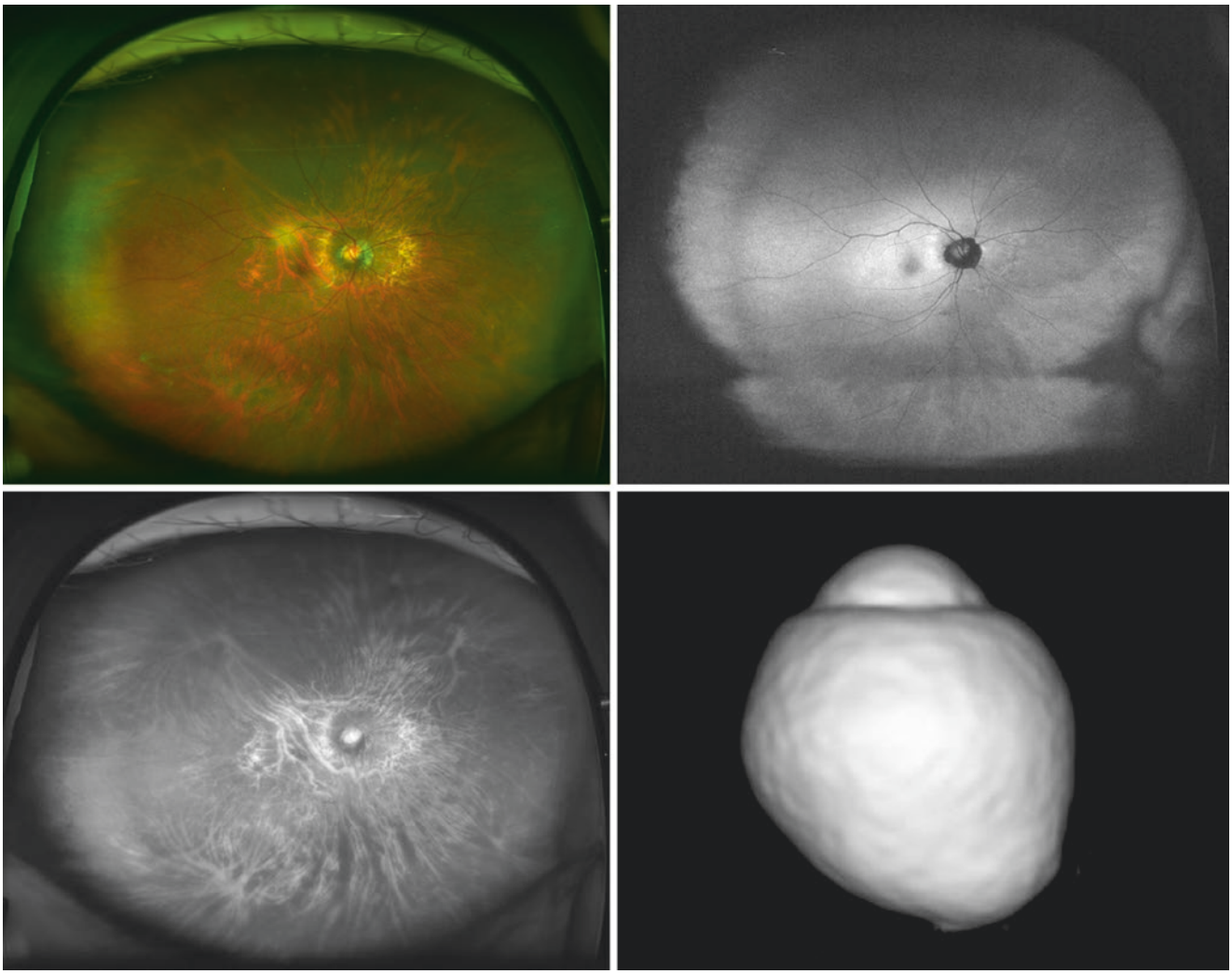

Fig. 6.3 Peripapillary staphyloma in the right fundus of a 67-year-old woman with an axial length of 26.9 mm. (Top left) Pseudo-color fundus photo shows yellowish depigmentation along the margin of peripapillary staphyloma. (Top right) Fundus autofluorescence image shows slight hyper-fluorescence along the temporal margin of the staphyloma and hypo-fluorescence along the nasal margin of the staphyloma. (Bottom left) Red-free fundus image shows a slight hyper-reflectance along the staphyloma border. (Bottom right) Three-dimensional magnetic resonance imaging (3D MRI) of the right eye viewed from the inferior shows the nasally distorted shape of the eye

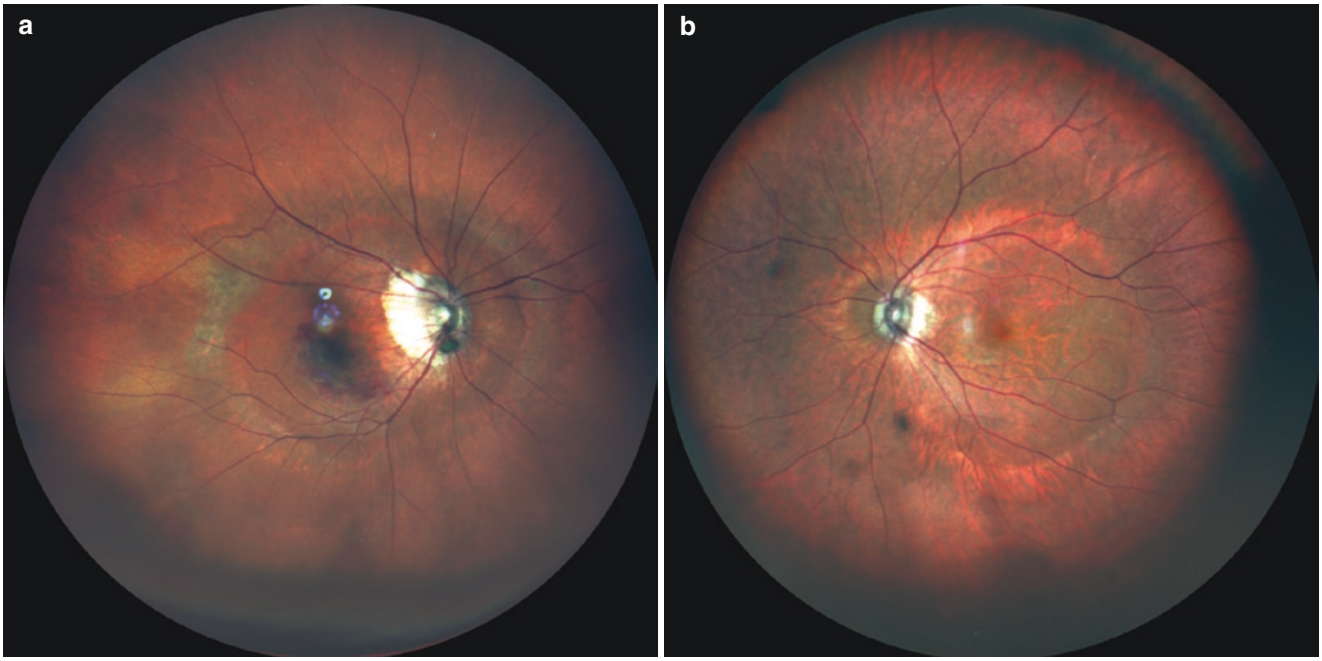

Fig. 6.4 Real color wide-field fundus image of posterior staphylomas obtained with Mirante (Nidek, Japan). (Left). Right fundus of a 67-year-old woman with an axial length of 27.3 mm shows wide macular staphyloma with depigmented staphyloma border. (Right) Left fundus of a 79-year-old woman with an axial length of 26.2 mm shows wide macular staphyloma with depigmented staphyloma border. Scleral ridge is seen temporal to the optic disc

References

1. Ohno-Matsui K. Proposed classification of posterior staphylomas based on analyses of eye shape by three-dimensional magnetic resonance imaging. Ophthalmology. 2014;121(9):1798–809.
2. Ohno-Matsui K, Alkabes M, Salinas C, et al. Features of posterior staphylomas analyzed in wide-field fundus images in patients with unilateral and bilateral pathologic myopia. Retina. 2017;37(3):477–86.
3. Ohno-Matsui K, Jonas JB. Posterior staphyloma in pathologic myopia. Prog Retin Eye Res. 2019;70:99–109.

Multimodal Imaging of Posterior Staphyloma

7

Muka Moriyama

Abstract

Recently, many different methods have been used to visualize posterior staphyloma. Each method has its strengths and limitations, thus, multimodal imaging is considered to be useful for visualizing many features of staphyloma.

Keywords

Staphyloma · 3D MRI · Wide-field OCT · Multimodal imaging

7.1 Wide Macular Staphyloma (Fig. 7.1)

Wide macular staphyloma is the most common type of staphylomas. It is usually horizontally long. Nasal margin of the staphyloma is away from the optic disc, and thus acquired megalodisc is often seen (Fig. 7.1a). The margin of the staphylomas shows pigmentary alterations, which is obvious in infrared images. Ultra-wide field OCT (UWF-OCT) shows the changes of scleral curvature along with the gradual choroidal thinning toward the staphyloma edges (Fig. 7.1c). The entire shape of the staphyloma is clearly imaged by 3D MRI. The image viewed from inferiorly clearly shows the degree of staphyloma (Fig. 7.1d), and the image viewed from the back clearly shows the area of staphyloma (Fig. 7.1e). Generally, wide staphylomas tend to be deep, whereas narrow staphylomas tend to be shallow.

7.2 Narrow Macular Staphyloma (Fig. 7.2)

In narrow macular staphyloma, nasal margin of staphylomas is close to the optic disc (Fig. 7.2a). Thus, the optic disc is usually tilted accompanying with temporal conus. Margin of staphyloma shows pigmentary alterations (Fig. 7.2a and b); however, pigmentary changes tend to be less obvious than those of wide macular staphylomas. UWF-OCT shows narrow staphyloma (Fig. 7.2c) with OCT features typical of staphyloma edges which are also seen in wide staphylomas. 3D MRI shows pointed shape of staphyloma (Fig. 7.2d and e).

7.3 Nasal Staphyloma (Fig. 7.3)

In nasal staphyloma, wide-field fundus image shows an ectasia of the nasal fundus (Fig. 7.3a). The optic disc is tilted nasally with the nasal conus. Diffuse choroidal atrophy is seen in the nasal fundus. The area of nasal diffuse atrophy shows an increased brightness in infrared image (Fig. 7.3b). UWF-OCT shows an incline of scleral curvature toward the optic nerve (Fig. 7.3c). Choroidal thickness changes toward staphyloma edges are not so obvious. 3D MRI viewed from inferiorly shows a nasally distorted shape of the eye (Fig. 7.3d). Scleral curvature changes at the border of nasal staphyloma are usually mild.

M. Moriyama (✉)
Ophthalmology and Visual Science Tokyo Medical and Dental University, Tokyo, Japan

K. Ohno-Matsui (ed.), *Atlas of Pathologic Myopia*, https://doi.org/10.1007/978-981-15-4261-9_7

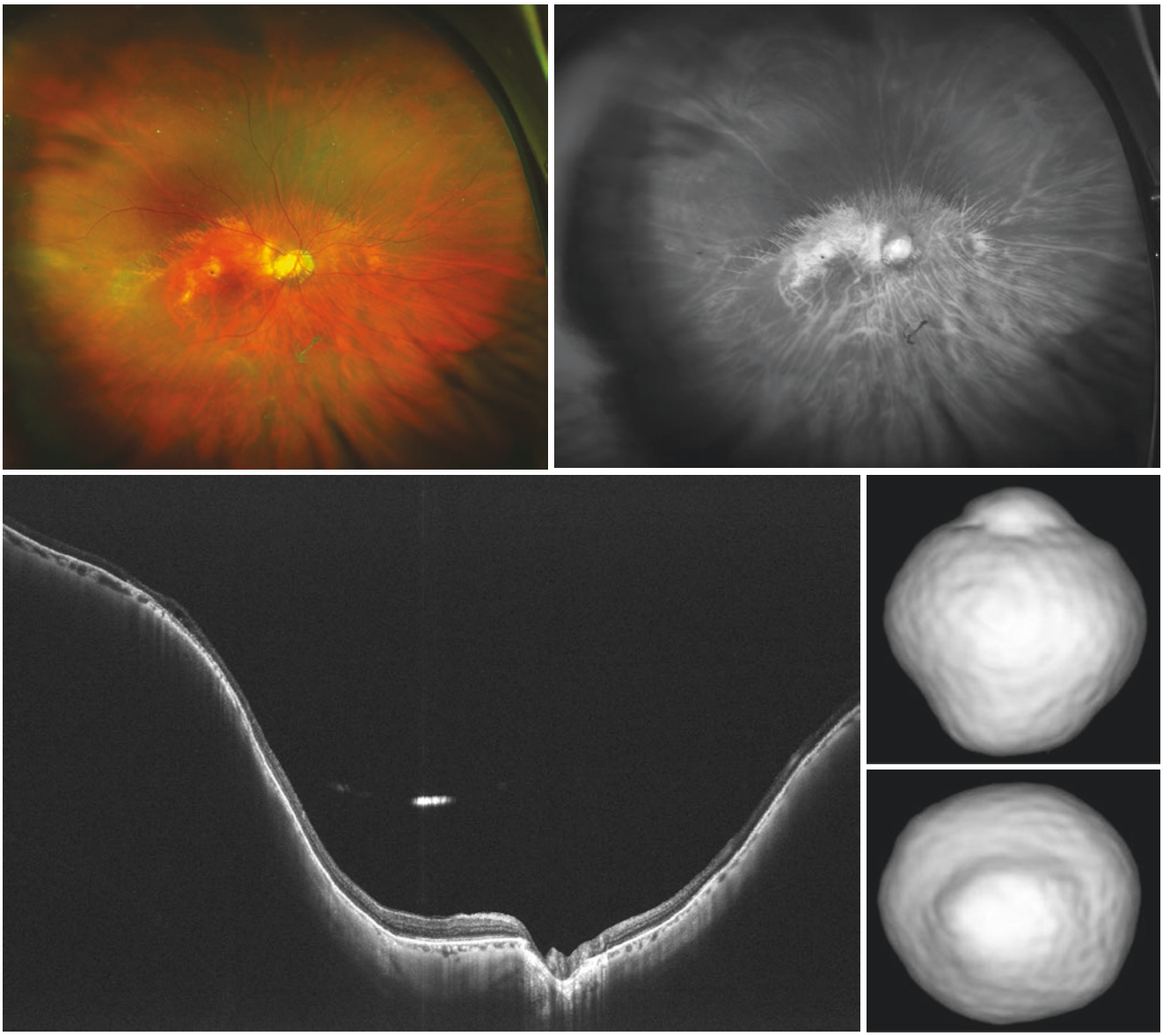

Fig. 7.1 Multimodal imaging of wide macular staphyloma in the right eye of a 73-year-old woman with an axial length of 27.3 mm (equivalent to Curtin's type I). Top Left: Wide-field fundus image shows horizontally long, wide macular staphyloma. The upper edge of the staphyloma shows pigmentary alterations. Top Right: Infrared image shows a pigmentary alteration along the upper edge of staphyloma. Bottom Left: Ultra wide-field OCT shows a posterior outpouching of the sclera in the staphylomatous area. Gradual choroidal thinning toward the staphyloma edge is clearly seen. Scleral inward protrusion is also seen at the staphyloma edge. Bottom Right: 3D MRI images of the eye. In the image viewed from inferior (upper image) as well as from the back (lower image) show a posterior outpouching of staphylomatous area

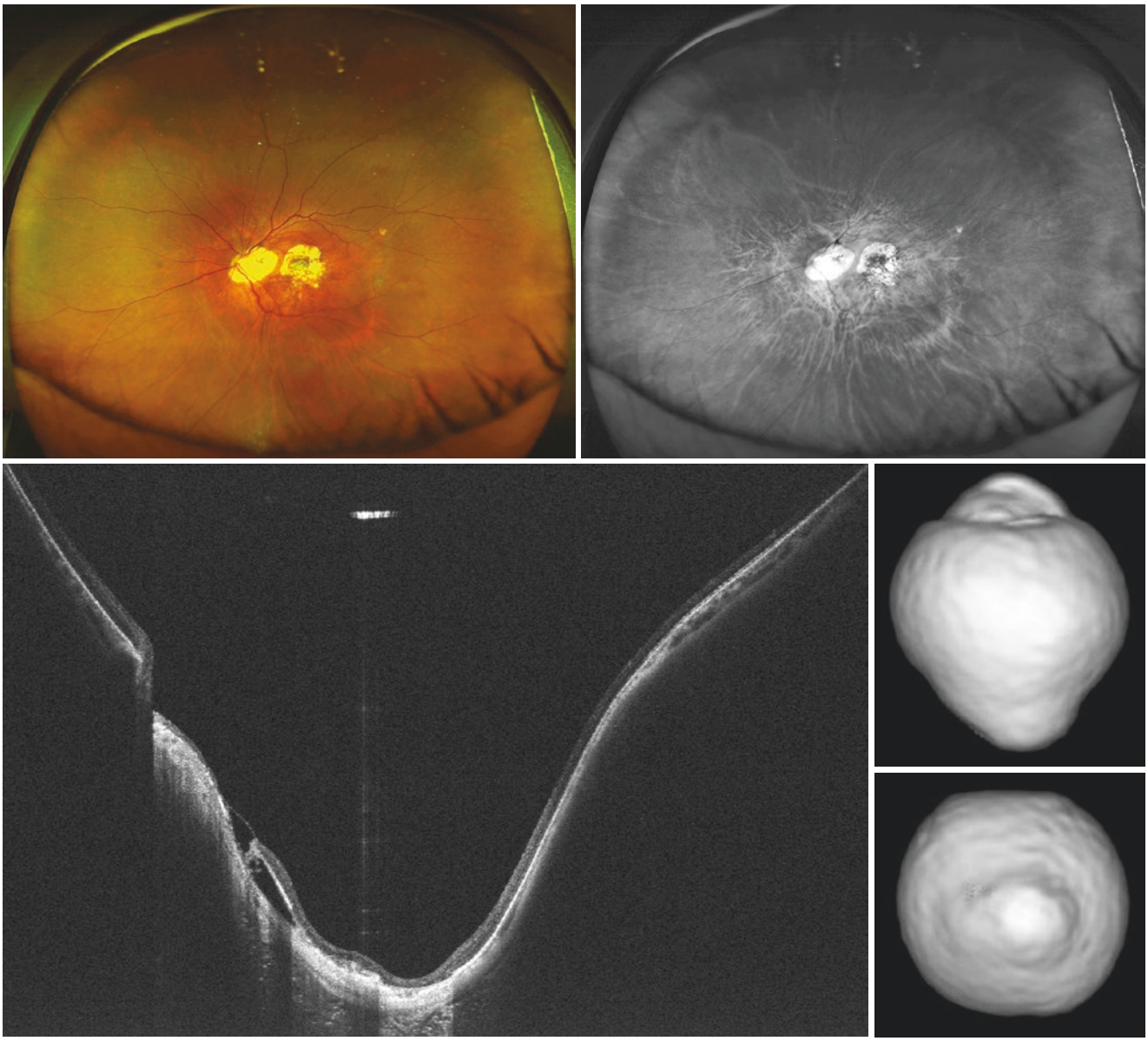

Fig. 7.2 Multimodal imaging of narrow macular staphyloma in the left eye of a 68-year-old man with an axial length of 28.1 mm (equivalent to Curtin's type II). Top Left: Wide-field fundus image shows narrow macular staphyloma. Different from wide staphylomas, the nasal margin of staphyloma is not far from the nasal edge of the optic disc. Staphyloma edges show mild pigmentary alterations. Top Right: Infrared image shows a pigmentary alteration along the edge of staphyloma. Bottom Left: Ultra-wide field OCT shows a posterior outpouching of the sclera in the staphylomatous area. Gradual choroidal thinning toward the staphyloma edge is clearly seen. Scleral inward protrusion is also seen at the staphyloma edge. Peripapillary intrachoroidal cavitation is seen. Bottom Right: 3D MRI images of the eye. In the image viewed from inferior (upper image) as well as from the back (lower image) show a posterior outpouching of a relative small area of the posterior segment

Fig. 7.3 Multimodal imaging of a nasal staphyloma in the left eye of a 70-year-old woman with an axial length of 28.5 mm (equivalent to Curtin's type IV). Top Left: Wide-field fundus image shows nasal staphyloma. The optic disc is tilted nasally and diffuse choroidal atrophy is seen in the nasal fundus. Top Right: Infrared image shows an increased reflectance in the area of nasal staphyloma. Bottom Left: Ultra wide-field OCT shows a gradual incline of scleral curvature toward the optic nerve. Bottom Right: 3D MRI of the left eye viewed from the inferior shows the nasally distorted shape of the eye

7.4 Inferior Staphyloma (Fig. 7.4)

In inferior staphyloma, wide-field fundus image shows an ectasia of the inferior fundus (Fig. 7.4a). The upper margin of inferior staphyloma shows pigmentary alterations (Fig. 7.4a and b). The optic disc is vertically tilted; however, some cases have inferior staphyloma without optic disc changes. Because the macula is often outside or along the margin of staphylomas, the axial length is not always long. In some eyes with unilateral high myopia, fellow eyes without high myopia often show this type of staphyloma. UWF-OCT and 3D MRI clearly show the protrusion of inferior segment of the eye (Fig. 7.4c and d).

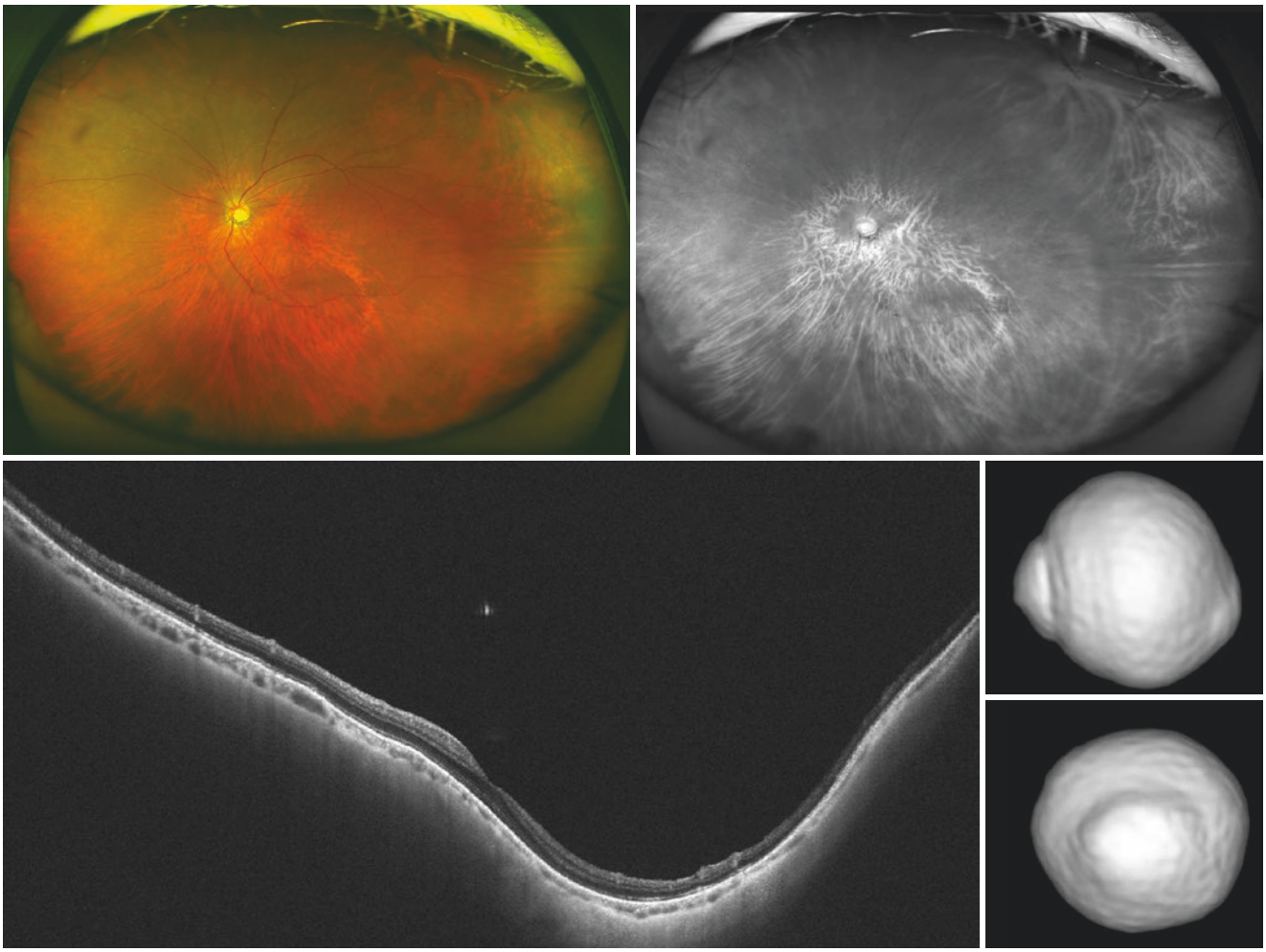

Fig. 7.4 Multimodal imaging of an inferior staphyloma in the left eye of a 74-year-old man with an axial length of 24.7 mm (equivalent to Curtin's type V). Top Left: Wide-field fundus image shows an inferior staphyloma. The upper margin of inferior staphyloma is slightly depigmented. Top Right: Infrared image shows an increased reflectance in the area and along the margin of inferior staphyloma. Bottom Left: A vertical section of ultra-wide field OCT shows a posterior outpouching of inferior fundus. Bottom Right: 3D MRI viewed from the side (upper image) shows an outpouching of the inferior segment of the eye. Inferior staphyloma is also seen in the image from the back (lower image)

Part IV

Myopic Maculopathy

Peripapillary Diffuse Atrophy (PDCA)

8

Tae Igarashi-Yokoi

Abstract

Diffuse choroidal atrophy first appears around the optic disc. In a recent longitudinal study, among 35 eyes of adult patients with signs of myopic maculopathy, 83% showed a peripapillary diffuse choroidal atrophy (PDCA) already in childhood. This study suggested that the presence of PDCA in children with high axial myopia might be an indicator of eventual pathologic myopia in adulthood. According to the study using swept-source OCT on children with PDCA, the segmental and abrupt thinning of the choroid in the temporal parapapillary region is characteristic to PDCA. The study also showed that a choroidal thickness measurement with cut-off value of <60 μm at 2500 μm nasal to the fovea can be used to detect children with PDCA with a 75.6% sensitivity and 100% specificity.

Keywords

Pathologic myopia · Myopic maculopathy · Peripapillary diffuse choroidal atrophy · Choroidal thickness

8.1 Peripapillary Diffuse Choroidal Atrophy (Category 2)

Generally, the area of diffuse choroidal atrophy first appears around the optic disc, as peripapillary diffuse chorioretinal atrophy (PDCA). In a recent longitudinal study [1], 35 eyes of 19 adult patients with signs of severe myopic maculopathy (mean age; 37.0 ± 5.1 years (range, 33-42 years) and mean axial length; 27.8 ± 1.2 mm (range, 25.5-29.7 mm)) were retrospectively analyzed. The results showed that 29 of the 35 eyes (83%) showed a PDCA at the initial visit (age 10.5 ± 2.6 years; range, 5-15 years. In those cases, PDCA was confined to the area temporal to the optic nerve head outside of the parapapillary alpha, beta, gamma, or delta zones (Figs. 8.1 and 8.2). This study suggested that the presence of PDCA in children with high axial myopia might be an important biomarker for eventual pathologic myopia in adulthood.

The following study investigating morphologic features of PDCA in children using swept-source OCT [2] revealed a profound segmental and abrupt thinning of the choroid in the temporal parapapillary region. The parapapillary segmental thinning of the choroid with an abrupt border in direction to the slightly thicker macular choroid was an OCT feature of PDCA (Figs. 8.3 and 8.4). Using a choroidal thickness cut-off value of <60 μm at 2500 μm nasal to the central fovea, 31 of the 41 eyes (76%) with PDCA and none of the eyes in the control group comprised of participants of the population-based Gobi Desert Children Eye Study (0/1463)-except for one child with PDCA-were positive for this sign. The study proposed a potentially useful cut-off value of choroidal thickness at a distance of 2500 μm nasal to the foveola may be the value of <60 μm, which may be helpful for the detection and diagnosis of PDCA in myopic children.

T. Igarashi-Yokoi (✉)
Department of Ophthalmology and Visual Science, Tokyo Medical and Dental University, Tokyo, Japan

K. Ohno-Matsui (ed.), *Atlas of Pathologic Myopia*, https://doi.org/10.1007/978-981-15-4261-9_8

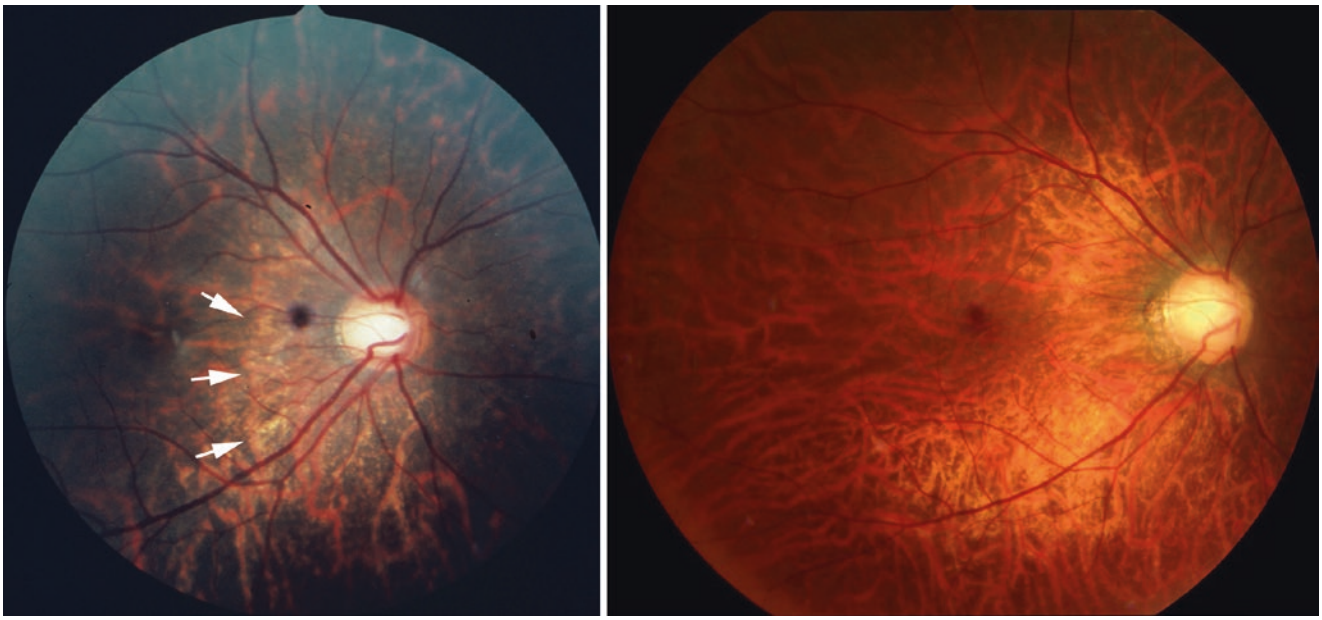

Fig. 8.1 Peripapillary diffuse choroidal atrophy (PDCA) seen in children who eventually develop severe myopic atrophy in adulthood (Reproduced with permission from [1]). (Left) Right fundus of a 12-year-old boy with a refractive error of -13.0 diopters (D) and axial length is 28.4 mm shows PDCA temporal to the optic disc. (Right) When the patient is 41-years old, diffuse atrophy has enlarged beyond the macular area (especially in the inferior fundus) and has become macular diffuse choroidal atrophy (MDCA). Refractive error has increased to -20.0 D and axial length has increased to 30.6 mm

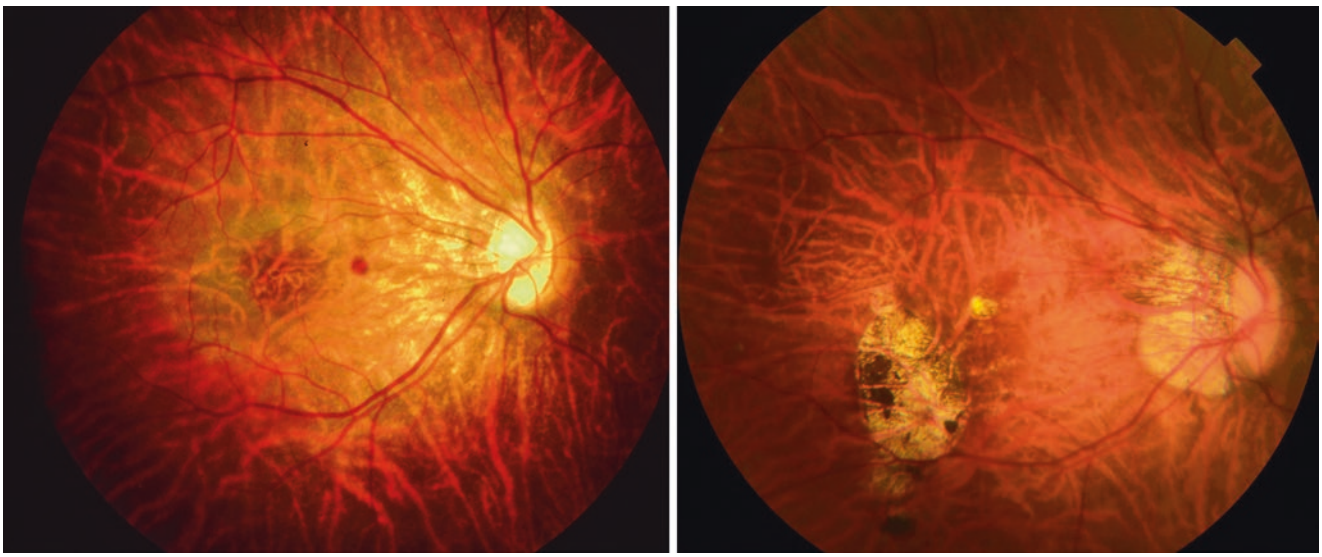

Fig. 8.2 Peripapillary diffuse choroidal atrophy (PDCA) seen in children who eventually develop severe myopic atrophy in adulthood (Reproduced with permission from [1]). (Left) Right fundus of a 11-year-old girl with a refractive error of -18.0 diopters (D) and an axial length of 27.2 mm shows PDCA temporal to the optic disc. (Right) When the patient is 41 years-old, diffuse atrophy has enlarged to cover the entire posterior fundus. Patchy atrophy is also seen temporal to the macula. Refractive error has increased to -20.5 D and an axial length has increased to 32.3 mm

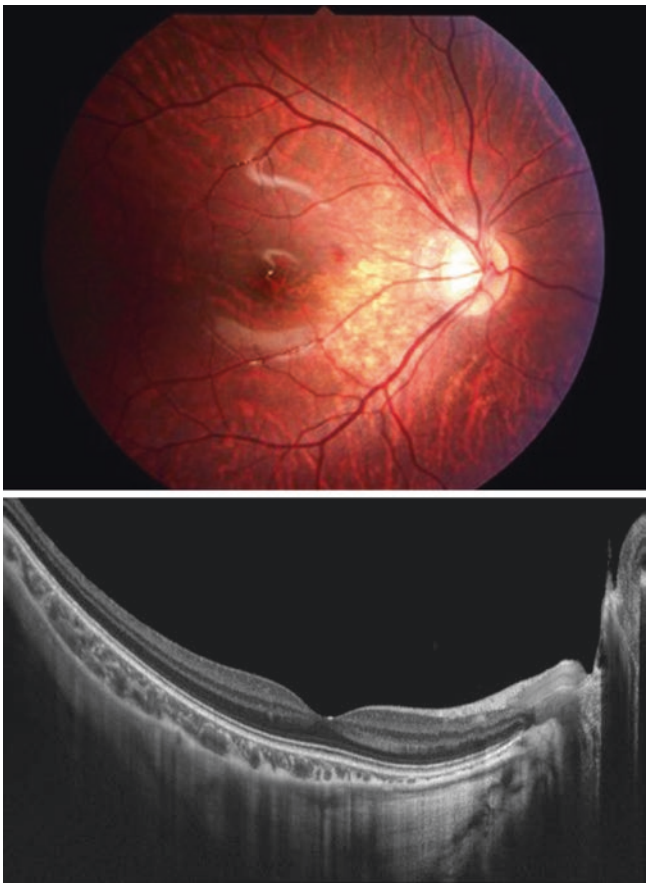

Fig. 8.3 Extreme and sudden thinning of the peripapillary choroid in a child with peripapillary diffuse choroidal atrophy (PDCA) (Reproduced with permission from [2]). (Top) Right fundus of an 11-year-old girl with refractive error of -11.0 D (spherical equivalent) and with axial length of 27.8 mm shows yellowish PDCA temporal to the gamma zone. (Bottom) A horizontal section of OCT shows extreme thinning of the choroid temporal to the optic nerve. Almost the entire thickness of the choroid has disappeared in the area of PDCA nasal to the central fovea, although the choroid seems to maintain its thickness temporal to the fovea. The transition from relatively normal choroid around the fovea to almost absent choroid in the area of PDCA is sudden

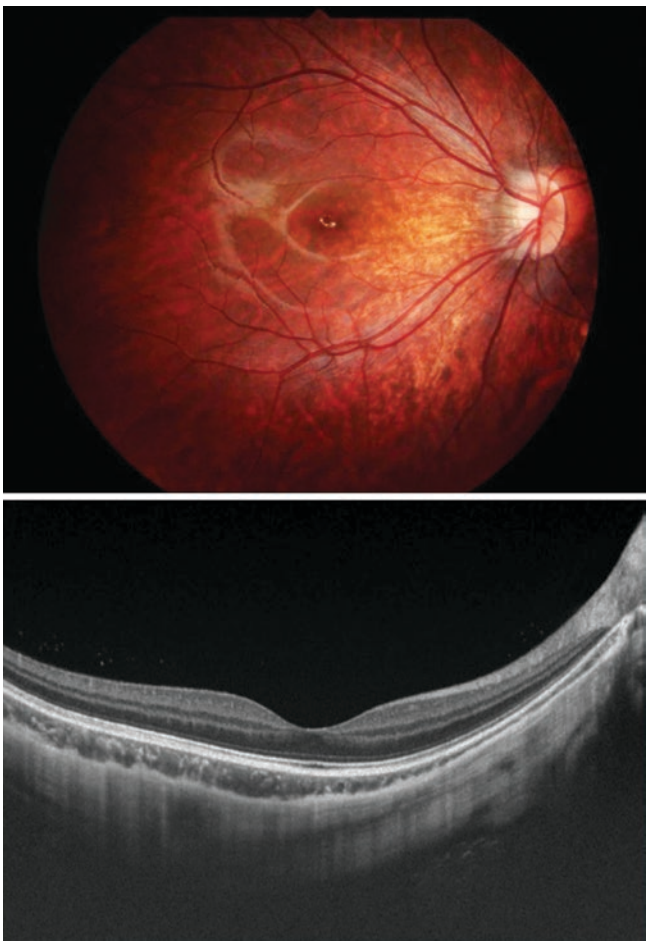

Fig. 8.4 Extreme and sudden thinning of the peripapillary choroid in a child with peripapillary diffuse choroidal atrophy (PDCA) (Reproduced with permission from [2]). (Top) Right fundus of a 9-year-old girl with refractive error of -10.25 D (spherical equivalent) and with an axial length of 26.4 mm shows yellowish PDCA temporal to the gamma zone. (Bottom) A horizontal section of OCT shows extreme thinning of the choroid in the area of PDCA. Almost the entire thickness of the choroid has disappeared in the area of PDCA nasal to the central fovea, although the subfoveal choroid seems to maintain its thickness. The transition from relatively normal choroid around the fovea to almost absent choroid in the area of PDCA is relatively sudden

References

1. Yokoi T, Jonas JB, Shimada N, Nagaoka N, Moriyama M, Yoshida T. Peripapillary diffuse Chorioretinal atrophy in children as a sign of eventual pathologic myopia in adults. Ophthalmology. 2016;123:1783–7.

2. Yokoi T, Zhu D, Bi HS, Jonas JB, Jonas RA, Nagaoka N. Parapapillary Diffuse Choroidal Atrophy in Children Is Associated With Extreme Thinning of Parapapillary Choroid. IOVS. 2017;58(2):901–6.

Macular Diffuse Choroidal Atrophy

9

Yuxin Fang

Abstract

Diffuse choroidal atrophy is observed as an ill-defined yellowish lesion in the posterior fundus. Diffuse atrophy starts from the peripapillary region and eventually extends to the macula. OCT shows a marked thinning of the choroid in the area of diffuse atrophy. In some cases, almost the entire choroid is lost leaving sporadically remaining large choroidal vessels.

Keywords

Diffuse choroidal atrophy · Peripapillary diffuse choroidal atrophy · Macular diffuse choroidal atrophy · Choroidal thinning · Choriocapillaris

Diffuse choroidal atrophy is observed as an ill-defined yellowish lesion in the posterior fundus (Fig. 9.1). Diffuse atrophy primarily occurs in the peripapillary region as "peripapillary diffuse choroidal atrophy (PDCA)" and eventually extends to the macula as "macular diffuse choroidal atrophy (MDCA)" [1–3]. MDCA is uncommon below the age 40 or axial length shorter than 27 mm [4]. Diffuse atrophy is not uniformly yellow but shows granular yellowish appearance. However, the fundus color may look different according to the degree of fundus pigmentation among races (Fig. 9.2). Thus, the diagnosis of diffuse atrophy solely depending on fundus photos tends to be tricky especially in less pigmented eyes, and OCT-based diagnosis is recommended.

OCT shows a marked thinning of the choroid in the area of diffuse atrophy (Figs. 9.3 and 9.4). The subfoveal choroidal thickness in eyes with MDCA is usually below 100 μm and the mean choroidal thickness is 50 μm based on a clinic-based study [4]. In most cases, the choroid is almost absent except for sporadically remaining large choroidal vessels. Large choroidal blood vessel can be observed to protrude to ward the retina [5]. However, even in the area where most of the choroidal layer is absent, can be as thin as 12 micron or so, the RPE layer and outer retina are present by OCT (Fig. 9.4). It might explain a relatively preserved vision in eyes with diffuse atrophy. Such disproportionate thinning of the choroid compared to the surrounding tissue (retina and sclera) might be a key phenomenon in diffuse atrophy.

OCT angiography (OCTA) can detect choriocapillaris flow impairment, even though the visualization of the choroidal circulation remains a challenge in eyes with pathologic myopia. The OCTA in eyes with diffuse atrophy shows the low-density choriocapillaris, while medium and large sized choroidal vessels remained (Fig. 9.3) [6, 7].

Y. Fang (✉)
Department of Ophthalmology and Visual Science, Tokyo Medical and Dental University, Tokyo, Japan

K. Ohno-Matsui (ed.), *Atlas of Pathologic Myopia*, https://doi.org/10.1007/978-981-15-4261-9_9

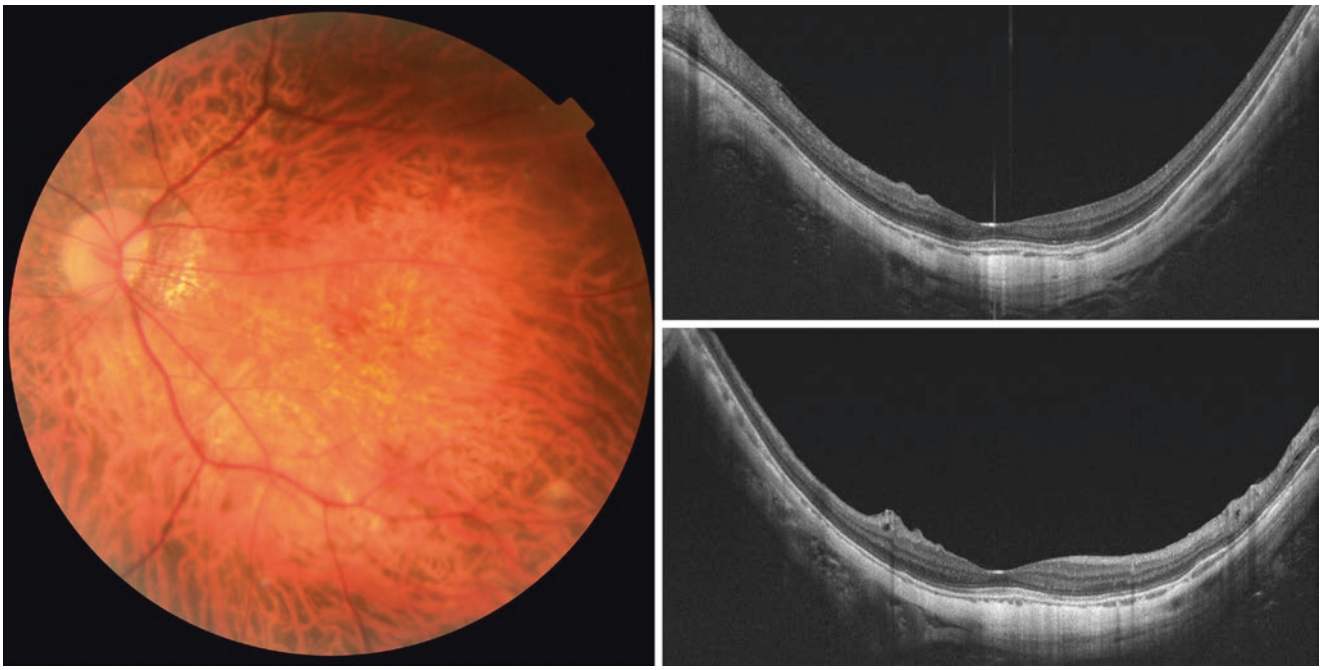

Fig. 9.1 Macular diffuse choroidal atrophy (MDCA) in an Asian patient. (Left) Left fundus of a 47-year-old woman with an axial length of 31.3 mm and with the best-corrected visual acuity (BCVA) of 1.0 shows granular yellowish, ill-defined MDCA covering almost the entire macular area. (Right) OCT images in a horizontal section (upper image) as well as in a vertical section (lower image) show that most of the choroid is absent and only large choroidal vessels are sporadically present. Subfoveal choroidal thickness is 40 μm

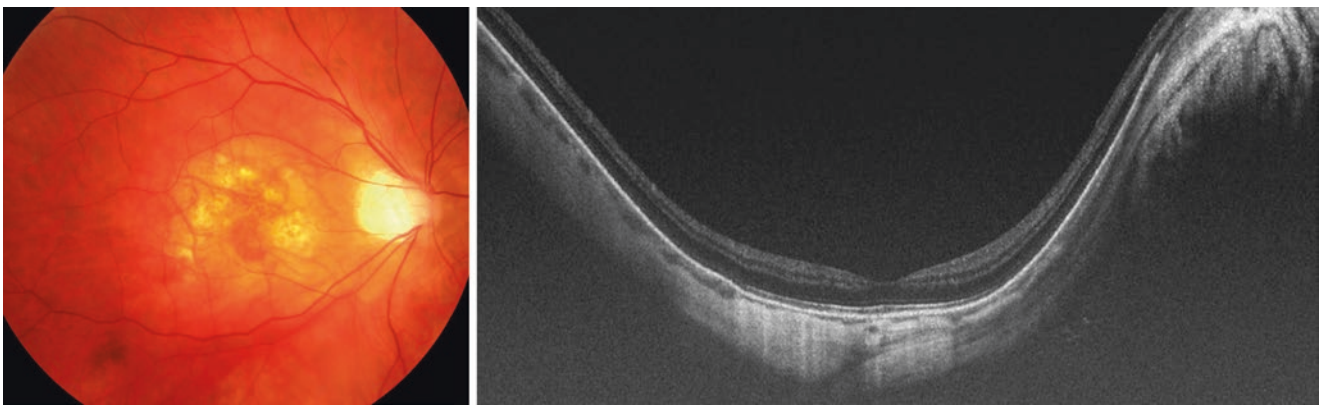

Fig. 9.2 Macular diffuse choroidal atrophy (MDCA) in a Caucasian patient. (Left) Right fundus of a 65-year-old Caucasian man with an axial length of 30.0 mm and with the best-corrected visual acuity (BCVA) of 1.0 shows MDCA. Lacquer cracks are also seen. (Right) A horizontal OCT section shows that the choroid is very thin and the subfoveal choroidal thickness is 25 μm

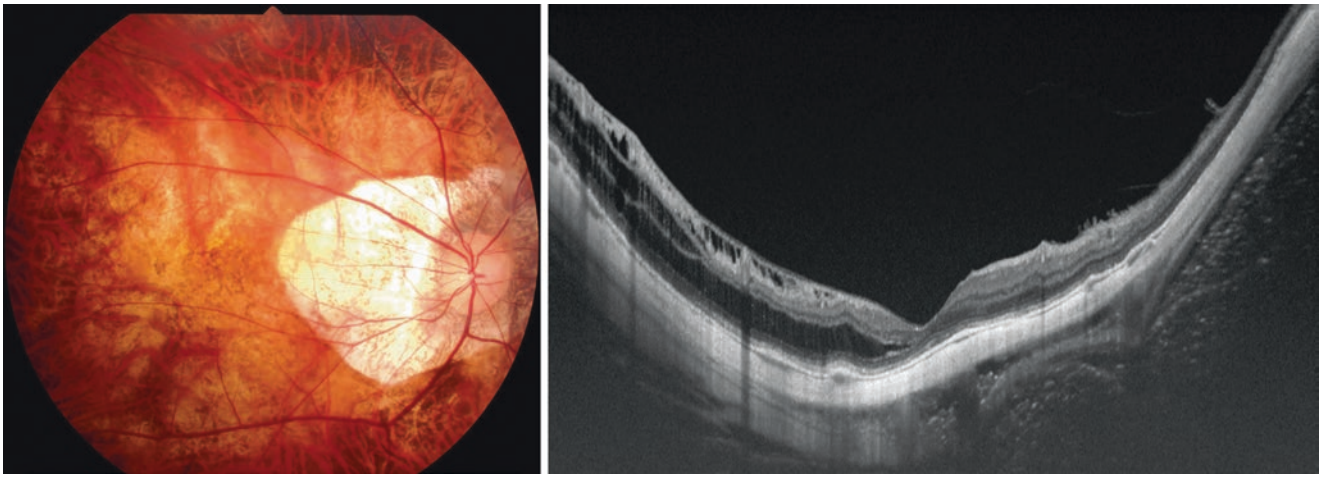

Fig. 9.3 Extremely thin choroid in a case with macular diffuse choroidal atrophy (MDCA). (Left) Right fundus of a 70-year-old woman with an axial length of 30.2 mm shows MDCA. (Right) Vertical OCT section shows that most of the choroid is absent and subfoveal choroidal thickness is as thin as 12 μm. However, the best-corrected visual acuity (BCVA) still maintains 1.5. OCT also shows myopic retinoschisis with an epiretinal membrane superior to fovea. The inferior sclera is also very thin and the orbital fat is clearly seen

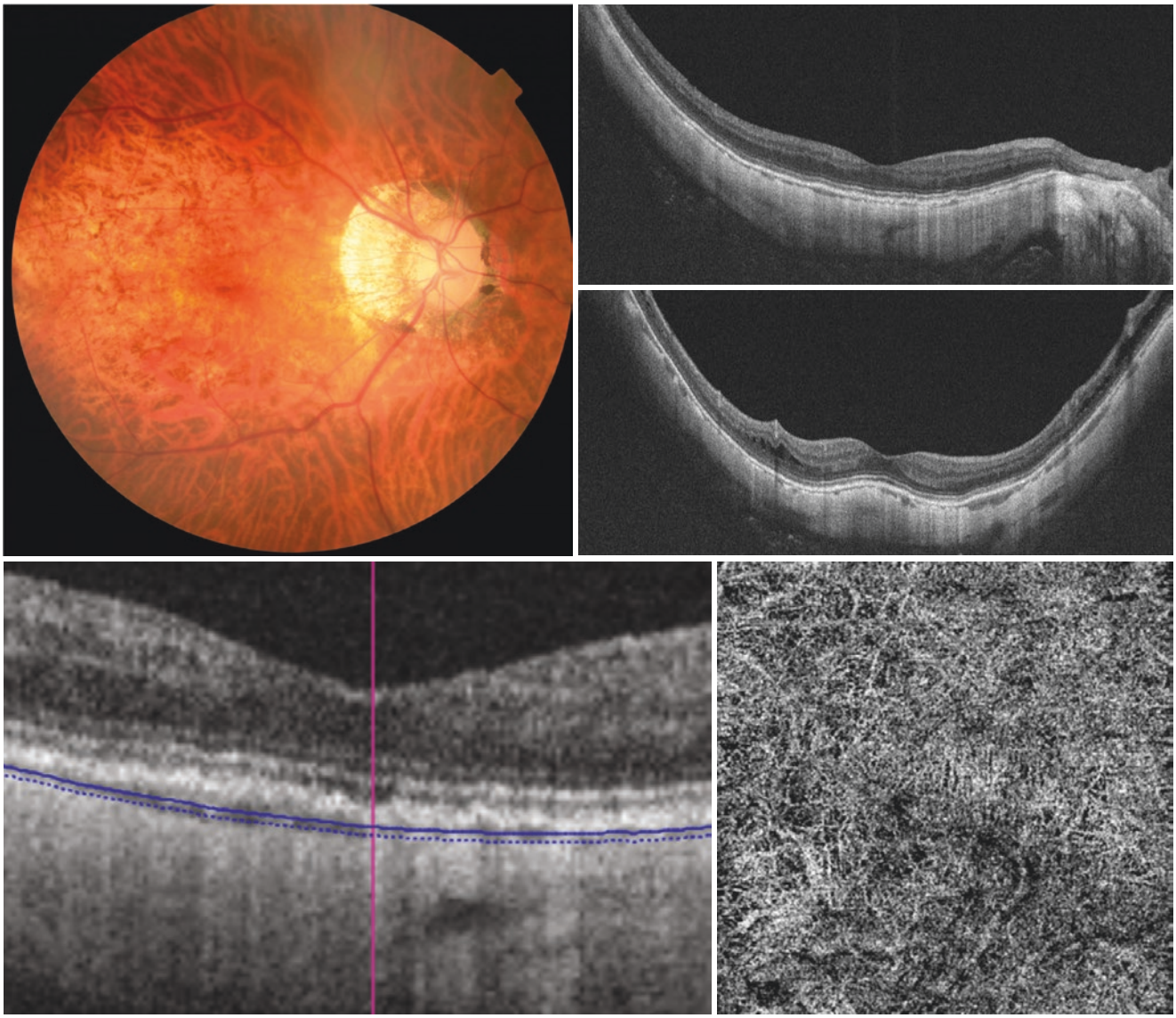

Fig. 9.4 Choroidal thinning and focal areas of choriocapillaris signal voids in a case with macular diffuse choroidal atrophy (MDCA). (Left) Right fundus of a 65-year-old man with an axial length of 30.3 mm and with the best-corrected visual acuity (BCVA) of 1.5 shows typical yellowish, ill-defined MDCA covering the entire macular area. (Right Top and Right Middle) OCT images show that the choroid is extremely thin in the area of MDCA and the subfoveal choroidal thickness is 30 μm. The entire thickness of the sclera is clearly visible. Vertical OCT image (Right, middle) also shows the inward bulge of the macular area, diagnosed as "dome-shaped macula." (Right bottom) OCT angiography shows the focal area of choriocapillaris signal voids with unmasking of the medium and large choroidal vessels seen as bright flow signals

References

1. Tokoro T. Types of fundus changes in the posterior pole. Atlas of posterior fundus changes in pathologic myopia. Tokyo: Springer; 1998. p. 5–22.
2. Hayashi K, Ohno-Matsui K, Shimada N, Moriyama M, Kojima A, Hayashi W, et al. Long-term pattern of progression of myopic maculopathy: a natural history study. Ophthalmology. 2010;117(8):1595–611.
3. Fang Y, Yokoi T, Nagaoka N, Shinohara K, Onishi Y, Ishida T, et al. Progression of myopic maculopathy during 18-year follow-up. Ophthalmology. 2018;125(6):863–77.
4. Fang Y, Du R, Nagaoka N, Yokoi T, Shinohara K, Xu X, et al. OCT-based diagnostic criteria for different stages of myopic maculopathy. Ophthalmology. 2019;126(7):1018–32.
5. Marchese A, Carnevali A, Sacconi R, Centoducati T, Querques L, Bandello F, et al. Retinal pigment epithelium humps in high myopia. Am J Ophthalmol. 2017;182:56–61.
6. Sayanagi K, Ikuno Y, Uematsu S, Nishida K. Features of the choriocapillaris in myopic maculopathy identified by optical coherence tomography angiography. Br J Ophthalmol. 2017;101(11):1524–9.
7. Wong CW, Teo YCK, Tsai STA, Ting SWD, Yeo YSI, Wong WKD, et al. Characterization of the choroidal vasculature in myopic maculopathy with optical coherence tomographic angiography. Retina (Philadelphia, Pa). 2018;

Patchy Choroidal Atrophy

10

Ran Du and Shiqi Xie

Abstract

Patchy choroidal atrophy is observed as a grayish-white and sharply margined atrophy in the posterior fundus. The shape of patchy atrophy is longitudinally oval, or round, or irregular when multiple lesions merge. Patchy atrophy can derive from lacquer cracks or diffuse atrophy. It rarely affects the central fovea. Fundus autofluorescence shows uniform hypo-autofluorescence in the area of patchy atrophy. OCT images show a loss of retinal pigment epithelium, with or without a Bruch's membrane defect.

Keywords

Patchy choroidal atrophy · Bruch's membrane · Retinal pigment epithelium

Patchy choroidal atrophy (known as Category 3 in META-PM classification [1]), is a grayish-white and well-margined atrophy in the posterior fundus [2]. It can derive from lacquer cracks or develop in the area of background diffuse atrophy. Patchy atrophy is longitudinally oval when it originates from lacquer cracks, or round when it originates from diffuse atrophy, or has an irregular shape when multiple lesions are merged.

Although patchy atrophy is seen in the posterior fundus [3–6], it rarely involves the central fovea itself. This location is different from CNV-related macular atrophy, which is almost always fovea-centered. As pathologic myopia progresses, multiple small patchy lesions enlarge and merge together or fuse with parapapillary atrophy. Some lesions of patchy atrophy occur in the mid-periphery [6]. In some rare cases, a very large merged lesion may finally cover almost the entire posterior pole and shows a "bare sclera" appearance.

Patchy atrophy shows a clear hypo-autofluorescence in fundus autofluorescence images (Fig. 10.1). In fluorescein angiogram (FA), patchy atrophy shows a hypo-fluorescence due to the choroidal filling defects in the early phase, and the edges show gradual hyper-fluorescence in the late phase (Fig. 10.2). In ICG angiogram, patchy atrophy shows hypo-fluorescence in the late phase. Intrascleral and retrobulbar blood vessels can be seen through the atrophic area. In OCT images, patchy atrophy is observed as a loss of retinal pigment epithelium, with or without a Bruch's membrane defect [6]. Following the loss of retinal pigment epithelium and Bruch's membrane, the choroid and the outer retina disappear and the inner retina directly sits on the sclera (Fig. 10.3). Pigmentation is often observed especially in and along large patchy atrophies. Perforating scleral vessels are sometimes detected within the atrophic area (Fig. 10.4) [7]. In that case, scleral pits are observed at the emissary of scleral perforating vessels.

R. Du (✉) · S. Xie
Department of Ophthalmology & Visual Science,
Tokyo Medical and Dental University, Tokyo, Japan

K. Ohno-Matsui (ed.), *Atlas of Pathologic Myopia*, https://doi.org/10.1007/978-981-15-4261-9_10

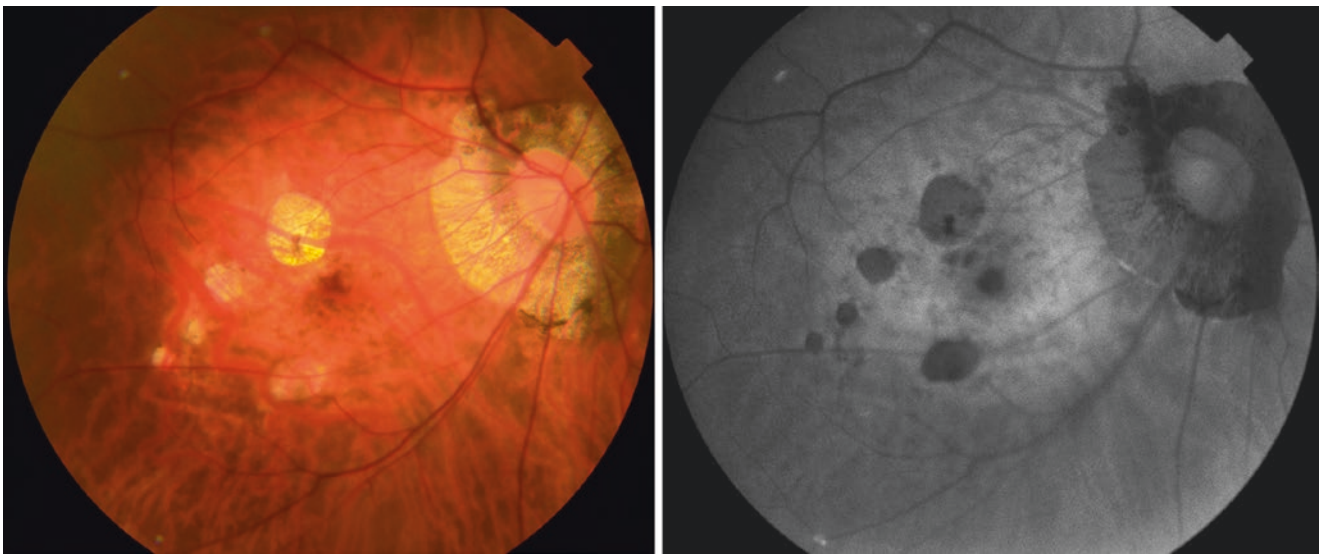

Fig. 10.1 Multiple lesions of patchy atrophy in the posterior fundus. (Left) Right fundus of a 57-year-old woman with axial length of 32.3 mm shows multiple lesions of patchy atrophy within the area of diffuse atrophy. (Right) Patchy atrophy is observed as uniform hypo-fluorescence in fundus autofluorescence image

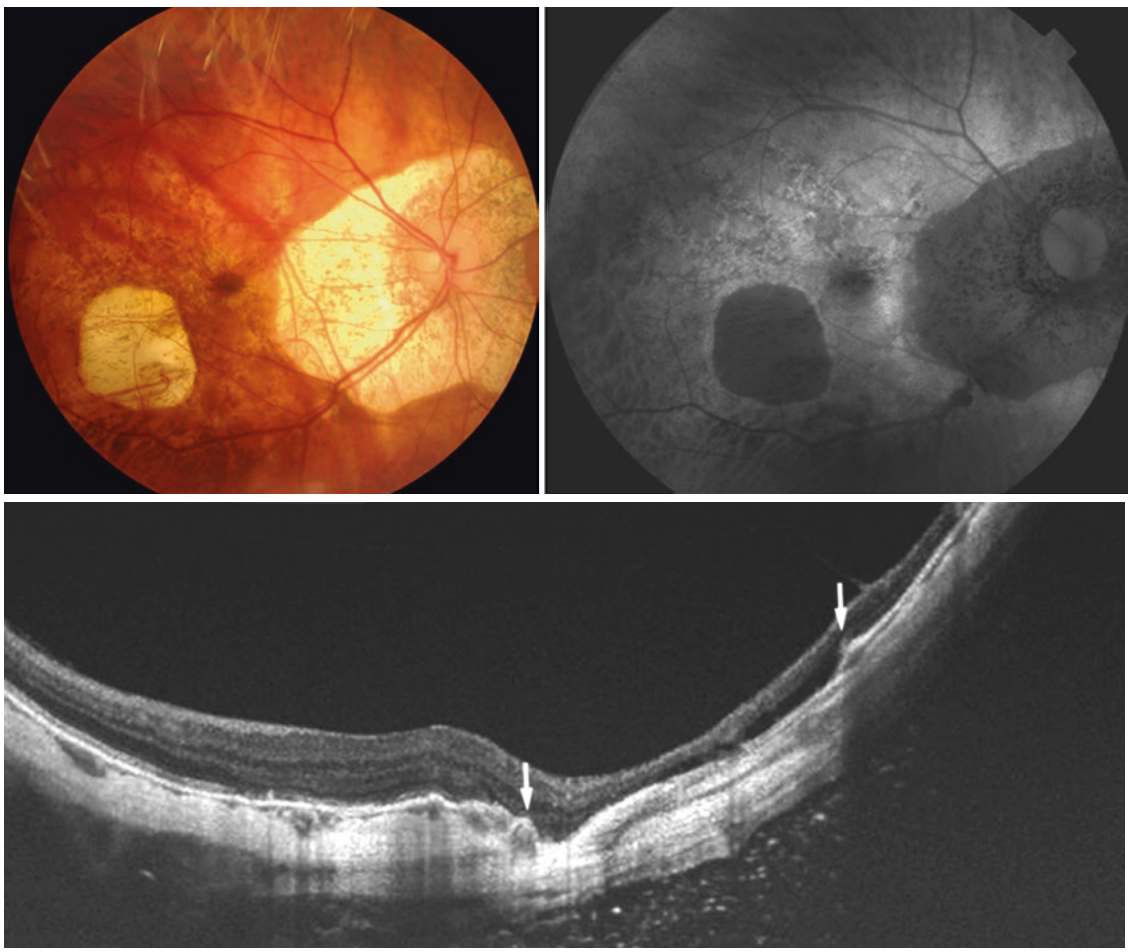

Fig. 10.2 Multimodal imaging of patchy atrophy. (Top Left) Right fundus of an 85-year-old man with axial length of 30.6 mm shows a circular patchy atrophy lower-temporal to the macula within the area of diffuse atrophy. Such circular-shaped patchy atrophy tends to develop from diffuse atrophy. (Top Right) The lesion of patchy atrophy shows uniform hypo-fluorescence in fundus autofluorescence image. (Middle) Swept-source OCT image across the patchy atrophy shows a defect of the retinal pigment epithelium (RPE) as well as Bruch's membrane. Arrows indicate the end of RPE. In the area of patchy atrophy, the outer retina and the choroid has also disappeared. Inner retina directly sits on the sclera. (Bottom) Fluorescein angiogram (FA) of the area of patchy atrophy shows hypo-fluorescence in the early phase (Left) and hyper-fluorescence along the edge of patchy atrophy in the late phase (Right)

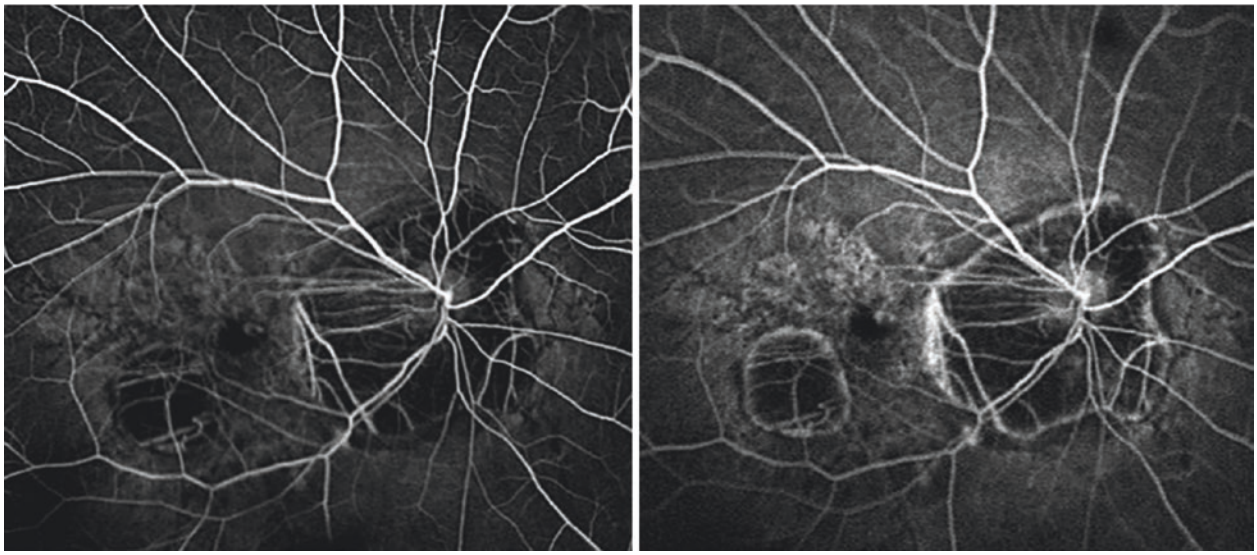

Fig. 10.2 (continued)

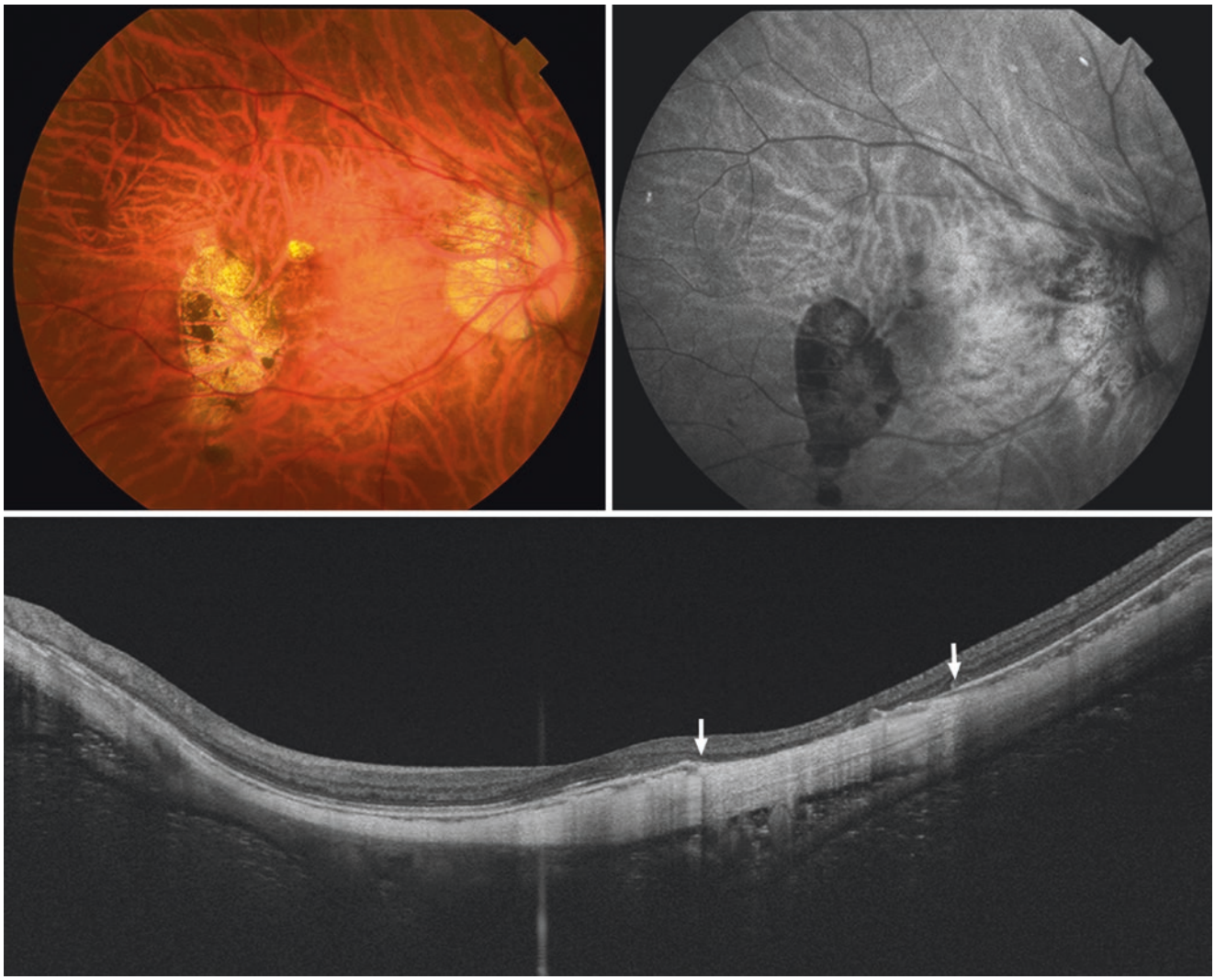

Fig. 10.3 Patchy atrophy originated from lacquer cracks. (Top Left) Left fundus of a 48-year-old woman with axial length of 34.8 mm shows vertically oval patchy atrophy temporal to the fovea. (Top Right) Fundus autofluorescence image shows hypo-fluorescence in the area of patchy atrophy. (Bottom) OCT image across the area of patchy atrophy shows a defect of the retinal pigment epithelium (RPE) as well as Bruch's membrane. Arrows indicate the end of RPE. In the area of patchy atrophy, the outer retina and the choroid has also disappeared. Inner retina directly sits on the sclera

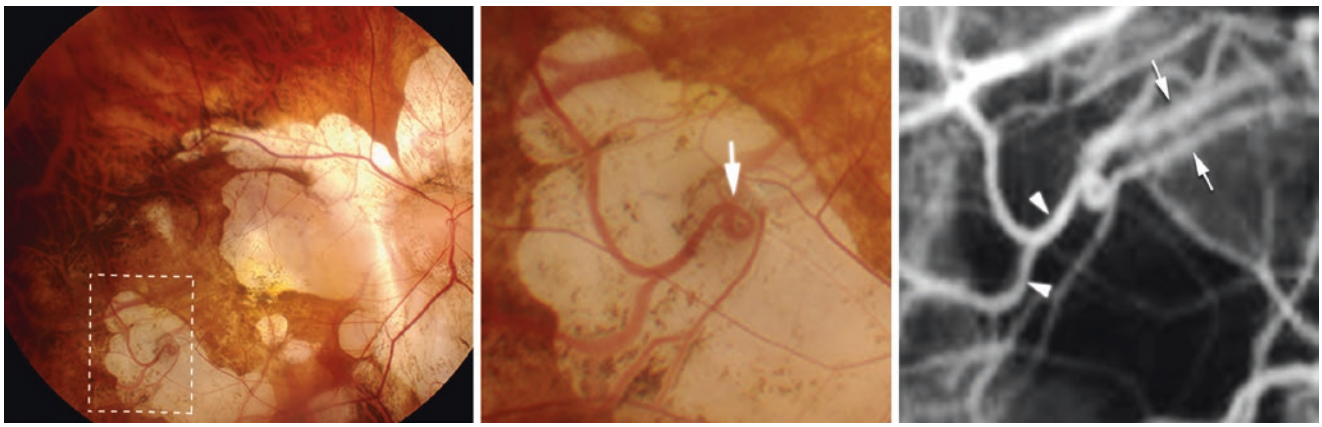

Fig. 10.4 (Cited with permission from [7]): Abruptly emerging vessel in the area of patchy atrophy. (Left) Right fundus of a 79-year-old woman with an axial length of 32.9 mm shows a large patchy atrophy lower to the fovea as well as a large parapapillary atrophy. (Middle) Magnified image of the squared area in the Left image shows that one large vessel has abruptly emerged (arrow), then takes a curled turn and then courses within the area of patchy atrophy, and finally continues as a choroidal vessel outside the patchy atrophy. (Right) Early phase of ICG angiography shows the more peripheral course of this emerging vessel (arrowheads). Two parallel running vessels (arrows, considered as intrascleral branches of short posterior ciliary arteries) seem to be continuous with this abruptly emerging vessel

References

1. Ohno-Matsui K, Kawasaki R, Jonas JB, Cheung CM, Saw SM, Verhoeven VJ, et al. International photographic classification and grading system for myopic maculopathy. Am J Ophthalmol. 2015;159(5):877–83.
2. Tokoro T. Atlas of posterior fundus changes in pathologic myopia. Tokyo: Springer; 1998. p. 5–22.
3. Hayashi K, Ohno-Matsui K, Shimada N, Moriyama M, Kojima A, Hayashi W, et al. Long-term pattern of progression of myopic maculopathy: a natural history study. Ophthalmology. 2010;117(8):1595–611.
4. Ohno-Matsui K, Akiba M, Moriyama M, Ishibashi T, Hirakata A, Tokoro T. Intrachoroidal cavitation in macular area of eyes with pathologic myopia. Am J Ophthalmol. 2012;154(2):382–93.
5. Ohno-Matsui K, Jonas JB, Spaide RF. Macular bruch membrane holes in highly myopic patchy chorioretinal atrophy. Am J Ophthalmol. 2016;166:22–8.
6. Du R, Fang Y, Jonas JB, Yokoi T, Takahashi H, Uramoto K, et al. Clinical features of patchy chorioretinal atrophy in pathologic myopia. Retina. 2019;
7. Xie S, Fang Y, Du R, Yokoi T, Takahashi H, Uramoto K, et al. Abruptly-emerging vessels in eyes with myopic patchy chorioretinal atrophy. Retina. 2019;

Myopic Macular Neovascularization (Diagnosis)

11

Yuka Onishi

Abstract

Myopic macular neovascularization (MNV) is one of the most common cause of the central vision loss in patients with pathologic myopia. It is classified into three phases: active, scar, and atrophic phase. MNV tends to be smaller and less active than choroidal neovascularization due to age-related macular degeneration. In addition, the presence of background choroidal atrophy makes the detection of MNV difficult in some cases. Thus, multimodal imaging is useful for diagnosing the MNV and determining its activity. MNV-related macular atrophy which is a long-term complication of MNV is also presented.

Keywords

Myopic macular neovascularization (MNV) · MNV-related macular atrophy

11.1 Incidence and Natural History

Myopic macular neovascularization (MNV) is one of the most common complications of the central vision loss in patients with pathologic myopia. MNV occurs in 7–10% of patients with high myopia [1], and one-third of the patients with MNV eventually become bilateral in the mean period of 8 years [2].

MNV is classified into three phases: active, scar, and atrophic phase [3]. The active phase is characterized by hemorrhage and/or serous retinal detachment. In the scar phase, the regressed MNV with fibrous scars is covered by the proliferated retinal pigment epithelial (RPE) cells, which was known as Fuchs' spot. In the atrophic phase, choroidal atrophy gradually develops and enlarges around the scarred MNV, which is featured by the formation of a hole of Bruch's membrane [4]. This atrophy is called "MNV-related macular atrophy" and is the main cause of long-term vision decrease of the patients with MNV.

A 10-year follow-up natural history study showed that 56% of the patients with MNV retained a visual acuity of better than 20/200 at 3 years after the onset; however, it dropped to 20/200 or less in 89% at 5 years and 96% at 10 years [5].

11.2 Diagnostic Imaging of Myopic Macular Neovascularization

11.2.1 Fundus Examination

Active phase of MNV is observed as a small, grayish membrane in the subfovea or parafovea (Figs. 11.1, 11.2). Small MNV tends to be missed in the area of background choroidal atrophy. Over time, it becomes scar with clear margin (Fig. 11.3). In a long-term (at least in a year), well-defined whitish (sometimes slightly pigmented) choroidal atrophy develops and enlarges around the scarred MNV, which is known as "MNV-related macular atrophy" (Figs. 11.5, 11.6, 11.7).

11.2.2 OCT

MNV in active phase is characterized by a highly reflective area above the RPE layer as a type 2 MNV (Fig. 11.1). Exudative changes such as subretinal fluid and hemorrhage are seen around MNV; however, exudative changes are usually much less compared to the MNV due to age-related macular

Y. Onishi (✉)
Department of Ophthalmology and Visual Science, Tokyo Medical and Dental University, Tokyo, Japan

K. Ohno-Matsui (ed.), *Atlas of Pathologic Myopia*, https://doi.org/10.1007/978-981-15-4261-9_11

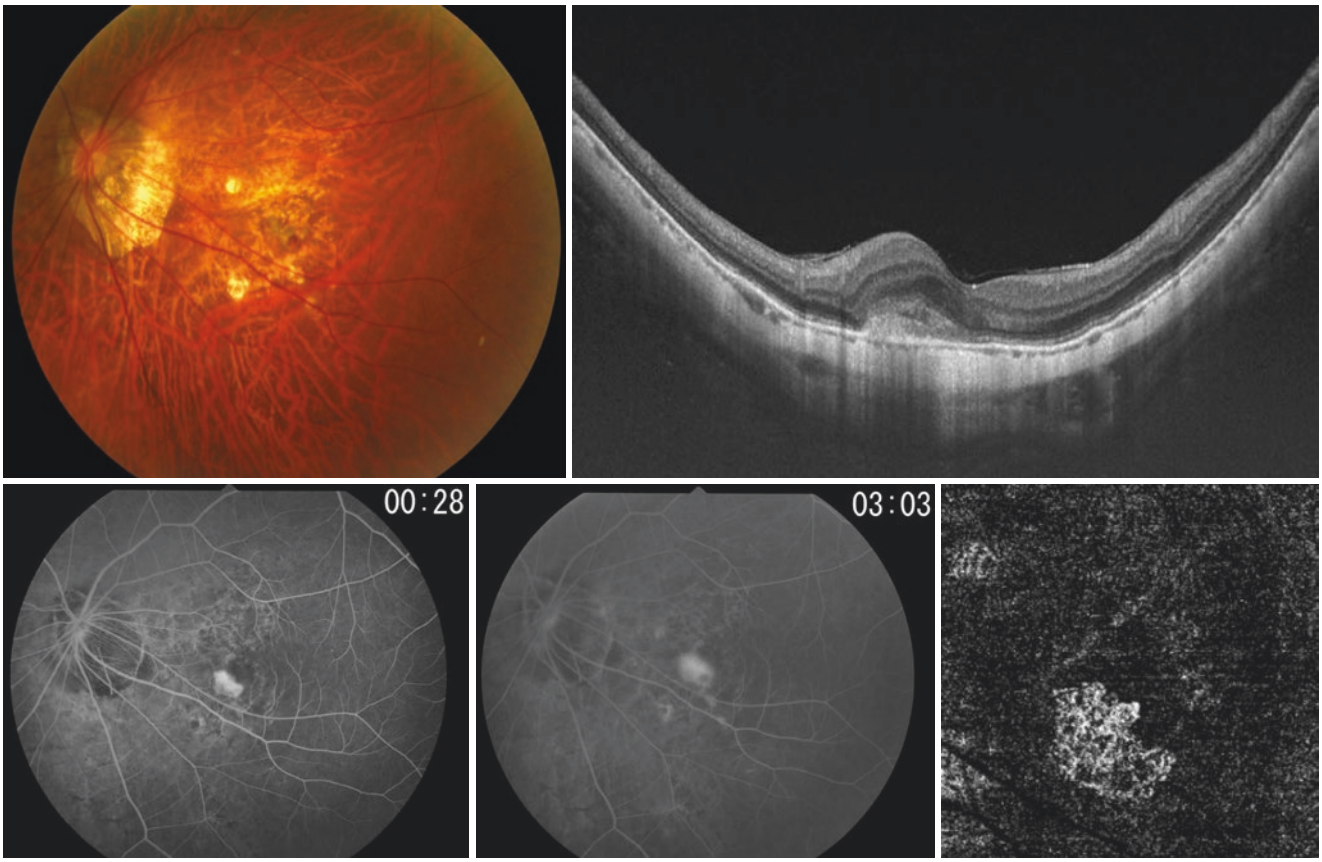

Fig. 11.1 Active phase of myopic macular neovascularization (MNV). (Top Left) Left fundus of a 65-year-old woman with refraction of -18.3D and axial length of 32.4 mm shows a grayish fibrovascular membrane in the area of background diffuse choroidal atrophy. (Top Right) Swept-source OCT image shows subretinal MNV and fibrin overlying the MNV. (Bottom Left and Middle) Fluorescein angiogram shows clear hyper-fluorescence in the early phase (left) and mild dye leakage in the late phase (middle) at the site of MNV. (Bottom Right) OCT angiographic image shows clear vascular network at the site of MNV

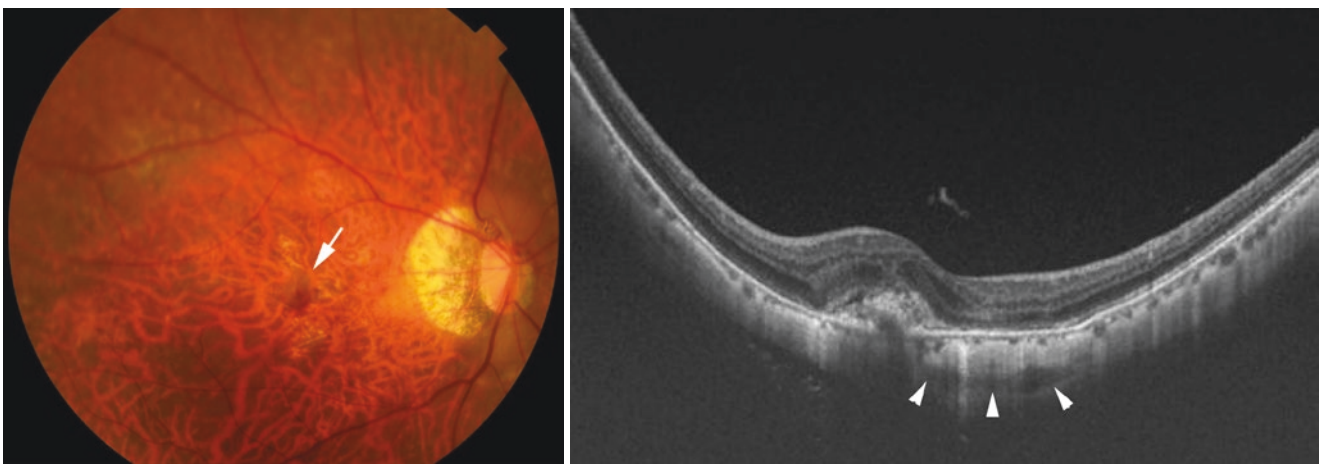

Fig. 11.2 Active phase of myopic macular neovascularization (MNV). (Top Left) Right fundus of a 78-year-old woman with axial length of 28.2 mm shows grayish fibrovascular membrane (arrow) in the background diffuse choroidal atrophy. (Top Right) Swept-source OCT image shows subretinal MNV. Small area of serous retinal detachment is seen around the MNV. Scleral vessel (arrowheads) seems to be running toward the MNV. (Bottom Left and Middle) Fluorescein angiogram shows clear hyper-fluorescence in the early phase (left) and mild dye leakage in the late phase (middle) at the site of MNV. (Bottom Right) OCT angiographic image shows clear vascular network at the site of MNV

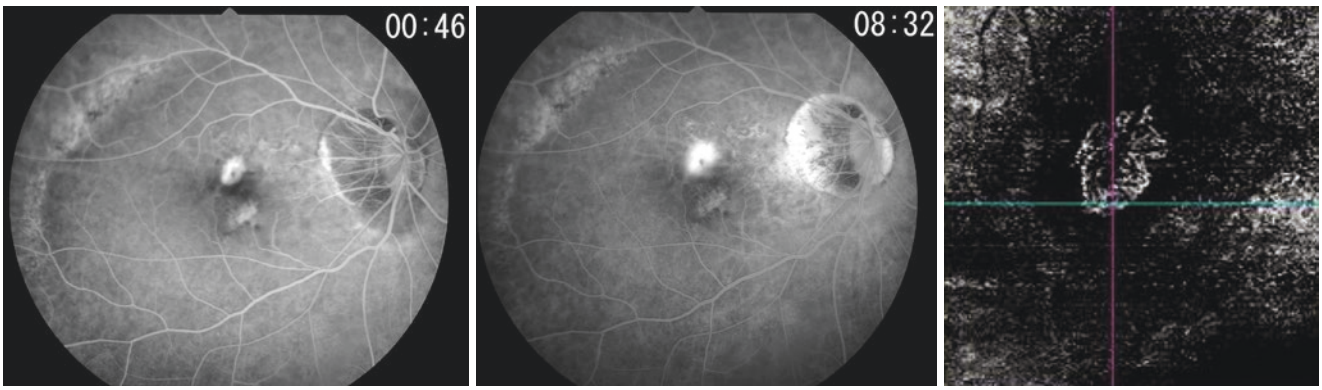

Fig. 11.2 (continued)

Fig. 11.3 Scar phase of myopic macular neovascularization (MNV). (Top Left) Left fundus of a 48-year-old man with refraction of -18.5D at 1 year after a single session of anti-VEGF therapy shows a grayish fibrovascular membrane surrounded by dark brown rim. Lacquer cracks are also seen around the MNV. (Top Right) Swept-source OCT shows a well-demarcated MNV. Proliferated RPE seems to cover the MNV. (Middle) Fluorescein angiogram shows clear hyper-fluorescence in the early phase (left) as well as in in the late phase (right) at the site of MNV. The size of hyper-fluorescence is the same between the two images, suggesting a lack of dye leakage. (Bottom Left and Middle) ICG angiogram in the early phase (left) and in the late phase (middle). MNV shows mild hyper-fluorescence in the late phase surrounded by a dark rim. Linear hypo-fluorescence due to lacquer cracks is clearly seen. (Bottom Right) OCT angiographic image shows clear vascular network at the site of scarred MNV

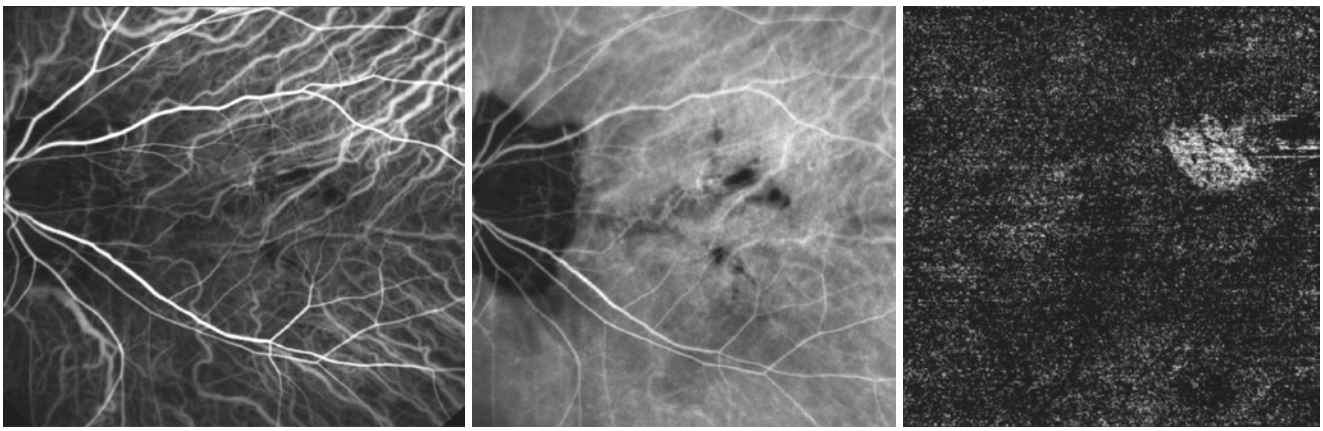

Fig. 11.3 (continued)

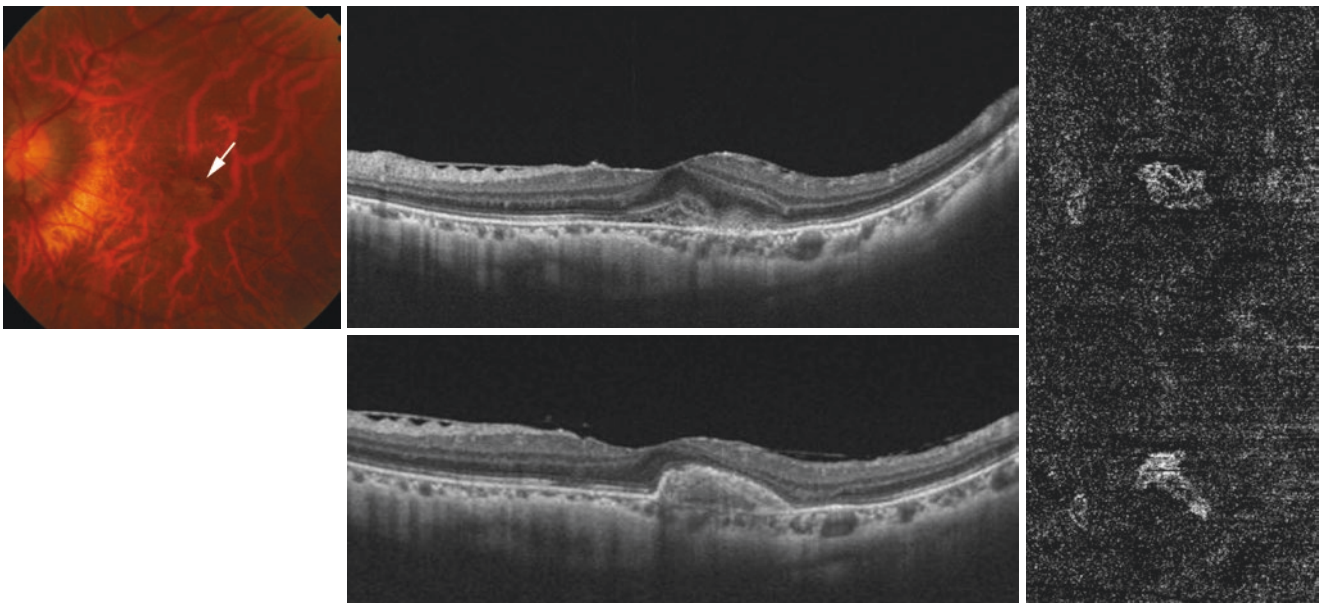

Fig. 11.4 Progression from active phase to scar phase. (Top Left) Left fundus of a 54-year-old woman with refraction of -19.0D and axial length of 30.0 mm shows grayish fibrovascular membrane (arrow) with hemorrhage. (Top Middle) Swept-source OCT image shows subretinal MNV with small area of serous retinal detachment. (Top Right) OCT angiographic image shows clear vascular network at the site of active MNV. (Bottom Left) Swept-source OCT image at 1 year after anti-VEGF therapy shows well-demarcated MNV encompassed with RPE. No exudative changes are seen. (Bottom Right) OCT angiographic image shows an irregular-shaped and shrunken MNV

degeneration. In some cases, swept-source OCT revealed that the intrascleral branches of short posterior ciliary arteries and MNV appeared to be continuous to short posterior ciliary arteries through a defect of Bruch's membrane, suggesting a non-choroidal origin for MNV in such eyes with extremely thin choroid (Figs. 11.2, 11.7) [6]. In scar phase, MNV is enclosed by RPE, and the line is drawn as a bright line on OCT (Figs. 11.3, 11.4). In the atrophic phase, an increased penetration of the light into the deeper tissue is found in the area of macular atrophy (Figs. 11.5, 11.6). Bruch's membrane is tattered and fragmentary in the area of atrophy.

11.2.3 OCT Angiography (OCTA)

OCTA shows clear vascular network at the site of MNV in all of the phases (active, scar, and atrophic) (Figs. 11.1, 11.2, 11.3, 11.7). A shrinkage or reduction of MNV size is well-observed when MNV is successfully treated (Fig. 11.4). Even in the atrophic phase, some MNVs maintain its blood flow. Thus, OCTA is useful for detecting MNV and differentiating it from simple macular bleeding which is caused by choriocapillaris injury due to new lacquer crack formation. However, it is difficult to determine the MNV activity by

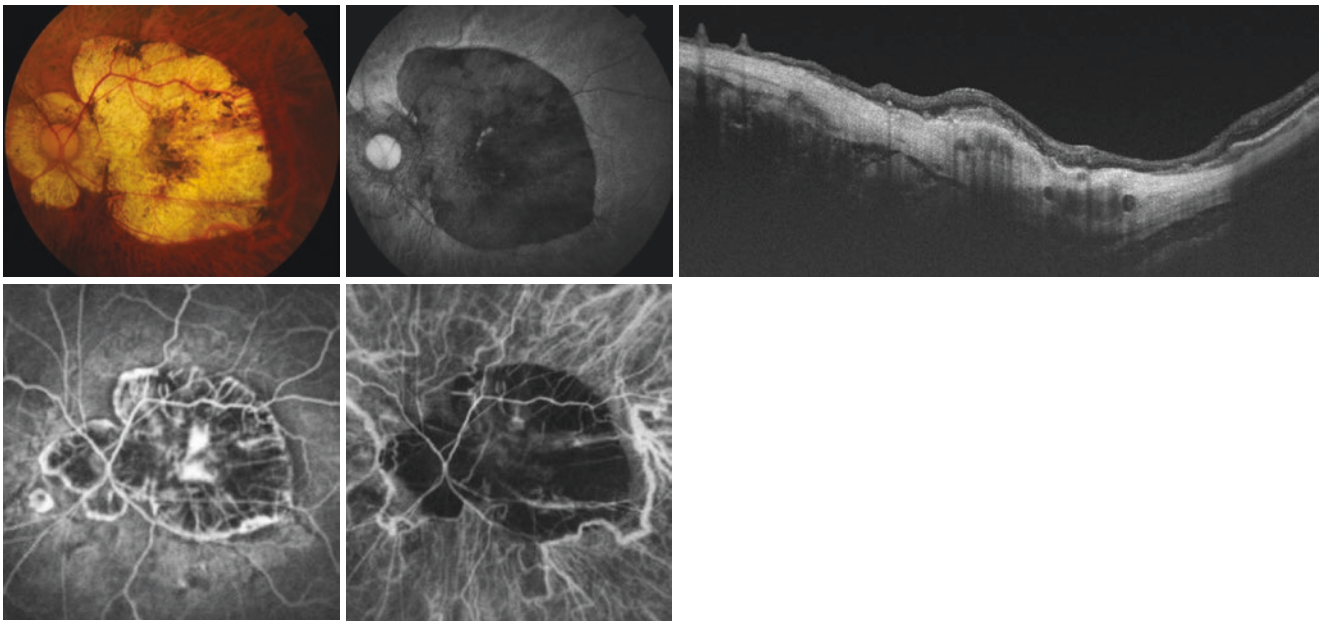

Fig. 11.5 Atrophic phase of myopic macular neovascularization (MNV) (MNV-related macular atrophy). (Top Left) Left fundus of a 75-year-old woman with axial length of 31.6 mm at 3 years after a single session of anti-VEGF therapy shows a large area of MNV-related macular atrophy. Scarred MNV with pigmentation (Fuchs' spot) is seen in the center of the atrophy. (Top Middle) Fundus autofluorescence shows clear hypo-fluorescence in the area of the MNV-related macular atrophy. (Top Right) Swept-source OCT image shows an increased penetration of the light into deeper tissues in the area of MNV-related macular atrophy. An oblique OCT section across the fovea shows scarred MNV as a subretinal elevation. Bruch's membrane is tattered and fragmented in the area of macular atrophy. (Bottom Left) Fluorescein angiogram in the late phase shows hypo-fluorescence in the area of MNV-related macular atrophy. The border of macular atrophy shows mild hyper-fluorescence. The scarred MNV also shows hyper-fluorescence. (Bottom Right) ICG angiogram in the late phase shows clear hypo-fluorescence in the area of macular atrophy. Posterior vortex vein is observed temporal to the macular atrophy

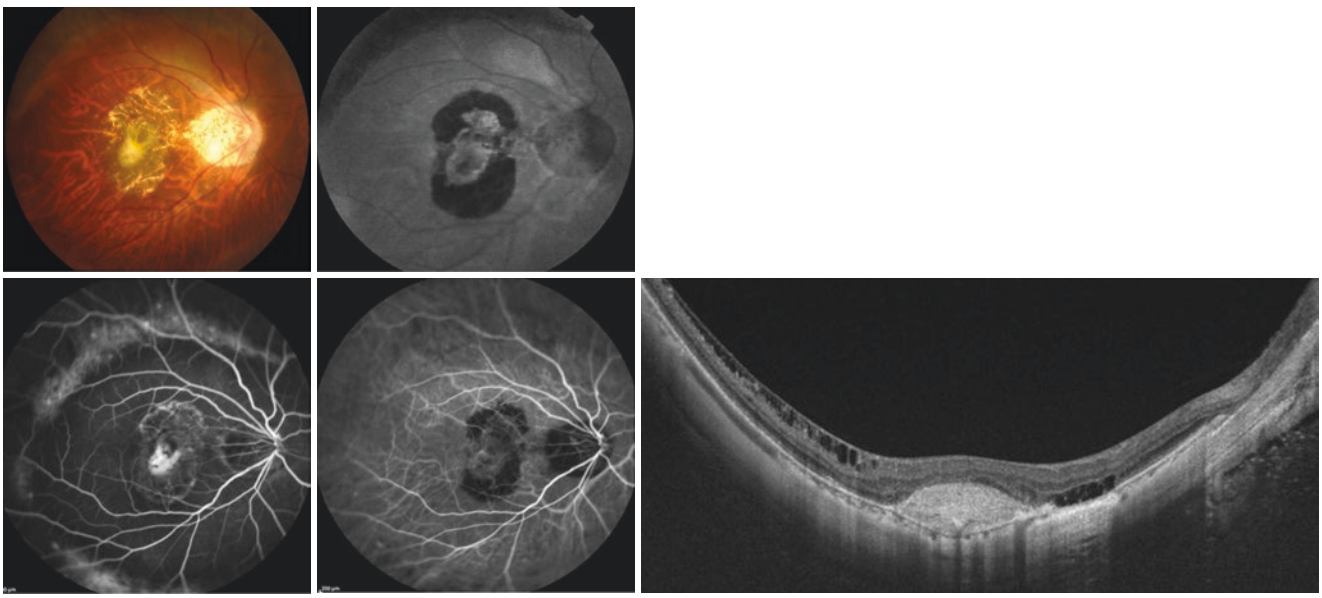

Fig. 11.6 Atrophic phase of myopic macular neovascularization (MNV). (Top Left) Right fundus of a 53-year-old woman with refraction of -13.0D and axial length of 27.9 mm at 3 years after anti-VEGF therapy shows a large MNV-related macular atrophy. Whitish scarred MNV is seen within macular atrophy. (Top Right) Fundus autofluorescence shows clear hypo-fluorescence in the area of the MNV-related macular atrophy. (Bottom Left) Fluorescein angiogram shows hypo-fluorescence in the early phase but shows mild hyper-fluorescence in the late phase at the area of MNV-related macular atrophy. The scarred MNV shows hyper-fluorescence. (Bottom, Middle) ICG angiogram in the late phase shows clear hypo-fluorescence in the area of macular atrophy. (Bottom, Right) Swept-source OCT image shows an increased penetration of the light into deeper tissues in the area of MNV-related macular atrophy. A scarred MNV is observed as a subretinal elevation

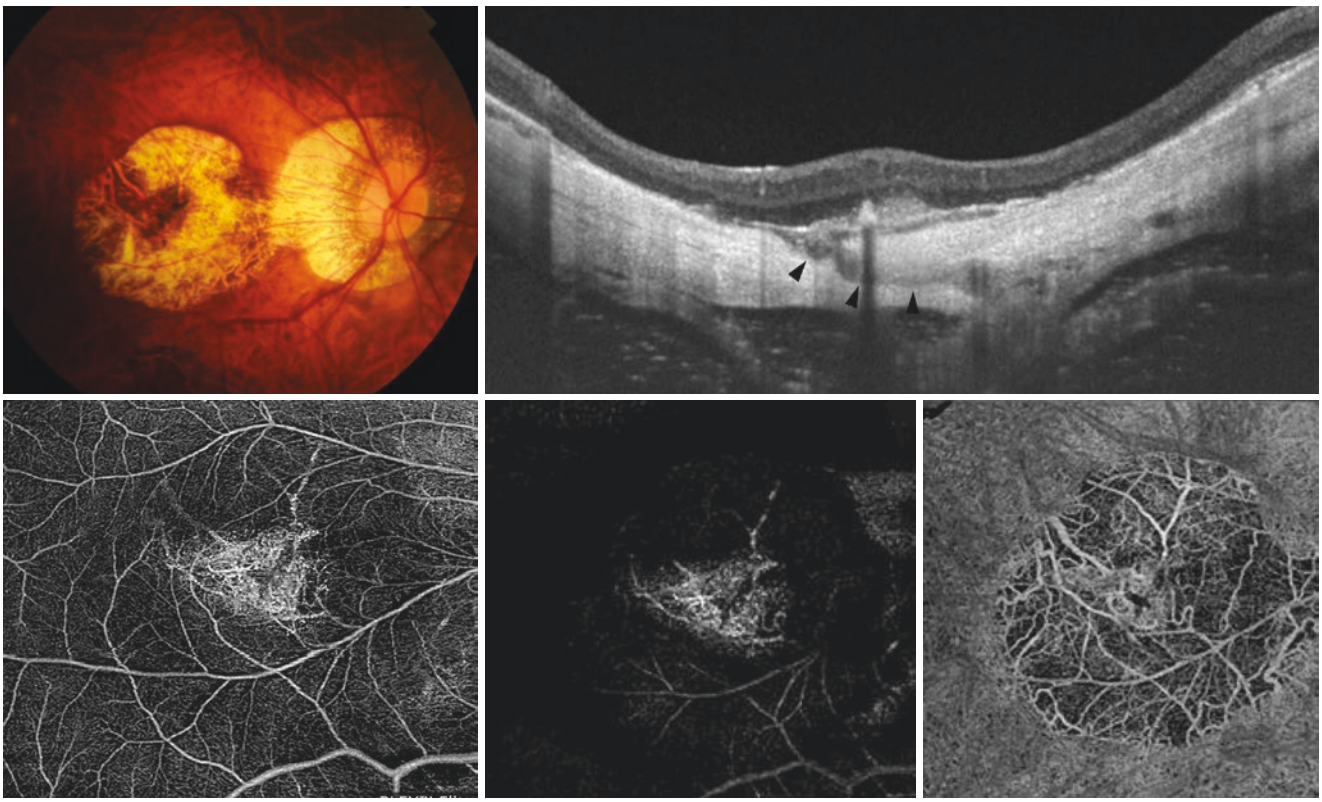

Fig. 11.7 Atrophic phase of myopic macular neovascularization (MNV) ([6] cited with permission). (Top Left) Right fundus of a 64-year-old woman with refraction of -18.0D and axial length of 29.5 mm shows a MNV-related macular atrophy around the scarred MNV. (Top right) Swept-source OCT image shows subretinal MNV. Scleral blood vessel (arrowheads) (confirmed as scleral branches of short posterior ciliary arteries by ICG angiography) appears to be continuous to the MNV through a defect of Bruch's membrane. (Bottom) OCT angiographic images at superficial retina slab (left), at outer retina slab (middle), and at choriocapillaris slab (right) show clear vascular network with blood flow

OCTA alone, because blood flow remains even in the scar phase or an atrophic phase.

11.2.4 Fluorescein Angiography (FA)

On FA, the active MNV shows clear hyper-fluorescence in the early phase with dye leakage in the late phase (Figs. 11.1, 11.2). Dye leakage is generally mild, thus it becomes obvious by a careful comparison of the MNV size between the early phase and the late phase. The scar phase MNV shows hyper-fluorescence without dye leakage (Fig. 11.3). The margin of MNV is clear throughout the entire angiographic phase. The area of MNV-related macular atrophy shows hypo-fluorescence in the early phase followed by mild staining in the late phase (Figs. 11.5, 11.6). The MNV remnants in the center of macular atrophy shows mild hyper-fluorescence in most cases.

11.2.5 ICG Angiography (ICGA)

MNV tends not to show clear hyper-fluorescence on ICGA. Thus, ICGA is not useful for the diagnosis or detecting activity of MNV. A dark rim surrounding MNV is sometimes found. Furthermore, ICGA is useful for the assessment of lacquer cracks surrounding MNV (Fig. 11.3). On ICGA, abnormally dilated choroidal veins or collaterals are sometimes seen below the MNV.

11.2.6 Fundus Autofluorescence (FAF)

FAF shows various inconsistent patterns at the MNV. FAF is the most useful for detecting MNV-related macular atrophy, which shows clear hypo-fluorescence (Figs. 11.5, 11.6).

11.2.7 Fundus Microperimetry (MP3)

For functional evaluation of the subfoveal retina, fundus perimetry (MP-3 Microperimeter, Nidek, Aichi, Japan) is a powerful tool. By combining with color fundus photos, OCT-A or OCT B scans, MP3 enables a precise determination of the spatial relationship between the structural abnormalities induced by MNV and retinal damage.

References

1. Wong TY, Ferreira A, Hughes R, Carter G, Mitchell P. Epidemiology and disease burden of pathologic myopia and myopic choroidal neovascularization: an evidence-based systematic review. Am J Ophthalmol. 2014;157:9–25.
2. Ohno-Matsui K, Yoshida T, Futagami S, Yasuzumi K, Shimada N, Kojima A, Tokoro T, Mochizuki M. Patchy atrophy and lacquer cracks predispose to the development of choroidal neovascularization in pathological myopia. Br J Ophthalmol. 2003;87:570–3.
3. Ohno-Matsui K, Kawasaki R, Jonas JB, Cheung CM, Saw SM, Verhoeven VJ, Klaver CC, Moriyama M, Shinohara K, Kawasaki Y, Yamazaki M, Meuer S, Ishibashi T, Yasuda M, Yamashita H, Sugano A, Wang JJ, Mitchell P, Wong TY, on behalf of META-PM study group. International photographic classification and grading system for myopic maculopathy. Am J Ophthalmol. 2015a;159:877–83.
4. Ohno-Matsui K, Jonas JB, Spaide RF. Macular Bruch's membrane holes in choroidal neovascularization-related myopic macular atrophy by swept-source optical coherence tomography. Am J Ophthalmol. 2015b;162:133–9.
5. Yoshida T, Ohno-Matsui K, Yasuzumi K, Kojima A, Shimada N, Futagami S, Tokoro T, Mochizuki M. Myopic choroidal neovascularization: a 10-year follow-up. Ophthalmology. 2003;110:1297–305.
6. Ishida T, Watanabe T, Yokoi T, Shinohara K, Ohno-Matsui K. Possible connection of short posterior ciliary arteries to choroidal neovascularisations in eyes with pathologic myopia. Br J Ophthalmol. 2019;103:457–62.

Myopic Macular Neovascularization; Treatment Outcome (Including MP3)

12

Mariko Yana and Yuka Onishi

Abstract

Intravitreal injection of anti-VEGF agents is the first-line therapy for myopic macular neovascularization (MNV). Among various anti-VEGF agents; ranibizumab has been approved for MNV in many countries and aflibercept in 99 countries at the point of August 2019. Bevacizumab is used off-label.

Keywords

Myopic macular neovascularization (MNV) · Anti-VEGF reagents · Ranibizumab · Aflibercept · macular atrophy

12.1 Clinical Trials of Anti-VEGF Therapy

The effectiveness and the safety of ranibizumab and aflibercept for MNV have been reported in large clinical trials; the REPAIR study [1], the RADIANCE study [2], and the MYRROR study [3].

In all of these studies, anti-VEGF therapy led to statistically significant improvement in visual acuity at 1 year. Further, these studies showed that the treatment of MNV with anti-VEGF therapies should be started as soon as possible after onset [2, 3]. Visual improvement by intravitreal ranibizumab guided by disease activity criteria was non-inferior to that guided by visual acuity stabilization criteria up to month 6 with a low number of injections.

M. Yana (✉) · Y. Onishi
Department of Ophthalmology and Visual Science, Tokyo Medical and Dental University, Tokyo, Japan
e-mail: yana-tmd@umin.org

12.2 Long-Term Studies of Anti-VEGF Therapy

There have been several studies reporting the visual outcome of patients with MNV treated with anti-VEGF agents with a follow-up period longer than 2 years.

These studies showed that the visual improvement was not statistically significant from that of the baseline in about 5 years [4–6]. Final vision was correlated with the size of the MNV-related macular atrophy, the baseline best-corrected visual acuity (BCVA), and MNV size [7, 8].

Although the long-term effect was inferior to the short-term course, Onishi et al. showed that the eyes treated with anti-VEGF reagents maintained significant better vision than non-treated historical controls in a long-term (in 5 years after the MNV onset) [8].

12.3 Prognostic Factors for Visual Outcome With Anti-VEGF Therapy

According to the systematic review of intravitreal bevacizumab, factors which were consistently associated with the improvement of BCVA were; smaller MNV size at baseline, younger age at baseline, and a lower rate of development of MNV-related macular atrophy [9]. The results of statistical analyses in earlier studies [4, 8, 10] showed that the decreased BCVA in longer follow-up periods by anti-VEGF therapy was significantly correlated with the development of MNV-related macular atrophy.

12.4 Treatment Strategy

It has been reported that in more than a half of the patients with MNV, the MNV regresses with a single session of anti-VEGF therapy [8]. Thus, unlike age-related macular degeneration (AMD), a single injection of anti-VEGF reagents followed by PRN treatment is recommended.

K. Ohno-Matsui (ed.), *Atlas of Pathologic Myopia*, https://doi.org/10.1007/978-981-15-4261-9_12

The detailed treatment strategy for MNV has been proposed by Wong et al. and Ohno-Matsui et al. [11–13]. According to Ohno-Matsui et al (Fig. 12.1). it is recommended that newly diagnosed patients initiating anti-VEGF treatment should be followed up by OCT monthly for the first 3 months, and then every 2–3 months. However, we also recommend fluorescein angiogram at 1 month after starting anti-VEGF therapy. Disappearance of dye leakage is earlier and more accurate marker to show a decreased activity of MNV than OCT or OCT angiography (OCTA). A shrinkage of MNV by OCTA is also a good marker to show the effectiveness of the treatment. However, the blood flow detected by OCTA tends to remain even after the MNV becomes inactive and even in its atrophic stage.

If there is no recurrence for a year, we can further extend the interval. The frequency of follow-up after the first year is every 6 months. However, it is recommended that the patients should come to the examination when new symptoms occur or symptoms change. After 1 year of the MNV onset, fundus autofluorescence (FAF) should be periodically conducted to detect the MNV-related macular atrophy.

Representative cases with MNV are shown in Figures (Figs. 12.2, 12.3, 12.4, 12.5).

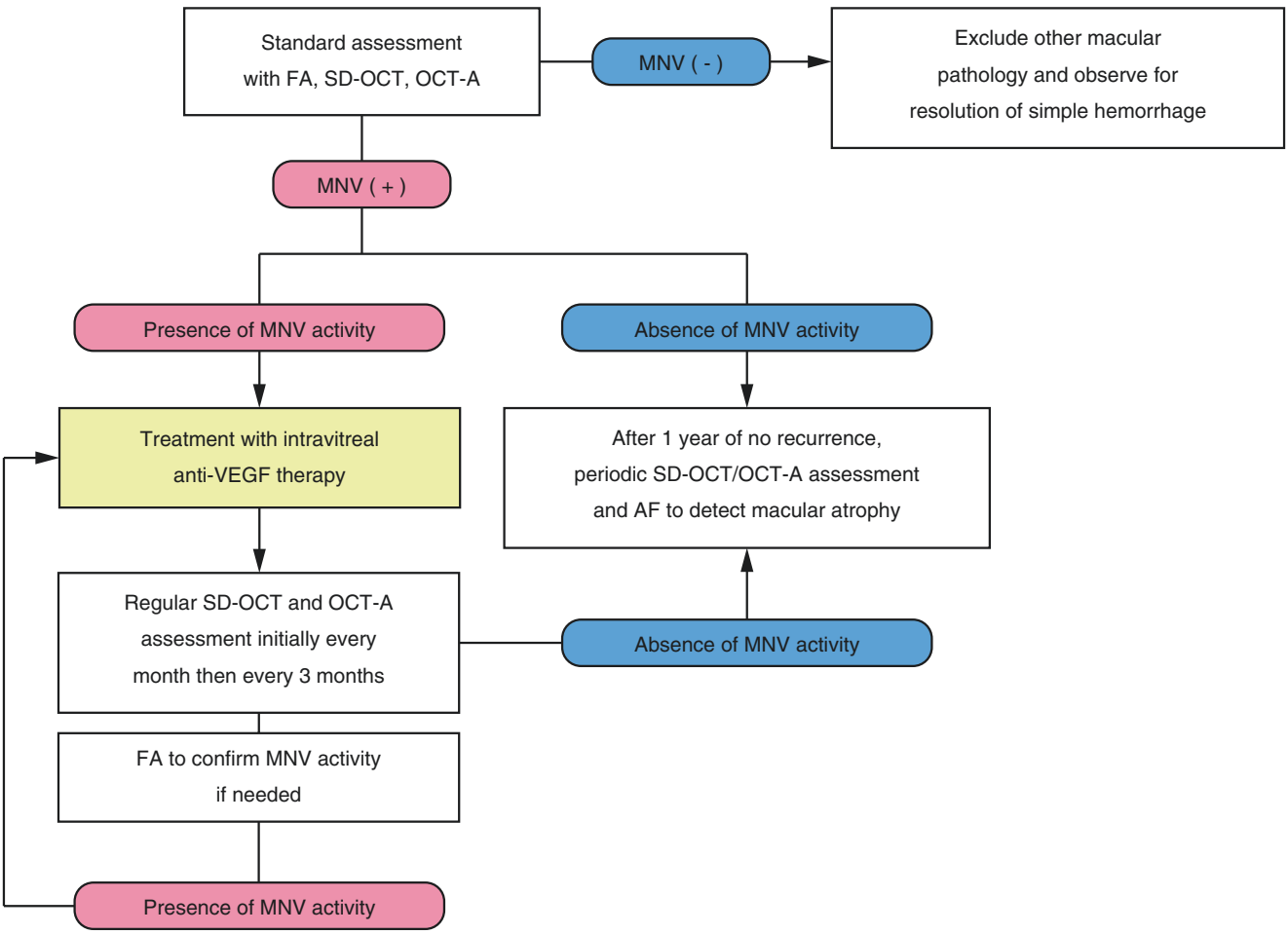

Fig. 12.1 Diagnostic and treatment flowchart for the management of suspected myopic macular neovascularization (MNV)

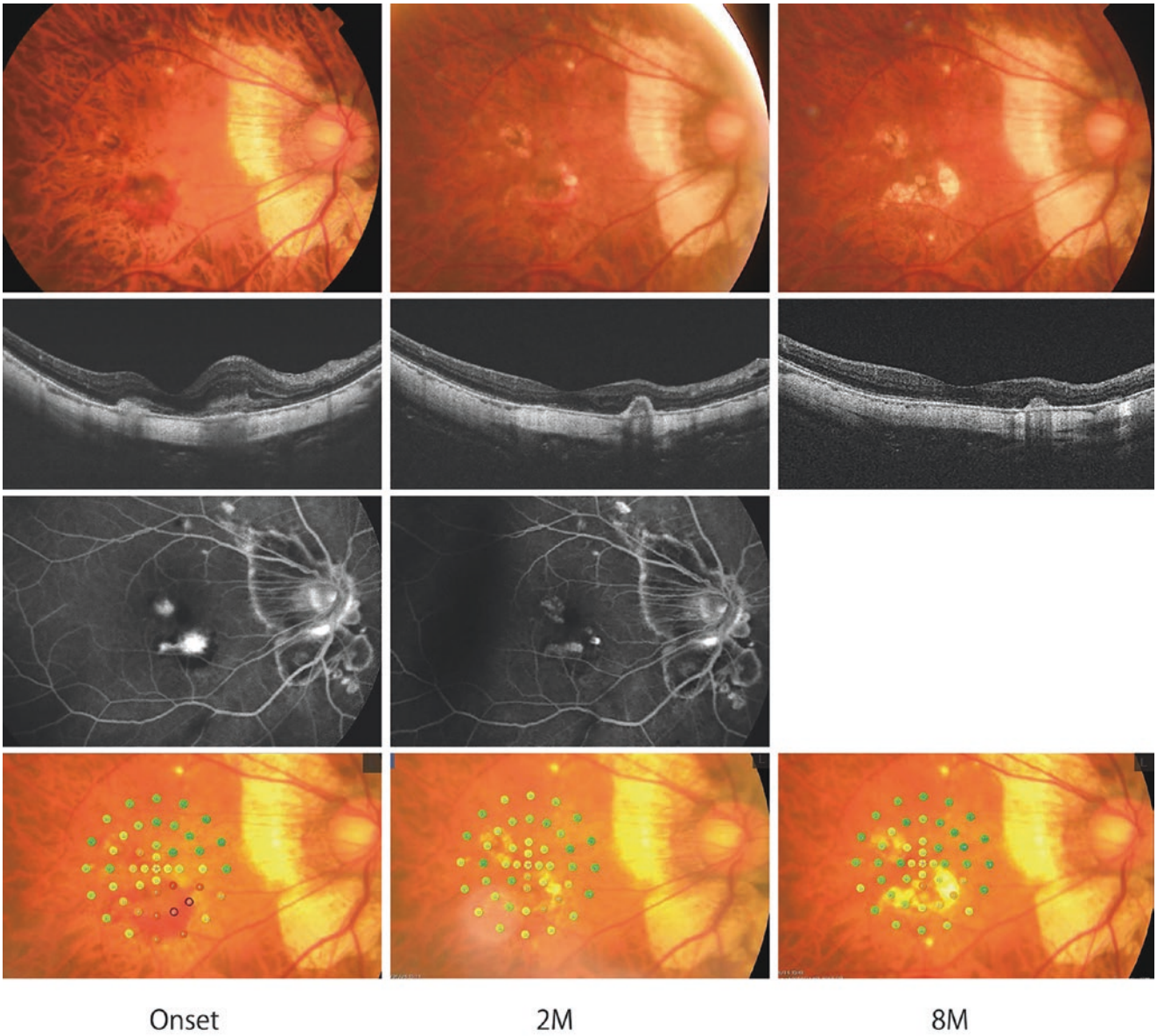

Fig. 12.2 Regression of myopic MNV and subsequent development of MNV-related macular atrophy after anti-VEGF therapy in the right fundus of a 53-year-old woman with refraction of -17.0 D and axial length of 31.7 mm. Before treatment (left row), the right fundus shows two hemorrhages in the macula. An oblique OCT section across the fovea shows two MNVs. Fluorescein angiogram (FA) shows dye leakage from the MNV. Fundus microperimetry with MP-3 shows a decreased sensitivity lower nasal to the fovea at the corresponding site of the MNV. Two months after a single session of intravitreal ranibizumab (middle row), the right fundus shows that the hemorrhage has been resolved. Small area of MNV-related macular atrophy has developed around the pigmented MNVs. OCT image shows well-demarcated MNV covered by the retinal pigment epithelium. FA shows an absence of dye leakage and a shrinkage of the MNV. MP3 shows an improvement of the retinal sensitivity. Eight months after a single session of intravitreal ranibizumab (right row), MNV-related macular atrophy has enlarged

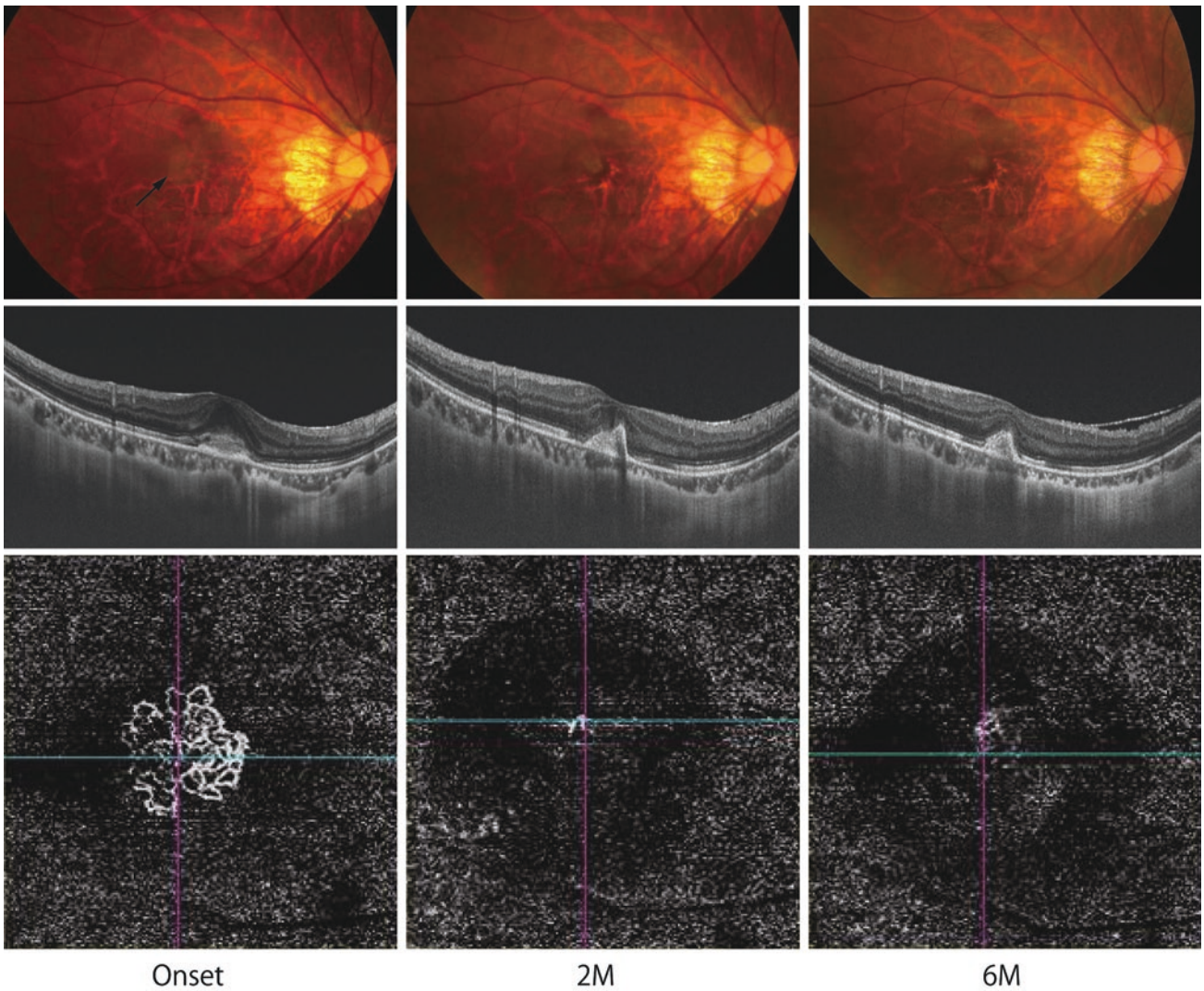

Fig. 12.3 A marked shrinkage of the vascular network of the myopic MNV after anti-VEGF therapy in the right fundus of a 42-year-old woman with refraction of -10.0 D and axial length of 29.8 mm. Before treatment (left row), the right fundus shows a blurred greyish area suggesting myopic MNV (arrow). OCT image shows subretinal MNV with serous retinal detachment. OCT angiography (OCTA) shows a clear vascular network at the MNV. Two months after intravitreal aflibercept (middle row), OCT shows that MNV has shrunken with a clear margin, and has been covered by the retinal pigment epithelium. No exudative changes are seen around the MNV. OCTA shows a marked reduction of the MNV size. New vessels with blood flow are barely detectable. Six months after a single session of intravitreal aflibercept (right row), OCT shows further shrinkage of the CNV. OCTA shows barely detectable vessels with blood flow

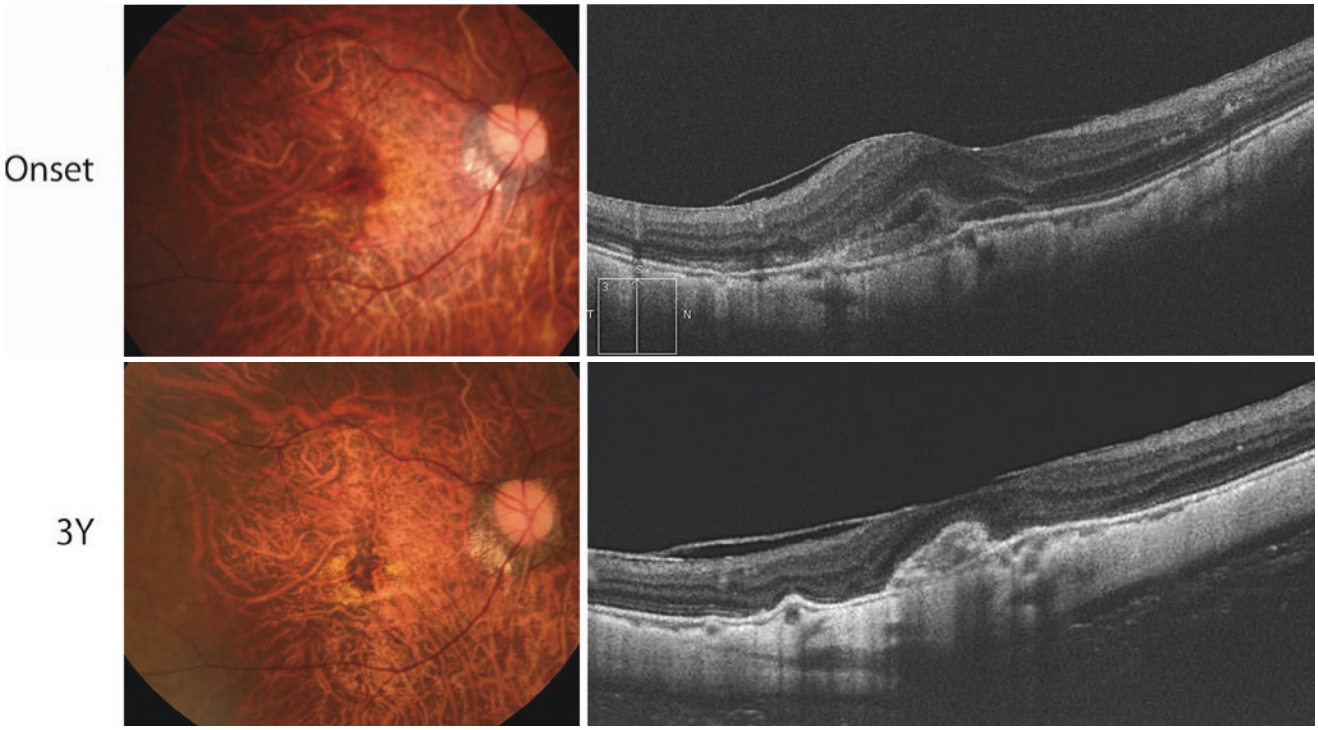

Fig. 12.4 Regression of myopic MNV without developing MNV-related macular atrophy in the right fundus of a 66-year-old woman with refraction of -11.0 D and axial length of 30.1 mm. At onset (top row), MNV with hemorrhage is observed lower to the fovea. OCT shows ill-defined MNV. Three years after a single session of intravitreal ranibizumab (bottom row), no exudative changes are seen around the MNV. MNV-related macular atrophy is not formed. OCT shows that MNV is well-defined and covered by the retinal pigment epithelium

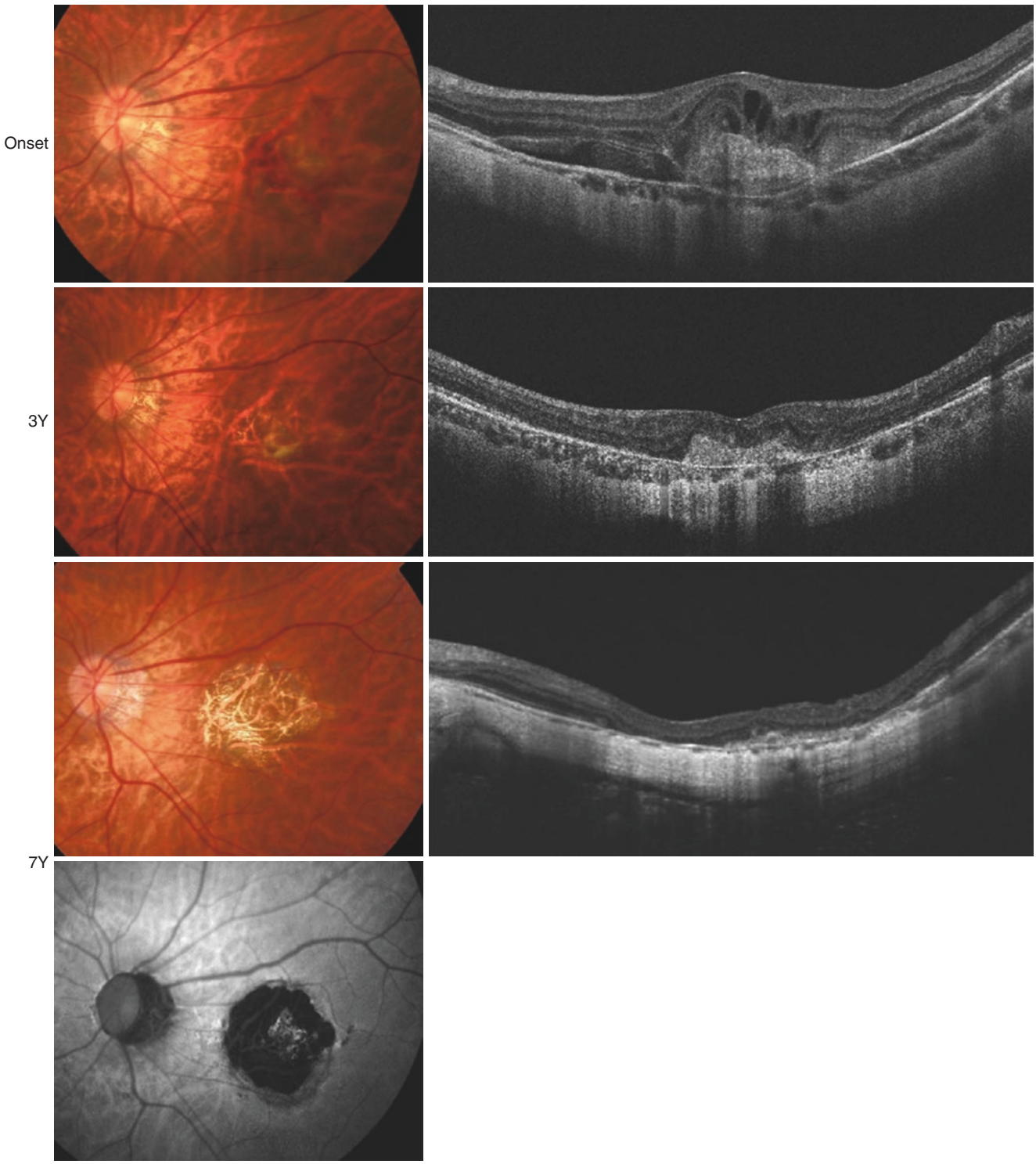

Fig. 12.5 Development of a large MNV-related macular atrophy around the regressed MNV in the left fundus of a 53-year-old woman with an axial length of 27.7 mm. At onset (top row), the MNV with exudative changes is seen in OCT image. Three years after intravitreal ranibizumab (the second row), the MNV has become a fibrotic scar. OCT image shows a shrunken and flattened MNV. Seven years after a single session of intravitreal ranibizumab (the third row and bottom row), a circular MNV-related macular atrophy has developed. Fundus autofluorescence (bottom) shows a clear hypo-fluorescence in the area of MNV-related macular atrophy. OCT image shows the remnants of MNV and an increased penetration of light is seen in the area of MNV-related macular atrophy

References

1. Tufail A, Narendran N, Patel PJ, et al. Ranibizumab in myopic choroidal neovascularization: the 12-month results from the REPAIR study. Ophthalmology. 2013;120(9):1944–5.
2. Wolf S, Balciuniene VJ, Laganovska G, Menchini U, Ohno-Matsui K, Sharma T, et al. RADIANCE: a randomized controlled study of ranibizumab in patients with cho- roidal neovascularization secondary to pathologic myopia. Ophthalmology. 2014;121(3):682–92.
3. Ikuno Y, Ohno-Matsui K, Wong TY, et al. Intravitreal aflibercept injection in patients with myopic choroidal neovascularization: the MYRROR study. Ophthalmology. 2015;122(6):1220–7.
4. Kasahara K, Moriyama M, Morohoshi K, Yoshida T, Simada N, Nagaoka N, Yokoi T, Shinohara K, Kaneko Y, Suga M, Ohno-Matsui K. Six-year outcomes of intravitreal bevacizumab for choroidal neovascularization in patients with pathologic myopia. Retina. 2016;37:1055–64.
5. Yoshida T, Ohno-Matsui K, Yasuzumi K, Kojima A, Shimada N, Futagami S, Tokoro T, Mochizuki M. Myopic choroidal neovascularization: a 10-year follow-up. Ophthalmology. 2003;110:1297–305.
6. Chhablani J, Paulose PM, Lasave AF, Wu L, Carpentier C, Maia M, et al. Intravitreal bevacizumab monotherapy in myopic choroidal neovascularisation: 5-year outcomes for the PAN-American collaborative retina study group. Br J Ophthalmol. 2018;102:455–9.
7. Tan NW, Ohno-Matsui K, Koh HJ, Nagai Y, Pedros M, Freitas RL, Macfadden W, Lai TY. Long-term outcomes of ranibizumab treatment of myopic choroidal neovascularization in east-Asian patients from the RADIANCE study. Retina. 2017;38(11):2228. https://doi.org/10.1097/IAE.0000000000001858.
8. Onishi Y, Yokoi T, Kasahara K, Yoshida T, Nagaoka N, Shinohara K, et al. Five-year outcomes of intravitreal ranibizumab for choroidal neovascularization in patients with pathologic myopia. Retina. 2018;39(7):1289–98. https://doi.org/10.1097/IAE.0000000000002164.
9. Wang J, Kang Z. Summary of prognostic factors for choroidal neovascularization due to pathological myopia treated by intravitreal bevacizumab injection. Graefes Arch Clin Exp Ophthalmol. 2012;250:1717–23.
10. Oishi A, Yamashiro K, Tsujikawa A, et al. Long-term effect of intravitreal injection of anti-VEGF agent for visual acuity and chorioretinal atrophy progression in myopic choroidal neovascularization. Graefes Arch Clin Exp Ophthalmol. 2013;251:1–7.
11. Ohno-Matsui K, Ikuno Y, Lai TYY, Gemmy Cheung CM, et al. Diagnosis and treatment guideline for myopic choroidal neovascularization due to pathologic myopia. Prog Retin Eye Res. 2018;63:92–106.
12. Wong TY, Ohno-Matsui K, Leveziel N, Holz FG, Lai TY, Yu HG, Lanzetta P, Chen Y, Tufail A. Myopic choroidal neovascularisation: current concepts and update on clinical management. Br J Ophthalmol. 2015;99:289–96.
13. Ohno-Matsui K, Jonas JB, Spaide RF. Macular Bruch membrane holes in choroidal neovascularization-related myopic macular atrophy by swept-source optical coherence tomography. Am J Ophthalmol. 2016;162:133–9.

13 Lacquer Cracks, Simple Macular Hemorrhage and Myopic Stretch Lines

Kengo Uramoto and Xian Xu

Abstract

Lacquer cracks are observed as yellowish linear lesions in the posterior fundus in 4.2–15.7% of highly myopic eyes. They represent healed and mechanical breaks of the retinal pigment epithelium (RPE), Bruch's membrane, and choriocapillaris complex. Their progression patterns are: increase in number, elongation, and progression to patchy atrophy.

Simple hemorrhage is macular hemorrhage that occurs in highly myopic eyes and is most likely caused by the mechanical rupture of Bruch's membrane and choriocapillaris complex without macular neovascularization. Subretinal bleeding is an indicator of a formation of new lacquer cracks.

Myopic stretch lines are observed as pigmented brown lines running alongside the large choroidal vessels, which represent a proliferation of RPE cells on and around the large choroidal vessels.

Keywords

Lacquer cracks · Simple macular hemorrhage · Myopic stretch lines

13.1 Lacquer Cracks

Lacquer cracks are found in the posterior fundus of 4.2–15.7% of highly myopic eyes [1–5]. They represent healed and mechanical breaks of the retinal pigment epithelium (RPE), Bruch's membrane, and choriocapillaris complex [2, 3]. Lacquer cracks are observed as yellowish linear lesions [2] (Fig. 13.1) and show linear hyper-fluorescence by fluorescein angiography (FA) [6] (Figs. 13.1, 13.2). Fundus autofluorescence (AF) shows hypo-autofluorescence, (Fig. 13.1) which is due to the atrophied RPE overlying the rupture. Lacquer cracks show hypo-fluorescence in the late-phase indocyanine green angiography (ICGA) [7] (Fig. 13.1).

Lacquer cracks are observed as discontinuities of the RPE and an increased penetration of the light through the choroid by optical coherence tomography (OCT) [8] (Figs. 13.1, 13.2, 13.3). OCT angiography shows a partial defect of choriocapillaris in the region of lacquer cracks [9] (Fig. 13.4).

Progression patterns of lacquer cracks are: an increase in number, elongation, and progression to patchy atrophy [10]. An increase in number of lacquer cracks is the most frequent progression pattern. New lacquer cracks tend to occur perpendicularly from the existing lacquer cracks (branching) (Figs. 13.5, 13.6), or in parallel with the existing lacquer cracks. An elongation of existing lacquer cracks is also observed. In some cases, focal disruption of outer retinal layers and RPE atrophy occurs, with increased penetration of light through the inner choroid. Lacquer cracks increase their width and progress to patchy atrophy with time (Fig. 13.7). In some eyes, this progression is not a uniform widening of pre-existing lacquer cracks but small circular areas of patchy atrophy first develop along the course of lacquer cracks, and then these circular areas enlarge and fuse with each other (Fig. 13.8).

In some cases, the lesions with punctate inner choroidopathy are aligned in a linear fashion, which needs to be differentiated from lacquer cracks.

K. Uramoto (✉)
Department of Ophthalmology and Visual Science, Tokyo Medical and Dental University, Tokyo, Japan

X. Xu
Department of Ophthalmology, Shanghai General Hospital, Shanghai Jiao Tong University, Shanghai, China

K. Ohno-Matsui (ed.), *Atlas of Pathologic Myopia*, https://doi.org/10.1007/978-981-15-4261-9_13

Fig. 13.1 Lacquer crack seen in the right fundus of a 52-year-old woman with a refractive error of -10.25 diopters and an axial length of 30.6 mm. (Top Left). Right fundus shows a lacquer crack (LC) inferior to the fovea as an yellowish linear lesion. The best-corrected visual acuity is 1.2. (Top Middle). Fundus autofluorescence (FAF) shows the LC as linear hypo-autofluorescence. (Top Right). Fluorescein angiogram (FA) shows linear hyper-fluorescence at the site of the LC. (Bottom Left). Late angiographic phase of indocyanine angiography (ICGA) shows hypo-fluorescence at the site of the LC. (Bottom Right). A vertical OCT section across the fovea shows a discontinuity of the retinal pigment epithelium and an increase in the light penetration into the deeper tissue

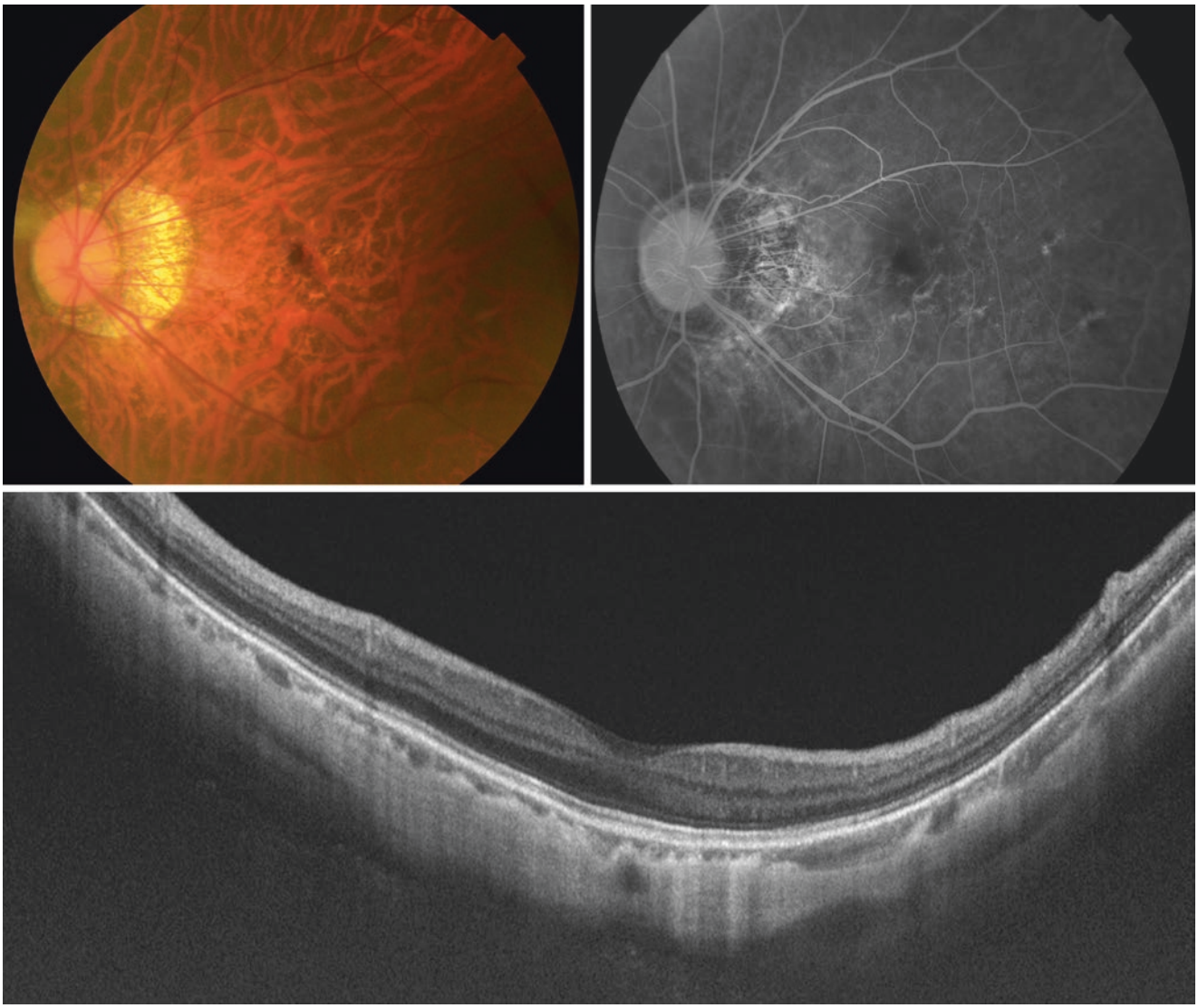

Fig. 13.2 Multiple lacquer cracks (LCs) in the left fundus of a 48-year-old man with refractive error of -12.0 diopters and an axial length of 30.5 mm. (Top Left). Left fundus shows multiple LCs mainly temporal to the fovea. The best-corrected visual acuity is 1.2. (Top Right). Fluorescein angiogram (FA) shows hyper-fluorescence at the site of the LCs. (Bottom). Swept-source OCT image shows an increased penetration of light into deeper tissue at the site of LCs

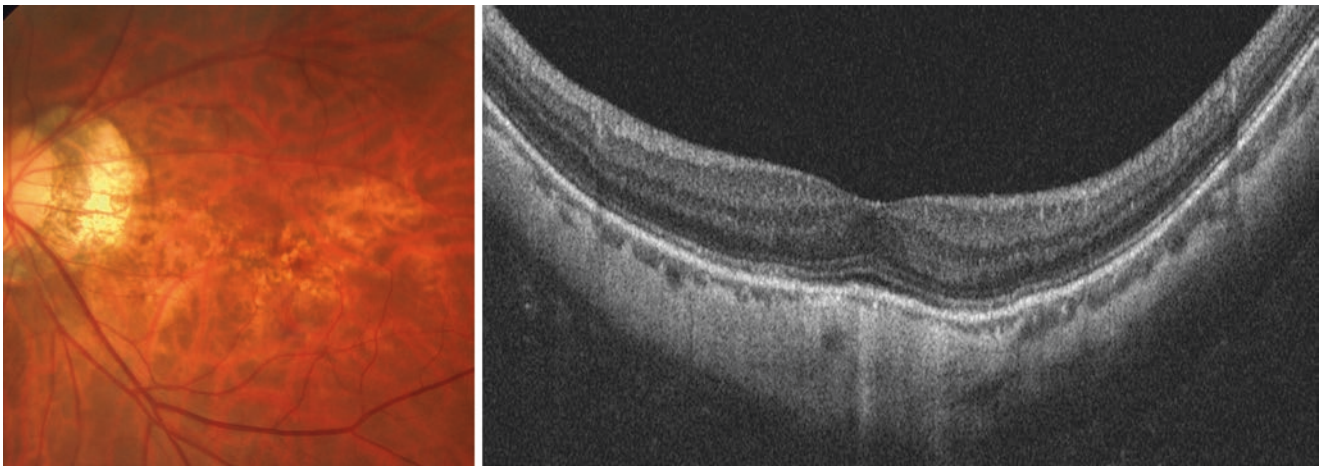

Fig. 13.3 Multiple lacquer cracks (LCs) in the left fundus of a 63-year-old woman with refractive error of -15.00 diopters and an axial length of 29.2 mm. (Left). Left fundus shows multiple LCs in the macular area. The best-corrected visual acuity is 0.8. (Right). An oblique section of swept-source OCT scans shows an increased penetration of the light at the subfovea at the sites of LCs

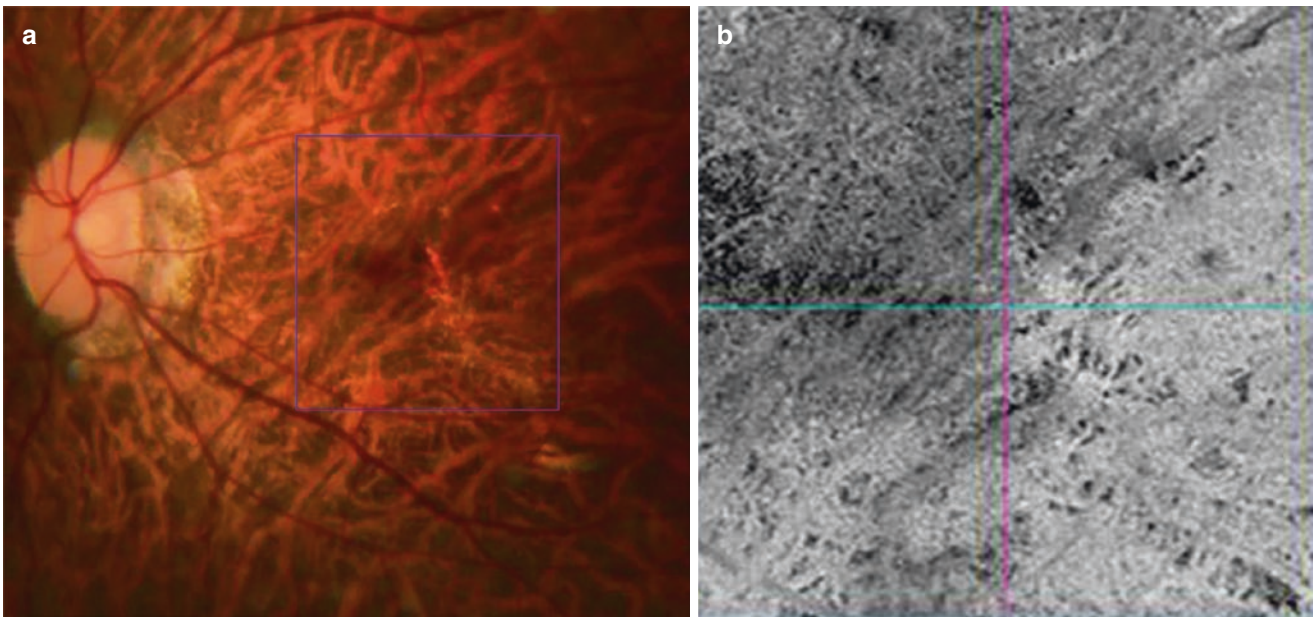

Fig. 13.4 Loss of choriocapillaris at the site of lacquer cracks (LCs) shown by OCT angiography (OCTA) in the left fundus of a 26-year-old man with refractive error of -14.25 diopters and an axial length of 31.2 mm. (Left) Left fundus shows multiple LCs in the macula. The best-corrected visual acuity is 1.2. The blue frame indicates an area scanned by OCTA. (Right) OCTA image shows a partial loss of the choriocapillaris in the area of the LCs

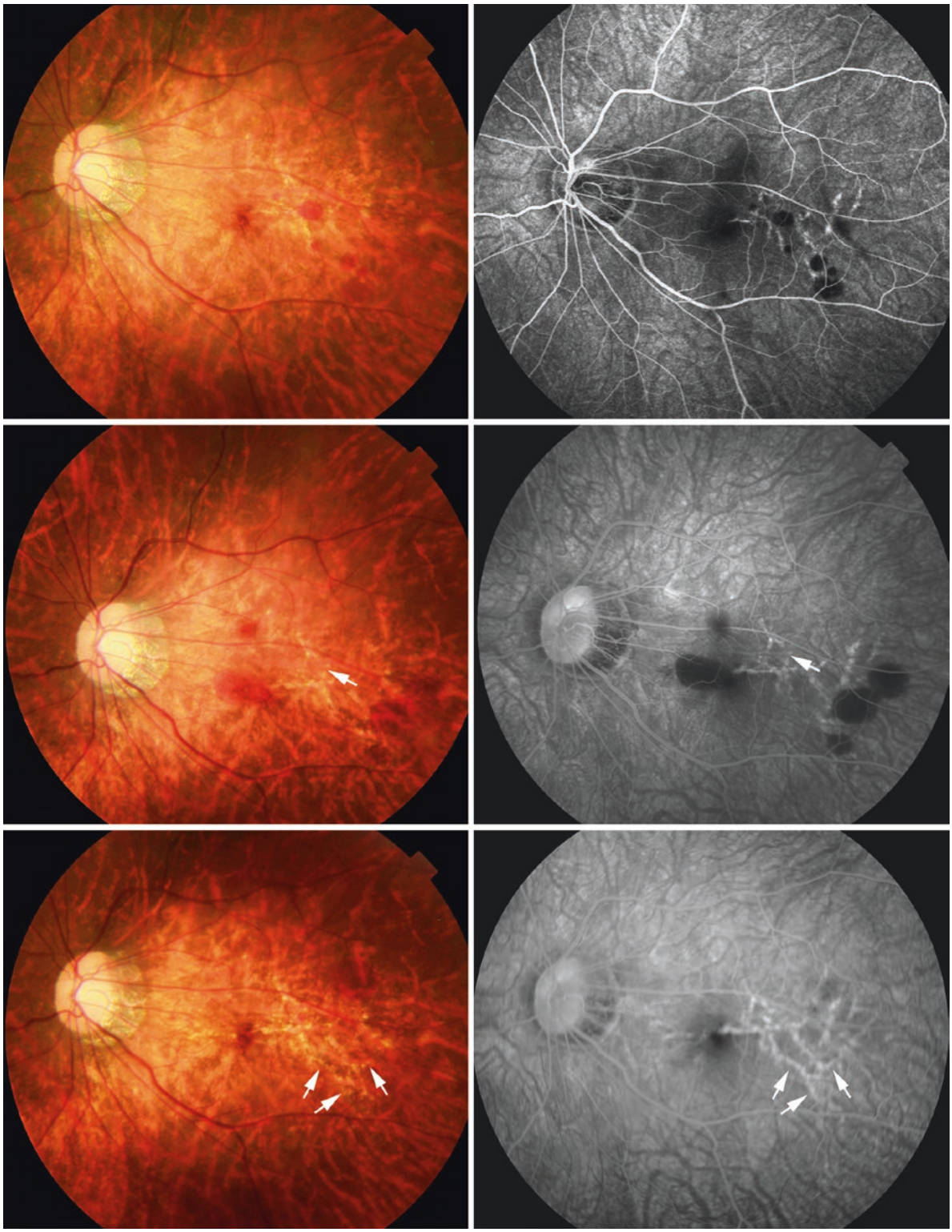

Fig. 13.5 Increase in number of lacquer cracks (LCs) by branching from the preexisting LCs in the left fundus of an 18-year-old woman with refractive error of -20.9 diopters and an axial length of 31.5 mm. (Top Left) Left fundus at the initial examination (December 2014) shows multiple LCs and spotty retinal hemorrhages temporal to the fovea. The best-corrected visual acuity is 1.0. (Top Right) Fluorescein angiogram (FA) at the initial examination shows linear hyper-fluorescence at the sites of the LCs. Blocked fluorescence due to simple hemorrhage (an indicator of new LC formation) is seen along the LCs. (Middle Left) Three months later (March 2015), new LC (arrow) with a branching pattern occurring from the existing LCs is seen. Multiple spots of simple bleeding have appeared. (Middle Right) FA at 3 months after the initial visit. New LC branched from the original LCs shows clear linear hyper-fluorescence (arrow). (Bottom Left) Left fundus at 9 months after the initial visit (September 2015) shows a formation of many new LCs branching from preexisting LCs. (Bottom Right) FA at 9 months after the initial visit shows clear linear hyper-fluorescence at the site of newly formed LCs

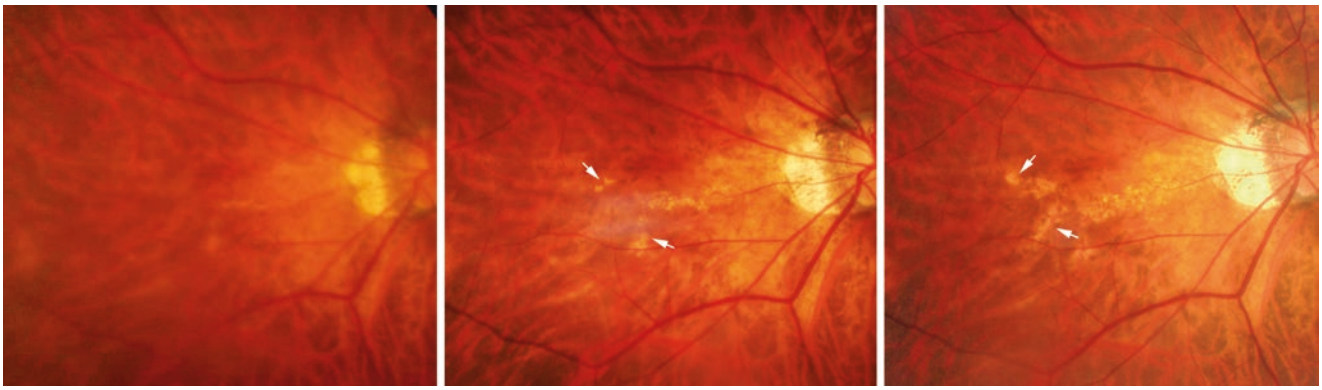

Fig. 13.6 Increase in number of lacquer cracks (LCs) by branching from the preexisting LCs in the right fundus of a 76-year-old woman with an axial length of 29.6 mm (Left). Right fundus at the initial examination shows a horizontal LC in the fovea. The best-corrected visual acuity is 0.9 (Middle). Eighteen months later, two new LCs have developed superior and inferior to the fovea (arrows) (Right). At 3.5 years after the initial visit, new LCs have developed temporal to the preexisting LCs (arrow) by branching and elongating from original LCs

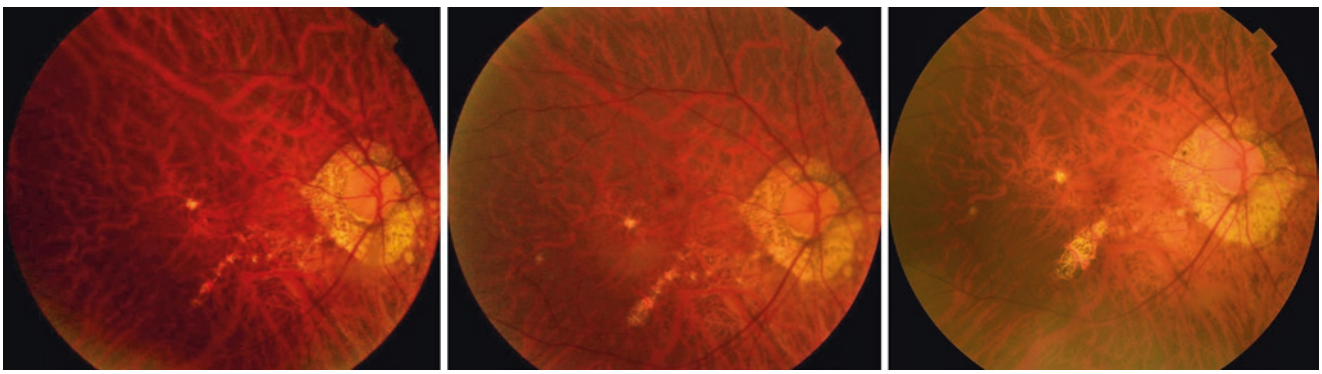

Fig. 13.7 Progression from lacquer cracks (LCs) to patchy atrophy in the right fundus of a 65-year-old man with refractive error of -11.4 diopters and an axial length of 29.2 mm. (Left) Right fundus at the initial examination shows yellowish LC inferior to macula. A small spotty lesion is seen upper temporal to the fovea. The best-corrected visual acuity is 0.9 (Middle) One year later, the LC has widened especially near its lowest end (Right) Six years after the initial examination, the LC has further widened and has progressed to patchy atrophy

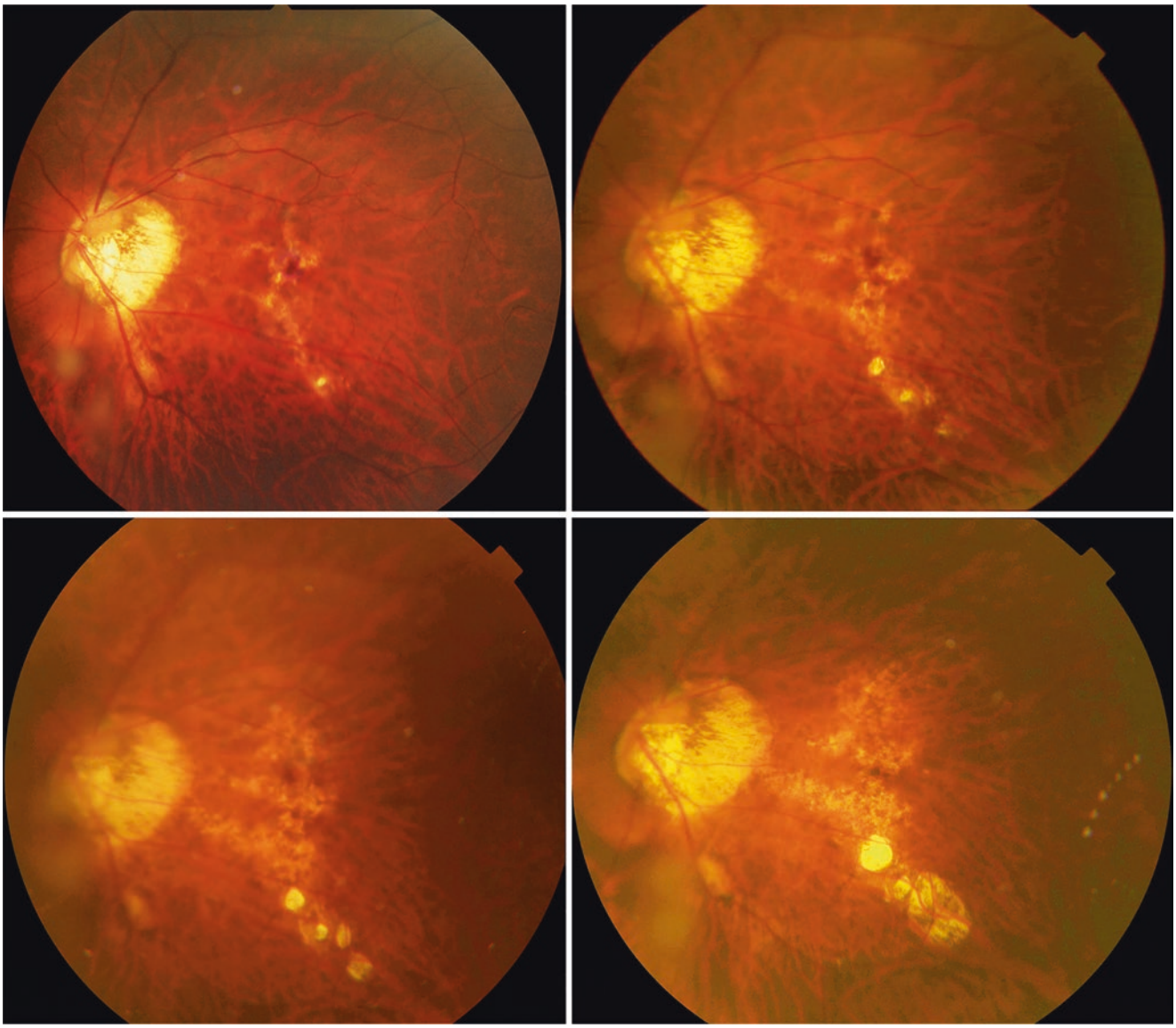

Fig. 13.8 Progression from lacquer cracks (LCs) to patchy atrophy in the left fundus of a 59-year-old woman with refractive error of -16.0 diopters and an axial length of 28.8 mm. (Top Left) Left fundus at the initial examination shows multiple lacquer cracks (LCs) in and lower to the macula. A tiny patchy atrophy is seen near the lowest end of LC. The best-corrected visual acuity is 1.0. (Top Right) Two years later, new lesions of patchy atrophy have appeared along the course of LC. (Bottom Left) Left fundus at 5 years after the initial examination shows an enlargement of the lesions of patchy atrophy. (Bottom Right) Left fundus at around 10 years after the first visit shows that the lesions of patchy atrophies have further enlarged and have coalesced with each other. Diffuse atrophy has also enlarged and original LCs have become less obvious

13.2 Simple Macular Hemorrhage

A rupture of Bruch's membrane and choriocapillaris complex results in subretinal bleeding, which is an indicator of new lacquer crack formation [11].

Simple hemorrhage is a term used for macular hemorrhage without macular neovascularization that occurs in highly myopic eyes and is most likely caused by the mechanical rupture of Bruch's membrane and choriocapillaris complex (Figs. 13.9, 13.10, 13.11).

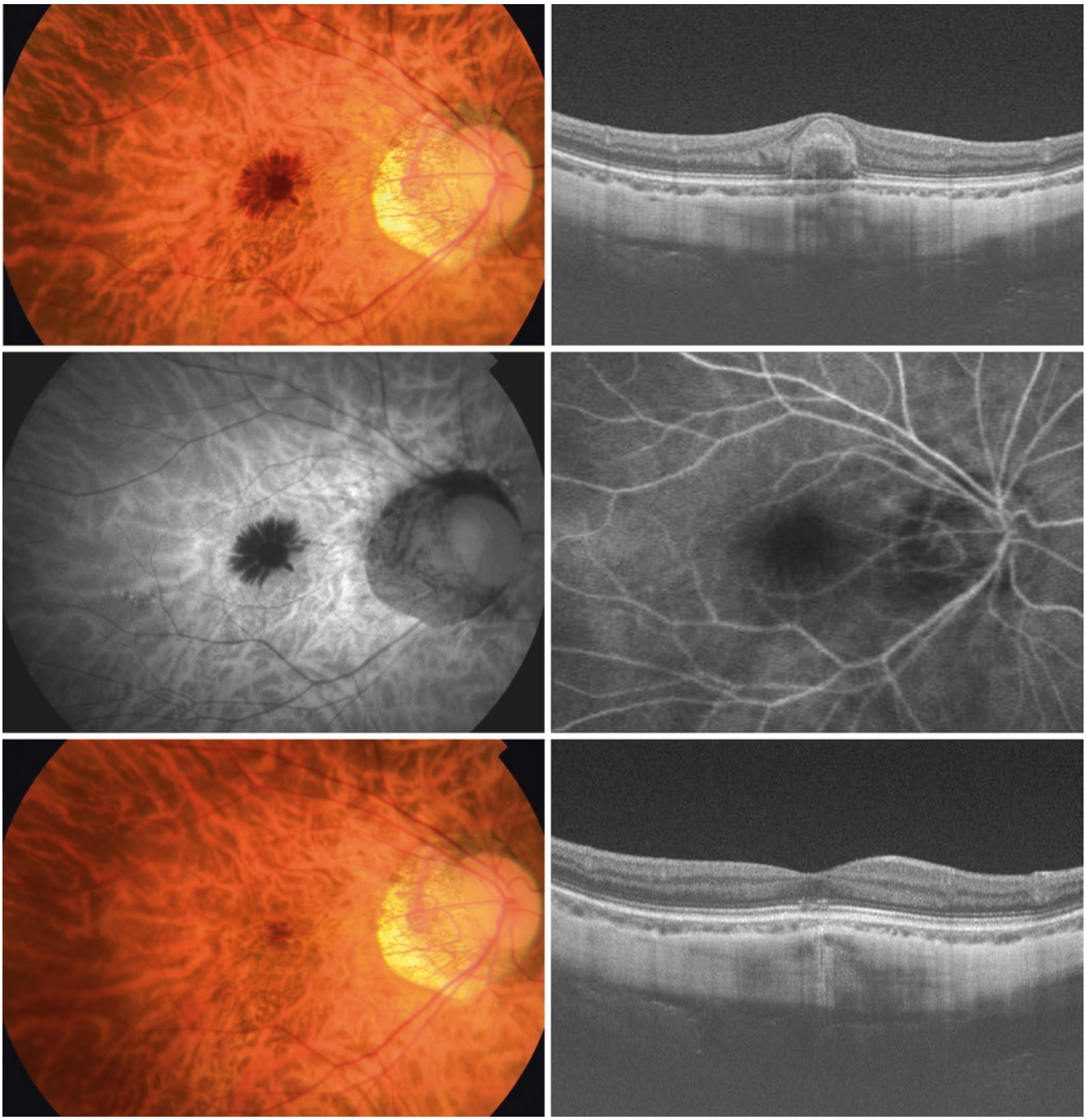

Fig. 13.9 Simple macular hemorrhage in the right fundus of a 49-year-old woman with refractive error of -14.3 diopters and an axial length of 30.5 mm. (Top Left) Right fundus shows macular hemorrhage. Hemorrhage shows projections along the Henle's layer. The best-corrected visual acuity (BCVA) is 0.1. (Top Right) OCT image shows well-demarcated subretinal hemorrhage. No exudative changes are seen. (Middle Left) Fundus autofluorescence (FAF) shows blocked auto-fluorescence at the site of hemorrhage. (Middle Right) Fluorescein angiogram (FA) shows no hyper-fluorescence indicating the macular neovascularization. (Bottom Left) Seven months later, the hemorrhage has disappeared and the BCVA has improved to 0.7. (Bottom Right) OCT image at 7 months after the onset shows a resolution of subretinal hemorrhage, leaving an irregularity of ellipsoid zone and an increase of the penetration of light into deeper tissues

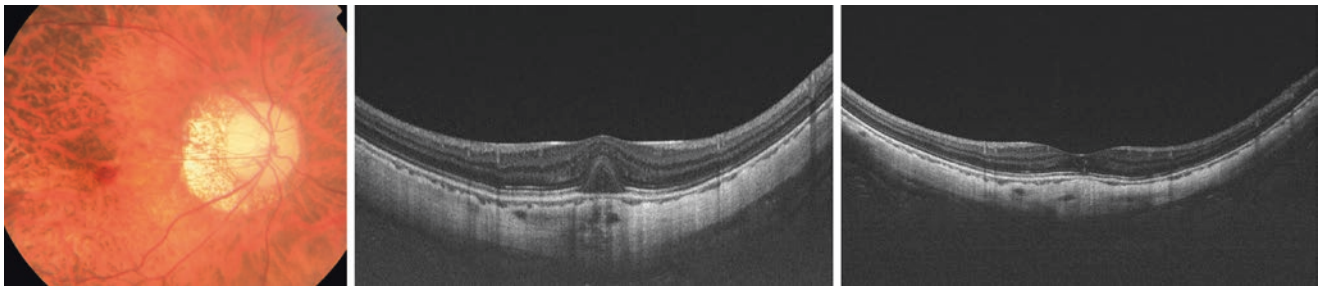

Fig. 13.10 Simple macular hemorrhage in the right fundus of a 36-year-old man with refractive error of -16.8 diopters and the axial length of 33.0 mm. (Left) Right fundus shows macular hemorrhage. The best-corrected visual acuity (BCVA) is 0.7. (Middle) OCT image shows subretinal hemorrhage. (Right) OCT image at 1 month after the onset shows a resolution of hemorrhage. A vertical strand is still seen at the site of previous hemorrhage. The BCVA has improved to 1.0

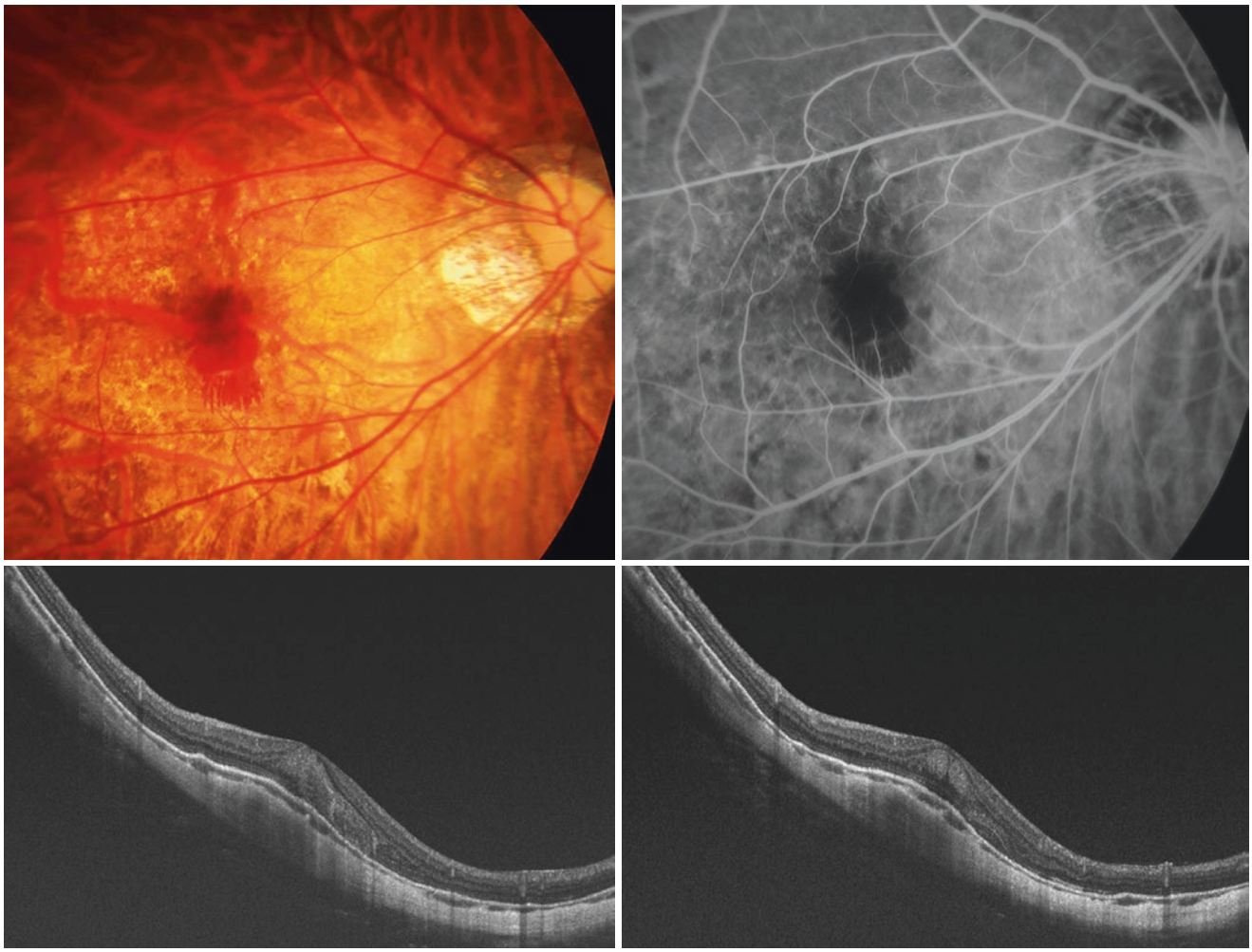

Fig. 13.11 Simple macular hemorrhage in the right fundus of a 50-year-old woman with an axial length of 33.5 mm. (Top Left) Right fundus shows macular hemorrhage. Projection of hemorrhage along the Henle's layer is observed. (Top Right) Fluorescein angiogram shows blocked fluorescence due to hemorrhage. (Second Row) Oblique OCT sections across the fovea show subretinal hemorrhage as well as bleeding penetrating to the inner retina. (Third Row, Left) Six months later, the right fundus shows that the hemorrhage is absorbed. Several lacquer cracks are observed in the macula. (Third Row, Right) Fundus autofluorescence shows slight hypo-autofluorescence at the site of previous hemorrhage. (Bottom) Oblique OCT section shows that the hemorrhage is almost completely resolved. A vertical strand is seen in the area of previous hemorrhage

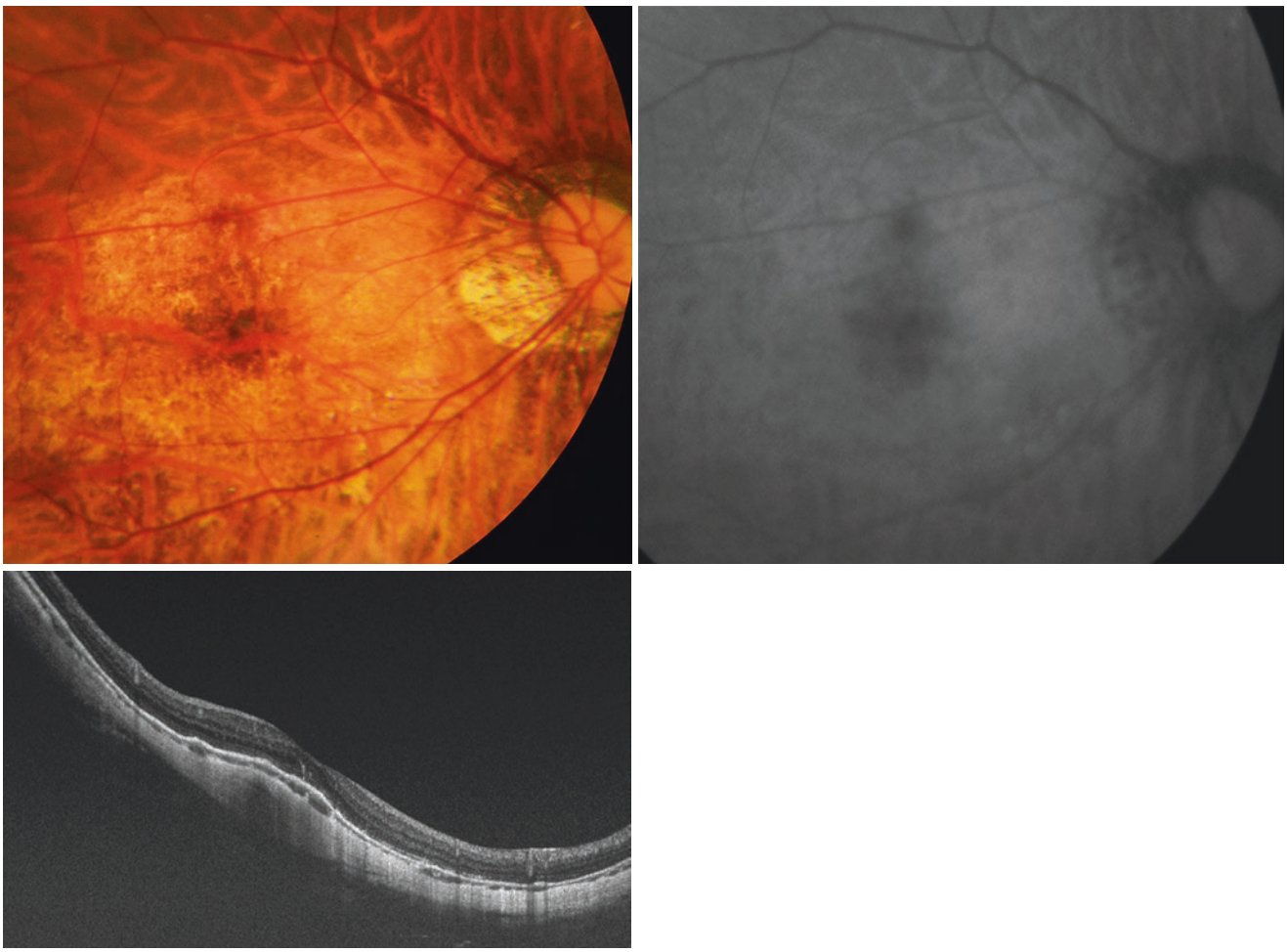

Fig. 13.11 (continued)

13.3 Myopic Stretch Lines

Myopic stretch lines are observed as pigmented brown lines running alongside the large choroidal vessels, in eyes with pathologic myopia. Different from lacquer cracks, fundus auto-fluorescence (FAF) shows linear hyper-autofluorescence. Different from lacquer cracks, myopic stretch lines are hypo-fluorescent in fluorescein angiogram (FA). OCT images show irregularities or clumps of RPE on and around the large choroidal vessels. These findings suggest that myopic stretch lines might represent a proliferation of RPE cells on and around the remaining large choroidal vessels in the area with almost absence of inner choroid [12]. Such proliferations or clumps of RPE cells are probably the source of the hyper-autofluorescence in the FAF images and the hypo-fluorescence both in FA and indocyanine angiography (ICGA) images due to the blockage of background fluorescence (Figs. 13.12, 13.13).

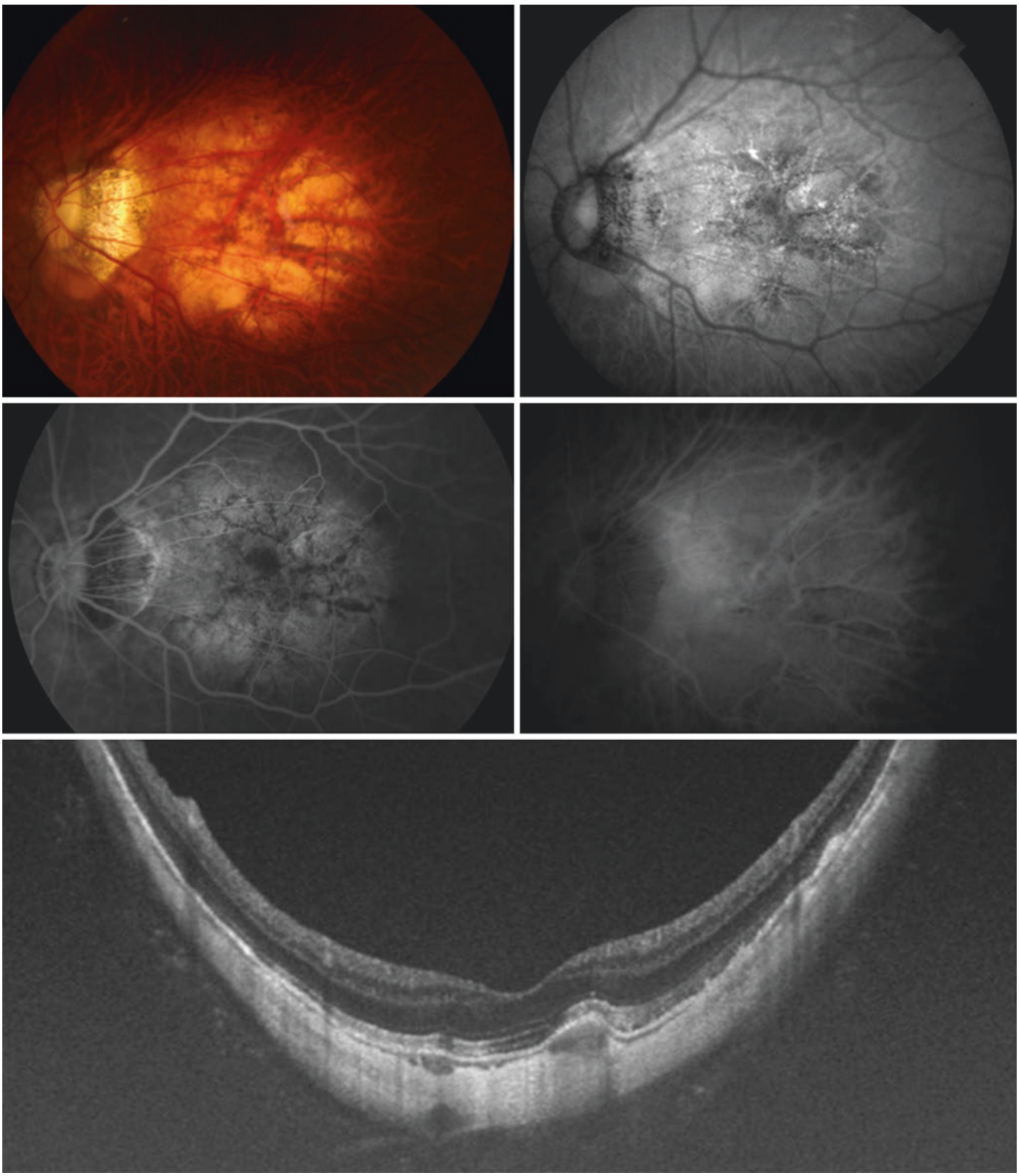

Fig. 13.12 Myopic stretch lines in the left fundus of a 62-year-old man with refractive error of -18.3 diopters and the axial length of 31.7 mm (modified with permission from [12]). (Top Left) Left fundus shows brownish pigmented linear lesions along the large choroidal vessels. The best-corrected visual acuity (BCVA) is 0.5. (Top Right) Fundus auto-fluorescence (FAF) shows linear hyper-AF at the site of myopic stretch lines. (Middle Left) Fluorescein angiogram (FA) shows linear hypo-fluorescence at the site of myopic stretch lines. FA features are distinctly different from lacquer cracks. (Middle Right) Indocyanine angiography (ICGA) shows linear hypo-fluorescence along the large choroidal vessels. (Bottom) A vertical OCT section across the fovea shows irregular clumping of the retinal pigment epithelium on and around the large choroidal vessel. This large choroidal vessel seems protruded toward the retina

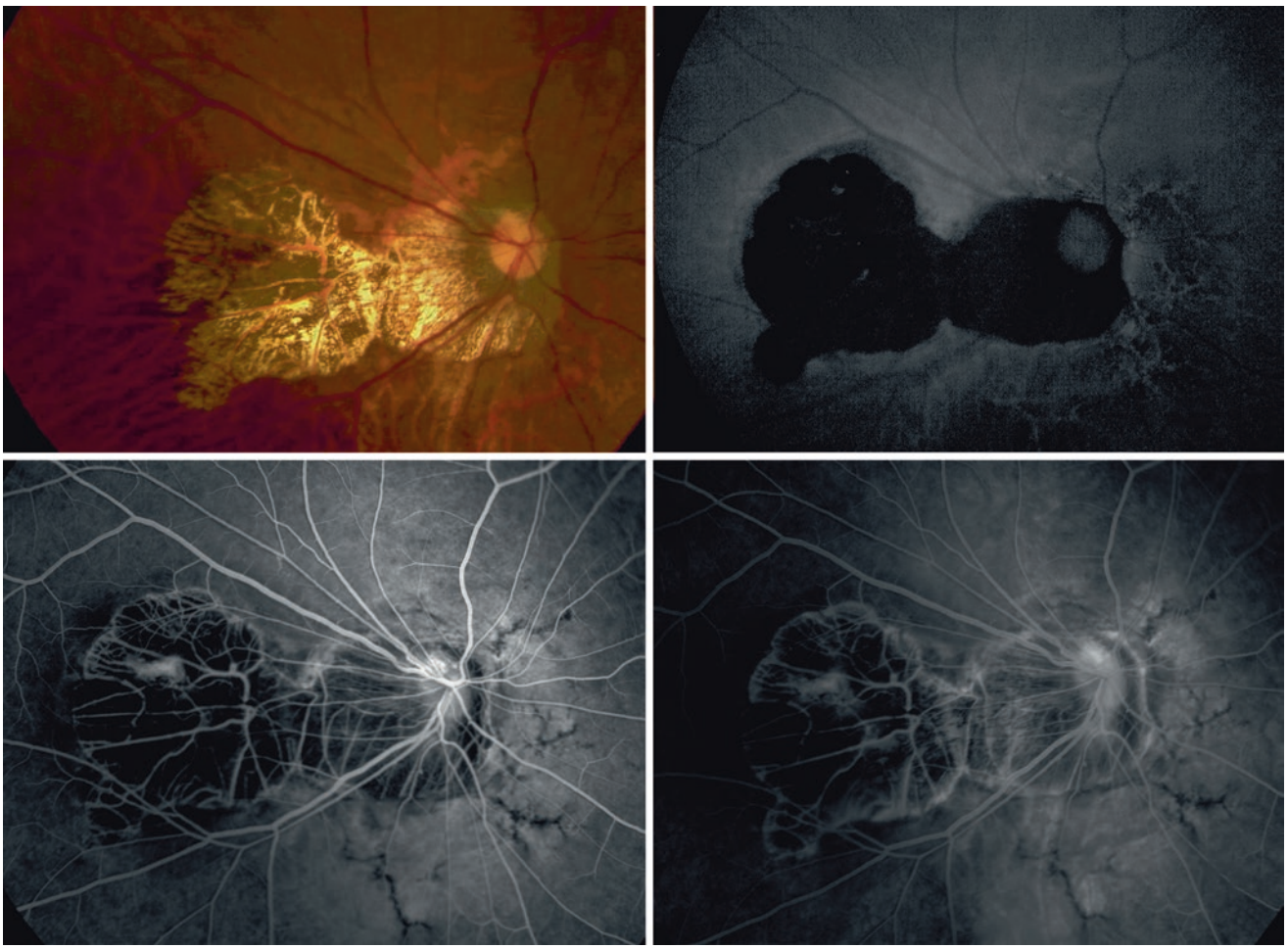

Fig. 13.13 Myopic stretch lines in the right fundus of a 64-year-old woman with refractive error of -18.0 diopters and an axial length of 30.9 mm. (Top Left) Right fundus shows myopic macular neovascularization (MNV)-related macular atrophy. Myopic stretch lines are barely detectable in this image. (Top Right) Fundus auto-fluorescence shows myopic stretch lines as linear hyper-autofluorescence (arrows) nasal to the optic disc. (Bottom) Fluorescein angiogram shows myopic stretch lines as consistent hypo-fluorescence (arrows) from the early (Left) to the late angiographic phase (Right)

References

1. Curtin BJ, Karlin DB. Axial length measurements and fundus changes of the myopic eye. Am J Ophthalmol. 1971;71(Pt 1):42–53.
2. Klein RM, Curtin BJ. Lacquer crack lesions in pathologic myopia. Am J Ophthalmol. 1975;79(3):386–92.
3. Grossniklaus HE, Green WR. Pathologic findings in pathologic myopia. Retina (Philadelphia, Pa). 1992;12(2):127–33.
4. Ohno-Matsui K, Yoshida T, Futagami S, Yasuzumi K, Shimada N, Kojima A, et al. Patchy atrophy and lacquer cracks predispose to the development of choroidal neovascularisation in pathological myopia. Br J Ophthalmol. 2003;87(5):570–3.
5. Chang L, Pan CW, Ohno-Matsui K, Lin X, Cheung GC, Gazzard G, et al. Myopia-related fundus changes in Singapore adults with high myopia. Am J Ophthalmol. 2013;155(6):991–9.
6. Liu CF, Liu L, Lai CC, Chou JC, Yeh LK, Chen KJ, et al. Multimodal imaging including spectral-domain optical coherence tomography and confocal near-infrared reflectance for characterization of lacquer cracks in highly myopic eyes. Eye. 2014;28(12):1437–45.
7. Ohno-Matsui K, Morishima N, Ito M, Tokoro T. Indocyanine green angiographic findings of lacquer cracks in pathologic myopia. Jpn J Ophthalmol. 1998;42(4):293–9.
8. Querques G, Corvi F, Balaratnasingam C, Casalino G, Parodi MB, Introini U, et al. Lacquer cracks and perforating scleral vessels in pathologic myopia: a possible causal relationship. Am J Ophthalmol. 2015;160(4):759–66.
9. Sayanagi K, Ikuno Y, Uematsu S, Nishida K. Features of the choriocapillaris in myopic maculopathy identified by optical coherence tomography angiography. Br J Ophthalmol. 2017;101(11):1524–9.
10. Xu X, Fang Y, Uramoto K, Nagaoka N, Shinohara K, Yokoi T, et al. Clinical features of lacquer cracks in eyes with pathologic myopia. Retina (Philadelphia, Pa). 2019;39(7):1265–77.
11. Ohno-Matsui K, Ito M, Tokoro T. Subretinal bleeding without choroidal neovascularization in pathologic myopia. A sign of new lacquer crack formation. Retina (Philadelphia, Pa). 1996;16(3):196–202.
12. Shinohara K, Moriyama M, Shimada N, Tanaka Y, Ohno-Matsui K. Myopic stretch lines: linear lesions in fundus of eyes with pathologic myopia that differ from lacquer cracks. Retina (Philadelphia, Pa). 2014;34(3):461–9.

Radial Tracts

14

Tomoka Ishida

Abstract

Radial tracts are linear or leaf-like lesions with abnormal autofluorescence and radiate toward periphery from the staphyloma edges. Unlike descending tracts seen in central serous chorioretinopathy, radial tracts run upwards against the gravity.

Keywords

Posterior staphyloma · Radial Tracts · Fundus autofluorescence

Radial tracts are linear or leaf-like lesions with abnormal autofluorescent (AF) patterns and radiate toward the periphery from staphyloma edges. Radial tracts are observed in 7.7% of high myopic eyes with posterior staphyloma [1]. Radial tracts are most commonly observed from the superior edge of the staphyloma. The number of the lesions is 1–4 per eye [1].

The AF patterns of radial tracts are divided into three patterns: (1) uniform hyper-AF, (2) granular hypo-AF surrounded by hyper-AF rim or (3) confluent hypo-AF [1].

Optical coherence tomographic images show serous retinal detachment and/or absence of outer retina/retinal pigmented epithelium (RPE) in the area of radial tracts [1]. Figures 14.1–14.4 are representative images of radial tracts.

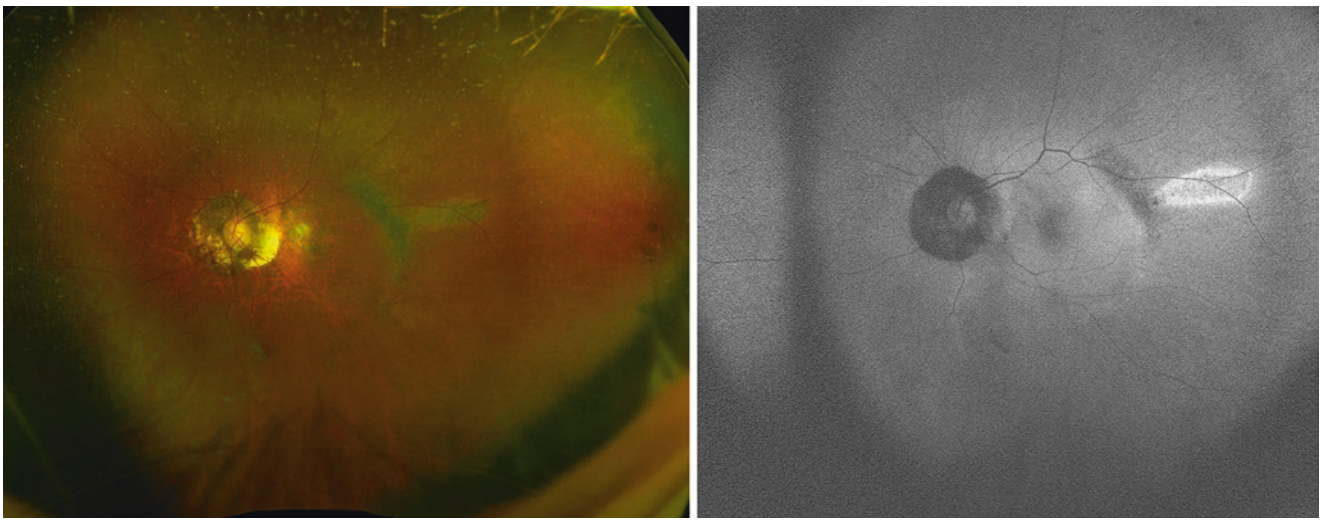

Fig. 14.1 Radial tracts with uniform hyper-autofluorescence (AF). Cited with permission from [1]. Left fundus of an 84-year-old woman with an axial length of 27.1 mm shows one radial tract emanating from the temporal edge of the staphyloma. AF image shows uniform hyper-AF in the area of the radial tract

T. Ishida (✉)
Department of Ophthalmology and Visual Science, Tokyo Medical and Dental University, Tokyo, Japan

Department of Ophthalmology, Kyorin University, Tokyo, Japan
e-mail: tom-oph@ks.kyorin-u.ac.jp

K. Ohno-Matsui (ed.), *Atlas of Pathologic Myopia*, https://doi.org/10.1007/978-981-15-4261-9_14

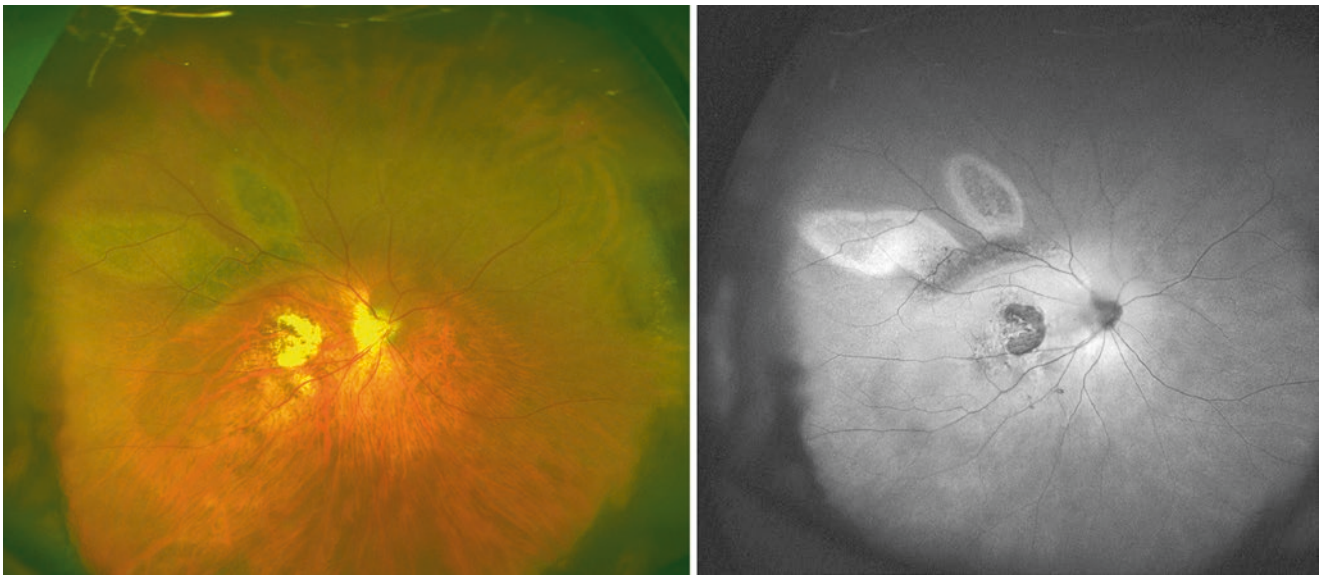

Fig. 14.2 Radial tracts with granular hypo-AF surrounded by hyper-AF rim. Cited with permission from [1]. Right fundus of a 75-year-old woman with an axial length of 28.2 mm shows two radial tracts spreading from the upper-temporal edge toward the periphery. AF image shows granular hypo-AF surrounded by hyper-AF rim in the area of the radial tracts. The left tract is wider and is bent like a dog ear

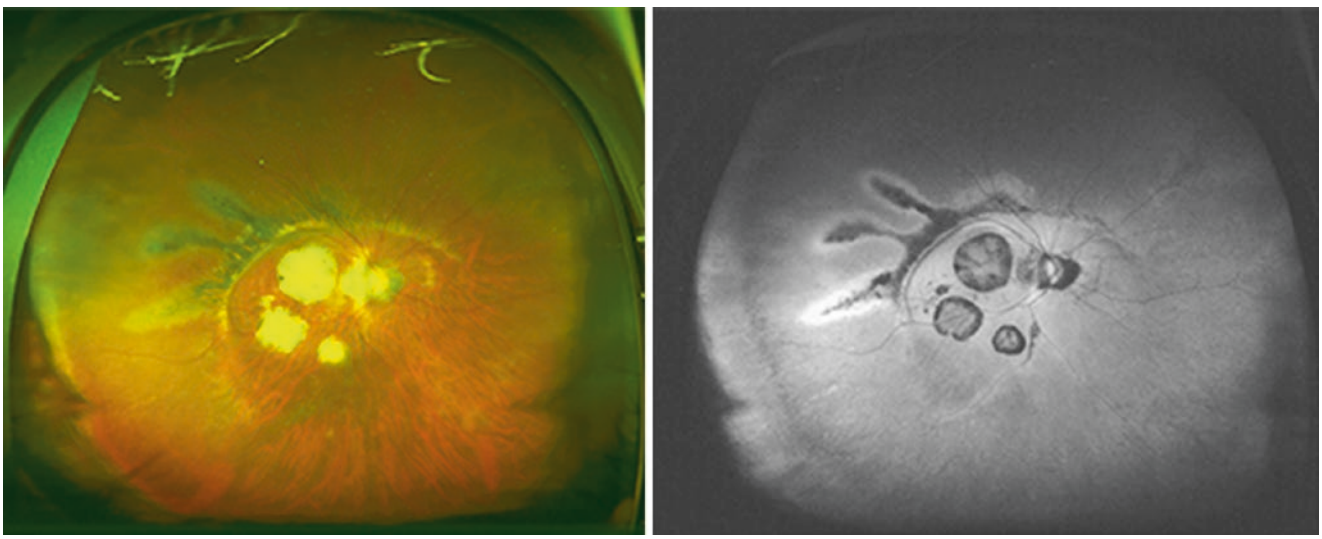

Fig. 14.3 Radial tracts with hypo-autofluorescence (AF). Cited with permission from [1]. Right fundus of a 60-year-old woman with an axial length of 29.3 mm shows three radial tracts radiating from the upper-temporal edge of wide macular staphyloma. AF image shows that these three tracts are granular hypo-AF surrounded by hyper-AF rim. In the leftmost tract, a patchy area of confluent hypo-AF is seen within the granular hypo-AF area

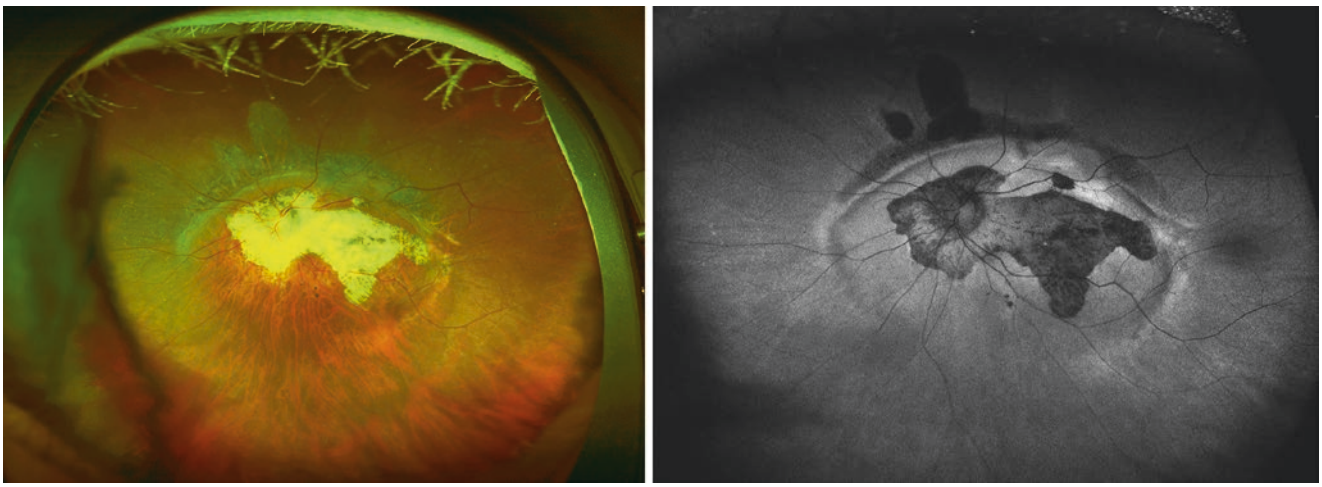

Fig. 14.4 Radial tracts with hypo-autofluorescence (AF). Cited with permission from [1]. Right fundus of an 81-year-old woman with an axial length of 27.4 mm shows three radial tracts emanating from the upper edge of the wide macular staphyloma. AF image shows that the two radial tracts in the left show confluent hypo-AF and the right one shows uniform hyper-AF

Reference

1. Ishida T, Moriyama M, Tanaka Y, Shinohara K, Shimada N, Yoshida T, Ohno-Matsui K. Radial tracts emanating from staphyloma edge in eyes with pathologic myopia. Ophthalmology. 2015;122(1):215–6. PMID: 25234014

Other Fundus Lesions

15

Yuichiro Kaneko

Abstract

In eyes with pathologic myopia, an alteration of retinal and choroidal vascular system is seen in a wide area of the fundus. Representative changes include peripheral retinal avascular zone and macular vortex veins. Wide-field fundus angiograms are powerful tools to examine the pathologies of retinal and choroidal vasculature in a wide area.

Keywords

Peripheral avascular zone · Macular vortex vein · Fluorescein angiogram · Indocyanine green angiogram

15.1 Peripheral Avascular Zone

Wide-field fluorescein angiography showed the areas of nonperfusion in the far periphery in 83% of the eyes with pathologic myopia [1] (Figs. 15.1 and 15.2). In addition to a closure of retinal capillaries, retinal arterioles and venules are all occluded as observed by an abrupt ending. In some patients, peripheral avascular zone reaches near the border of posterior staphyloma. The pathogenesis of peripheral avascular zone is not fully clear; however, one possibility is that the vessel-free zone that normally exists in the far periphery becomes wider in axially elongated eyes.

Also, retinal capillary telangiectasia and microaneurysms are commonly seen in the periphery of eyes with pathologic myopia.

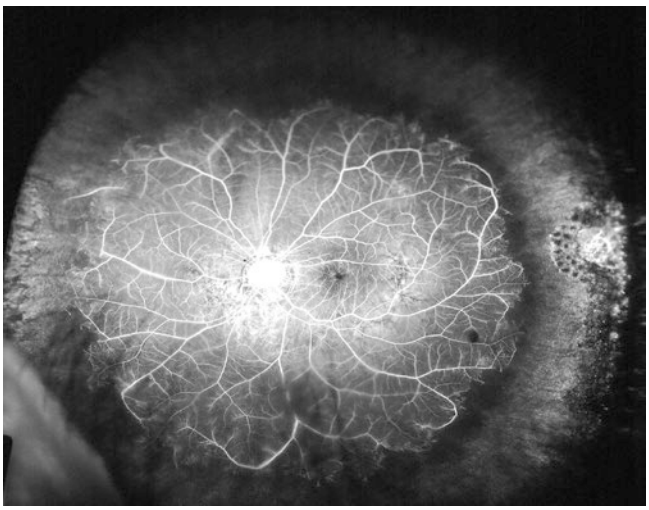

Fig. 15.1 Wide-field fluorescein angiogram showing the peripheral avascular zone in the left fundus of a 59-year-old man with an axial length of 33.0 mm. Reproduced with permission from [1]. Retinal nonperfused area is seen in 360 degree in the peripheral fundus. Retinal capillaries, retinal arterioles, and venules all end abruptly in the periphery. This patient has a history of laser photocoagulation for retinal hole in the temporal fundus

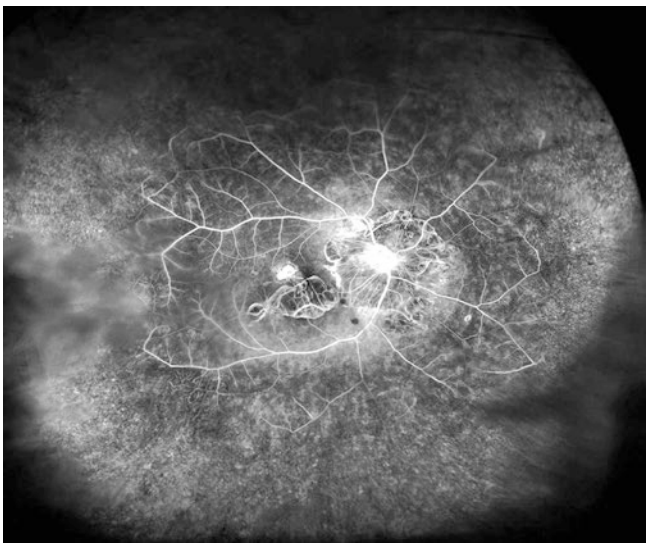

Fig. 15.2 Wide-field fluorescein angiogram showing a very large peripheral avascular zone in the right fundus of a 78-year-old woman with an axial length of 29.0 mm. Reproduced with permission from [1]. All of the retinal arterioles, venules, and capillaries end in the midperiphery. A wide area of granular hyperfluorescence suggesting the changes of the retinal pigmented epithelium is present in the non-perfused area

Y. Kaneko (✉)
Department of Ophthalmology and Visual Science, Tokyo Medical and Dental University, Tokyo, Japan

K. Ohno-Matsui (ed.), *Atlas of Pathologic Myopia*, https://doi.org/10.1007/978-981-15-4261-9_15

15.2 Macular vortex vein (posterior vortex vein)

Choroidal venous blood is usually drained through vortex veins situated in the equator of the eye. However, about 25% of eyes with pathologic myopia have additional vortex veins in the macula (macular vortex vein), and they work as a main venous drainage route in the posterior fundus [2] (Fig. 15.3). The prevalence of posterior staphyloma is significantly higher in eyes with macular vortex veins than those without macular vortex veins [3]. In eyes with macular vortex veins, the orientation of choroidal venous flow is opposite at around mid-peripheral fundus; choroidal venous flow in the posterior segment flows to macular vortex veins, and venous flow outside the posterior segment flows to peripheral vortex veins. In extreme cases, macular vortex veins collect most of the choroidal venous blood, and only scanty vortex veins remain in the periphery (Fig. 15.4) [3]. Branches of macular vortex veins are often dilated. Such stagnation of venous flow may affect the development of myopic maculopathy [4]. In addition to a drainage around the macula, the drainage around the optic disc is also common (Fig. 15.5).

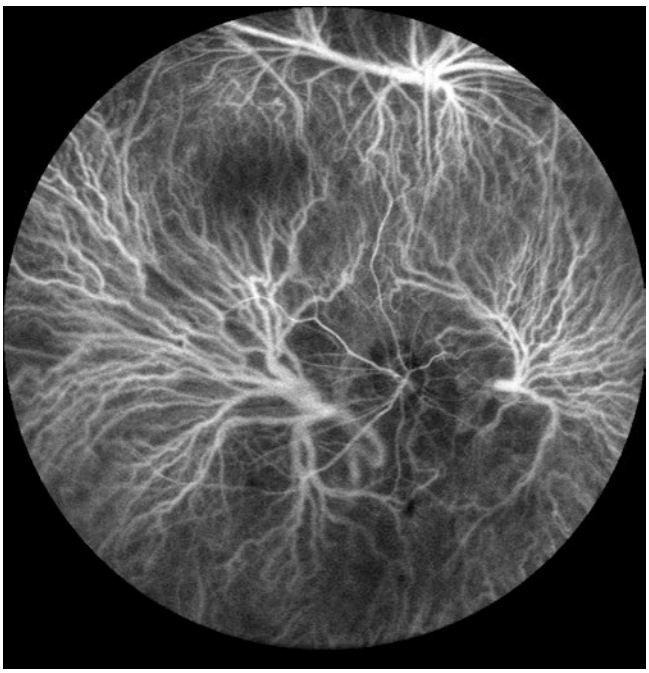

Fig. 15.4 (Reproduced with permission from [3]). Wide-field ICG angiogram showing two posterior vortex veins which cover a very wide area of the fundus. A large posterior vortex vein forms a wide trunk of the ampulla and exits the eye in the macula. This vortex vein covers a wide area up to the periphery. There is another posterior vortex vein draining to nasal to the optic disc. One very small vortex vein remains in the upper periphery

Fig. 15.3 Macular vortex vein in the left fundus of a 62-year-old woman with axial length of 32.3 mm. Macular vortex vein appears to exit the eye at around the fovea. Branches of macular vortex vein are dilated

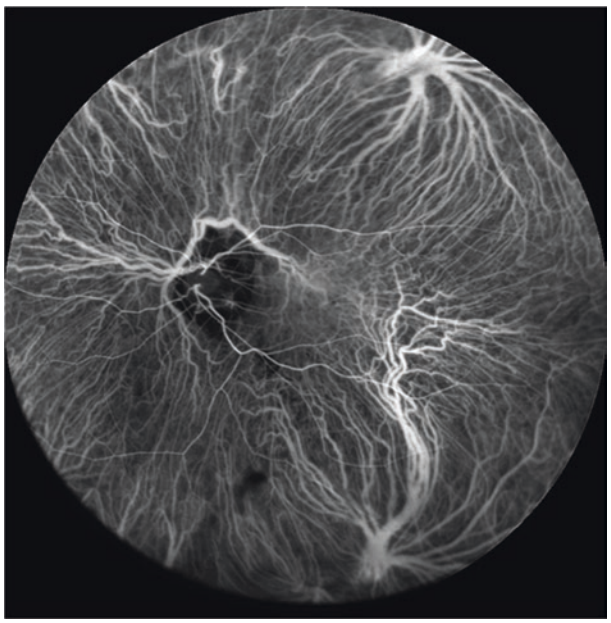

Fig. 15.5 Wide-field ICG angiogram showing posterior vortex vein draining to nasal to the optic disc. This posterior vortex vein seems to collect the venous blood of nasal fundus

References

1. Kaneko Y, Moriyama M, Hirahara S, Ogura Y, Ohno-Matsui K. Areas of nonperfusion in peripheral of eye with pathologic myopia detected by ultra-widefield fluorescein angiography. Invest Ophthalmol Vis Sci. 2014;55(3):1432–9.
2. Ohno-Matsui K, Morishima N, et al. Posterior routes of choroidal blood outflow in high myopia. Retina. 1996;16:419–25.
3. Moriyama M, Cao K, et al. Detection of posterior vortex veins in eyes with pathologic myopia by ultra-widefield indocyanine green angiography. Br J Ophthalmol. 2017;101(9):1179–84.
4. Moriyama M, Ohno-Matsui K, et al. Morphology and long-term changes of choroidal vascular structure in highly myopic eyes with and without posterior staphyloma. Ophthalmology. 2007;114(9):1755–62.

Choroidal Circulatory Changes by Using Wide-Field ICG Angiography

16

Muka Moriyama

Abstract

Various changes of choroidal vasculature are seen in eyes with pathologic myopia especially when they have posterior staphylomas. In addition to "macular vortex vein" shown in the Chap. 15, short posterior ciliary arteries and veins undergo various alterations according to an axial elongation and a staphyloma formation. Such alterations may underlie a development of myopic maculopathy.

Keywords

ICG angiography · Posterior staphyloma · Wide-field fundus imaging · Choroidal circulation

Various features of choroidal circulation in eyes with pathologic myopia are shown by ICG angiography and wide-field angiography, as below.

16.1 Peripheral displacement of emissaries of short posterior ciliary arteries (Fig. 16.1)

A peripheral displacement of emissaries of short posterior ciliary arteries are commonly seen in eyes with pathologic myopia. As a result, there are fewer short posterior ciliary arteries in the posterior fundus than non-highly myopic eyes [1].

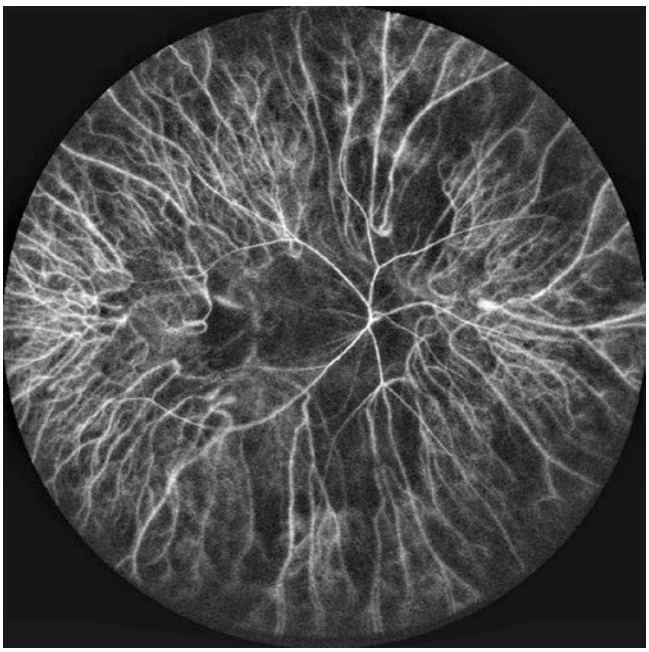

Fig. 16.1 Arterial phase of ICG angiogram shows that short posterior ciliary arteries enter the eye away from the macula, and thus emissaries of short posterior ciliary arteries are shifted peripherally. There are few short posterior ciliary arteries seen in the posterior fundus. [Axial length is 30.0 mm]

16.2 Changes of courses of choroidal veins as well as dilation of choroidal veins (Figs. 16.2 and 16.3)

In some eyes with pathologic myopia, large choroidal veins are less numerous and remaining veins are dilated (Fig. 16.1). Especially in eyes with steep staphyloma edges, choroidal venous flow appears to be stopped at the border of the staphyloma (Fig. 16.2). With time, the choroidal veins change their course through vascular remodeling and tend to flow over less steep edges of staphyloma

M. Moriyama (✉)
Department of Ophthalmology and Visual Science, Tokyo Medical and Dental University, Tokyo, Japan

K. Ohno-Matsui (ed.), *Atlas of Pathologic Myopia*, https://doi.org/10.1007/978-981-15-4261-9_16

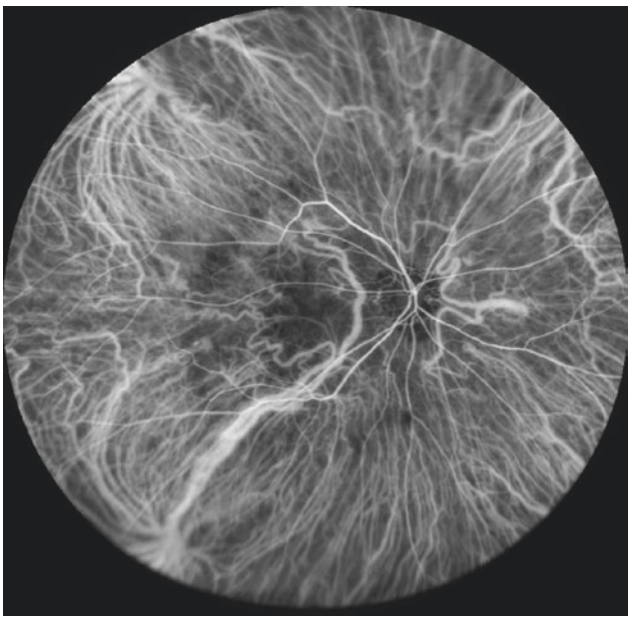

Fig. 16.2 Dilated choroidal veins in pathologic myopia. Venous phase of ICG angiogram shows dilated and tortuous choroidal veins in and around the macula, as well as nasal to the optic disc. Most choroidal venous flow in the posterior fundus flows to lower-temporal vortex vein. Nasal choroidal venous flow exits the eye nasal to the optic disc after forming an ampulla. Axial length is 28.7 mm

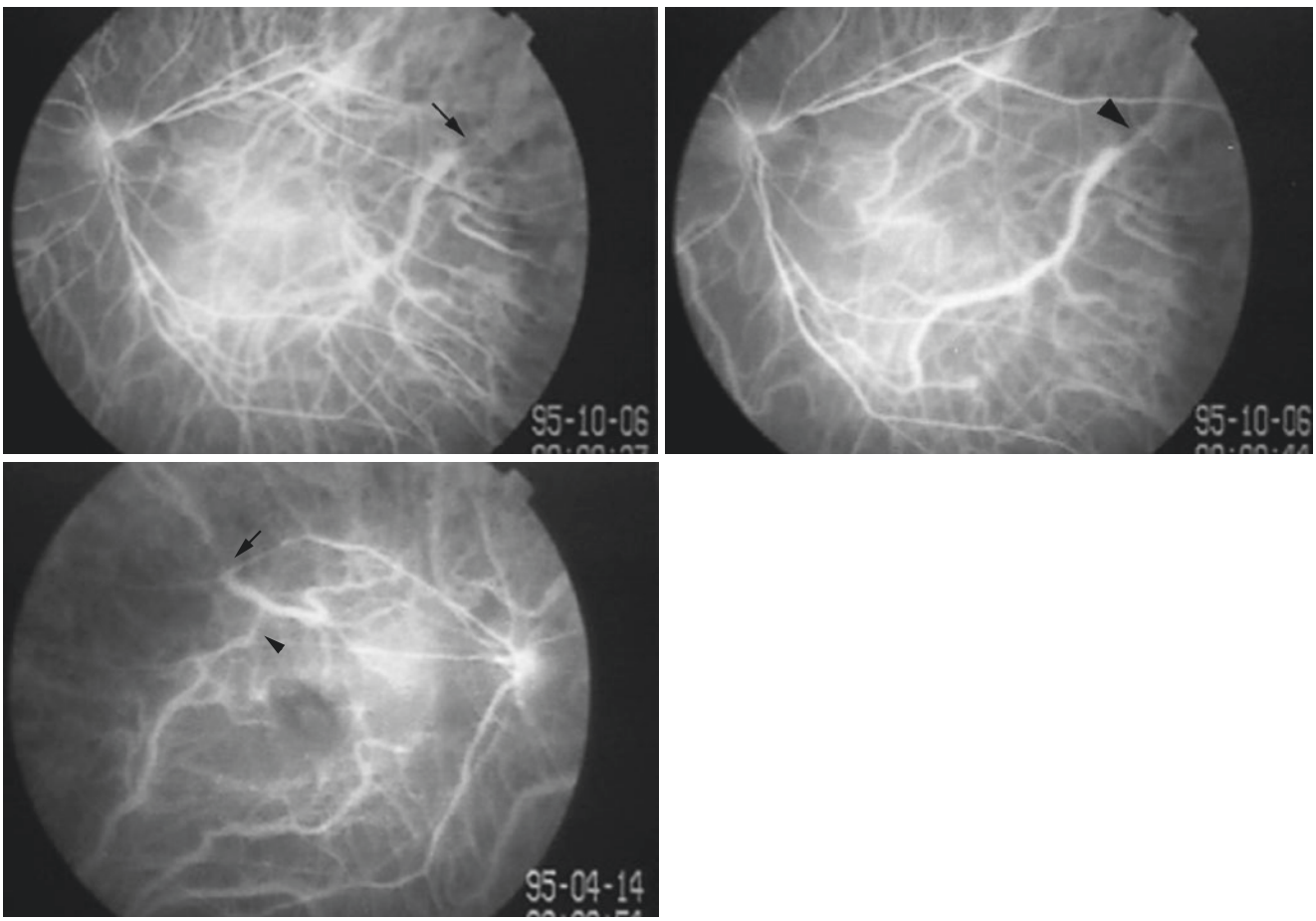

Fig. 16.3 (Top) Disturbed choroidal venous flow at the border of staphyloma. The left fundus of a 62-year-old woman with an axial length of 27.6 mm (Cited with permission from [1]). (Top Left) Twenty seconds after ICG dye injection, the choroidal venous flow appears to be stopped (arrow) at the border of staphyloma. (Top Right) One minute after the dye injection, the choroidal venous flow has gone slowly toward the periphery (arrowhead). (Bottom) Discontinuous choroidal venous flow at the staphyloma margin. The right fundus of a 61-year-old woman with an axial length of 27.7 mm (Cited with permission from [1]). The choroidal venous flow toward the upper periphery is discontinuous at the border of the staphyloma (arrow) and appears to change direction to go toward the inferior periphery through a collateral channel (arrowhead)

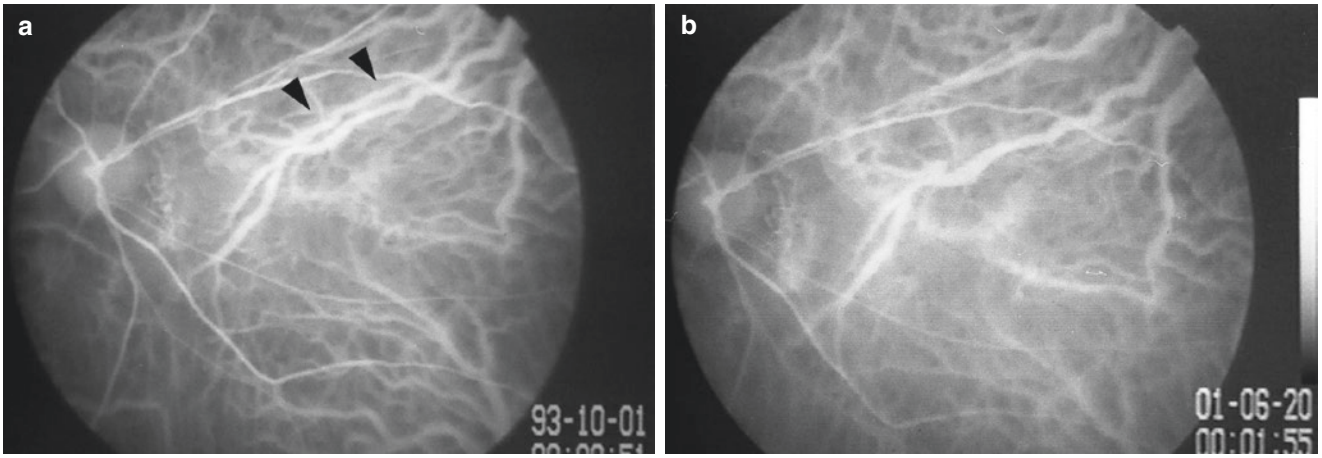

Fig. 16.4 Marked attenuation of a large choroidal vein during a long-term follow-up in the left fundus of a 56-year-old woman with an axial length of 30.4 mm (Cited with permission from [1]). (Left) Two parallel choroidal veins are seen at the initial examination. (Right) Eight years later, one choroidal vein shown by arrowheads in the left image is barely detected

Fig. 16.5 Direct shunt between large choroidal veins. Choroidal veins flowing to upper vortex vein and lower vortex vein directly communicate across the macula. Ampulla of upper vortex vein is not seen. Axial length is 30.0 mm

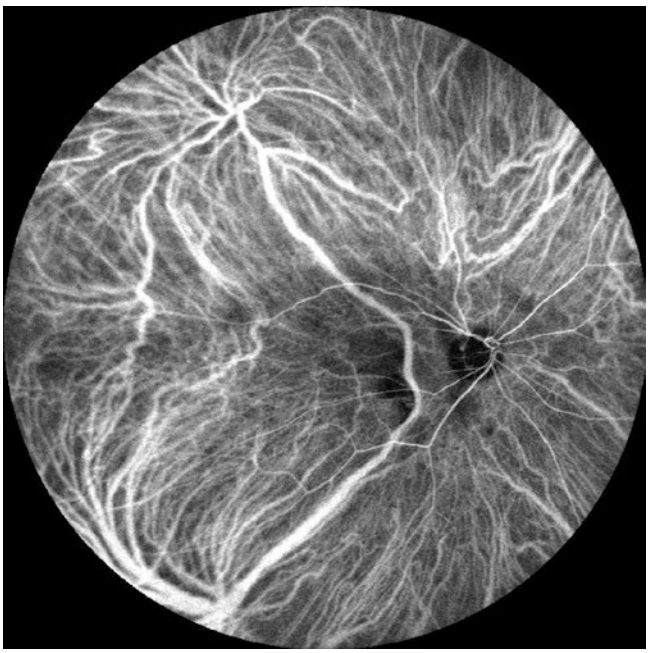

(Fig. 16.3) [1]. Marked attenuation or disappearance of large choroidal veins occurs in a long-term (Fig. 16.4). It seems that when choroidal circulatory disturbance progresses, not all choroidal veins become attenuated uniformly, but only selected veins markedly attenuate or disappear instead.

Such stagnation of choroidal venous flow at the staphyloma edges and the disappearance of selected veins may cause a remarkable change in choroidal vasculature pattern. In some eyes with pathologic myopia, a direct shunt between large choroidal veins is seen (although it is rare) (Fig. 16.3).

16.3 Cilioretinal artery originated from Zinn–Haller arterial circle (Fig. 16.4)

In highly myopic eyes with large conus, Zinn–Haller arterial circle is clearly seen. Although cilioretinal artery is generally considered to originate from short posterior ciliary arteries, ICG angiogram shows that 40% of cilioretinal arteries is originated from Zinn–Haller arterial circle in highly myopic eyes [2]. This origin of cilioretinal arteries may also be true in eyes without pathologic myopia. In addition, cilioretinal arteries in pathologic myopia cover wide region of fundus (in some cases, almost an entire upper fundus).

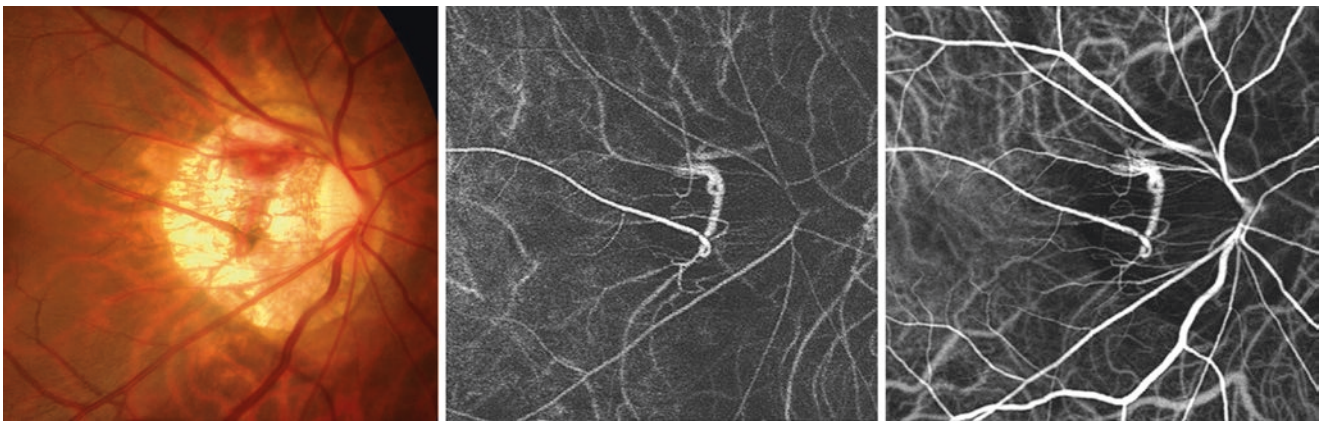

Fig. 16.6 Cilioretinal artery originated from Zinn-Haller arterial circle (Cited with permission from [2]). Axial length is 28.1 mm. (Left) Right fundus shows a part of Zinn–Haller arterial circle (ZHAC) and cilioretinal artery (CA) branching from ZHAC. Arterial phase (Middle) as well as early venous phase of ICG angiogram (Right) show ZHAC within temporal conus and CA branching from ZHAC

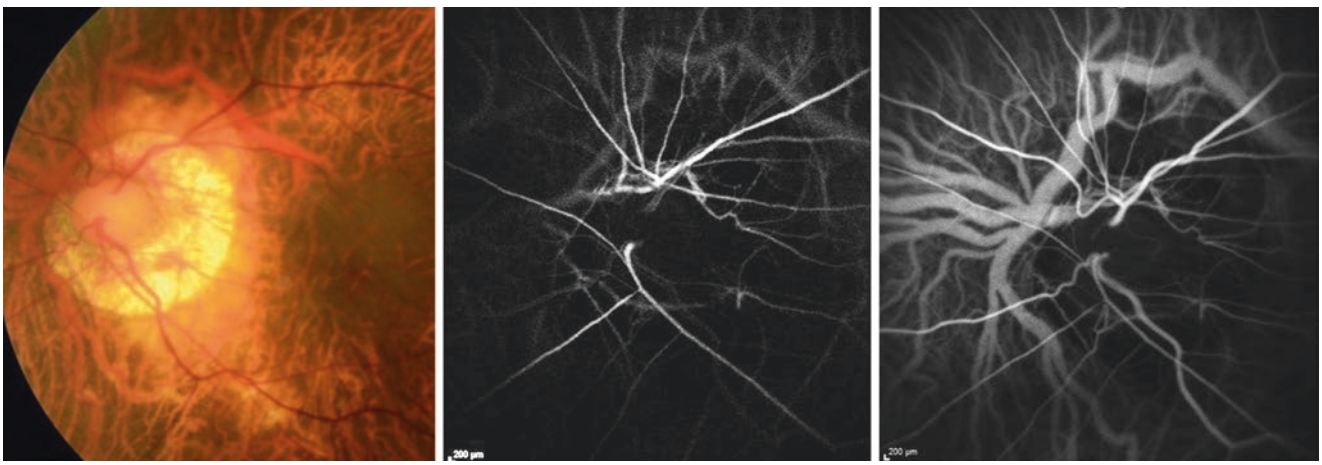

Fig. 16.7 Cilioretinal vein (Cited with permission from [2]). (Left) Left fundus shows cilioretinal arteries and veins in the upper and lower parts of the optic disc. (Middle) Arterial phase of ICG angiogram shows two cilioretinal arteries in the upper as well as the lower parts of the optic disc. The upper cilioretinal artery directly originates from short posterior ciliary artery. (Right) Venous phase of ICG angiogram shows two cilioretinal veins draining into the upper as well as the lower parts of the optic disc. Dilated posterior vortex vein is seen adjacent to the optic disc, and it seems that the upper cilioretinal vein drains into this posterior vortex vein

16.4 Cilioretinal vein (Fig. 16.5)

Cilioretinal veins were mainly reported as opticociliary shunt vessels developing after central retinal vein occlusion. However, in eyes with pathologic myopia, cilioretinal veins can occur without retinal vein occlusions [2]. Although it is not clear whether cilioretinal veins are congenital or acquired, this occurrence may be because of an extreme enlargement of the optic disc area. Instead of flowing into central retinal venous trunk, retinal veins flow into nearby choroidal veins around the optic disc in some cases.

References

1. Moriyama M, Ohno-Matsui K, et al. Morphology and long-term changes of choroidal vascular structure in highly myopic eyes with and without posterior staphyloma. Ophthalmology. 2007;114(9):1755–62.
2. Watanabe T, Kasahara K, et al. Cilioretinal arteries and Cilioretinal veins in eyes with pathologic myopia. Sci Rep. 2019;29(1):2451.

OCT-Based Classification of Myopic Maculopathy

17

Yuxin Fang

Abstract

The choroid in high myopia is markedly thin compared to normal eyes. Choroidal thickness is negatively correlated with severity of myopic maculopathy from tessellated fundus to macular diffuse choroidal atrophy. However, there is no significant difference in choroidal thickness between eyes with macular diffuse choroidal atrophy and patchy choroidal atrophy. By using swept-source OCT, macular Bruch's membrane defects in patchy atrophy and CNV-related macular atrophy have also been shown. Using receiver operating characteristic curve, the cut-off value of 56.5 μm for the nasal choroidal thickness (3000 μm from fovea) is able to predict peripapillary diffuse choroidal atrophy from the tessellation, and cut-off value of 62 μm at subfovea is able to predict the macular diffuse choroidal atrophy. OCT-based classification of myopic maculopathy is presented.

Keywords

OCT-based classification · Myopic maculopathy · Choroidal thickness · Bruch's membrane defect · Cut-off value

Over the past two decades, optical coherence tomography (OCT) has greatly enhanced our understanding of various retinal pathologies. Recent advance in OCT technologies, including enhanced depth imaging OCT and swept-source OCT, has provided the high-resolution images and highly reliable measurements of the choroid in highly myopic eyes [1–20]. It has been well-known that the choroid of highly myopic eyes is markedly thinned compared to normal eyes in both histological study [21] and in OCT studies [6, 9, 19].

Y. Fang (✉)
Department of Ophthalmology and Visual Science, Tokyo Medical and Dental University, Tokyo, Japan

OCT images of eyes with pathologic myopia show an extreme thinning of the choroid with a presence of sporadically remaining large choroidal vessels in the area of diffuse choroidal atrophy [22]. Peripapillary diffuse atrophy in children, which is a sign of eventual pathologic myopia in adults, is characterized by a profound thinning of the nasal choroid [23]. Choroidal thickness can also be more precise biometric than axial length or refractive error in predicting the formation of lacquer cracks [24]. In addition, choroidal thinning is correlated with age [1, 2, 4, 6, 7, 12, 16, 20], refractive error [1–4, 6, 7, 16, 20], and axial length [2–4, 6, 13, 16, 19, 20]. All of previous studies support the theory that choroidal abnormalities may play a key role in the pathogenesis of myopic maculopathy. By using swept-source OCT, macular Bruch's membrane defects in patchy atrophy and myopic macular neovascularization (MNV)-related macular atrophy have also been found [25–27]. These studies showed that patchy atrophy and MNV-related macular atrophy are not simply a chorioretinal atrophy but are Bruch's membrane holes. Moreover, new macular lesions which cannot be detected in fundus photographs are also found by OCT, such as myopic traction maculopathy [28] and dome-shaped macula [29].

17.1 Why the OCT-Based Classification is Needed for Myopic Maculopathy?

Nowadays, the diagnosis of diffuse atrophy relies on its yellowish appearance on ophthalmoscopy. However, fundus color may look different among ethnic groups. Integrating choroidal thickness into the classification system would offer the objective information, and therefore make the diagnosis more accurate and reproducible. Choroidal thickness may also act as a variable that has biologic plausibility to both influence visual function and preserve associated tissue. Moreover, other myopic macular lesions such as myopic traction maculopathy and dome-shaped macula were not included in the META-PM classification because only fundus photographs were used in this classification.

K. Ohno-Matsui (ed.), *Atlas of Pathologic Myopia*, https://doi.org/10.1007/978-981-15-4261-9_17

Table 17.1 Characteristics and choroidal thickness of highly myopic eyes for each type of myopic maculopathy

	All highly myopic eyes	No maculopathy	Tessellated fundus	PDCA	MDCA	Patchy atrophy	MNV-MA	Patchy-MA
No. of eyes	1487	18	266	392	355	268	178	10
Age (years)	58.4 ± 16.3	28.7 ± 18.5	46.1 ± 18.8	54.5 ± 16.1	62.5 ± 10.9	65.8 ± 10.6	67.8 ± 10.6	71.9 ± 8.9
Axial length (mm)	29.87 ± 1.99	27.47 ± 0.89	28.51 ± 1.43	29.33 ± 1.67	30.55 ± 1.75	30.97 ± 2.04	30.14 ± 1.91	31.73 ± 4.01
Refractive error (D)	−13.2 ± 4.0	−10.6 ± 2.8	−11.4 ± 2.7	−12.9 ± 3.8	−15.2 ± 3.7	−15.1 ± 4.8	−12.6 ± 4.4	−11.1 ± 2.3
BCVA (logMAR units)	0.218 ± 0.419	−0.024 ± 0.195	0.015 ± 0.219	0.061 ± 0.231	0.128 ± 0.261	0.272 ± 0.403	0.971 ± 0.42	0.557 ± 0.431
CT (μm)								
Subfoveal	72.7 ± 55.1	274.5 ± 54.8	129.1 ± 58.5	84.6 ± 41.9	50.2 ± 22.4	48.6 ± 24.7	27.3 ± 29.1	3.5 ± 9.4
Nasal	30.8 ± 34.0	153.1 ± 42.5	61.3 ± 37.9	32.3 ± 24.9	21.3 ± 23.7	14.5 ± 21.0	15.3 ± 21.3	8.9 ± 17.8
Temporal	94.7 ± 62.7	254.9 ± 56.1	156.3 ± 60.5	112.7 ± 48.4	62.0 ± 34.2	62.3 ± 42.6	58.2 ± 48.3	17.0 ± 30.1
Superior	98.2 ± 64.8	297.7 ± 64.9	164.6 ± 67.0	112.4 ± 44.7	66.1 ± 33.5	63.2 ± 38.2	62.2 ± 48.7	35.7 ± 37.3
Inferior	82.3 ± 54.0	261.7 ± 47.5	136.3 ± 52.6	92.6 ± 38.1	56.5 ± 28.4	51.6 ± 33.4	49.5 ± 36.2	18.3 ± 24.0

BCVA Best-Corrected Visual Acuity, *logMAR* logarithm of minimal angle of resolution, *CT* Choroidal thickness, *PDCA* peripapillary diffuse choroidal atrophy, *MDCA* macular diffuse choroidal atrophy, *MNV* myopic macular neovascularization, *MA* macular atrophy, *MNV-MA* myopic macular neovascularization-related macular atrophy, *patchy-MA* patchy atrophy-related macular atrophy. Reproduced with permission from *Ophthalmology*

Thus, this chapter presents OCT features, especially choroidal thickness, of each lesion of myopic maculopathy. The OCT-based classification of myopic maculopathy is also presented in this chapter.

Fang et al. [20] collected the data from a clinic-based cross-sectional study on 1487 eyes of 884 highly myopic patients who were examined by swept-source OCT at Tokyo Medical and Dental University (TMDU). The mean age was 58.4 ± 16.3 years, the mean axial length was 29.9 ± 2.0 mm, and the mean refractive error was -13.2 ± 4.0 D [20]. The distribution of myopic maculopathy in our series is shown in Table 17.1.

17.2 Choroidal Thickness in Highly Myopic Eyes

The subfoveal choroidal thickness in highly myopic eyes has previously been reported to vary between 84 and 166 μm for all range of age [1, 2, 4, 6–8, 16]. The mean subfoveal choroidal thickness in the study by Fang et al. [20] for all eyes was extremely thin; 72.7 ± 55.1 μm. According to the definition of pathologic myopia defined as eyes having equal or severe atrophic lesions than diffuse choroidal atrophy or a presence of plus lesions, the subfoveal choroidal thickness was 58.6 ± 44.0 μm in eyes with pathologic myopia and 144.6 ± 64.8 μm in highly myopic eyes without pathologic myopia [20]. Choroidal thickness was the thickest at the superior and temporal location followed by the inferior, subfoveal, and the nasal locations, which was consistent with other studies in highly myopic Asians [2, 7, 11, 20] and highly myopic Caucasians [1, 6]. In contrast, the subfoveal CT was the thickest in normal eyes [30].

17.3 Choroidal Thickness is an Indicator for Severity of Myopic Maculopathy

Only a few studies showed that the choroidal thickness was negatively correlated with the severity of myopic maculopathy based on META-PM classification [11, 17, 20]. According to the modified classification [31], the choroidal thickness in each lesion of myopic maculopathy from our database is shown in Table 17.1. The characteristic fundus photographs and OCT images in each myopic maculopathy is seen in Fig. 17.1. Fang et al. [20] reported that the mean subfoveal choroidal thickness was 274.5 μm in eyes with a normal fundus (category 0), 129.1 μm in eyes with tessellated fundus, 84.6 μm in eyes with peripapillary diffuse choroidal atrophy, 50.2 μm in eyes with macular diffuse choroidal atrophy, 48.6 μm in eyes with patchy atrophy, 27.3 μm in eyes with myopic macular neovascularization (MNV)-related macular atrophy, and 3.5 μm in eyes with patchy-related macular atrophy (Fig. 17.2). In this series, choroidal thickness in all locations decreased from normal fundus to tessellated fundus, to peripapillary diffuse choroidal atrophy, and to macular diffuse choroidal atrophy, as the severity of the myopic maculopathy increased. However, there was no significant difference in the choroidal thickness between eyes with macular diffuse choroidal atrophy and patchy atrophy in all locations except for those at nasally. The subfoveal choroidal thickness in eyes with macular atrophy (MNV-related macular atrophy and patchy-related macular atrophy) was significantly thinner than that in any other groups. The subfoveal choroidal thickness in eyes with patchy-related macular atrophy was even thinner than that in MNV-related macular atrophy. It is noted that there was no difference in the choroidal thickness at temporal, nasal, superior, and inferior locations among MNV-related macular atrophy, macular diffuse choroidal atrophy and patchy atrophy (Fig. 17.2).

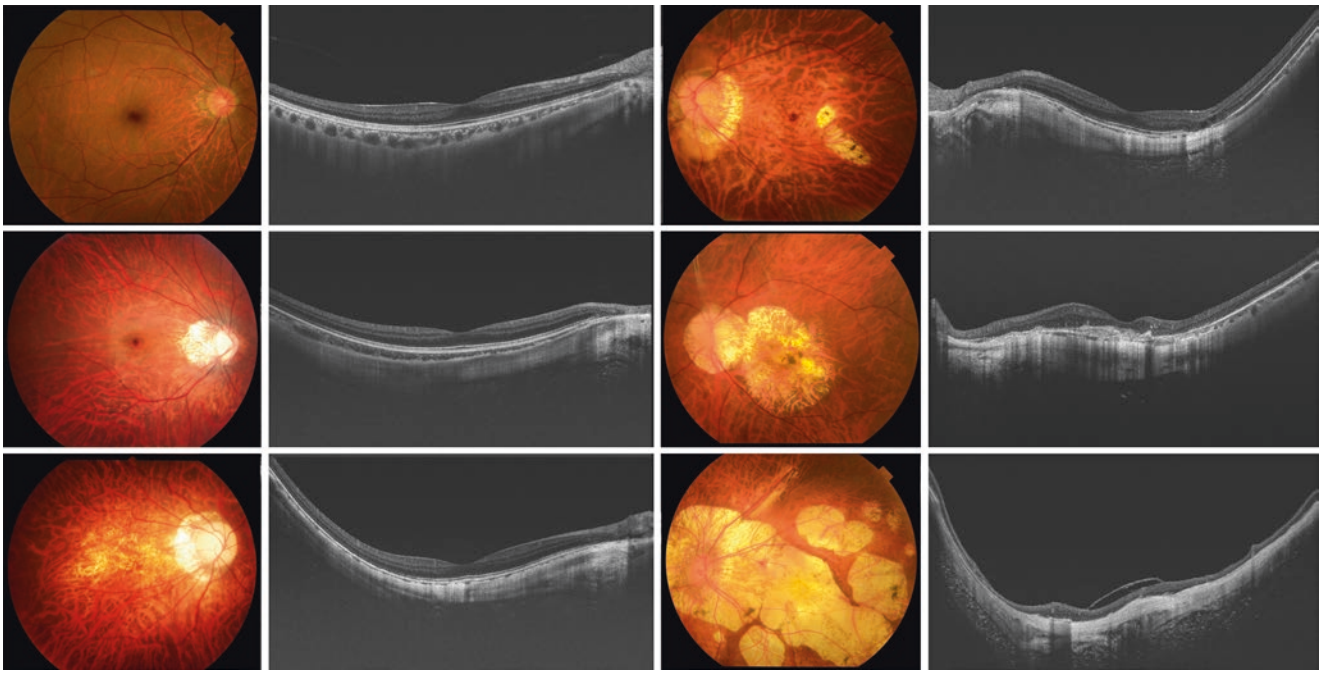

Fig. 17.1 Representative fundus photographs and swept-source optical coherence tomographic images of each lesion of myopic maculopathy. (Top Left and Top Second from left). Tessellated fundus in a 51-year-old man with an axial length of 27.2 mm. The choroidal thickness (CT) is 174 μm in the subfovea, 209 μm in the temporal, and 76 μm in the nasal location. (Middle Left and Middle Second from left). Peripapillary diffuse chorioretinal atrophy in a 30-year-old woman with an axial length of 30.9 mm. The subfoveal CT is 95 μm, temporal CT is 146 μm, and nasal CT is 47 μm. (Bottom Left and Bottom Second from left). Macular diffuse chorioretinal atrophy in a 44-year-old woman with axial length of 30.91 mm. The subfoveal CT was 52 μm, temporal CT was 36 μm, and nasal CT was 27 μm. (Top Third from Left and Top Right). Patchy atrophy in a 49-year-old woman with an axial length of 30.5 mm. The subfoveal CT is 53 μm and the temporal CT is 63 μm. There is no choroid on the nasal side. OCT image across the area of patchy atrophy shows the end of the retinal pigment epithelium (RPE). Bruch's membrane (BM) shows discontinuities and stops within the margin of the RPE defect. In the area of the defective of BM, almost the entire choroid is absent and the inner retina is in direct contact with the sclera. (Middle Third from Left and Middle Right). Macular atrophy (macular neovascularization-related) in a 73-year-old woman with an axial length of 27.4 mm. The subfoveal CT is 15 μm, temporal CT is 93 μm, and nasal CT is 24 μm. (Bottom Third from Left and Bottom Right). Macular atrophy (patchy atrophy-related) in a 63-year-old woman with an axial length of 30.6 mm. There is a severe loss of the choroid, RPE, and BM. Reproduced with permission from [20]

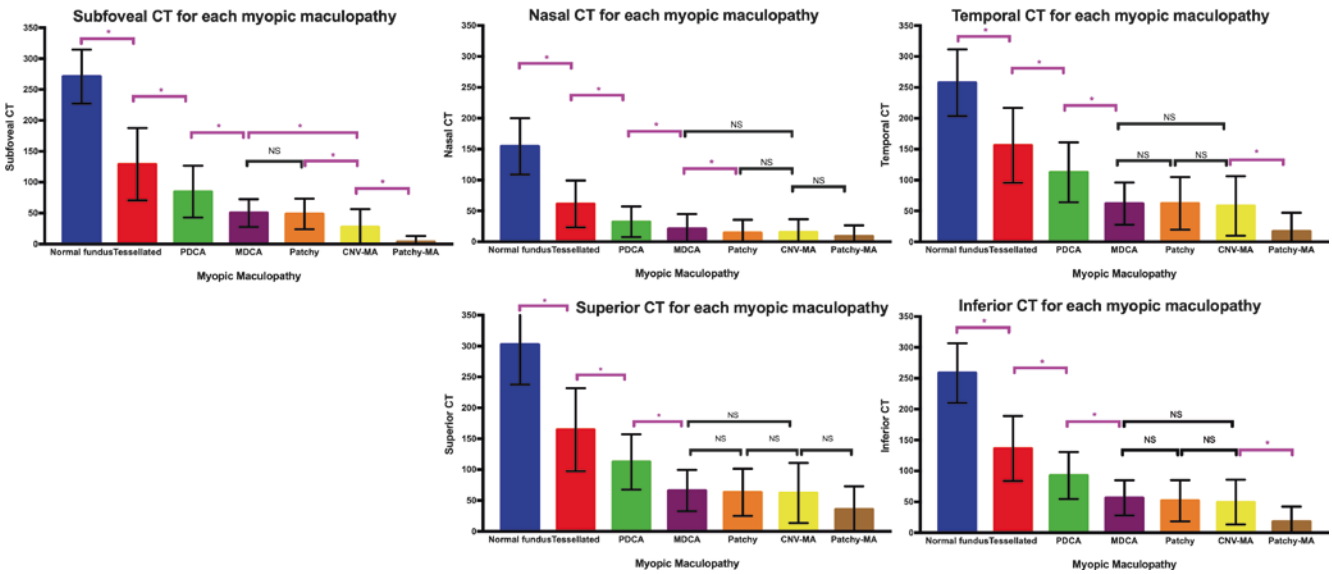

Fig. 17.2 The choroidal thickness (CT) (mean with standard deviation) at each location in each lesion of myopic maculopathy. Choroidal thickness decreases significantly from normal fundus to tessellated fundus, to peripapillary diffuse atrophy (PDCA), and to macular diffuse atrophy (MDCA) in all locations. There is no significant difference in CT between eyes with MDCA and patchy atrophy in all locations except for nasal CT. It is noted that only subfoveal CT in macular neovascularization (MNV)-macular atrophy (MA) is significantly thinner than CT in MDCA and patchy atrophy while there is no difference in CT in other locations. $^{*}P < 0.05$, *NS* Not significant

Another high myopia clinic-based study from the Zhongshan Ophthalmic Center [17] also investigated the choroidal thickness in a large population of highly myopic eyes with different categories of myopic maculopathy according to META-PM classification. In this study, the median subfoveal choroidal thickness was 165 μm in normal fundus (C0), 80 μm in tessellated fundus (C1), 49 μm in diffuse atrophy (C2), 35 μm in patchy atrophy (C3) and 6.5 μm in macular atrophy (C4). It showed that the subfoveal choroidal thickness became significantly thinner with the increasing severity of maculopathy in C0–C4 but the eyes with C3–C4 shared similar parafoveal choroidal thickness, leading to the conclusion that C4 was not the result of progression from C3, which was consistent with long-term follow-up study [31].

17.4 Topography of Choroidal Thickness in Eyes with Different Lesions of Myopic Maculopathy (Fig. 17.3)

The topography of the choroidal thickness in highly myopic eyes with normal fundus is different from that in eyes with pathologic myopia. In highly myopic eyes with no myopic maculopathy, the subfoveal choroidal thickness is the thickest in horizontal sections, which is in same pattern with non-highly myopic eyes [30]. In contrast, the temporal choroidal thickness is the thickest in eyes with myopic maculopathy (Fig. 17.3a). In vertical sections, the inferior choroid is the thinnest in normal fundus, whereas in eyes with myopic maculopathy, the subfoveal choroidal is the thinnest (Fig. 17.3b). This finding is also consistent with another study comparing choroidal thickness in vertical sections between eyes with tessellated fundus and those with normal fundus [32]. Actually, the distribution pattern of choroidal thickness in eyes with tessellated fundus is similar to the eyes with other lesions of myopic maculopathy, e.g., peripapillary diffuse choroidal atrophy, macular diffuse choroidal atrophy, and patchy atrophy. This suggested that the tessellated fundus might be the first sign for myopic eyes to become pathologic.

17.5 Cut-off Values of Choroidal Thickness to Classify Lesions of Myopic Maculopathy

The diagnosis of peripapillary diffuse choroidal atrophy (PDCA) and macular diffuse choroidal atrophy (MDCA) had been based on fundus examination, which was somewhat subjective. Since there was a significant difference in the choroidal thickness between eyes with tessellation and those with PDCA, as well as PDCA and MDCA, it is worth to see if the choroidal thickness can be used as a diagnostic tool for both entities.

Fang et al.[20] used the receiver operating characteristic (ROC) curve and Youden's index to determine the optimal cut-off CT value for the diagnosis of PDCA and MDCA (Fig. 17.4). In predicting the eyes with PDCA from the tessellated fundus, the cut-off value for the nasal choroidal thickness (3000 μm from the fovea) was 56.5 μm with a high sensitivity of 90% and a good specificity of 88% in the group with age < 20, which was consistent with previous findings [23]. The area under curve (AUC) of the choroidal thickness in each location became lower in the older age group. For the group with age 60–79, only the subfoveal choroidal thickness can be used for the diagnosis.

To differentiate eyes with MDCA from PDCA, the nasal choroidal thickness was not useful. Instead, the choroidal

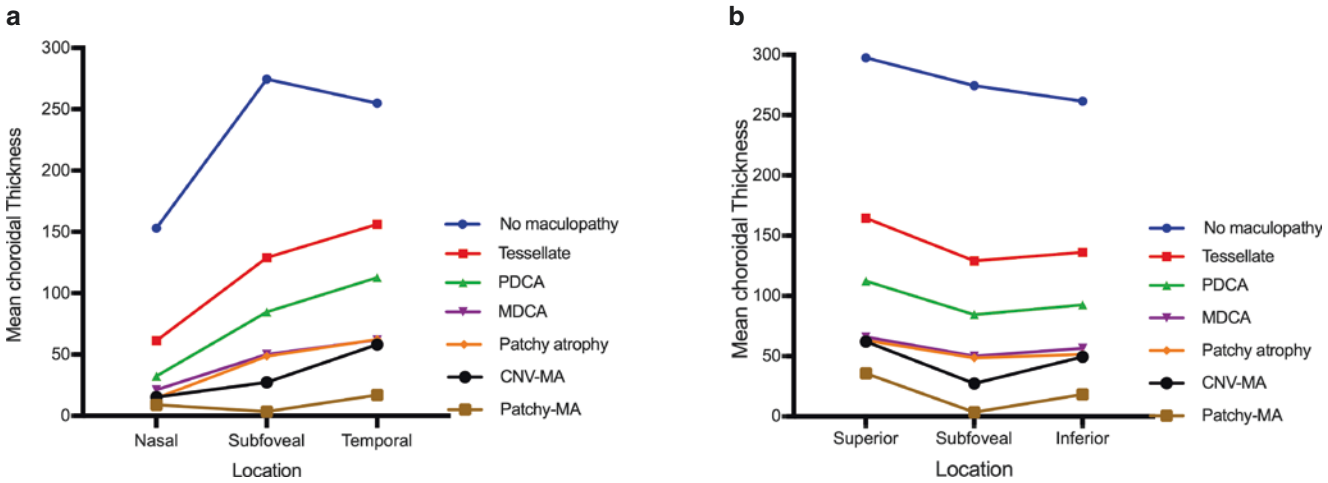

Fig. 17.3 Graphs showing the topography of choroidal thickness (CT) in each lesion of myopic maculopathy in a horizontal direction (Left) and in a vertical direction (Right). The CT was measured at the subfoveal region and at 3 mm nasal, temporal, superior, and inferior to the fovea. The pattern of the CT in highly myopic eyes with normal fundus (= no maculopathy) was different from that in eyes with myopic maculopathy, i.e., ≥ tessellated fundus. In eyes with myopic maculopathy (≥ tessellated fundus), the temporal CT was thicker than the subfoveal CT or nasal CT (Left). In the vertical scan, the subfoveal CT was thinner than the superior CT or inferior CT (Right). Reproduced with permission from [20]

thickness cut-off value of 62 μm at subfovea (sensitivity: 71%; specificity: 72%), 73 μm at temporal (sensitivity: 67%; specificity: 90%), 83 μm at superior (sensitivity: 67%; specificity: 80%), 85 μm at inferior (sensitivity: 81%; specificity: 65%), can be used to define the eyes with MDCA. Although the area under curve (AUC) of subfoveal choroidal thickness was not the largest among all locations, the cut-off value differentiating MDCA from PDCA was still based on the subfoveal choroidal thickness since the detection of the fovea is easier and more accurate than the parafoveal points.

17.6 OCT-Based Classification of Myopic Maculopathy (Table 17.2)

Combining all the hallmarks of myopic maculopathy in pathologic myopia including myopic traction maculopathy and dome-shaped macula, we propose a new classification based on OCT findings [20]. In this new system, diffuse choroidal atrophy (PDCA and MDCA) should be named as "peripapillary choroidal thinning" and "macular choroidal thinning." Based on our results, the cut-off value of the cho-

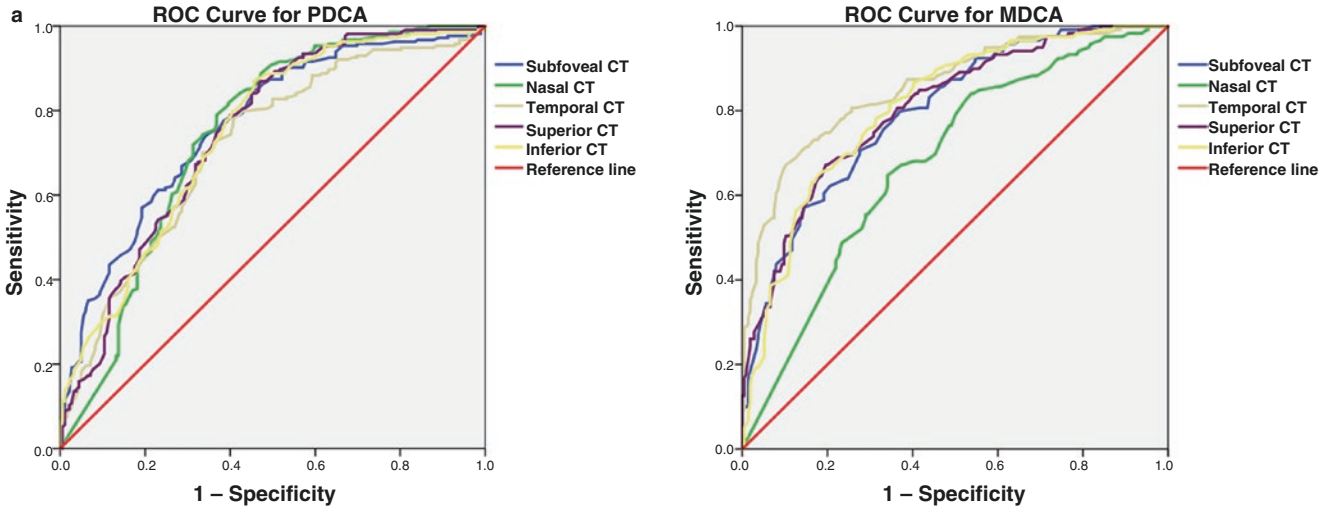

Fig. 17.4 Graphs showing the receiver operating curve (ROC) of optimal choroidal thickness for each location to predict PDCA (Left) and MDCA (Right). *PDCA* peripapillary diffuse choroidal atrophy, *MDCA* macular diffuse choroidal atrophy. Reproduced with permission from [20]. *Ophthalmology*

Table 17.2 OCT-based classification of myopic maculopathy

New terminology	Details	Old terminology
Peripapillary choroidal thinning	CT <56.5 μm at 3000 μm nasal from the fovea	PDCA
Macular choroidal thinning	CT <62 μm at subfovea	MDCA
Linear BM defects	Yellowish linear lesions. Discontinuities of the RPE and increased hyper-transmission into deeper tissues beyond the RPE in OCT image.	Lacquer cracks
Extrafoveal BM defects	Well-defined, grayish white, round lesion(s) in the macular, extrafoveal area. The BM defect is usually surrounded by a slightly wider RPE defect. In the region of the BM defect, the outer retinal layer, the RPE, the choriocapillaris and most of the medium-sized choroidal vessel layer are absent, and a medium-sized or large choroidal vessel may occasionally be present. The middle and inner retinal layers, more or less thinned, are in direct contact with the inner scleral surface	Patchy atrophy
Myopic MNV	MNV occurring in eyes with at least peripapillary or macular choroidal thinning	CNV
Foveal BM defects	The OCT-based histology is similar to the histology of extrafoveal BM defects	Macular atrophy
Foveal BM defects MNV-related	Well-defined, round lesion including the fovea and expanding centrifugally around the fovea. The edges of the macular BM defect are often upturned. In the center, remnants of BM can be present, folded up in the process of the RPE-associated scar formation.	CNV-MA
Foveal BM defects, Patchy-related	Develops outside of the foveal area and enlarges or coalesces with other extrafoveal BM defects.	Patchy-MA
Macular traction maculopathy	Schisis-like inner retinal fluid, schisis-like outer retina fluid, foveal retinal detachment, lamellar or full-thickness macular hole and/or retinal detachment	
Dome-shaped macula	Inward bulge of the RPE line in either horizontal or vertical scan with a height of >50 μm above a base line connecting the RPE lines on both side outside the dome.	

OCT Optical Coherence Tomography, *PDCA* peripapillary diffuse choroidal atrophy, *MDCA* macular diffuse choroidal atrophy, *CT* Choroidal thickness, *MNV* myopic macular neovascularization, *MNV-MA* myopic macular neovascularization-related macular atrophy, *patchy-MA* patchy atrophy-related macular atrophy, *BM* Bruch's membrane, *RPE* retinal pigment epithelium. Reproduced with permission from [20]

roidal thickness as a diagnostic tool for diffuse atrophy has been added to this system. That is, peripapillary choroidal thinning is defined as the choroidal thickness < 56.5 mm at 3000 mm nasal from the fovea and macular choroidal thinning is defined as the choroidal thickness < 62 mm at subfovea. The patchy atrophy and macular atrophy are not simply due to atrophy but the holes of Bruch's membrane. Patchy atrophy is seen as a well-defined, grayish white lesion in fundus photographs rarely involving the central fovea. These two lesions should be called "extrafoveal Bruch's membrane defects" in OCT classification system. On the other hand, macular atrophy (Category 4 in META-PM classification, both MNV-related and patchy-related) should be named as "foveal Bruch's membrane defects". In addition, myopic traction maculopathy and dome-shaped macula that only can be detected by OCT are also included in this OCT-based classification of myopic maculopathy.

17.7 Predictors of Subfoveal Choroidal Thickness (Fig. 17.5)

17.7.1 Predictors of Subfoveal Choroidal Thickness in All Highly Myopic Eyes

The choroid thickness has been found to vary inversely with the age, an axial length, and the amount of refractive error in eyes with high myopia [1–4, 6, 7, 12, 16, 19, 20]. Fang et al. [20] reported that the subfoveal choroid thickness decreased by 1.75 μm per year of age and 9.87 μm per mm of axial length. By using the model of age and the refractive error, the reduction of the subfoveal choroid thickness was 2.00 μm/year and 4.14 μm/diopter. The age-related rate of the choroidal thinning in highly myopic eyes varied from 1.19 to 1.78 μm/year in earlier studies [1, 6, 7]. It is interesting that the reduction of choroidal thickness with age is approximately the same in absolute amounts between normal eyes (1.56 μm/year) and those with high myopia [30].

The female sex, a presence of MNV, a severity of myopic maculopathy, and a presence of myopic traction maculopathy were also independent predictors for subfoveal choroidal thickness. In addition, the dome-shaped macula was correlated with subfoveal choroidal thickening [20]. Thus, clinicians should take all of these parameters into account when interpreting the data on the choroidal thickness.

17.7.2 Predictors of Subfoveal Choroidal Thickness in Each lesion of Myopic Maculopathy

As the severity of myopic maculopathy should be taken into account in the choroidal thickness, a correlation between the subfoveal choroid thickness and the age, an axial length and a refractive error in each lesion of myopic maculopathy is shown in Fig. 17.5. In eyes with tessellated fundus, the rate of CT decrease (1.465 μm/year) was very close to the rate of choroidal thinning in normal eyes (1.56 μm/year) [30]. This rate slowed down as the severity of the myopic maculopathy increased especially in eyes with MDCA and patchy atrophy.

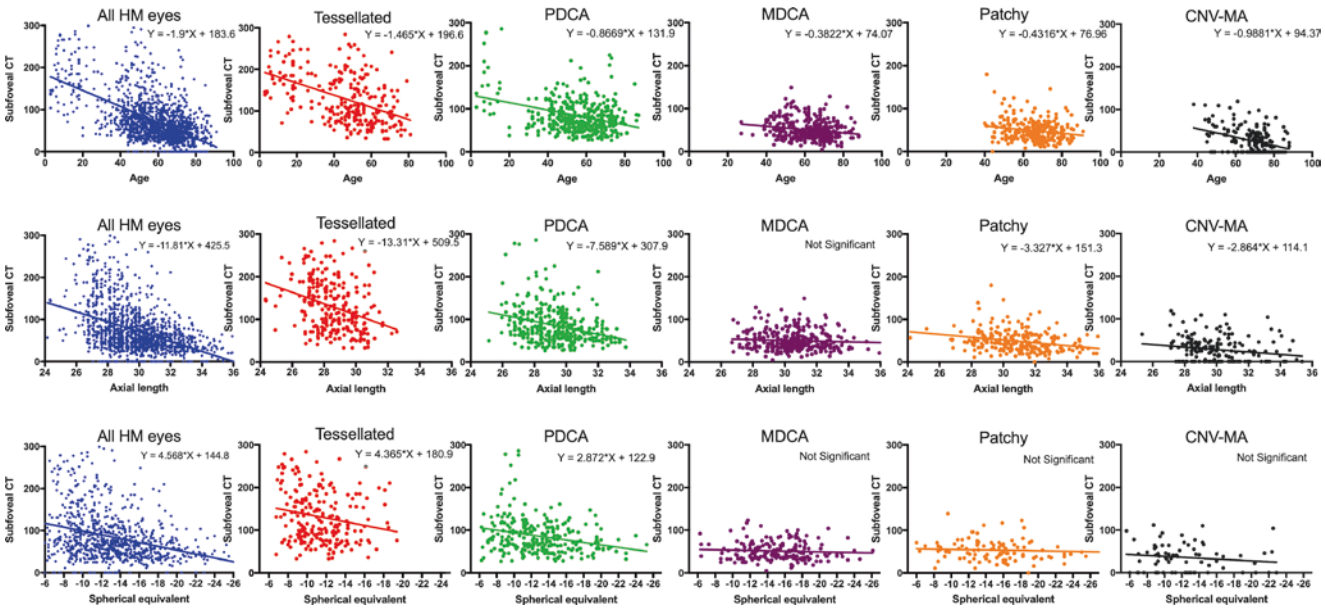

Fig. 17.5 Scatterplots showing a negative correlation between the subfoveal choroidal thickness and the age, a negative correlation between the subfoveal choroid thickness and an axial length (mm), and a negative correlation between the subfoveal choroid thickness and a refractive error (spherical equivalents) in diopters in all highly myopic eyes and in each lesion of myopic maculopathy. The equation shown in each scatterplot is statistical results based on each single regression analysis

However, when the eyes had myopic macular neovascularization (MNV) and progressed to MNV-related macular atrophy (MA), the age-related attenuation in the subfoveal choroid thickness slightly accelerated again. Combining the distribution of the subfoveal choroid thickness for different lesions of myopic maculopathy, the results indicated that the choroid might maintain at its extreme thinnest threshold unless MNV-related MA developed.

17.7.3 Predictors of Subfoveal Choroidal Thickness in Each Age Group

All patients were divided into the following five age groups: ≤20, 21–39, 41–59, 61–79, and ≥ 80 years [20]. The subfoveal choroidal thickness was significantly correlated with the age and an axial length in groups aged 21–39, 41–59, 61–79 years. For ages ≤20 years, an axial length was the only independent factor and for aged ≥80 years neither an axial length or the age were related with the subfoveal choroid thickness. In a large population of school-based study enrolling children aged 6–19 years in Shanghai, China, Xiong et al. found that the central foveal choroidal thickness increased with age in emmetropic eyes. However, an axial length but not age was significantly correlated with the choroidal thickness in highly myopic children (≤ -5.0 D) and moderately myopic children (-5.0 D < spherical equivalents ≤ -3.0 D), suggesting that the protective effect of normal choroidal growth with age disappeared while axial elongation became the dominant determinant of the choroidal thickness in myopic children [15].

In a normal population study, Ruiz-Medrano et al. [33] reported that the choroidal thickness decreased with age (0.85 μm/year) especially after the age 40. Ding et al. [34] also reported that the age-related thinning occurred only in age older than 60 in 210 healthy Chinese volunteers. In contrast, the rate of the subfoveal choroidal thinning in highly myopic eyes was faster at a relatively younger age (ages 20–39, 4.91 μm/year) [20]. The rate slowed down with aging and turned out to be 1.66 μm/year in subjects aged 40–59 and 1.03 μm/year in subjects aged 61–80 [20]. These findings suggested that the choroidal thinning with age in highly myopic eyes was not steadily progressive but had periods of accelerated thinning. It may help us to construct a picture of choroidal attenuations in the entire life of highly myopic patients.

References

1. Fujiwara T, Imamura Y, Margolis R, Slakter JS, Spaide RF. Enhanced depth imaging optical coherence tomography of the choroid in highly myopic eyes. Am J Ophthalmol. 2009;148(3):445–50.
2. Ikuno Y, Tano Y. Retinal and choroidal biometry in highly myopic eyes with spectral-domain optical coherence tomography. Invest Ophthalmol Vis Sci. 2009;50(8):3876–80.
3. Wang NK, Lai CC, Chu HY, Chen YP, Chen KJ, Wu WC, et al. Classification of early dry-type myopic maculopathy with macular choroidal thickness. Am J Ophthalmol. 2012;153(4):669–77. 677 e1–2
4. Nishida Y, Fujiwara T, Imamura Y, Lima LH, Kurosaka D, Spaide RF. Choroidal thickness and visual acuity in highly myopic eyes. Retina (Philadelphia, Pa). 2012;32(7):1229–36.
5. Takahashi A, Ito Y, Iguchi Y, Yasuma TR, Ishikawa K, Terasaki H. Axial length increases and related changes in highly myopic normal eyes with myopic complications in fellow eyes. Retina (Philadelphia, Pa). 2012;32(1):127–33.
6. Flores-Moreno I, Lugo F, Duker JS, Ruiz-Moreno JM. The relationship between axial length and choroidal thickness in eyes with high myopia. Am J Ophthalmol. 2013;155(2):314–9. e1
7. Ho M, Liu DT, Chan VC, Lam DS. Choroidal thickness measurement in myopic eyes by enhanced depth optical coherence tomography. Ophthalmology. 2013;120(9):1909–14.
8. Flores-Moreno I, Ruiz-Medrano J, Duker JS, Ruiz-Moreno JM. The relationship between retinal and choroidal thickness and visual acuity in highly myopic eyes. Br J Ophthalmol. 2013;97(8):1010–3.
9. Gupta P, Saw SM, Cheung CY, Girard MJ, Mari JM, Bhargava M, et al. Choroidal thickness and high myopia: a case-control study of young Chinese men in Singapore. Acta Ophthalmol. 2015;93(7):e585–92.
10. Pang CE, Sarraf D, Freund KB. Extreme choroidal thinning in high myopia. Retina (Philadelphia, Pa). 2015;35(3):407–15.
11. Wong CW, Phua V, Lee SY, Wong TY, Cheung CM. Is Choroidal or scleral thickness related to myopic macular degeneration? Invest Ophthalmol Vis Sci. 2017;58(2):907–13.
12. Zhou LX, Shao L, Xu L, Wei WB, Wang YX, You QS. The relationship between scleral staphyloma and choroidal thinning in highly myopic eyes: the Beijing eye study. Sci Rep. 2017;7(1):9825.
13. Abdolrahimzadeh S, Parisi F, Plateroti AM, Evangelista F, Fenicia V, Scuderi G, et al. Visual acuity, and macular and Peripapillary thickness in high myopia. Curr Eye Res. 2017;42(11):1468–73.
14. Lee JH, Lee SC, Kim SH, Koh HJ, Kim SS, Byeon SH, et al. Choroidal thickness and chorioretinal atrophy in myopic choroidal neovascularization with anti-vascular endothelial growth factor therapy. Retina (Philadelphia, Pa). 2017;37(8):1516–22.
15. Xiong S, He X, Deng J, Lv M, Jin J, Sun S, et al. Choroidal thickness in 3001 Chinese children aged 6 to 19 years using swept-source OCT. Sci Rep. 2017;7:45059.
16. Liu B, Wang Y, Li T, Lin Y, Ma W, Chen X, et al. Correlation of subfoveal choroidal thickness with axial length, refractive error, and age in adult highly myopic eyes. BMC Ophthalmol. 2018;18(1):127.
17. Zhao X, Ding X, Lyu C, Li S, Liu B, Li T, et al. Morphological characteristics and visual acuity of highly myopic eyes with different severities of myopic Maculopathy. Retina (Philadelphia, Pa). 2018;40(3):461–7.
18. Fledelius HC, Jacobsen N, Li XQ, Goldschmidt E. Choroidal thickness at age 66 years in the Danish high myopia study cohort 1948 compared with follow-up data on visual acuity over 40 years: a clinical update adding spectral domain optical coherence tomography. Acta Ophthalmol. 2018;96(1):46–50.
19. Chalam KV, Sambhav K. Choroidal thickness measured with swept source optical coherence tomography in posterior staphyloma strongly correlates with axial length and visual acuity. Int J Retina and Vitreous. 2019;5:14.
20. Fang Y, Du R, Nagaoka N, Yokoi T, Shinohara K, Xu X, et al. OCT-based diagnostic criteria for different stages of myopic Maculopathy. Ophthalmology. 2019;126(7):1018–32.
21. Grossniklaus HE, Green WR. Pathologic findings in pathologic myopia. Retina (Philadelphia, Pa). 1992;12(2):127–33.
22. Ohno-Matsui K. Myopic Chorioretinal atrophy. In: Spaide RF, Ohno-Matsui K, Yannuzzi LA, editors. Pathologic myopia. New York: Springer; 2014. p. 187–210.

23. Yokoi T, Zhu D, Bi HS, Jonas JB, Jonas RA, Nagaoka N, et al. Parapapillary diffuse Choroidal atrophy in children is associated with extreme thinning of Parapapillary choroid. Invest Ophthalmol Vis Sci. 2017;58(2):901–6.
24. Wang NK, Lai CC, Chou CL, Chen YP, Chuang LH, Chao AN, et al. Choroidal thickness and biometric markers for the screening of lacquer cracks in patients with high myopia. PLoS One. 2013;8(1):e53660.
25. Ohno-Matsui K, Jonas JB, Spaide RF. Macular Bruch membrane holes in Choroidal neovascularization-related myopic macular atrophy by swept-source optical coherence tomography. Am J Ophthalmol. 2016;162:133–9. e1
26. Ohno-Matsui K, Jonas JB, Spaide RF. Macular Bruch membrane holes in highly myopic patchy Chorioretinal atrophy. Am J Ophthalmol. 2016;166:22–8.
27. Du R, Fang Y, Jonas JB, Yokoi T, Takahashi H, Uramoto K, et al. Clinical features of patchy Chorioretinal atrophy in pathologic myopia. Retina (Philadelphia, Pa). 2019; https://doi.org/10.1097/IAE.0000000000002575.
28. Panozzo G, Mercanti A. Optical coherence tomography findings in myopic traction maculopathy. Arch Ophthalmol. 2004;122(10):1455–60.
29. Gaucher D, Erginay A, Lecleire-Collet A, Haouchine B, Puech M, Cohen SY, et al. Dome-shaped macula in eyes with myopic posterior staphyloma. Am J Ophthalmol. 2008;145(5):909–14.
30. Margolis R, Spaide RF. A pilot study of enhanced depth imaging optical coherence tomography of the choroid in normal eyes. Am J Ophthalmol. 2009;147(5):811–5.
31. Fang Y, Yokoi T, Nagaoka N, Shinohara K, Onishi Y, Ishida T, et al. Progression of myopic Maculopathy during 18-year follow-up. Ophthalmology. 2018;125(6):863–77.
32. Zhou Y, Song M, Zhou M, Liu Y, Wang F, Sun X. Choroidal and retinal thickness of highly myopic eyes with early stage of myopic Chorioretinopathy: tessellation. J Ophthalmol. 2018;2018:2181602.
33. Ruiz-Medrano J, Flores-Moreno I, Pena-Garcia P, Montero JA, Duker JS, Ruiz-Moreno JM. Macular choroidal thickness profile in a healthy population measured by swept-source optical coherence tomography. Invest Ophthalmol Vis Sci. 2014;55(6):3532–42.
34. Ding X, Li J, Zeng J, Ma W, Liu R, Li T, et al. Choroidal thickness in healthy Chinese subjects. Invest Ophthalmol Vis Sci. 2011;52(13):9555–60.

Part V

Myopic Traction Maculopathy

TMDU Classification of Myopic Traction Maculopathy Based on OCT and Ultra Wide-Field OCT (UWF-OCT)

18

Noriaki Shimada

Abstract

Myopic traction maculopathy (MTM) is considered a preexisting lesion of macular hole retinal detachment. The diagnosis of MTM is made by the existence of one of the macular lesions; epiretinal membrane, vitreomacular traction, retinal thickening, retinoschisis, macular hole (lamellar or full thickness), and retinal detachment. Tokyo Medical and Dental University (TMDU) classification of MTM is established based on the size and the location of the retinoschisis and the presence of six foveal pathologies. Progression from retinoschisis to retinal detachment is classified into four stages starting with a development of outer lamellar hole.

Keyword

Retinoschisis · Epiretinal membrane · Vitreomacular traction · Macular hole · Retinal detachment

The terminology of myopic macular retinoschisis, myopic foveoschisis, or myopic retinoschisis has not been consistent. Retinoschisis is the most frequent form of tractional retinal changes before the development of a macular hole retinal detachment (MHRD) in eyes with pathologic myopia [1]. However, in some eyes, MHRD can develop without retinoschisis. Panozzo et al. [2] proposed to unify all of the pathologic features generated by traction in the myopic environment under the name of myopic traction maculopathy (MTM) in 2004. The diagnosis of MTM is made by the existence of one of the macular lesions; epiretinal membrane, vitreomacular traction, retinal thickening, retinoschisis, macular hole (lamellar or full thickness), and retinal detachment (RD). Other causes of RDs, such as those caused by intrachoroidal cavitation [3], myopic macular neovascularization, or dome-shaped macula, should be excluded.

MTM is thought to be the preexisting lesion before the development of MHRD. Tractional mechanisms causing the MTM are diverse. Therefore, OCT images of MTM are also diverse. OCT examinations must be performed over the entire area of macula, as wide as possible with a use of wide-field OCT.

Tokyo Medical and Dental University (TMDU) classification of MTM is shown in Table 18.1. Firstly, the images over the entire area of the retinoschisis need to be thoroughly examined. Retromode imaging is also useful for detecting a characteristic fingerprint pattern at the corresponding area of the retinoschisis [4] (Fig. 18.1). When the entire area of the retinoschisis is examined, the eyes are classified into five groups based on the area and the extent of the retinoschisis: no retinoschisis (S0), extra-foveal retinoschisis (S1), foveal only retinoschisis (S2), foveal but not entire macular area retinoschisis (S3), and entire macular area retinoschisis (S4) (Fig. 18.2).

Next, other foveal pathologies should be identified in OCT images; such as an epiretinal membrane (M), a vitreomacular traction (V), an inner lamellar MH (L), a full thickness macular hole (H), a retinal detachment (D) and a retinal atrophy (A). A retinal detachment is classified into four stages according to its progression from retinoschisis [5] (Fig. 18.3). Retinal atrophy is included in TMDU classification of MTM because a retinal atrophy with outer retinal damage such as myopic macular neovascularization may worsen MTM [6], and may affect surgical outcome.

Natural course of the MTM is generally stable [7]. 3.9% showed a decrease or complete resolution of the retinoschisis. However, 11.6% had a progression of the MTM. The progression rate was high (42.9%) in the more advanced MTM (S4), whereas the progression rate was as low as 7.8% in the milder MTM, such as S1 to S3.

N. Shimada (✉)
Department of Ophthalmology and Visual Science, Tokyo Medical and Dental University, Tokyo, Japan
e-mail: shimada.oph@tmd.ac.jp

K. Ohno-Matsui (ed.), *Atlas of Pathologic Myopia*, https://doi.org/10.1007/978-981-15-4261-9_18

Table 18.1 Tokyo Medical and Dental University (TMDU) classification of myopic traction maculopathy

Area of the retinoschisis	S0: No retinoschisis S1: Extra-foveal retinoschisis S2: Foveal only retinoschisis S3: Foveal but not entire macular area retinoschisis S4: Entire macular area retinoschisis
Foveal pathologies	M: Epiretinal membrane V: Vitreomacular traction L: Inner lamellar macular hole H: Full thickness macular hole D: Retinal detachment (D1~4) A: Retinal atrophy
Retinal detachment (if accompanied)	D1: Irregularity of the thickness of the external retinal layer D2: Formation of outer lamellar hole D3: Vertically increased outer lamellar hole D4: Attachment of the edge of outer retina to the upper part of the retinoschisis layer

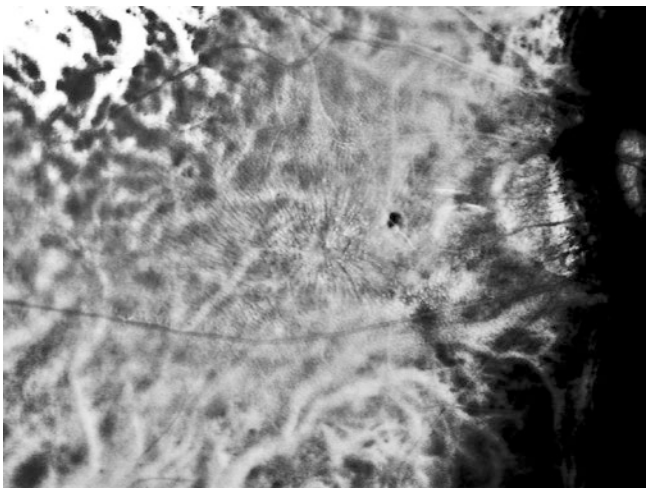

Fig. 18.1 Representative retromode image of an eye with a retinoschisis. Retromode image shows a fingerprint pattern consisting of central radiating retinal striae and surrounding multiple dots and lines. Many lines appear in parallel or in a whorled pattern

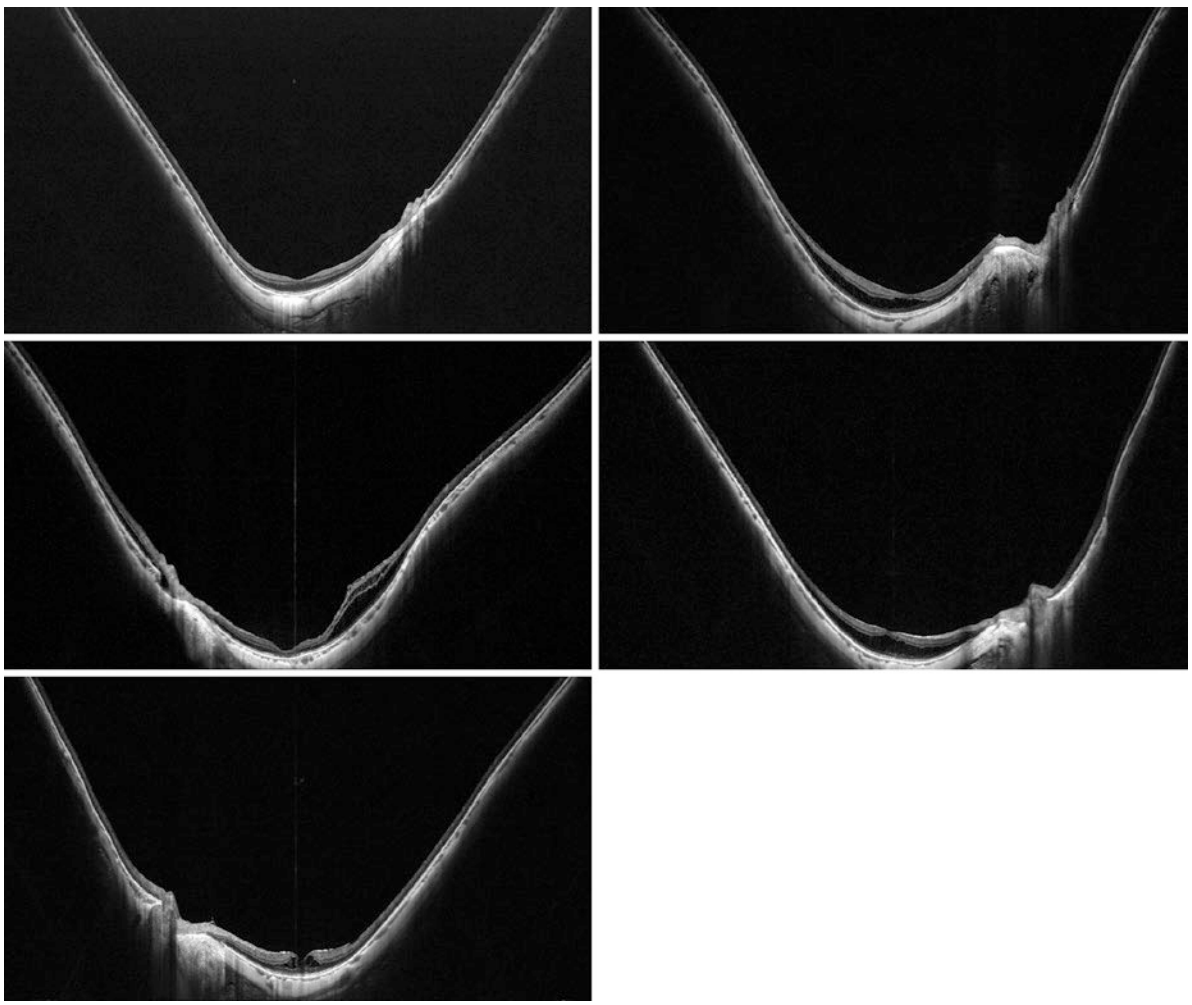

Fig. 18.2 Wide-field OCT images of five groups according to the size of the retinoschisis in Tokyo Medical and Dental University (TMDU) classification of myopic traction maculopathy. (Top Left) no retinoschisis (S0), (Second Row, Left) extra-foveal retinoschisis (S1), (Bottom Left) foveal only retinoschisis (S2), (Top Right) foveal but not entire macular area retinoschisis (S3), (Second Row, Right) entire macular area retinoschisis (S4)

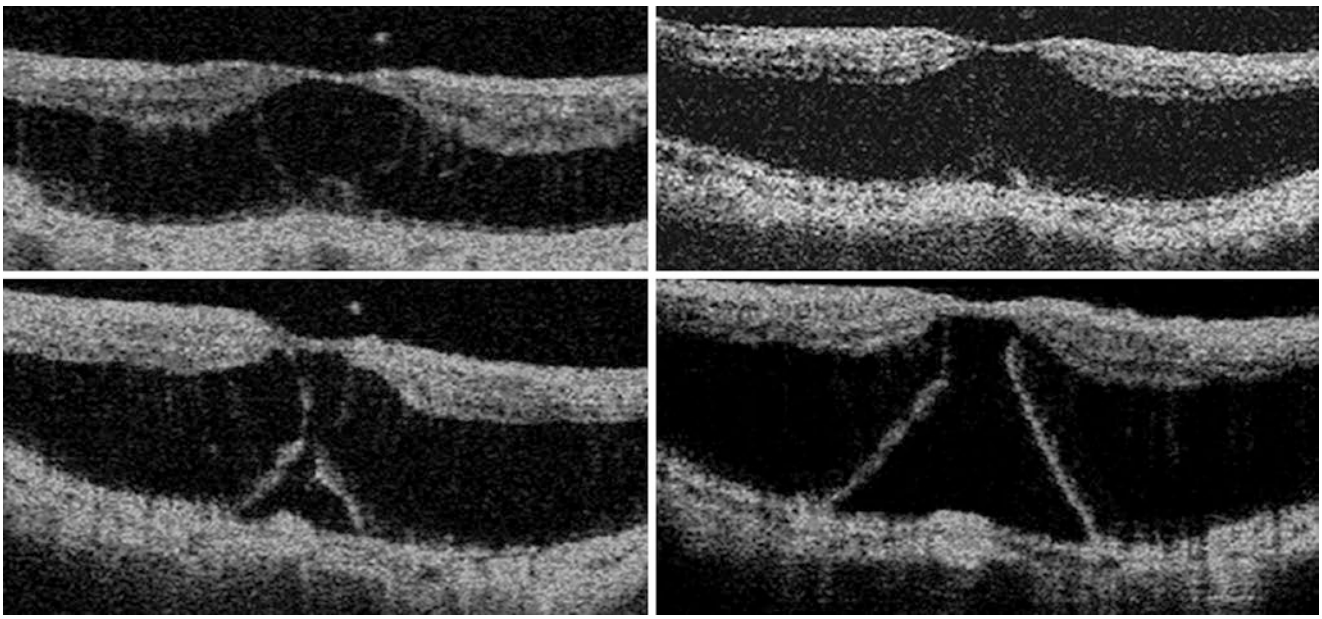

Fig. 18.3 Different stages in the progression from the retinoschisis to the retinal detachment in Tokyo Medical and Dental University (TMDU) classification of MTM. In stage D1 (Top Left), OCT image shows an irregularity of the thickness of the outer retinal layer. In stage D2 (Top Right), an outer lamellar hole has developed in the thickened area of the outer retina. In stage D3 (Bottom Left), the column-like structures within the retinoschisis layer overlying the lamellar hole appear to be separated horizontally, and consequently the hole is enlarged vertically. The outer margins of the outer retinal layer around the hole are further elevated, and the area of the retinal detachment is enlarged. In stage D4 (Bottom Right), the upper edge of external retina around the hole is attached to the upper part of the retinoschisis layer, and retinal detachment is further enlarged accompanied by a resolution of the retinoschisis

References

1. Takano M, Kishi S. Foveal retinoschisis and retinal detachment in severely myopic eyes with posterior staphyloma. Am J Ophthalmol. 1999;128(4):472–6.
2. Panozzo G, Mercanti A. Optical coherence tomography findings in myopic traction maculopathy. Arch Ophthalmol. 2004;122(10):1455–60.
3. Shimada N, Ohno-Matsui K, Iwanaga Y, et al. Macular retinal detachment associated with peripapillary detachment in pathologic myopia. Int Ophthalmol. 2009;29:99–102.
4. Tanaka Y, Shimada N, Ohno-Matsui K, et al. Retromode retinal imaging of macular retinoschisis in highly myopic eyes. Am J Ophthalmol. 2010;149:635–40.
5. Shimada N, Ohno-Matsui K, Yoshida T, et al. Progression from macular retinoschisis to retinal detachment in highly myopic eyes is associated with outer lamellar hole formation. Br J Ophthalmol. 2008;92(6):762–4.
6. Shimada N, Ohno-Matsui K, Yoshida T, et al. Development of macular hole and macular retinoschisis in eyes with myopic choroidal neovascularization. Am J Ophthalmol. 2008;145(1):155–61.
7. Shimada N, Tanaka Y, Tokoro T, et al. Natural course of myopic traction maculopathy and factors associated with progression or resolution. Am J Ophthalmol. 2013;156:948–57.

Outer and Inner Retinoschisis, Foveal Retinal Detachment

19

Kosei Shinohara

Abstract

The outer retinoschisis is defined as a splitting of the outer retinal layers, mainly between the outer plexiform layer and the outer nuclear layer. The inner retinoschisis is defined as a retinoschisis involving the inner layer of the retina. Posterior staphylomas are strongly associated with outer retinoschisis, whereas the inner retinoschisis is strongly associated with inward tractional lesions. Foveal retinal detachment is a complication of the outer retinoschisis, and a high risk for developing the full thickness macular hole with retinal detachment.

Keywords

Myopic macular retinoschisis · Outer retinoschisis · Inner retinoschisis · Foveal retinal detachment

A myopic macular retinoschisis (MRS) is a common complication of pathologic myopia. MRS is classified to inner retinoschisis and outer retinoschisis according to the region of the retinoschisis [1]. The outer retinoschisis is defined as a splitting of the outer retinal layers, mainly between the outer plexiform layer and the outer nuclear layer. Highly reflective layer representing the external limiting membrane (ELM) and the ellipsoid zone are observed in the anterior and posterior border of the retinoschisis (Fig. 19.1) [2]. The inner retinoschisis is defined as a retinoschisis involving the inner layer of the retina. The inner retinoschisis is observed as a splitting of the inner plexiform layer (IPL) or an internal limiting membrane (ILM) detachment. In the space beneath the ILM and within the IPL, multiple columnar structures are observed similar to those found in the outer retinoschisis (Fig. 19.1) [2]. Inner retinoschisis is not observed in the foveolar area because of a lack of the inner retina, and is rarely seen in areas without outer retinoschisis. The outer retinoschisis is usually stable when the retinoschisis is restricted within the macular area. However, once the retinoschisis extends over the entire macular area, it frequently progresses and tends to impair the vision. On the other hand, the inner retinoschisis usually does not affect the vision. Both of the inner and outer retinoschises are occasionally resolved in the natural course secondary to posterior vitreous detachment or spontaneous disruption of ILM [3].

Recent study using ultra-wide field OCT (UWF-OCT) has revealed an association between myopic macular retinoschisis and posterior staphylomas [4]. Outer retinoschisis is strongly associated with the presence of a posterior staphyloma (Figs. 19.2 and 19.3). In the study by Shinohara et al. [4], a posterior staphyloma was observed in 86.0%; 117 of the 136 highly myopic eyes with outer retinoschisis, which was significantly higher than 61.6%; 365 of the 593 highly myopic eyes without outer retinoschisis. An outer retinoschisis without a posterior staphyloma is rare; however, a wide outer retinoschisis is occasionally observed in eyes without staphylomas when the posterior vitreous diffusely adheres to retinal surface (Fig. 19.4). On the other hand, the inner retinoschisis is not strongly associated with the presence of a staphyloma, however, it is strongly associated with inward tractional lesions such as epiretinal membrane, vitreomacular traction, and traction caused by retinal vessels (Fig. 19.5). In eyes with a dome-shaped macula and MRS, an outer retinoschisis spares the foveal area, suggesting that the dome-shaped macula would act protectively against the development of foveal retinoschisis because the sclera of the foveal region protrudes inwardly, and this protrusion might

Electronic Supplementary Material The online version of this chapter (https://doi.org/10.1007/978-981-15-4261-9_19) contains supplementary material, which is available to authorized users.

K. Shinohara (✉)
Department of Ophthalmology and Visual Science, Tokyo Medical and Dental University, Tokyo, Japan

Musashino Red-Cross Hospital, Tokyo, Japan

K. Ohno-Matsui (ed.), *Atlas of Pathologic Myopia*, https://doi.org/10.1007/978-981-15-4261-9_19

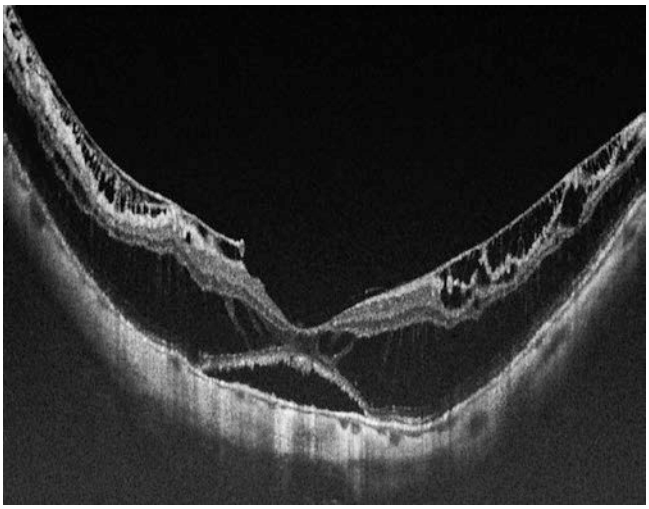

Fig. 19.1 An OCT image showing inner retinoschisis, outer retinoschisis, and foveal retinal detachment

weaken the outward tractional force by a staphyloma and the inward tractional force by epiretinal lesions (Fig. 19.6).

Foveal retinal detachment (foveal RD) is seen in the process of the progression of the outer retinoschisis (Fig. 19.1). In the study by Shinohara et al, foveal RD was observed only in eyes with wide outer retinoschisis including the entire macular area [4]. Foveal RD frequently affects the central vision and is a high risk for a development of full thickness macular hole with retinal detachment [3].

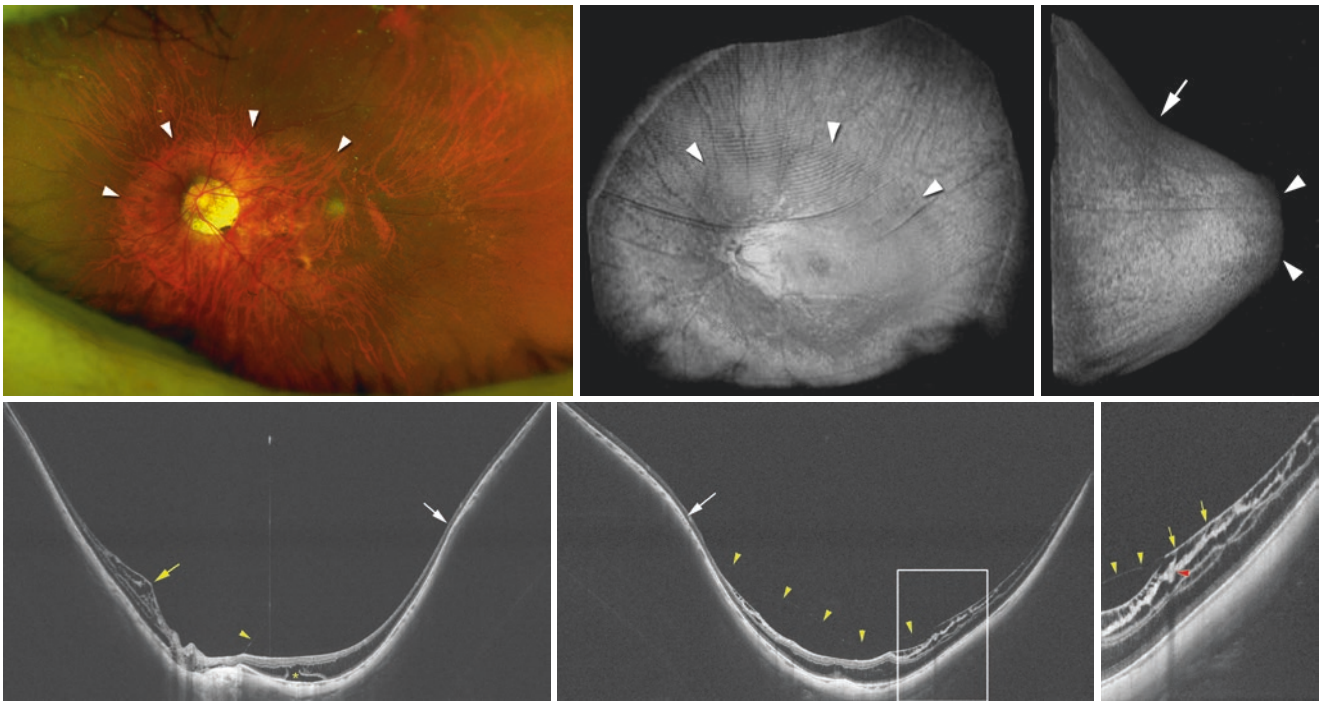

Fig. 19.2 Outer and inner retinoschisis within the area of a wide macular posterior staphyloma in images obtained by ultra-wide field optical coherence tomography (UWF-OCT) (Reproduced with permission from [4]). (Top left) Left fundus of a 72-year-old woman (axial length, 29.7 mm) with a wide macular staphyloma (arrowheads). (Top middle and Top right) Three-dimensional UWF-OCT images viewed from the front (middle) and from the temporal side (right) show a scleral outpouching (arrowheads) due to a wide macular staphyloma. The edges of the staphyloma are marked by a notch (arrow in top right image). (Bottom) UWF-OCT images in a horizontal section (Left) and in a vertical section (middle) (Bottom right) Magnified image of the bottom middle image. White arrows show the staphyloma edge, associated with a slight inward protrusion of the sclera and a gradual thinning of the choroid from the periphery toward the staphyloma edge and a gradual re-thickening of the choroid from the staphyloma edge toward the posterior pole. An outer retinoschisis with a circumscribed macular retinal detachment (asterisk) does not extend beyond the staphyloma edge. Epiretinal membrane with inner limiting membrane (arrows in bottom right image) can be seen within the area of the inner retinoschisis. The outer surface of the posterior vitreous (yellow arrowheads) is adhered to a retinal vessel (red arrowhead)

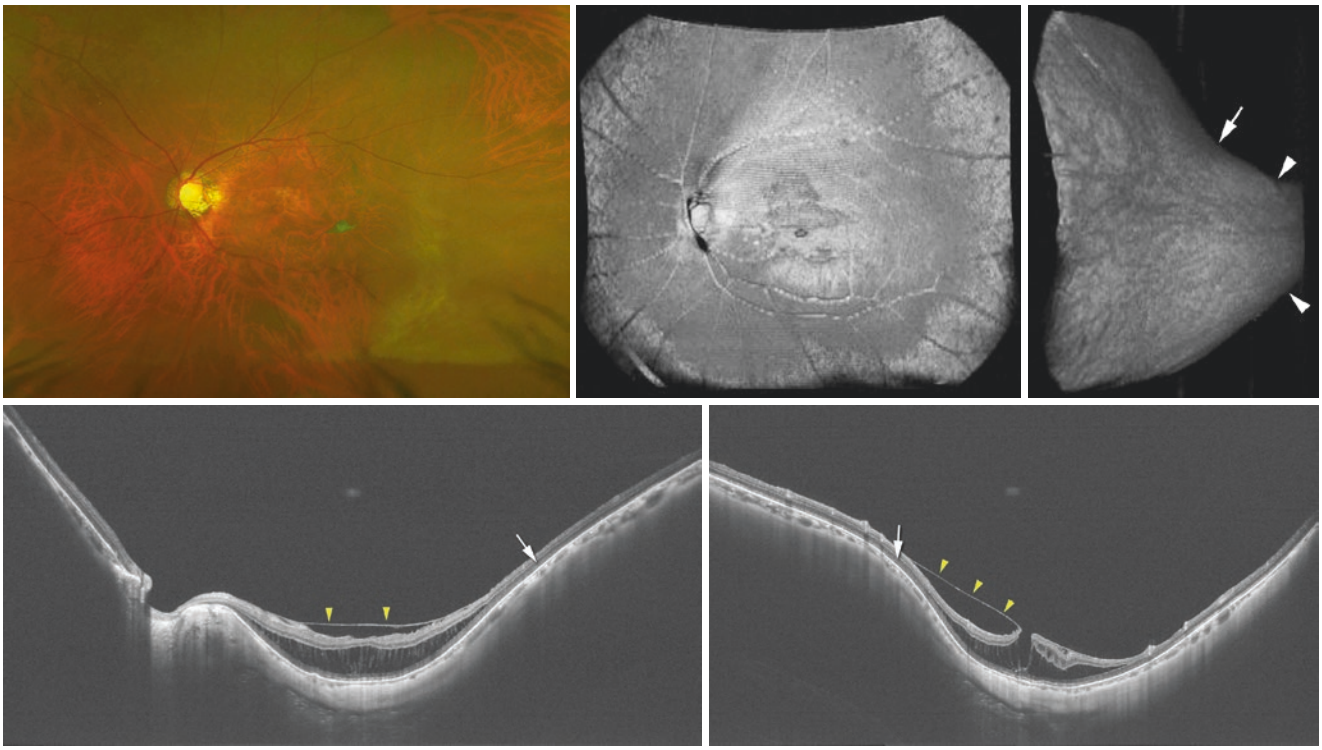

Fig. 19.3 Outer retinoschisis within an area of a narrow macular staphyloma (Reproduced with permission from [4]). (Top Left) Left fundus of an 80-year-old woman (axial length: 28.2 mm). The edge of the staphyloma is not obvious in the fundus photo. (Top middle and right) Three-dimensional UWF-OCT images viewed from the front (middle) and from the temporal side (right) showing a scleral outpouching (arrowheads) due to a narrow macular staphyloma. The staphyloma edge is marked by a notch (arrow). Bottom; UWF-OCT images in a horizontal section (Left) and in a vertical section (Right). At the staphyloma edge (arrows), a local inward protrusion of the sclera as well as a localized thinning of the choroid are seen. An outer retinoschisis is observed in a wide area but it does not extend beyond the staphyloma edge. The posterior vitreous (arrowheads) is attached to the retinal surface except for the foveal region. Posterior vitreous is adhered to the staphyloma edge and it lifts the fovea, resulting in a formation of an inner lamellar hole

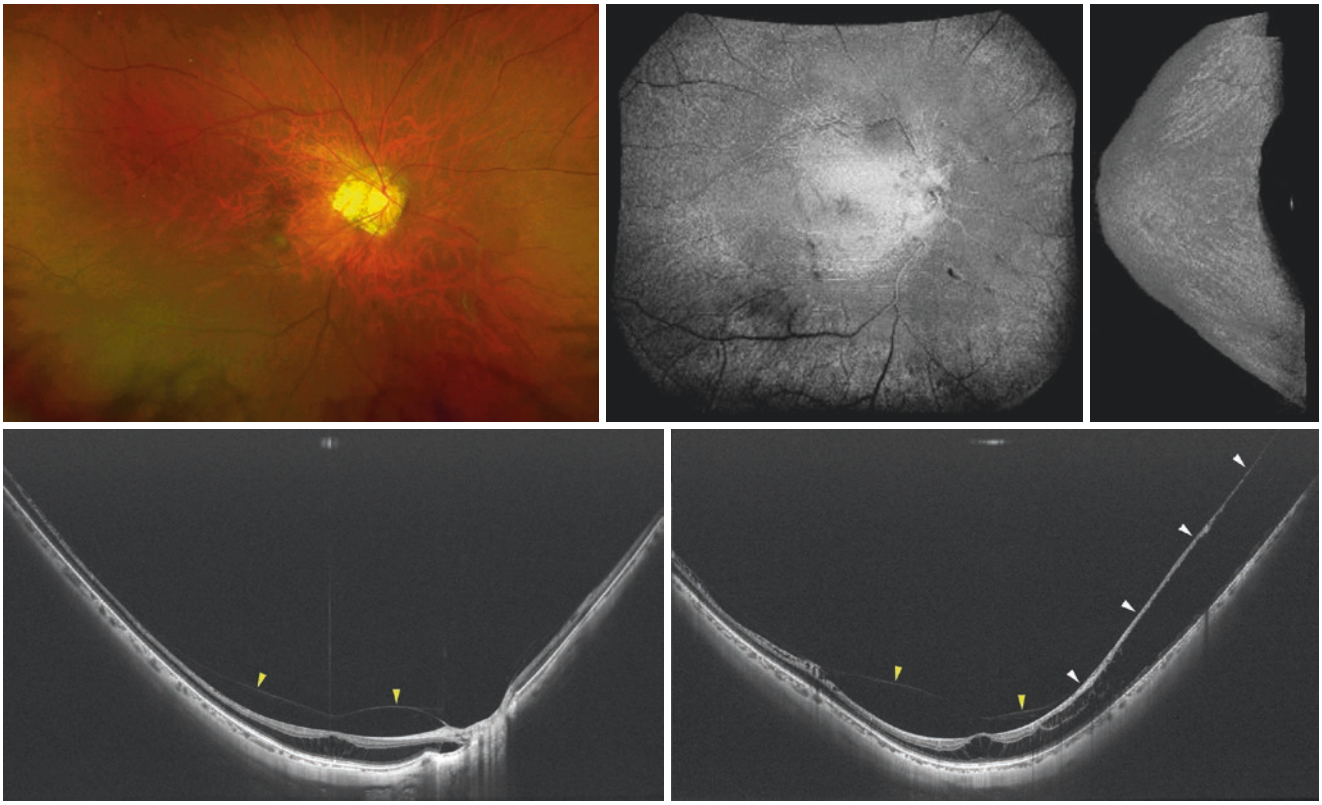

Fig. 19.4 UWF-OCT images of an outer retinoschisis without a posterior staphyloma (Reproduced with permission from [4]). (Top Left) Right fundus of a 59-year-old man (axial length: 28.2 mm). The edge of the staphyloma is not obvious in the fundus photo. (Top middle and Top right) Three-dimensional UWF-OCT images viewed from the front (middle) and from the temporal side (right). Both images do not show a posterior outpouching of the posterior segment suggesting a posterior staphyloma. (Bottom) UWF-OCT images in a horizontal section (Left) and in a vertical section (Right). An outer retinoschisis is observed in a wide area. In the vertical section, the outer retinoschisis spreads inferiorly. Posterior vitreous (yellow arrowheads) is seen. It is diffusely adhered to the inferior fundus (white arrowheads)

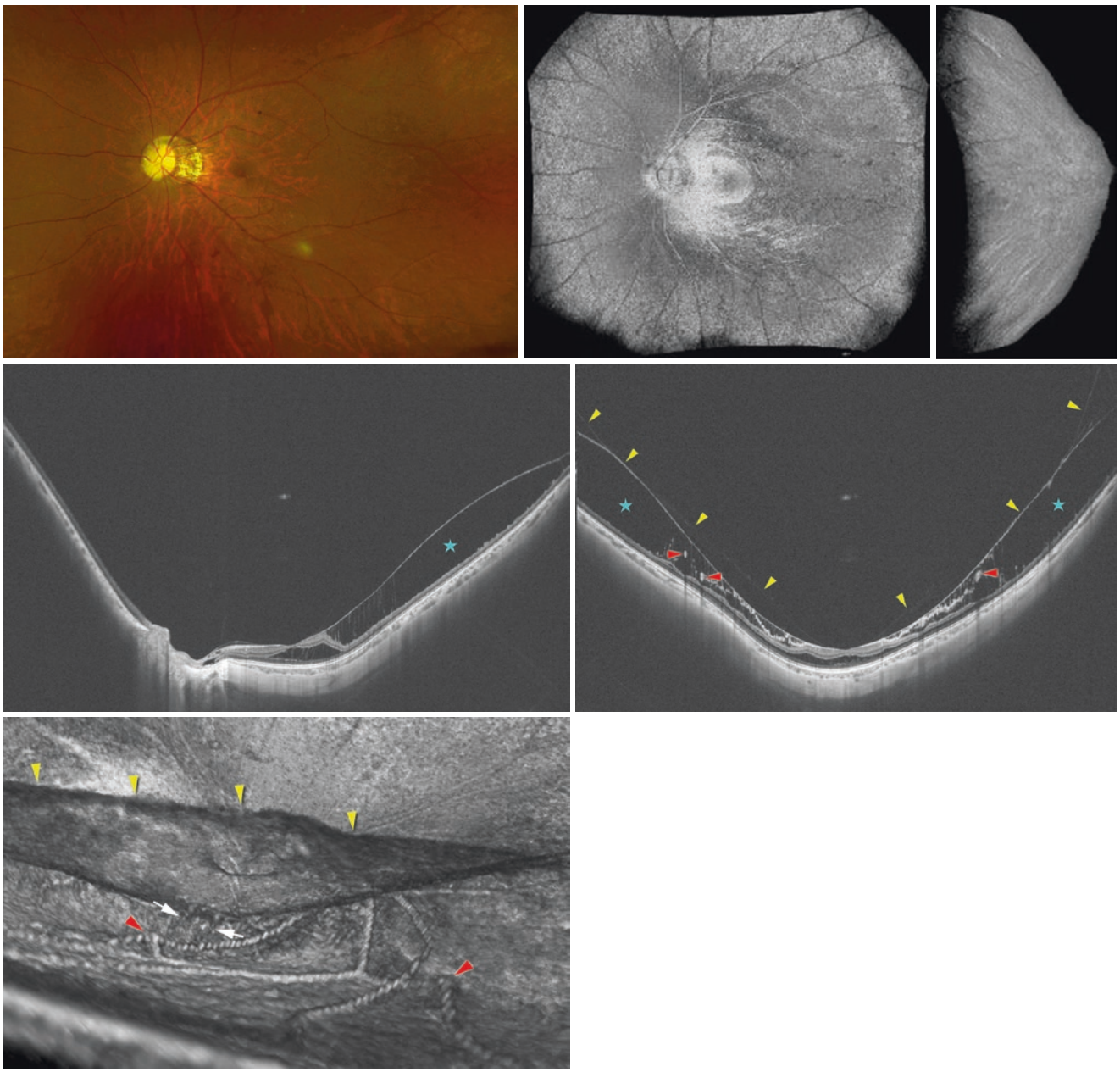

Fig. 19.5 Extended inner retinoschisis in an eye without a posterior staphyloma (Reproduced with permission from [4]). (Top Left) Left fundus of a 44-year-old woman (axial length: 29.0 mm). The edge of the staphyloma is not obvious in the fundus photo. (Top middle and Top right) Three-dimensional UWF-OCT images viewed from the front (middle) and from the temporal side (right) do not show a posterior outpouching of the posterior segment suggesting a posterior staphyloma. (Middle row) UWF-OCT images in a horizontal section (Left) and in a vertical section (Right). An outer retinoschisis can be seen only in the macular area. An extended inner retinoschisis (blue stars) can be seen. The retinal vessels (red arrowheads) appear to be pulled upwards and to be floating in the space of the inner retinoschisis. Yellow arrowheads show the posterior vitreous attached to the retinal surface in the region of the inner retinoschisis. (Bottom) Three-dimensional view constructed from a map scan shows a layer of detached inner limiting membrane (yellow arrowheads). Under the detached inner limiting membrane, retinal vessels are lifted up (red arrowheads). Columnar structures appear to connect the inner limiting membrane and the retinal vessels (arrows)

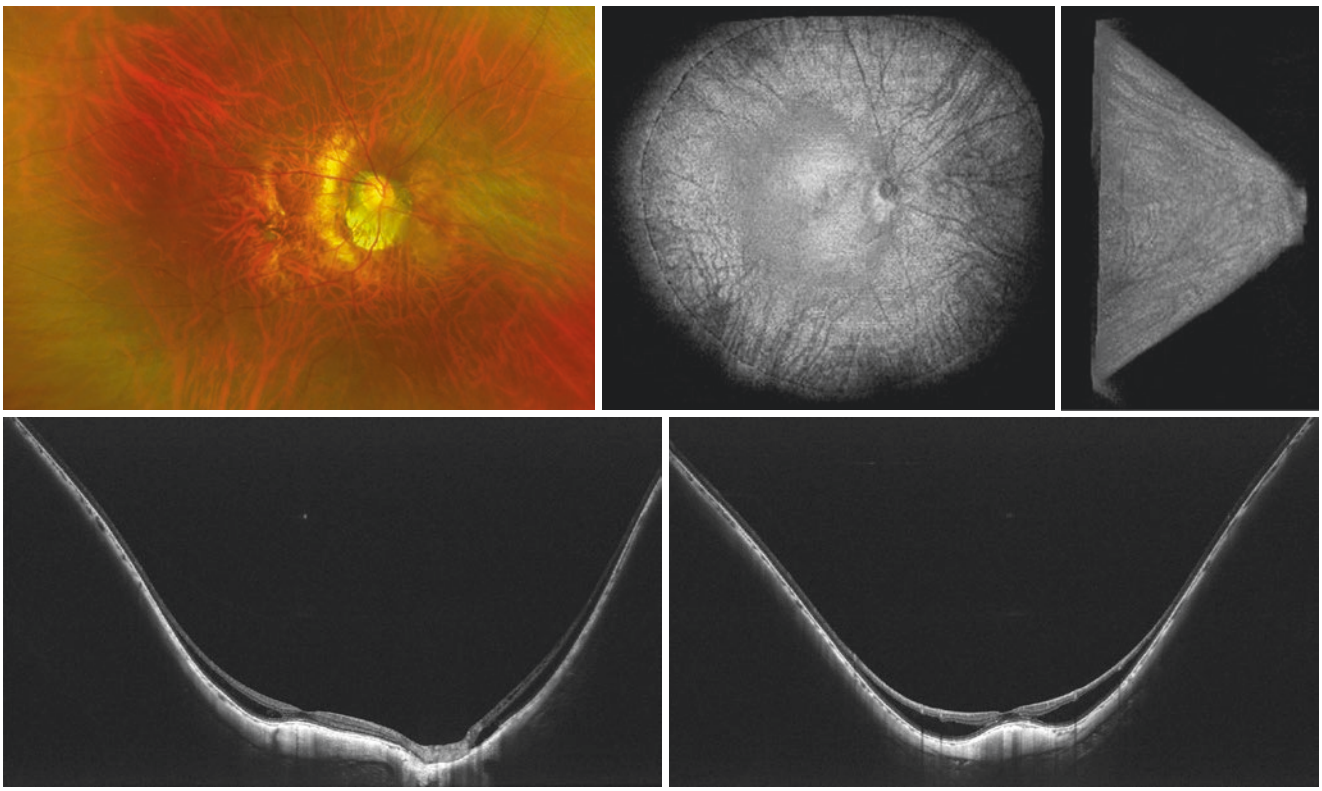

Fig. 19.6 Fovea-sparing outer retinoschisis in a patient with dome-shaped macula (Reproduced with permission from [4]). (Top Left) Right fundus of a 60-year-old woman (axial length: 30.3 mm). Staphyloma edges are not obvious in the fundus photo. (Top middle and Top right) Three-dimensional UWF-OCT images viewed from the front (middle) and from the nasal side (right). The images do not show a posterior outpouching of the posterior segment suggesting a posterior staphyloma. (Bottom) UWF-OCT images in a horizontal section (Left) and in a vertical section (Right). An outer retinoschisis, grade S4(D), surrounds a dome-shaped macula

References

1. Benhamou N, Massin P, Haouchine B, Erginay A, Gaudric A. Macular retinoschisis in highly myopic eyes. Am J Ophthalmol. 2002;133(6):794–800. https://doi.org/10.1016/s0002-9394(02)01394-6.
2. Fujimoto M, Hangai M, Suda K, Yoshimura N. Features associated with foveal retinal detachment in myopic macular retinoschisis. Am J Ophthalmol. 2010;150(6):863–70. https://doi.org/10.1016/j.ajo.2010.06.023.
3. Shimada N, Tanaka Y, Tokoro T, Ohno-Matsui K. Natural course of myopic traction maculopathy and factors associated with progression or resolution. Am J Ophthalmol. 2013;156(5):948–957.e1. https://doi.org/10.1016/j.ajo.2013.06.031.
4. Shinohara K, Tanaka N, Jonas JB, Shimada N, Moriyama M, Yoshida T, et al. Ultrawide-field OCT to investigate relationships between myopic macular Retinoschisis and posterior staphyloma. Ophthalmology. 2018;125(10):1575–86. https://doi.org/10.1016/j.ophtha.2018.03.053.

Macular Hole and Macular Hole Retinal Detachment

20

Hiroyuki Takahashi

Abstract

Myopic traction maculopathy (MTM) is a common complication of pathologic myopia. It is caused by outward tractional force due to a posterior staphyloma combined with inward tractional force of posterior vitreous. Among various lesions of MTM, macular hole retinal detachment causes a severe and an irreversible vision impairment. It is sometimes difficult to diagnose MTM with ophthalmoscopy because of the presence of chorioretinal atrophy in the macula, and thus optical coherence tomography is necessary to detect subtle retinal changes such as macular hole, macular retinoschisis, and foveal retinal detachment.

Keywords

Pathologic myopia · High myopia · Myopic traction maculopathy · Posterior staphyloma · Macular hole · Retinal detachment · Macular retinoschisis · Pars plana vitrectomy

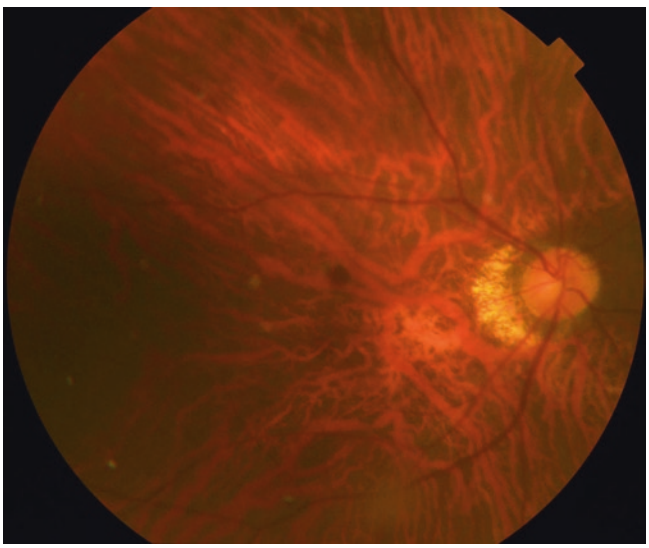

Fig. 20.1 Right eye of a 64-year-old highly myopic woman with a full-thickness macular hole. The axial length is 28.4 mm. Because of the tessellated fundus, macular hole is hard to recognize

20.1 Macular Hole

Pathologic myopia is a known risk factor for the development of macular hole (MH). In eyes with pathologic myopia, abnormal vitreoretinal adhesion is present in the macular area as well as in the peripheral area, which causes MH formation in younger subjects compared to idiopathic MH. Also, different from MH in non-myopic patients, retinal detachment may result from MH in highly myopic patients.

In eyes with pathologic myopia, the presence of fundus tessellation and macular chorioretinal atrophy prevent accurate diagnosis of MH on fundus examination (Fig. 20.1). Thus, optical coherence tomography (OCT) is needed for detecting MH as well as the coexisting lesions like epiretinal membrane, macular retinoschisis, and epiretinal proliferative tissue, which are reported to be predictive factors of poor visual outcome [1] (Fig. 20.2).

Pars plana vitrectomy combined with dye-assisted internal limiting membrane (ILM) peeling and intraocular gas tamponade has been widely accepted as a worthwhile treatment for myopic MH as well as idiopathic MH (Fig. 20.2). Previous case-control studies showed a successful closure of MH, however, visual improvement after surgery was more difficult to achieve in highly myopic eyes than in non-highly myopic eyes [2–4]. Accordingly, newly invented techniques including inverted ILM flap or autologous retinal free flap are effective for enhancement of surgical closure of myopic MH.

H. Takahashi (✉)
Department of Ophthalmology and Visual Science, Tokyo Medical and Dental University (TMDU), Tokyo, Japan
e-mail: t.hiroyuki.oph@tmd.ac.jp

K. Ohno-Matsui (ed.), *Atlas of Pathologic Myopia*, https://doi.org/10.1007/978-981-15-4261-9_20

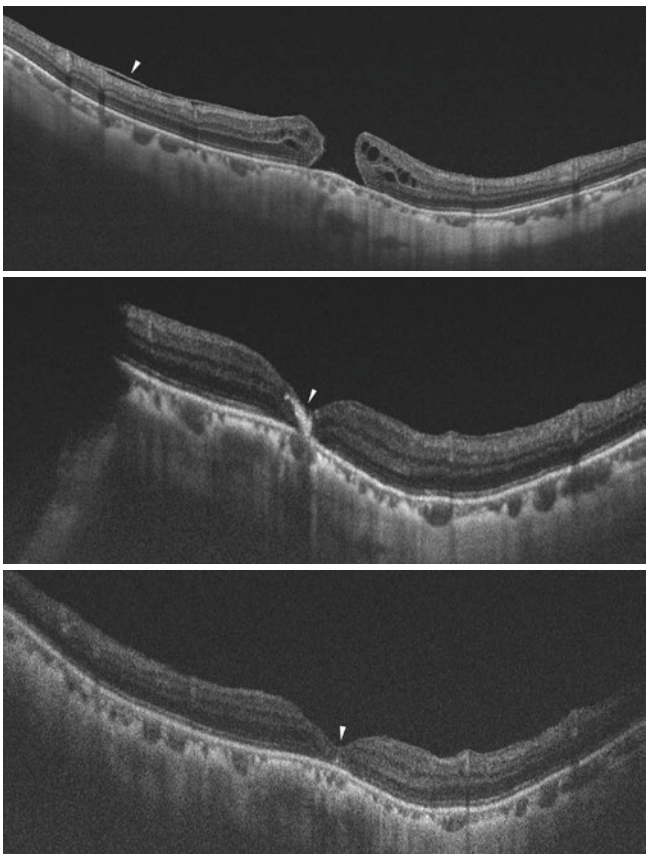

Fig. 20.2 A course of a closure of full-thickness macular hole after vitrectomy in a patient with pathologic myopia. (Top) A vertical scan of swept-source OCT shows full-thickness macular hole accompanied with epiretinal membrane (arrowhead). Ten days after pars plana vitrectomy with inverted internal limiting membrane (ILM) flap technique, the vertical scan of swept-source OCT shows a closure of macular hole and hyper-reflective tissue stuffed in a closed macular hole (arrowhead). The OCT images of superior part of the fundus is not available due to intraocular sulfur hexafluoride. At 3 months after surgery, a macular hole is closed in a vertical scan of swept-source OCT (arrowhead). Retinal microstructure is restored around the fovea, but it still remains disorganized at the fovea

Fig. 20.3 (Top) Right eye of 64-year-old highly myopic woman with macular hole retinal detachment. The axial length is 28.5 mm. Fundus image shows retinal detachment covering the entire posterior pole (margined by arrowheads). Macular chorioretinal atrophy is present beneath the detached retina (arrow). (Bottom) A vertical section of ultra-widefield swept-source OCT shows a retinal detachment and full-thickness macular hole. The fundus at 1 year after surgery is shown in Figs. 20.4 and 20.5

20.2 Macular Hole Retinal Detachment

Macular hole retinal detachment (MHRD) is one of the most vision-threatening complications of pathologic myopia. MHRD requires immediate surgical intervention because it can lead to irreversible retinal damages [5, 6]. Compared to retinal breaks in the peripheral retina, MH rarely causes retinal detachment. Actually, MHRD accounts for 0.5 to 4% of all patients of rhegmatogeneous retinal detachment [7]. High myopia, trauma, and proliferative vitreoretinopathy are causative factors for MHRD [8].

In eyes with pathologic myopia, MHRD has been reported to be due to tangential macular traction generated by the vitreoretinal interface, presence of a posterior staphyloma, or an atrophy of the retinal pigment epithelium [9, 10]. In addition, complications including epiretinal membrane, macular retinoschisis, an abrupt change of scleral curvature in the macular area and macular chorioretinal atrophy contribute to the development of MHRD (Figs. 20.3 and 20.4). Accordingly, a removal of the epiretinal membrane is necessary, and a removal of the internal limiting membrane (ILM) is effective for reattachment of neurosensory retina. Among newly invented surgical procedures, inverted ILM flap technique is useful to form a base for the tissue closing MH and to induce the recovery of foveal microstructure (Fig. 20.5).

Fig. 20.4 (Top) One year after pars plana vitrectomy combined with internal limiting membrane (ILM) removal, the fundus shows reattachment of the retina. Macular atrophy is seen more obviously than prior to surgery. (Bottom) A horizontal section of swept-source OCT shows retinal reattachment at 1 year after surgery. The macular hole is closed with scarred tissue, however, retinal microstructure is not restored yet. Retina is very thinned in the area of macular atrophy

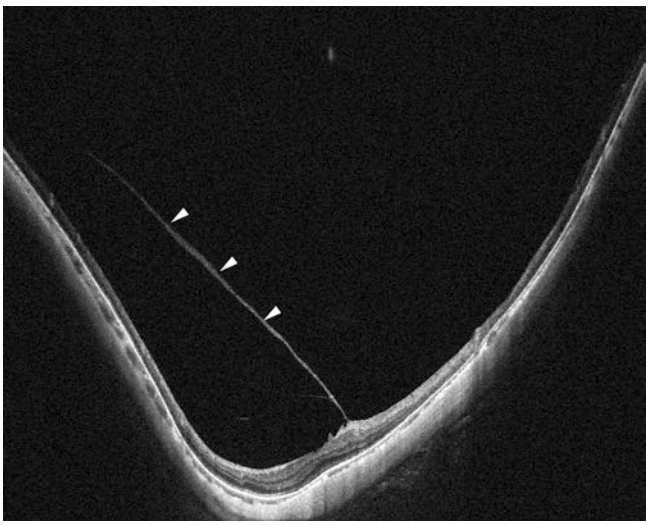

Fig. 20.5 The vertical scanning image of ultra-widefield swept-source OCT shows asymmetrical posterior vitreous detachment (PVD) in the right eye of 57-year-old highly myopic woman with an axial length of 30.9 mm. The area of PVD (arrowheads) corresponds to the area where the sclera protrudes posteriorly

Visual prognosis of MHRD is not satisfactory yet even when successful retinal reattachment and MH closure are achieved. Restoration of photoreceptor cells is complicated by the presence of macular chorioretinal atrophy. In addition, recurrences of retinal detachment sometimes occur because the remnants of vitreous cortex cause tangenital vitreoretinal traction on the surface of retina. Thus, a long-term follow-up after surgery is necessary.

20.3 Vitreous Changes in Eyes with Pathologic Myopia

20.3.1 Early Liquefaction and Large Premacular Bursae

An earlier liquefaction and a larger cistern of the vitreous are detected in highly myopic eyes by slit-lamp observation. In OCT examination, a large empty spaces are present above the macula, so-called premacular bursae. The liquefactions of vitreous body may cause floaters in the vision even in young patients.

20.3.2 Early and Asymmetrical Posterior Vitreous Detachment

In highly myopic eyes, posterior vitreous detachment (PVD) is present in younger subjects than in non-highly myopic eyes [11]. In addition, highly myopic eyes more frequently had residual vitreous cortex that is adhered to the surface of the retina. As PVD progresses in highly myopic eyes, posterior vitreous detaches from the retinal surface in an asymmetrical fashion [12]. The area of the PVD corresponds to the area where the sclera protrudes most posteriorly (Fig. 20.6).

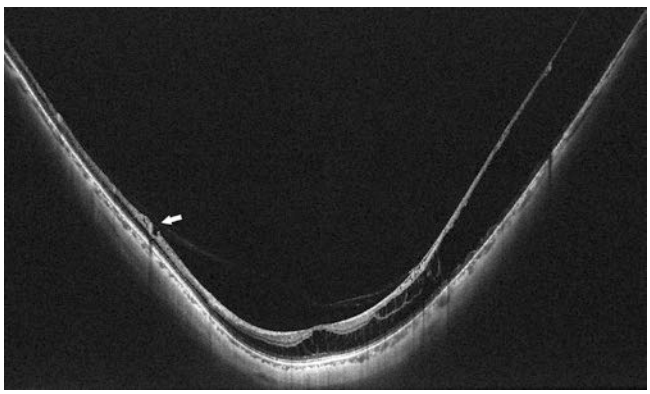

Fig. 20.6 The vertical scanning image of ultra-widefield swept-source OCT shows myopic retinoschisis in the right eye of 59-year-old highly myopic man with an axial length of 28.2 mm. Posterior vitreous adheres to retinal vessel and causes paravascular lamellar hole (arrow)

20.3.3 Vitreous Adhesion to Retinal Vessels, Which is Associated with Retinoschisis

Posterior vitreous adheres to retinal vessels. Retinal vessels are lifted by posterior vitreous and paravascular retinal lesions such as paravascular retinal cysts and paravascular lamellar holes develop. Vitreal tractions onto retinal surface also cause retinoschisis extending to the macular area.

References

1. Jo Y, Ikuno Y, Nishida K. Retinoschisis: a predictive factor in vitrectomy for macular hole without retinal detachment in highly myopic eyes. Br J Opthalmol. 2012;96(2):197–200.
2. Sulkes DJ, Smiddy WE, Flynn HW, Feuer W. Outcomes of macular hole surgery in severely myopic eyes: a case-control study. Am J Ophthalmol. 2000;130:335–9.
3. Patel SC, Loo RH, Thompson JT, Sjarrda RN. Macular hole surgery in high myopia. Ophthalmology. 2001;108:377–80.
4. Kwok AK, Lai TY. Internal limiting membrane removal in macular hole surgery for severely myopic eyes: a case-control study. Br J Ophthalmol. 2003;87:885–9.
5. Morita H, Ideta H, Ito K, Yonemoto J, Sasaki K, Tanaka S. Causative factors of retinal detachment in macular holes. Retina. 1991;11:281–4.
6. Ripandelli G, Rossi T, Scarinci F, et al. Macular vitreoretinal interface abnormalities in highly myopic eyes with posterior staphyloma: 5 year follow-up. Retina. 2012;32:1531–8.
7. Margherio RR, Schepens CL. Macular breaks. I. Diagnosis, etiology, and observations. Am J Ophthalmol. 1972;74:219–32.
8. Aaberg TM, Blair CJ, Gass JDM. Macular holes. Am J Ophthalmol. 1970;69:555–62.
9. Siam A. Macular hole with central retinal detachment in high myopia with posterior staphyloma. Br J Ophthalmol. 1969;53:62–3.
10. Stripe M, Micheals RG. Retinal detachment in highly myopic eyes due to macular holes and epiretinal traction. Retina. 1990;10:113–4.
11. Itakura H, Kishi S, Li D, et al. Vitreous changes in high myopia observed by swept-source optical coherence tomography. Invest Ophthalmol Vis Sci. 2014;55(3):1447–52.
12. Takahashi H, Tanaka N, Shinohara K, et al. Ultra-widefield optical coherence tomographic imaging of posterior vitreous in eyes with high myopia. Am J Ophthalmol. 2019;206:102–12.

Surgical Outcome

21

Kosei Shinohara

Abstract

Vitrectomy with inner limiting membrane (ILM) peeling is the common treatment for myopic macular retinoschisis (MRS). Postoperative full-thickness macular hole is a severe complication of this treatment, and fovea-sparing ILM peeling has been proposed to prevent this complication. Fovea-sparing ILM peeling is an effective method for the improving morphology and function of the retina in eyes which have MRS with or without foveal retinal detachment; however, postoperative microscotomas occasionally develop after vitrectomy with ILM peeling.

Keywords

Myopic macular retinoschisis · Vitrectomy · Fovea-sparing inner limiting membrane peeling · Microscotoma

To treat MRS and to prevent the progression of MRS to more serious complications, surgical procedures including vitrectomy with or without inner limiting membrane (ILM) peeling [1–4], macular buckling [5, 6], and scleral imbrication [7] have been applied. All of them have been reported effective for the resolution of MRS. Vitrectomy is the most commonly used method among them because of the relatively low invasiveness; however, the development of a full-thickness macular hole (MH) after vitrectomy is a severe complication especially in eyes with a foveal retinal detachment (fRD) (Fig. 21.1) [8]. To prevent this complication, Ho et al. [9] and Shimada et al. [10] reported that vitrectomy with fovea-sparing ILM peeling was an effective and a safe method to treat an MRS with a fRD (Fig. 21.2). According to the report by Shimada et al., [10] 11 of 15 eyes that had undergone fovea-sparing ILM peeling had an improvement of the best-corrected visual acuity (BCVA) by >0.2 logarithm of the minimum angle of resolution (logMAR) units, and none of the eyes developed a full-thickness MH (Fig. 21.3). On the other hand, 5 of 30 eyes treated with complete macular ILM peeling developed a full-thickness MH postoperatively. Later, Shinohara et al. [11] reported the functional improvement by using microperimetry in the eyes who had vitrectomy with fovea-sparing ILM peeling to treat MRS with or without fRD. The postoperative BCVA, the central retinal sensitivity, and the retinal sensitivity at 2° were significantly better than the preoperative values (Figs. 21.4 and 21.5). However, 16 eyes developed postoperative microscotomas at paracentral 2° and/or 6° (Fig. 21.6). These results suggest that a careful follow-up should be performed to detect postoperative microscotomas. Figure 21.7 shows the cases who have absolute and relative indications of fovea-sparing ILM peeling. Recently, Fang et al. [12] reported vitrectomy-related macular atrophy after surgery for MTM, as an important surgical complication in a long-term.

K. Shinohara (✉)
Department of Ophthalmology and Visual Science, Tokyo Medical and Dental University, Tokyo, Japan

Musashino Red-Cross Hospital, Tokyo, Japan

K. Ohno-Matsui (ed.), *Atlas of Pathologic Myopia*, https://doi.org/10.1007/978-981-15-4261-9_21

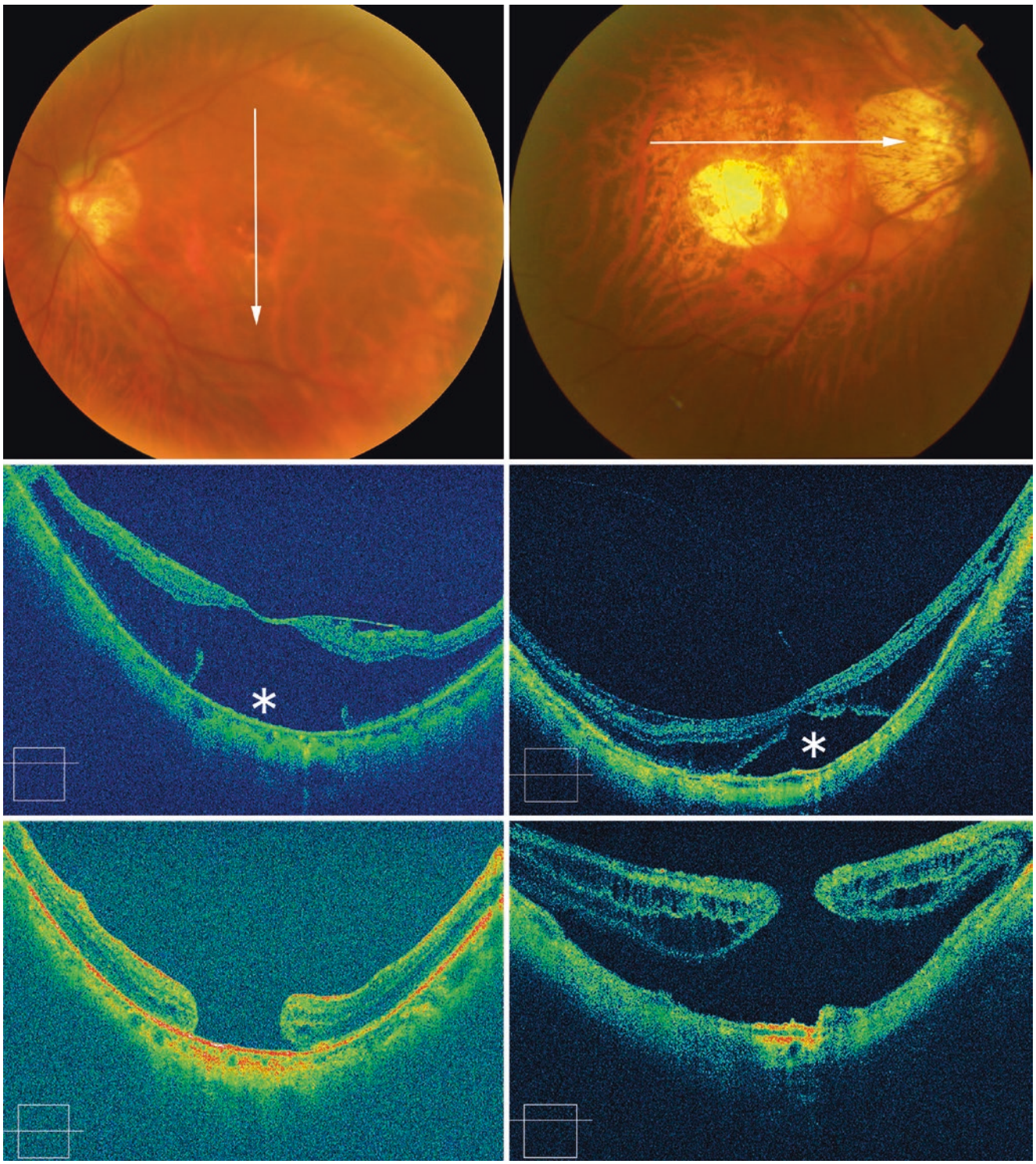

Fig. 21.1 Two representative cases that developed a full-thickness macular hole (MH) after vitrectomy with complete internal limiting membrane (ILM) peeling and gas tamponade to treat myopic foveal retinal detachment (fRD) (Reproduced with permission from [10]). (Top Left) Preoperative fundus photograph of the left eye of a 69-year-old woman with axial length of 27.4 mm. An arrow indicates the optical coherence tomography (OCT) scan line. The best-corrected visual acuity (BCVA) is 0.05. (Middle Left) Preoperative OCT image shows the fRD (asterisk) and macular retinoschisis. (Bottom Left) At 1 month after surgery, the retinoschisis is resolved, but a full-thickness MH is present. The BCVA has been reduced to 0.03. (Top Right) Preoperative fundus photograph of the right eye of a 63-year-old woman with axial length of 28.7 mm. An arrow indicates the OCT scan line. The BCVA is 0.1. (Middle Right) Preoperative OCT image shows the fRD (asterisk) and macular retinoschisis. (Bottom Right) At 2 months after surgery, a full-thickness MH with RD has developed

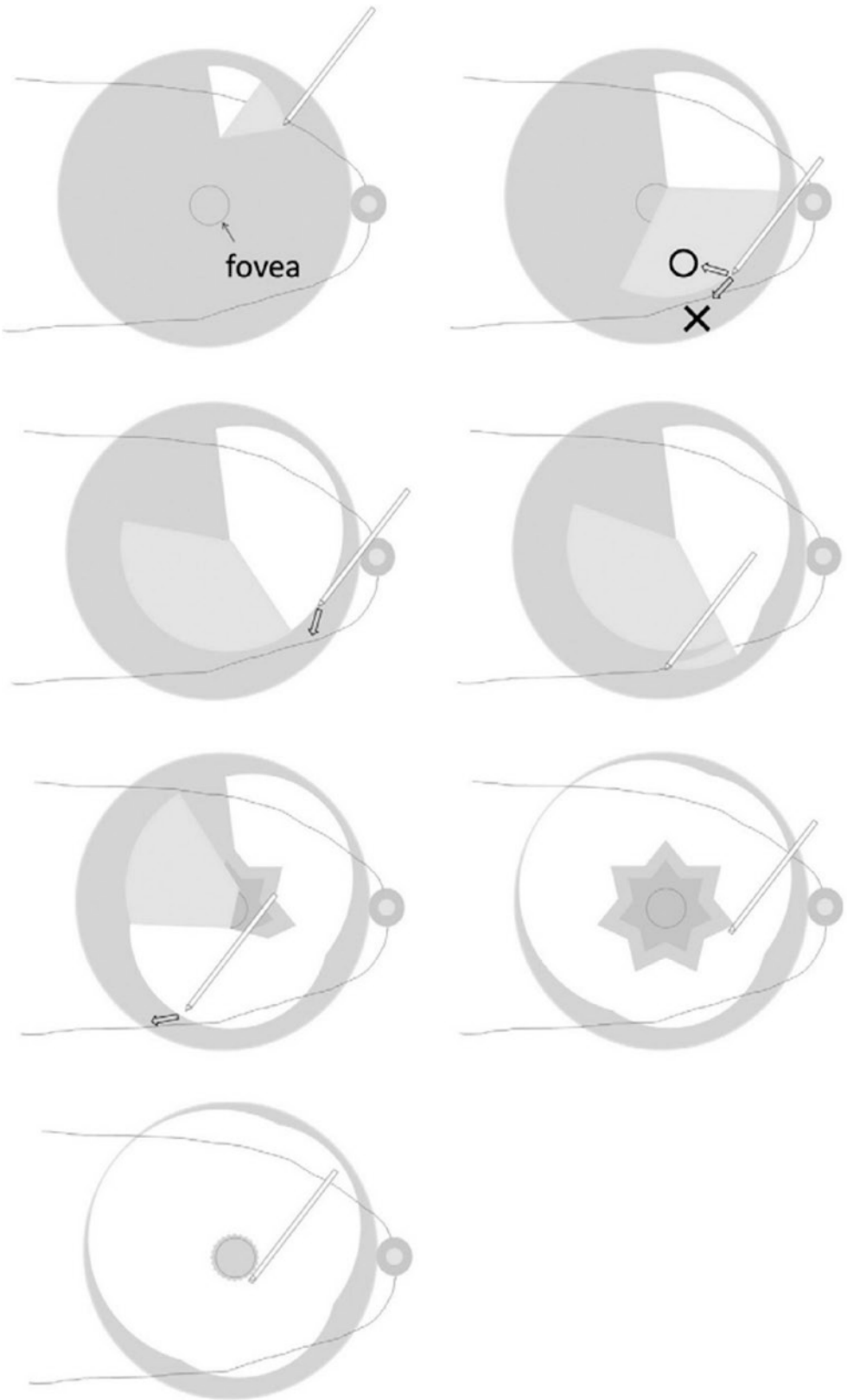

Fig. 21.2 Schematic drawings of fovea-sparing internal limiting membrane (ILM) peeling (Reproduced with permission from [10]). (Top left) Start ILM peeling away from the central fovea. (Top right) Proceed with the ILM peeling. (Second row left) When the peeled ILM flap comes close to the central fovea, stop and start ILM peeling from a new site. (Second row right) Proceed with ILM peeling from the new site with special attention not to peel the ILM around the central fovea. (Third row left) Start the ILM peeling from several new sites and proceed to peel ILM from the entire macular area away from the central fovea. (Third row right) Trim the ILM that remains on and around the fovea with a vitreous cutter. (Bottom left) Completed fovea-sparing ILM peeling

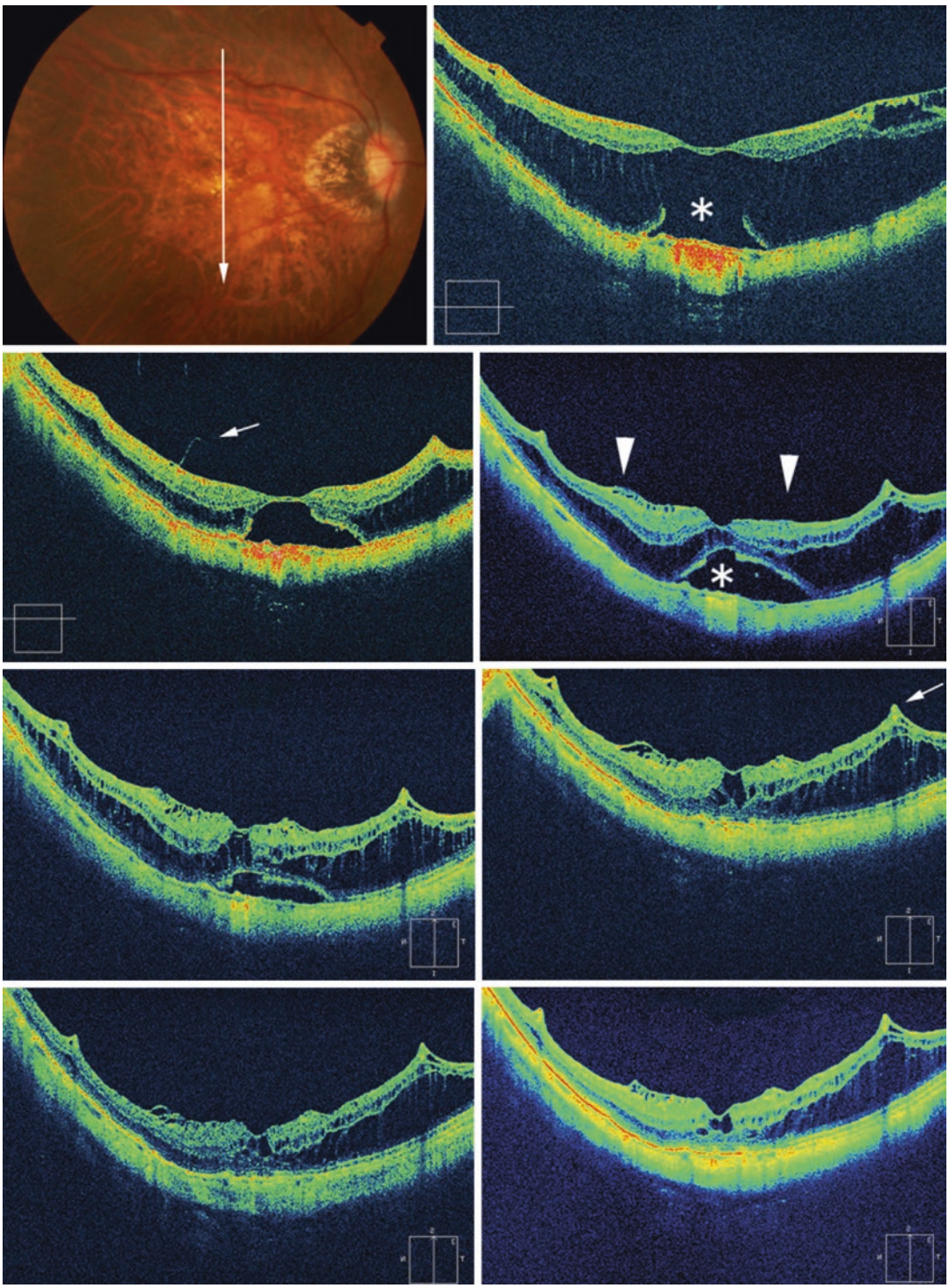

Fig. 21.3 Changes in optical coherence tomographic (OCT) findings after vitrectomy with fovea-sparing internal limiting membrane peeling and gas tamponade to treat myopic foveal retinal detachment (fRD) (Reproduced with permission from [10]). (Top left) Preoperative fundus photograph of the right eye of a 66-year-old woman with an axial length of 28.0 mm. Arrow indicates the OCT scan line. The best-corrected visual acuity (BCVA) is 0.2. (Top right) Preoperative OCT image shows foveal RD with large outer lamellar macular hole (asterisk) and macular retinoschisis. (Second row left) At 1 month after fovea-sparing ILM peeling, the retinoschisis is decreased along with the intraocular gas absorption. The fRD is still present, although reduced. The rolled edges of the ILM (arrow) can be seen. The BCVA is 0.3. (Second row right) At 3 months after surgery, the residual ILM (between arrowheads) appears to have contracted and thickened. The retinoschisis is slightly increased and fRD is still present. However, the outer lamellar hole has become smaller (asterisk). The BCVA is 0.3. (Third row left) At 6 months after surgery, the retinoschisis and fRD are still present, but decreased. The BCVA is 0.3. (Third row right) At 12 months after surgery, the fRD is completely resolved and the retinoschisis is also decreased except at the lower macular area around the retinal artery, which is observed as a retinal vascular microfold (arrow). The BCVA is 0.4. (Bottom) At 18 months (left) and 24 months (right) after surgery, the retinoschisis has been absorbed. The BCVA has improved to 0.7 at 24 months after the fovea-sparing ILM peeling

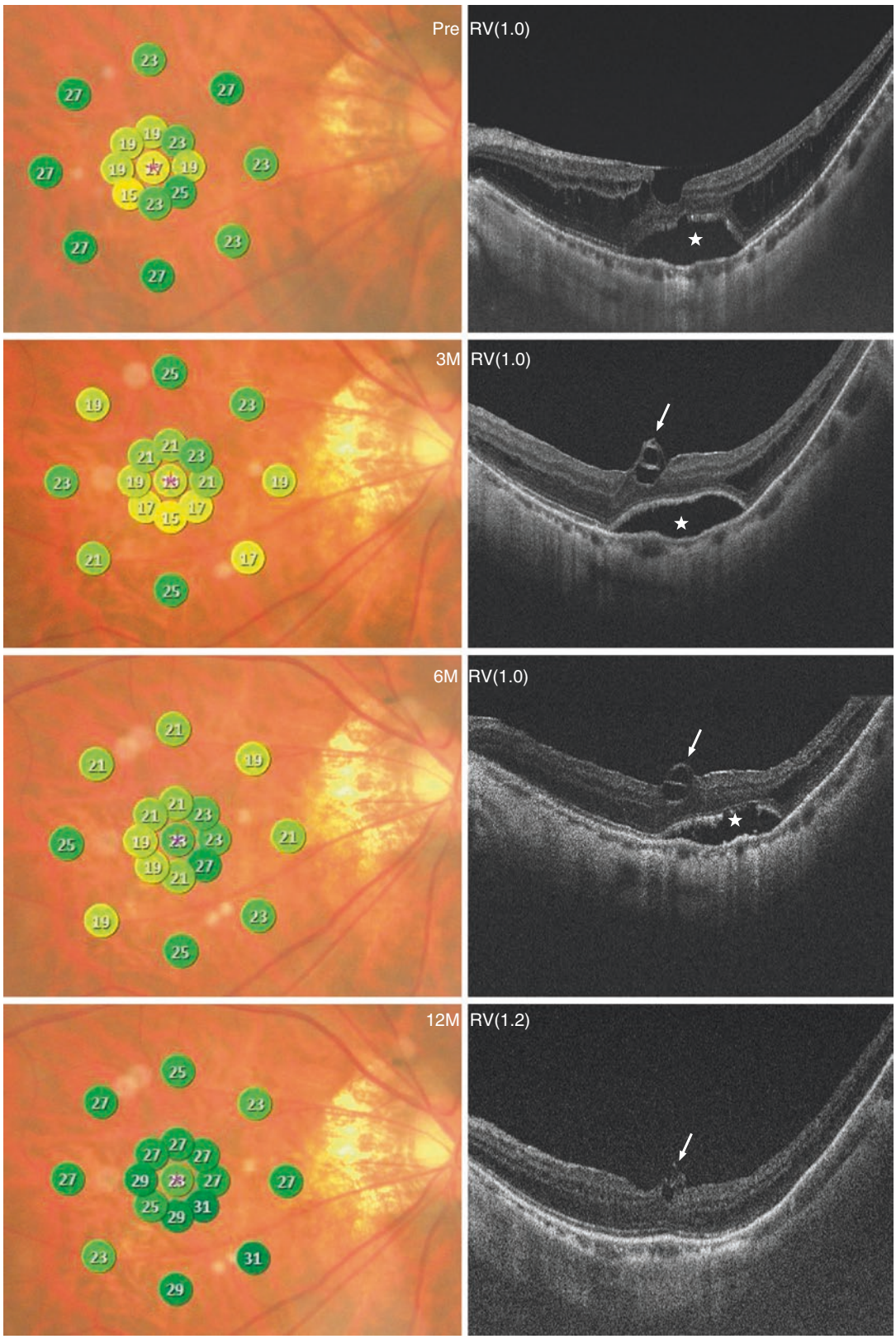

Fig. 21.4 Microperimetric and morphologic changes of the right eye with a foveal retinal detachment (fRD) in a 52-year-old woman (Reproduced with permission from [11]). The axial length is 31.2 mm. The time course is from the top row to the bottom row. The fRD (asterisk) is observed preoperatively and is gradually improved. The spared internal limiting membrane is observed until 12 months after the surgery (arrows). The central and paracentral retinal sensitivity at 2° has gradually improved after the surgery. The paracentral 6° retinal sensitivity has decreased 3 months after the surgery, but has gradually been improved until 12 months

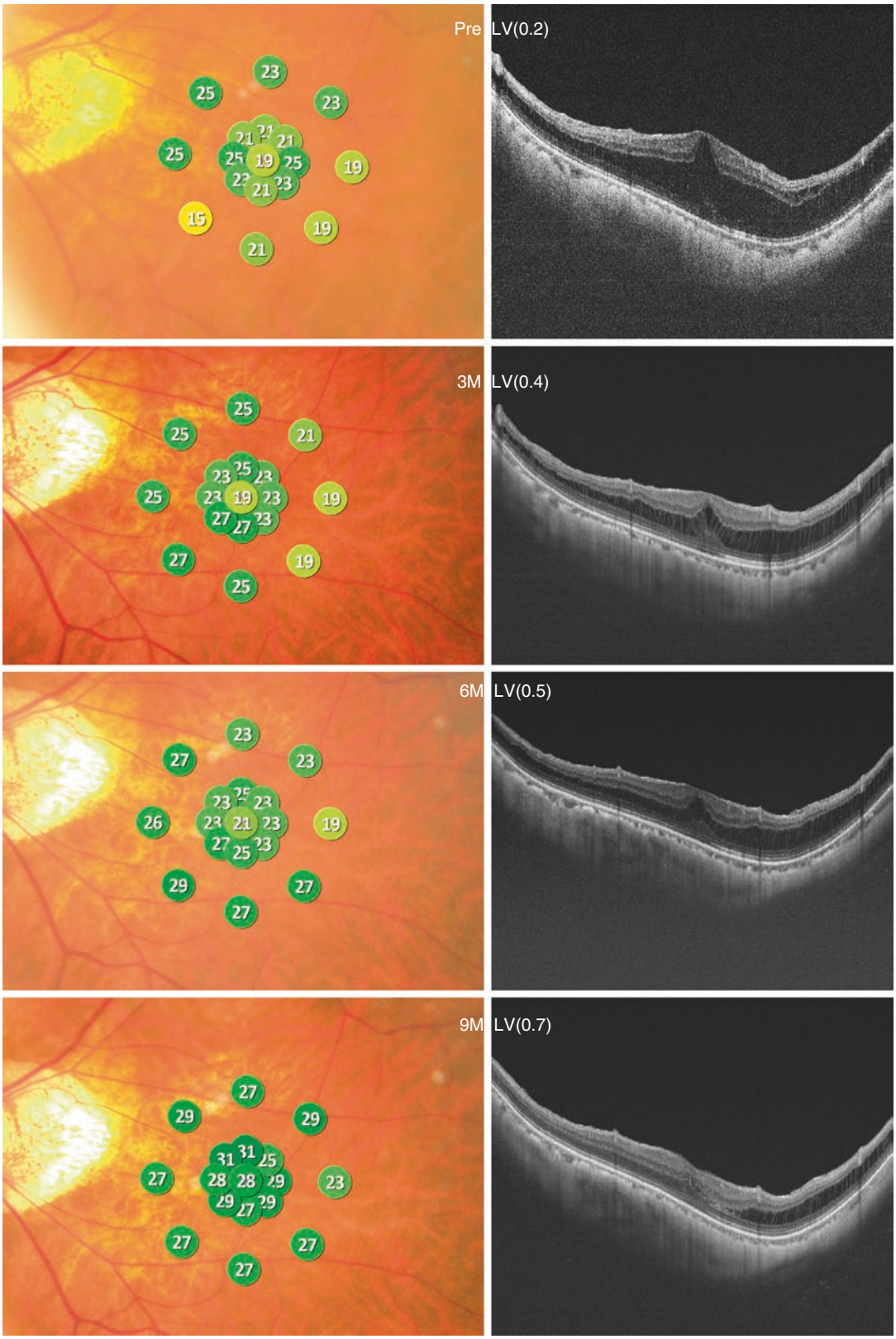

Fig. 21.5 Microperimetric and morphologic changes of the left eye of a 73-year-old man with a severe macular retinoschisis without a fRD. The axial length is 27.6 mm (Reproduced with permission from [11]). The time course is from the top row to the bottom row. The retinoschisis has gradually improved after the surgery. The visual acuity, central retinal sensitivity, paracentral 2° retinal sensitivity, and paracentral 6° retinal sensitivity have gradually improved after the surgery as the retinoschisis is resolved

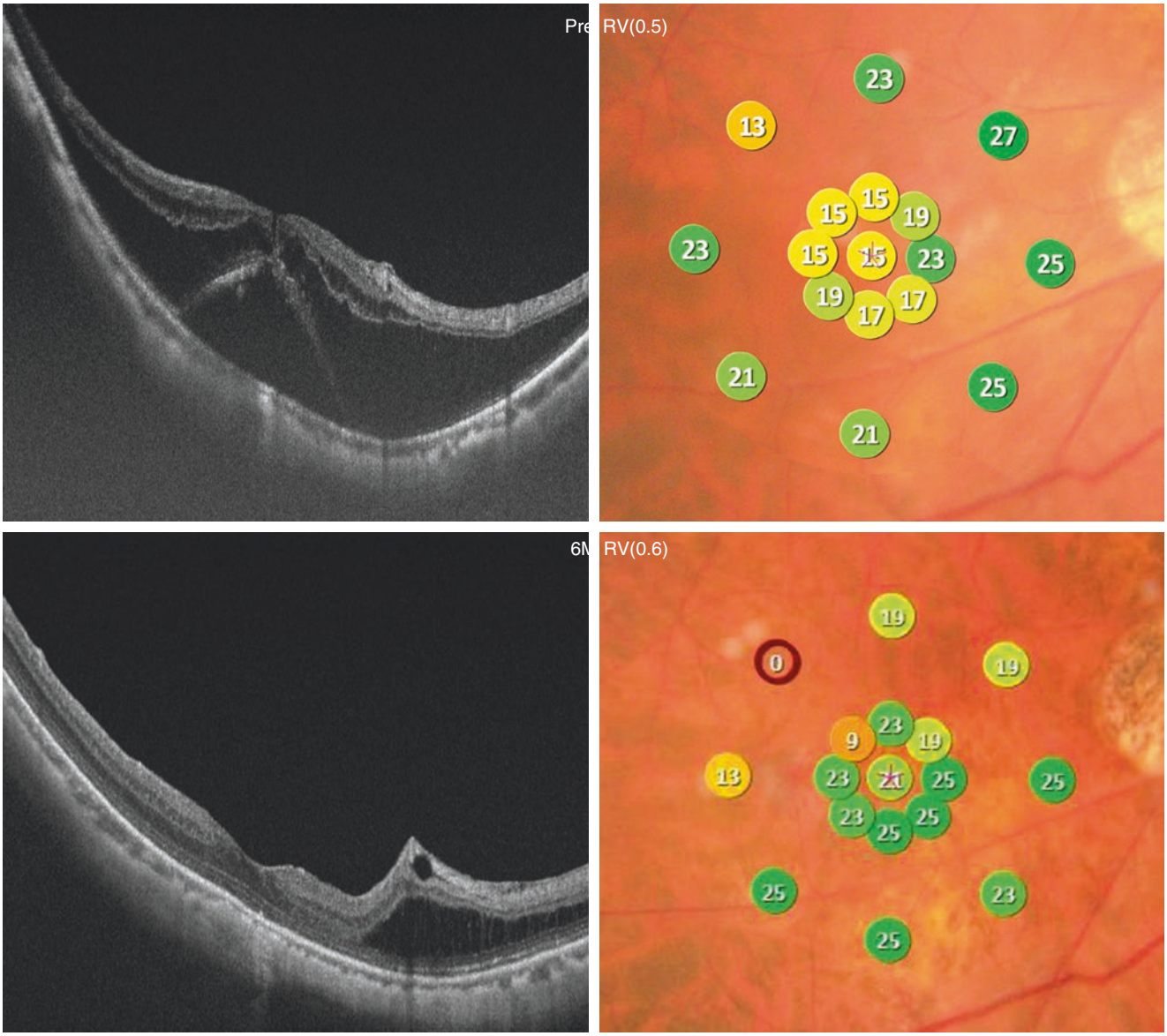

Fig. 21.6 Microperimetric and morphologic changes of the right eye with a severe macular retinoschisis and fRD in a 77-year-old woman developing microscotomas postoperatively. At 6 months after surgery (Bottom Row). The fRD and retinoschisis are morphologically improved and the visual acuity has also improved from (0.5) to (0.6) after surgery, however microscotomas at the upper temporal macula has developed

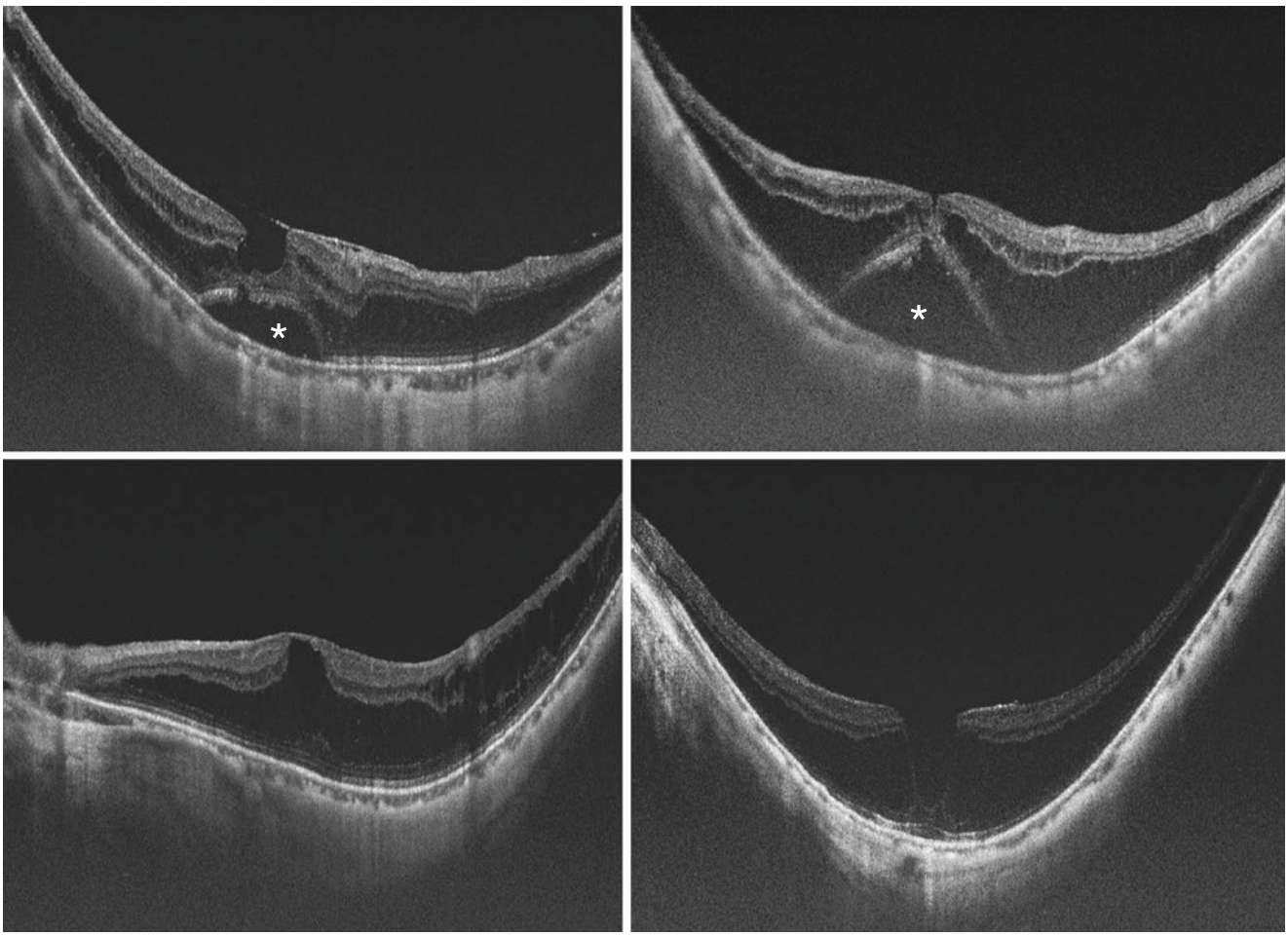

Fig. 21.7 Representative cases of absolute and relative indications for fovea-sparing ILM peeling. (Top row) Cases with absolute indications for fovea-sparing ILM peeling. The fRD (asterisk) is observed and the foveal retinal thickness is very thin. (Bottom row) Cases with relative indications for fovea-sparing ILM peeling. Severe MRS without fRD is observed

References

1. Panozzo G, Mercanti A. Vitrectomy for myopic traction maculopathy. Arch Ophthalmol. 2007;125(6):767–72.
2. Ho TC, Yang CM, Huang JS, et al. Long-term outcome of foveolar internal limiting membrane nonpeeling for myopic traction maculopathy. Retina. 2014;34(9):1833–40.
3. Ikuno Y, Sayanagi K, Ohji M, et al. Vitrectomy and internal limiting membrane peeling for myopic foveoschisis. Am J Ophthalmol. 2004;137(4):719–24.
4. Kim KS, Lee SB, Lee WK. Vitrectomy and internal limiting membrane peeling with and without gas tamponade for myopic foveoschisis. Am J Ophthalmol. 2012;153(2):320–6.
5. Baba T, Tanaka S, Maesawa A, et al. Scleral buckling with macular plombe for eyes with myopic macular retinoschisis and retinal detachment without macular hole. Am J Ophthalmol. 2006;142(3):483–7.
6. Mateo C, Bures-Jelstrup A, Navarro R, Corcostegui B. Macular buckling for eyes with myopic foveoschisis secondary to posterior staphyloma. Retina. 2012;32(6):1121–8.
7. Ando Y, Hirakata A, Ohara A, et al. Vitrectomy and scleral imbrication in patients with myopic traction maculopathy and macular hole retinal detachment. Graefes Arch Clin Exp Ophthalmol. 2017;255(4):673–80.
8. Hirakata A, Hida T. Vitrectomy for myopic posterior retinoschisis or foveal detachment. Jpn J Ophthalmol. 2006;50(1):53–61.
9. Ho TC, Chen MS, Huang JS, et al. Foveola nonpeeling technique in internal limiting membrane peeling of myopic foveoschisis surgery. Retina. 2012;32(3):631–4.
10. Shimada N, Sugamoto Y, Ogawa M, et al. Fovea-sparing internal limiting membrane peeling for myopic traction Maculopathy. Am J Ophthalmol. 2012;154(4):693–701.
11. Shinohara K, Shimada N, Takase H, Ohno-Matsui K. Functional and structural outcomes after fovea-sparing internal limiting membrane peeling for myopic macular retinoschisis by microperimetry. Retina. 2019; https://doi.org/10.1097/IAE.0000000000002627.
12. Fang Y, Yokoi T, Shimada N, et al. Development of macular atrophy after pars plana vitrectomy for myopic traction maculopathy and macular hole retinal detachment in pathologic myopia. Retina. 2019; https://doi.org/10.1097/IAE.0000000000002709.

Part VI

Dome-Shaped Macula

Dome-Shaped Macula

22

Yuxin Fang

Abstract

Dome-shaped macula (DSM) is an inward bulge of the macula identified with OCT. DSM is a local thickening of macular sclera. It can be classified into three morphologic patterns: round dome, horizontal ridge, and vertical ridge. Macular complications of DSM include serous retinal detachment, retinal pigment epithelial abnormalities, and macular neovascularization. DSM can be also detected in highly myopic children. The pathogenesis of DSM remains unclear.

Keywords

Dome-shaped macula (DSM) · Horizontal ridge · Vertical ridge · Macular bulge · Serous retinal detachment

Dome-shaped macula (DSM) was first described as an inward bulge of the macula in OCT images [1]. Quantitative definition of DSM is macular bulge height of >50 μm in the most convex scan in either vertical or horizontal scan [2]. DSM is an important finding in highly myopic eyes, but it is also found in mildly myopic or even in emmetropic eyes [3]. The prevalence of DSM in high myopic eyes has been estimated up to 20% in Japan [4] and about 10.7% in Europe [1]. DSM is considered to be irregularities of posterior scleral curvature independent of posterior staphylomas [5].

OCT examination is indispensable for the diagnosis of DSM. Three-dimensional (3D) reconstructions of OCT allow the precise investigations of DSM. DSM is classified into three morphologic patterns: round dome, horizontal ridge, and vertical ridge [6]. The round dome is seen as a round and radially symmetric inward bulge which can be seen in both horizontal and vertical scans (Fig. 22.1). However, the majority of DSM is not a typical round dome but horizontal ridge-shaped in which the inward bulge can be detected only in vertical axis and horizontal axis is either slightly elevated or flat (Fig. 22.2). Vertical ridge-shaped DSM, relatively rare in Japanese patients, is characterized by the inward bulge presenting only in the horizontal sections (Fig. 22.3). Regarding the significant variations of morphology in DSM, radial OCT scans or at least both vertical and horizontal scans should be used for screening, examining, and a follow-up of the eyes with DSM. Besides OCT findings, the appearance of a horizontal ridge connecting the optic disc and the fovea (Fig. 22.4), and the existence of macular pigmentation in fundus photographs may also provide the important clues to suspect the presence of DSM [4]. It is also noted that the eyes with inferior staphylomas (type V in Curtin's classification) including titled disc syndrome, in which the upper edge of staphyloma is across the fovea, should be differentiated from eyes with horizontal ridge-shaped DSM.

Macular bulge height is a useful indicator for dynamic changes of DSM. The macular bulge height in highly myopic eyes with DSM is around 152–188 μm in Japanese groups [2, 4], but is much higher, around 400 μm, in European group [6, 7]. Over time, the macular bulge height increases (Fig. 22.2). It is suspected that the apparent increase of dome height is related to the more profound scleral thinning in the parafoveal area than at the foveal center during a follow-up [8].

The pathogenesis of DSM remains unclear. Several hypotheses have been suggested including localized thickening of the choroid [1], local thickening of the subfoveal sclera which is adaptive or compensatory response to the defocus of the image on the fovea [5] and macular Bruch's membrane defects [9].

Macular complications of DSM include serous retinal detachment (Fig. 22.1), retinal pigment epithelial abnormalities, and macular neovascularization (Fig. 22.5). The prevalence of serous RD is markedly variable from 2 to 67% depending on the series, which is rare in Asians [2, 4, 10] and much higher in Europeans [1, 11]. The presence of

Y. Fang (✉)
Department of Ophthalmology and Visual Science, Tokyo Medical and Dental University, Tokyo, Japan

K. Ohno-Matsui (ed.), *Atlas of Pathologic Myopia*, https://doi.org/10.1007/978-981-15-4261-9_22

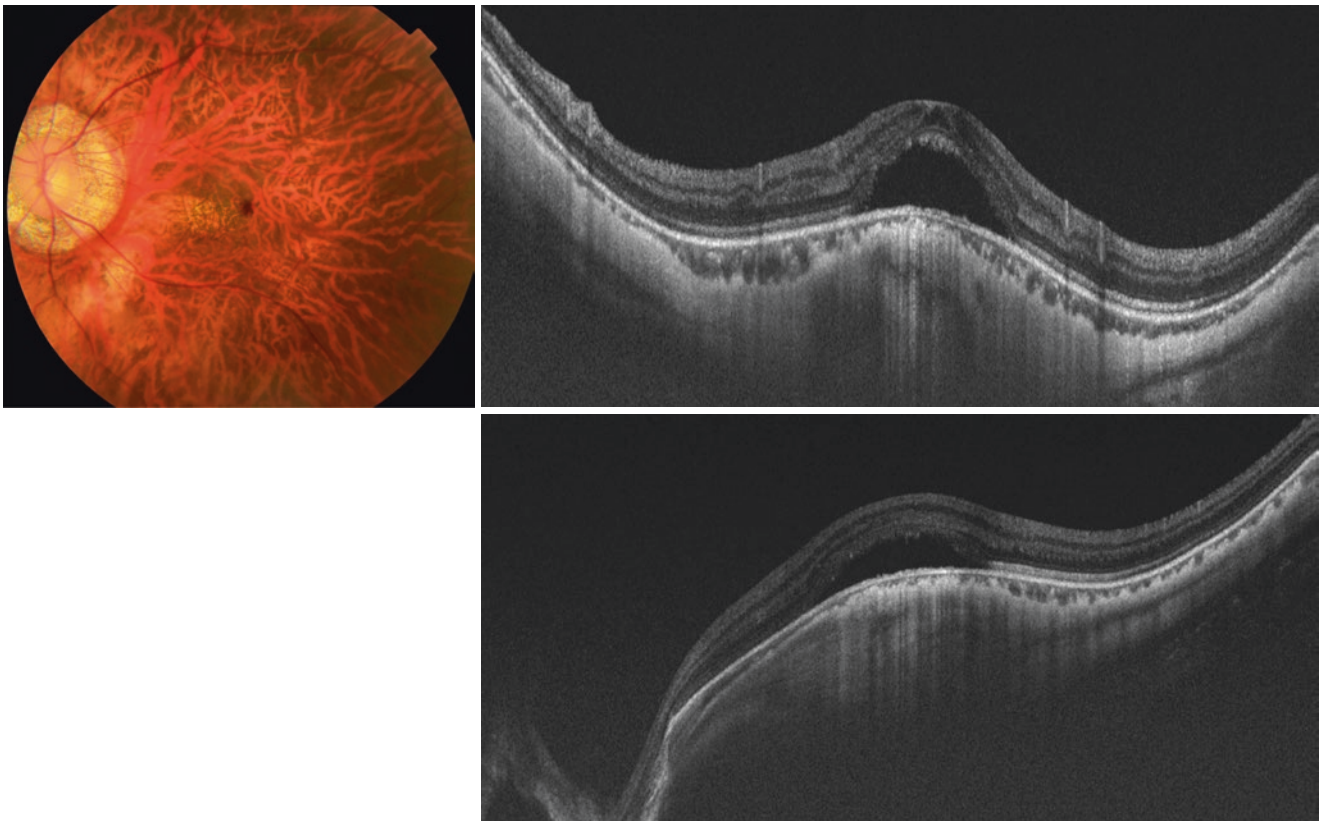

Fig. 22.1 Round type of dome-shaped macula (DSM) accompanying with serous retinal detachment (RD). Left fundus of a 42-year-old man with an axial length of 31.1 mm and the best-corrected visual acuity of 0.5 shows severe tessellation and granular pigmentary changes in the macula. Both vertical (Top Right) and horizontal (Bottom) OCT scans show an inward bulge of the macula with subretinal fluid on the top of the dome. The macular bulge height is 221 μm. Vertical scan also (Top Left) shows the superior and inferior choroid appears deepened around the dome which is called peri-dome choroidal deepening

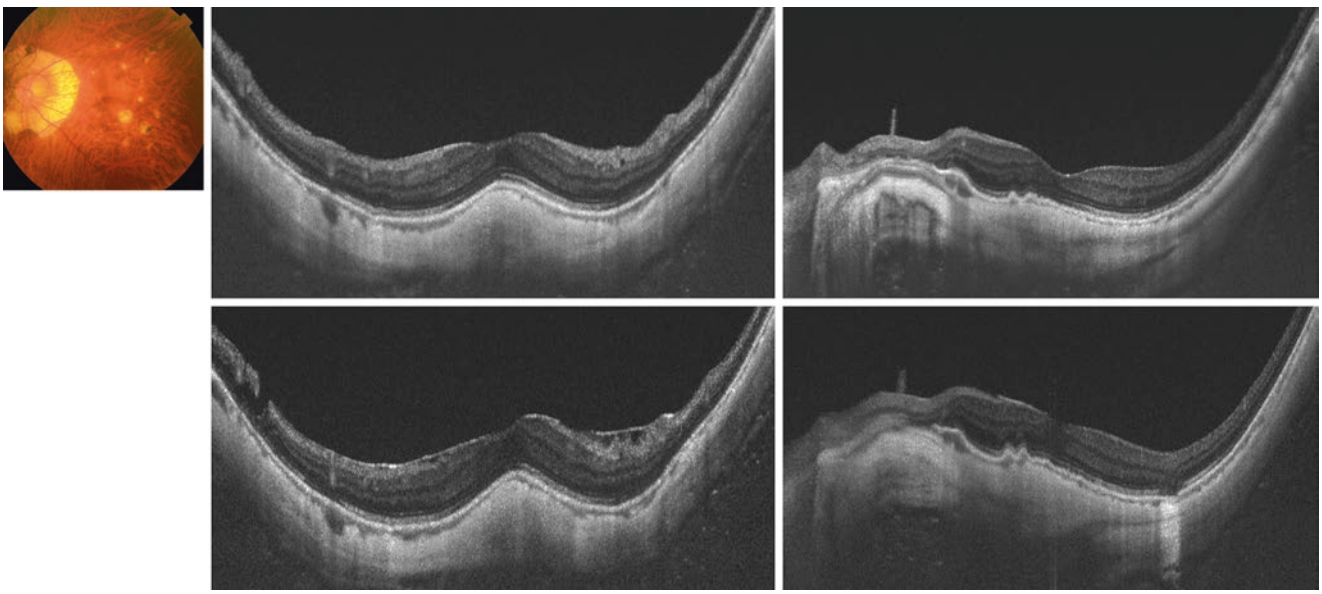

Fig. 22.2 Horizontal ridge-shaped dome-shaped macula (DSM). Left fundus of a 63-year-old man with an axial length of 33.4 mm and the best-corrected visual acuity of 0.7 shows multiple lesions of patchy atrophy. An inward protrusion of the macula is seen in vertical OCT scan across the fovea (Top Middle image). The horizontal scan (Top Right) shows the flat contour of the macula. The macular bulge height is 144 μm. After 4 years, the macular bulge has increased to 184 μm (Bottom Left image). The horizontal scan (Bottom Right) still show the flat contour

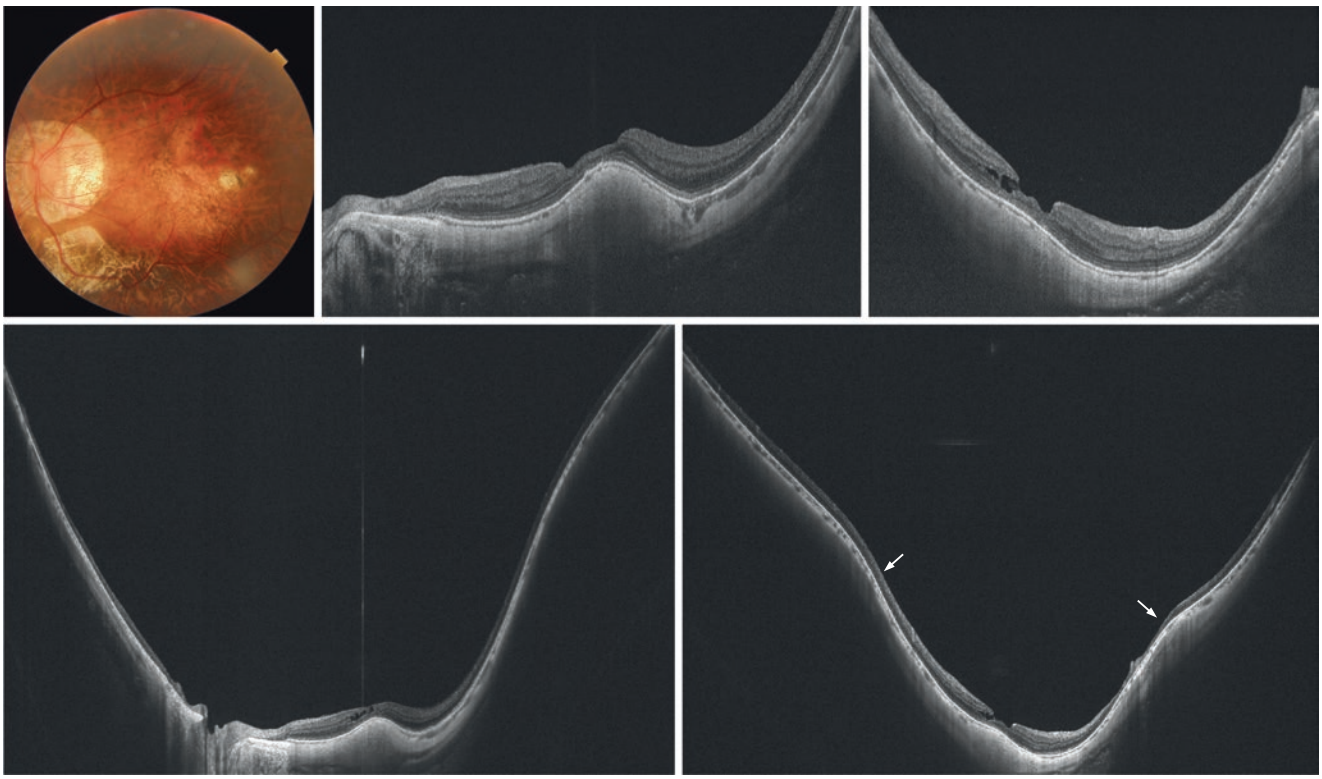

Fig. 22.3 Vertical ridge-shaped dome-shaped macula (DSM). Left fundus of a 65-year-old woman with an axial length of 31.3 mm and the best-corrected visual acuity of 0.8 shows macular diffuse atrophy and patchy atrophy. An inward bulge due to DSM is observed only in the horizontal section (Top Middle and Bottom Left) and not in the vertical section (Top Right and Bottom Right) in both conventional and ultra-widefield OCT images. OCT images also show the presence of inner lamellar macular hole. Arrows show the staphyloma edge in the vertical scan of ultra-widefield OCT (Bottom Right)

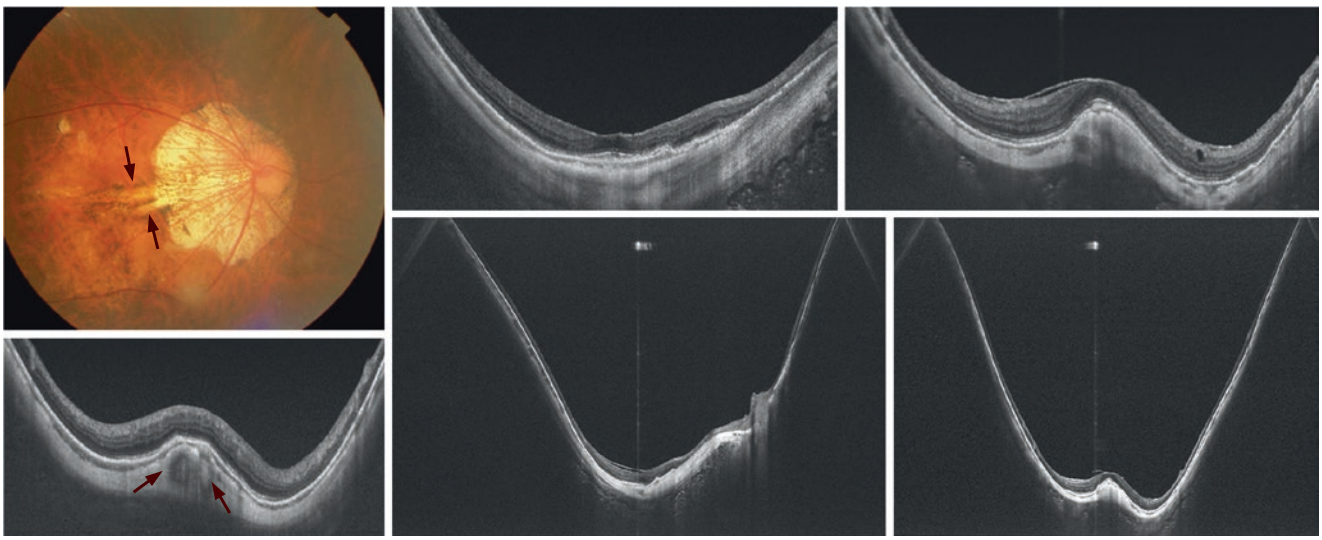

Fig. 22.4 Yellowish linear lesions connecting the optic disc and macula in a 73-year-old woman with dome-shaped macula (DSM). Right fundus with an axial length of 30.2 mm shows two yellowish linear lesions connecting the optic disc and the macula horizontally (arrows). An inward bulge due to DSM is observed only in the vertical OCT section (Top Right and Bottom Right) and not in the horizontal section (Top Middle and Bottom Middle). Vertical OCT across the horizontal ridge nasal to the fovea shows two hyporeflective structures (arrows, Bottom Left) are observed in the sclera. Staphyloma edges are not obvious in ultra-widefield OCT images. Reproduced with permission from [4]

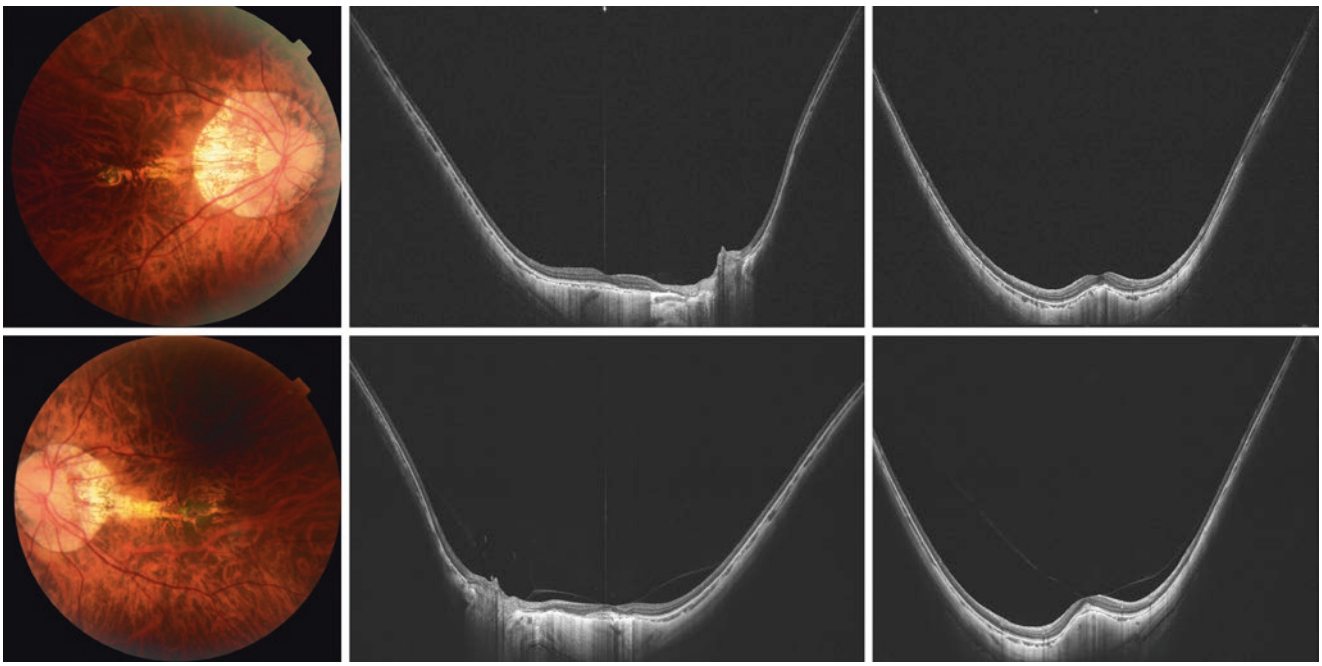

Fig. 22.5 Dome-shaped macula (DSM) accompanying with myopic macular neovascularization (MNV). A 36-year-old woman with bilateral DSM and myopic MNV with refractive error of -13.8 diopters in right eye and -12.0 diopters in the left eye. The axial length is 29.5 mm in her right eye and 28.9 mm in her left eye. The best-corrected visual acuity is 0.7 in both eyes. Fundus photographs show peripapillary diffuse atrophy, pigmentary changes in the macula, and yellowish linear lesions connecting the optic disc and the macula horizontally. Ultra-widefield OCT images show an inward bulge in vertical scans across the fovea. A macular elevation is not detected in the horizontal scans. Horizontal and vertical scans of the left eye show the perifoveal posterior vitreous detachment. (Bottom middle and Bottom Right)

serous RD in DSM is thought to be related to the sclera thickening under the dome which may result in choroidal outflow resistance. Other factors such as a higher macular bulge height [6, 11] and vertically oriented domes [2, 6] are also considered. The eyes with serous RD may have a higher rate of abrupt change in choroidal thickness and associated pachyvessels which may cause RPE dysfunction and serous RD [12]. At present, there is no specific treatment for serous RD associated with DSM. Although extrafoveal retinoschisis is found in around 18% of eyes with DSM [2, 4], it is interesting that the foveal schisis is uncommon suggesting that the DSM may be protective against the development of foveal schisis.

It is noted that the DSM also can be detected in 9% of highly myopic children and in young adults (Fig. 22.6) [13]. Compared to DSM in elderly patients, the domes in children are detected only in the vertical OCT scans and have a wider basis and smoother slope of the elevation without the presence of macular Bruch's membrane defects or a posterior staphyloma.

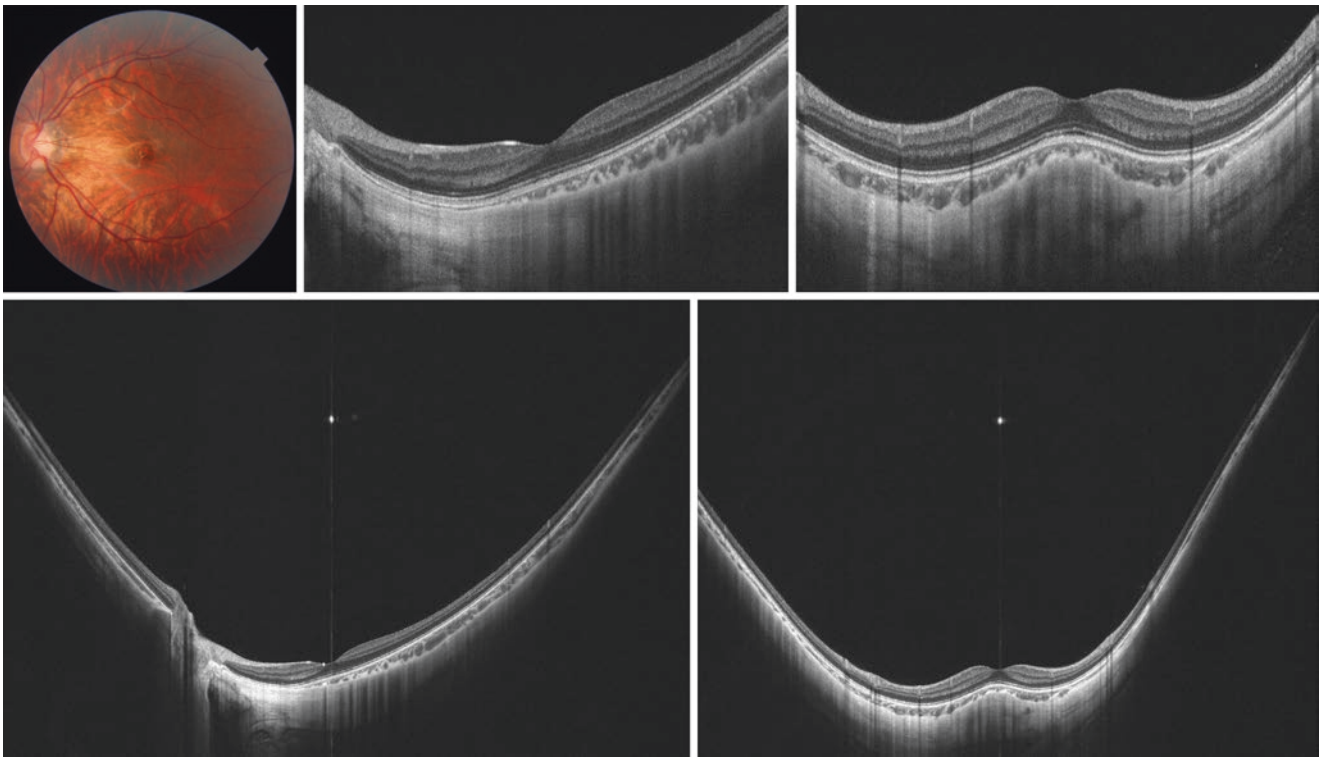

Fig. 22.6 Dome-shaped macula (DSM) seen in children. Left fundus of a 16-year-old girl with refractive error of -11.3 diopters shows DSM. The axial length is 26.8 mm and the best-corrected visual acuity is 1.0. Fundus photograph shows peripapillary diffuse atrophy. OCT image shows an inward bulge in vertical scans across the fovea. The dome height is 147 μm, and the base of the elevation is 4081 μm. A macular elevation is not detected in the horizontal scan

References

1. Gaucher D, Erginay A, Lecleire-Collet A, Haouchine B, Puech M, Cohen SY, et al. Dome-shaped macula in eyes with myopic posterior staphyloma. Am J Ophthalmol. 2008;145(5):909–14.
2. Ellabban AA, Tsujikawa A, Matsumoto A, Yamashiro K, Oishi A, Ooto S, et al. Three-dimensional tomographic features of dome-shaped macula by swept-source optical coherence tomography. Am J Ophthalmol. 2013;155(2):320–8. e2
3. Errera MH, Michaelides M, Keane PA, Restori M, Paques M, Moore AT, et al. The extended clinical phenotype of dome-shaped macula. Graefes Arch Clin Exp Ophthalmol. 2014;252(3):499–508.
4. Liang IC, Shimada N, Tanaka Y, Nagaoka N, Moriyama M, Yoshida T, et al. Comparison of clinical features in highly myopic eyes with and without a dome-shaped macula. Ophthalmology. 2015;122(8):1591–600.
5. Imamura Y, Iida T, Maruko I, Zweifel SA, Spaide RF. Enhanced depth imaging optical coherence tomography of the sclera in dome-shaped macula. Am J Ophthalmol. 2011;151(2):297–302.
6. Caillaux V, Gaucher D, Gualino V, Massin P, Tadayoni R, Gaudric A. Morphologic characterization of dome-shaped macula in myopic eyes with serous macular detachment. Am J Ophthalmol. 2013;156(5):958–67.e1.
7. Soudier G, Gaudric A, Gualino V, Massin P, Nardin M, Tadayoni R, et al. Macular choroidal thickness in myopic eyes with and without a dome-shaped macula: a case-control study. Ophthalmologica Journal international d'ophtalmologie International journal of ophthalmology Zeitschrift fur Augenheilkunde. 2016;236(3):148–53.
8. Ellabban AA, Tsujikawa A, Muraoka Y, Yamashiro K, Oishi A, Ooto S, et al. Dome-shaped macular configuration: longitudinal changes in the sclera and choroid by swept-source optical coherence tomography over two years. Am J Ophthalmol. 2014;158(5):1062–70.
9. Fang Y, Jonas JB, Yokoi T, Cao K, Shinohara K, Ohno-Matsui K. Macular Bruch's membrane defect and dome-shaped macula in high myopia. PLoS One. 2017;12(6):e0178998.
10. Zhao X, Ding X, Lyu C, Li S, Lian Y, Chen X, et al. Observational study of clinical characteristics of dome-shaped macula in Chinese Han with high myopia at Zhongshan ophthalmic Centre. BMJ Open. 2018;8(12):e021887.
11. Viola F, Dell'Arti L, Benatti E, Invernizzi A, Mapelli C, Ferrari F, et al. Choroidal findings in dome-shaped macula in highly myopic eyes: a longitudinal study. Am J Ophthalmol. 2015;159(1):44–52.
12. Tan ACS, Yzer S, Freund KB, Dansingani KK, Phasukkijwatana N, Sarraf D. Choroidal changes associated with serous macular detachment in eyes with staphyloma, dome-shaped macula or tilted disk syndrome. Retina (Philadelphia, Pa). 2017;37(8):1544–54.
13. Xu X, Fang Y, Jonas JB, Du R, Shinohara K, Tanaka N, et al. Ridge-shaped macula in young myopic patients and its differentiation from typical dome-shaped macula in elderly myopic patients. Retina (Philadelphia, Pa). 2018; https://doi.org/10.1097/IAE.0000000000002395.

Part VII

Optic Disc Changes

Optic Disc Changes in Pathologic Myopia

23

Natsuko Nagaoka and Takeshi Yoshida

Abstract

Visual field defects due to optic nerve changes are common in eyes with pathologic myopia (PM). However, it is sometimes difficult to suspect the presence of visual field defects because of the existing deformity of the optic disc. Optical coherence tomography (OCT) is useful to detect structural abnormalities in and around the optic nerve, such as acquired optic disc pits, acquired conus pits, focal lamina defects, and peripapillary intrachoroidal cavitation (ICC).

Keywords

Pathologic myopia · High myopia · Glaucoma · Parapapillary atrophy · Intrachoroidal cavitation · Optic disc pit · Conus pit · Lamina defect

23.1 Introduction

Pathologic myopia (PM) causes serious visual field defects which are associated with morphological alterations of the optic nerve due to the extreme elongation and deformity of the globe. The optic disc of the eyes with PM shows various deformities including an extreme tilting, acquired megalodisc, irregular-shaped optic disc, and a large gamma and delta zone of peripapillary atrophy. Because of such deformities of the optic disc, it is difficult to suspect the presence of visual field defects based on optic disc appearance. To overcome this issue, optical coherence tomography (OCT) is a useful tool to detect optic disc abnormalities which may be responsible for visual field defects in eyes with PM, such as acquired optic disc pits [1], acquired conus pits, focal lamina defects [2], and peripapillary intrachoroidal cavitation (ICC) [3, 4]. This chapter focuses on the association between the optic disc alterations and visual field defects in eyes with PM.

N. Nagaoka (✉) · T. Yoshida
Department of Ophthalmology and Visual Science, Tokyo Medical and Dental University, Tokyo, Japan
e-mail: nanaoph@tmd.ac.jp

23.2 Tilting of the Optic Disc

Tilt and torsion of the optic disc are commonly seen in myopic eyes [5]. Sawada et al. reported that the tilt ratio (defined as the ratio between the longest and shortest diameters of the optic disc) was significantly greater in the eyes with faster progression of visual field (VF) defects than those with slower progression in myopic glaucomatous subjects [2, 6].

In eyes with PM, the degree of tilt and torsion increases and in some cases, due to an extreme tilting of the optic disc, the optic disc itself is not visible funduscopically. Because of the tilting, the temporal part of the optic disc is stretched which may facilitate the development of laminar cribrosa defects along the temporal margin of the optic disc. In addition, the retinal nerve fiber is severely bent and distorted along the nasal margin.

23.3 Acquired Megalodisc and Small Disc

Various patterns in size of the optic disc are seen in eyes with PM (Figs. 23.1 and 23.2).

Nagaoka et al. assessed the prevalence of glaucoma in 336 eyes with high myopia, and reported that the proportion of small discs, normal sized discs, and megalodiscs was 64 eyes (19%), 173 eyes (52%), and 99 eyes (29%). Larger disc area was associated with a longer axial length [7, 8]. Such large optic disc is also known as "acquired megalodisc." According to the Beijing Eye Study, "megalodiscs" were defined as discs larger than 3.79 mm^2 [9]. The size of acquired megalodisc ranged from 3.79 to 13.96 mm^2 with a mean of

K. Ohno-Matsui (ed.), *Atlas of Pathologic Myopia*, https://doi.org/10.1007/978-981-15-4261-9_23

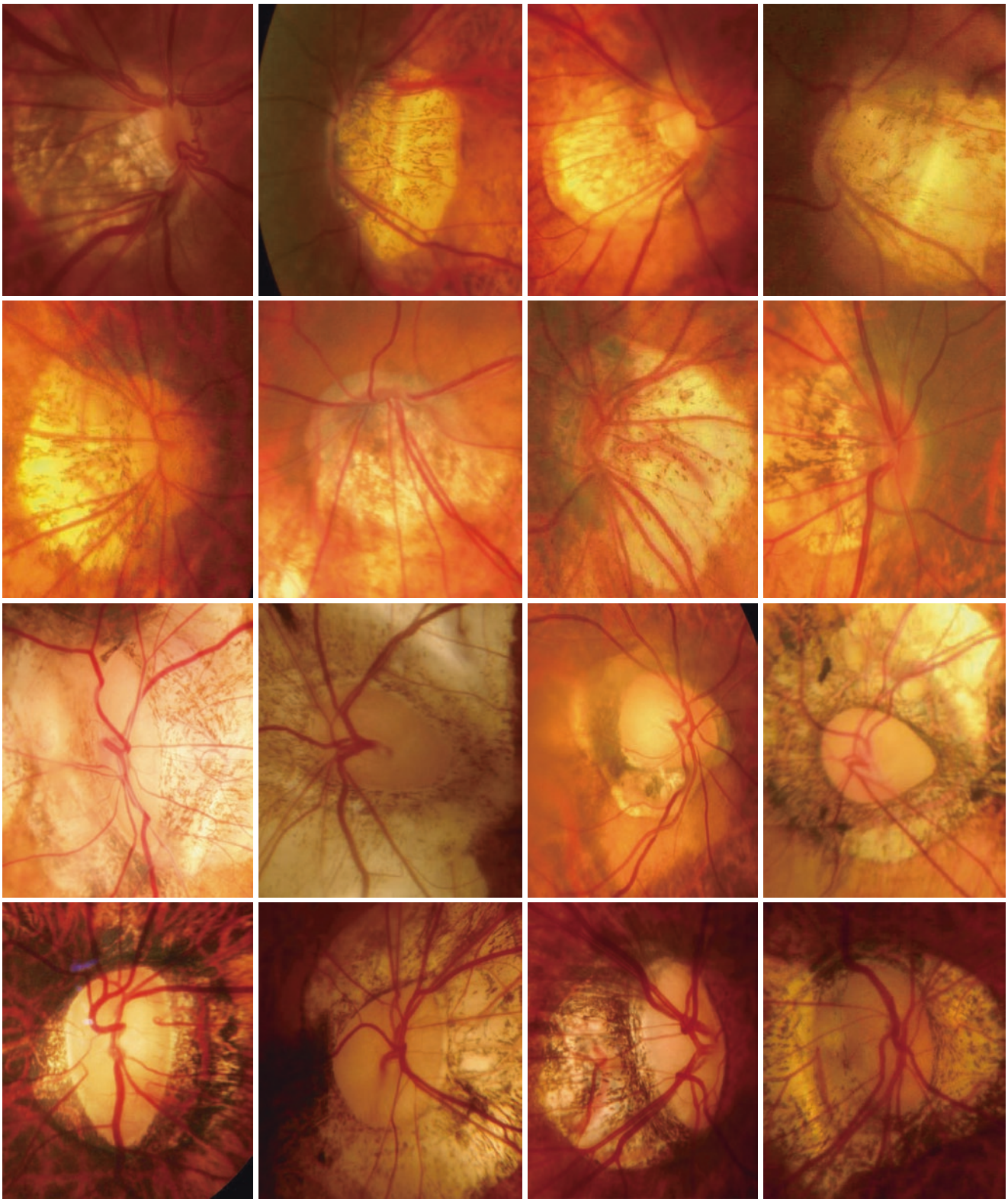

Fig. 23.1 Fundus photographs of various shape of the optic disc in pathologic myopia. The upper two rows show extremely tilted discs and small discs. The bottom two rows show acquired megalodiscs and irregular-shaped discs

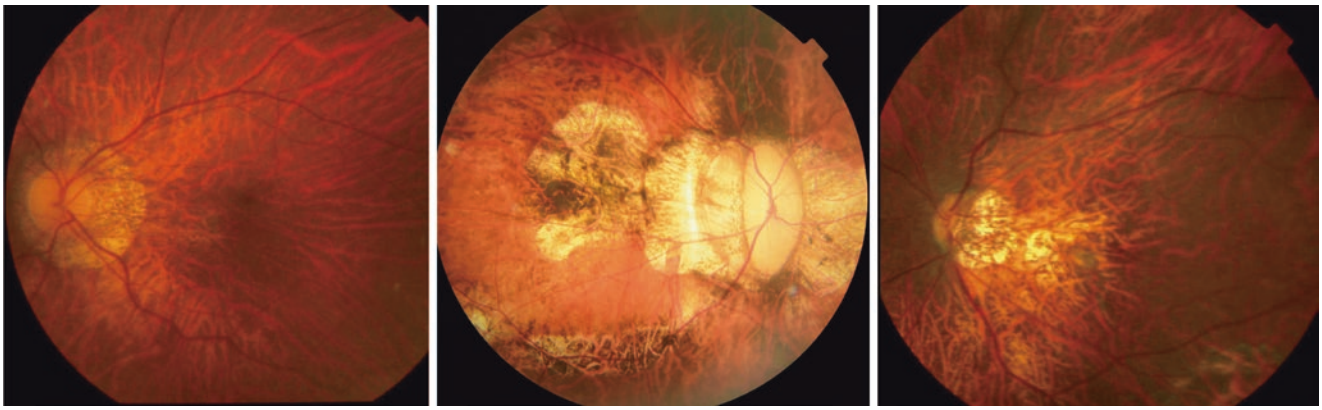

Fig. 23.2 Representative fundus images of normal sized disc (Left, 2.80 mm^2), megalodisc (Middle, 5.15 mm^2) and small disc (Right, 0.66 mm^2) in highly myopic eyes

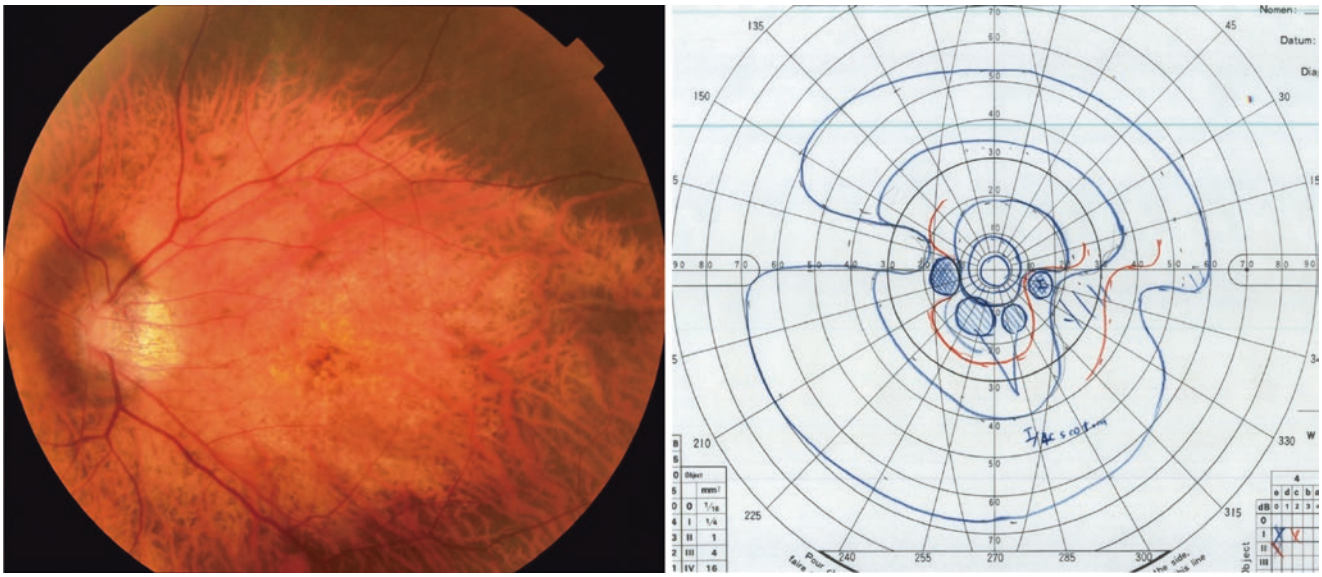

Fig. 23.3 Small optic disc with irregular visual field defects in the left fundus of a 83-year-old man with an axial length of 29.4 mm. (Left) Left fundus shows small optic disc with disc area of 0.51 mm^2. (Right) Goldmann perimetry shows atypical gourd-shaped visual field defects with both temporal and nasal defects

5.39 mm^2 in the study by Nagaoka et al. [7]. In multivariate analysis, the prevalence of glaucoma defined by glaucomatous optic disc and glaucomatous visual field defects was 3.2 times higher in megalodiscs than in normal-sized discs or small discs after adjusting for the age. Glaucoma prevalence increased by a factor of 1.39 for each increase of optic disc area by 1 mm^2. In summary, in highly myopic eyes, glaucoma prevalence increased with larger optic disc size beyond a disc area of 3.8 mm^2.

The reasons for the increased glaucoma susceptibility in highly myopic eyes with megalodiscs may be histological changes in the lamina cribrosa and in the parapapillary tissue [10, 11]. Previous investigations revealed that eyes with myopic axial elongation as compared to eyes with normal axial length showed a marked thinning of the lamina cribrosa. It has been postulated that the thinning of the lamina cribrosa led to the shortening of the distance between the intraocular compartment and the retrobulbar optic nerve compartment. The parapapillary scleral flange is the continuation of the inner half of the posterior sclera and continues to the lamina cribrosa. In eyes with acquired megalodisc, the parapapillary scleral flange markedly elongates and thins. Since the parapapillary scleral flange is the biomechanical anchor of the lamina cribrosa, the elongation and thinning of the parapapillary scleral flange may have consequences in the lamina cribrosa including the susceptibility for glaucomatous optic neuropathy [12].

Small optic disc (defined as disc size <1.51 mm^2) was also found in 19% of 336 eyes with high myopia [7]. Different from normal sized disc or megalodisc, the eyes with small optic disc tend to show atypical visual field defects, such as gourd-shaped defects accompanying with both temporal and nasal defects (Fig. 23.3).

23.4 Parapapillary Gamma Zone and Delta Zone (Fig. 23.4)

Jonas et al. histomorphometrically examined the parapapillary region of human eyes [10]. They measured the distance between Bruch's membrane (BM) end and the optic nerve margin ("Gamma zone"); BM end and retinal pigment epithelium (RPE) ("Beta zone"); BM end and the beginning of non-occluded choriocapillaris; and BM end and the beginning of photoreceptor layer. "Delta zone" was defined as a part of gamma zone in which blood vessels of at least 50 μm diameter were not present over a length of >300 μm. Beta zone was significantly larger in the glaucoma group than in the non-glaucomatous group, however, it was not significantly associated with an axial length. In contrast, gamma zone was associated with axial length with an increase starting at an axial length of 26.5 mm. It was not significantly associated with glaucomatous optic neuropathy. In summary, parapapillary gamma zone (parapapillary sclera without overlying choroid, Bruch's membrane and deep retinal layers) was related to axial elongation and was independent of glaucoma. Delta zone was present only in highly axially elongated globes and was not related to glaucoma. Recently they reported that larger gamma and delta zones were correlated with larger optic disc and more marked vertical optic disc rotation, longer disk-fovea distance, higher number of chorioretinal atrophic lesions, and a longer vertical distance between the superior and inferior temporal arterial arcade [11].

23.5 Scleral Ridge Temporal to the Optic Disc

Vertically oriented scleral ridge temporal to the optic disc is not uncommon in eyes with PM. This was also reported as type IX staphyloma by Curtin [13]. OCT examinations showed that such changes of scleral curvature occurred at the attachment of the dura mater of subarachnoid space to the peripapillary sclera [14]. Funduscopically, the location of scleral ridge often coincides the border between gamma zone and delta zone (Fig. 23.5).

The importance of the scleral ridge lies in a high prevalence of coexisting visual field defects. Ohno-Matsui et al. reported that significant visual field defects (defined as 10% or more loss of V4 isopter and which were not explained by myopic maculopathy or peripheral fundus lesions) were newly developed in 13.2% of 492 highly myopic eyes during a mean follow-up of 11.6 years [15]. An abrupt change of the scleral curvature represented by scleral ridge formation was the only factor significantly

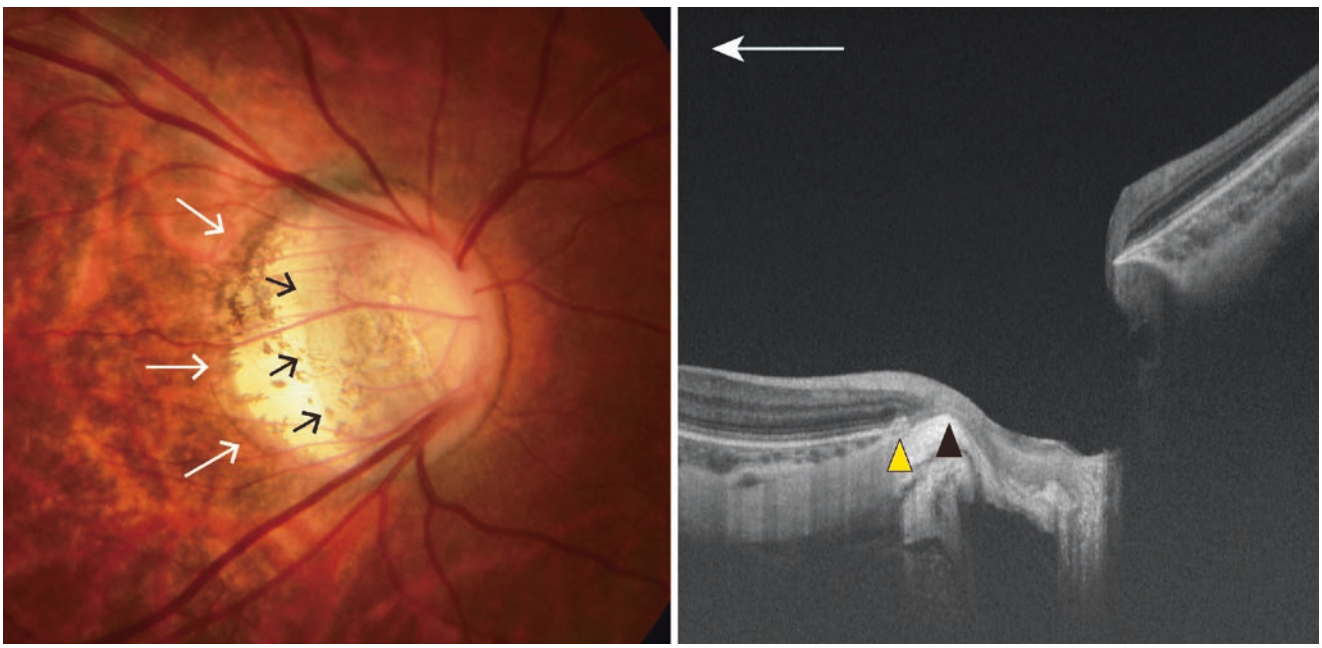

Fig. 23.4 Parapapillary gamma zone and delta zone in the right fundus of a 18-year-old man with an axial length of 28.9 mm. (Left) Right fundus shows parapapillary gamma zone (white arrows; the area without Bruch's membrane) and delta zone (black arrows; no blood vessels >50 μm diameter within gamma zone). (Right) OCT image shows the margin of gamma zone (yellow arrowhead) and the margin of delta zone (black arrowhead)

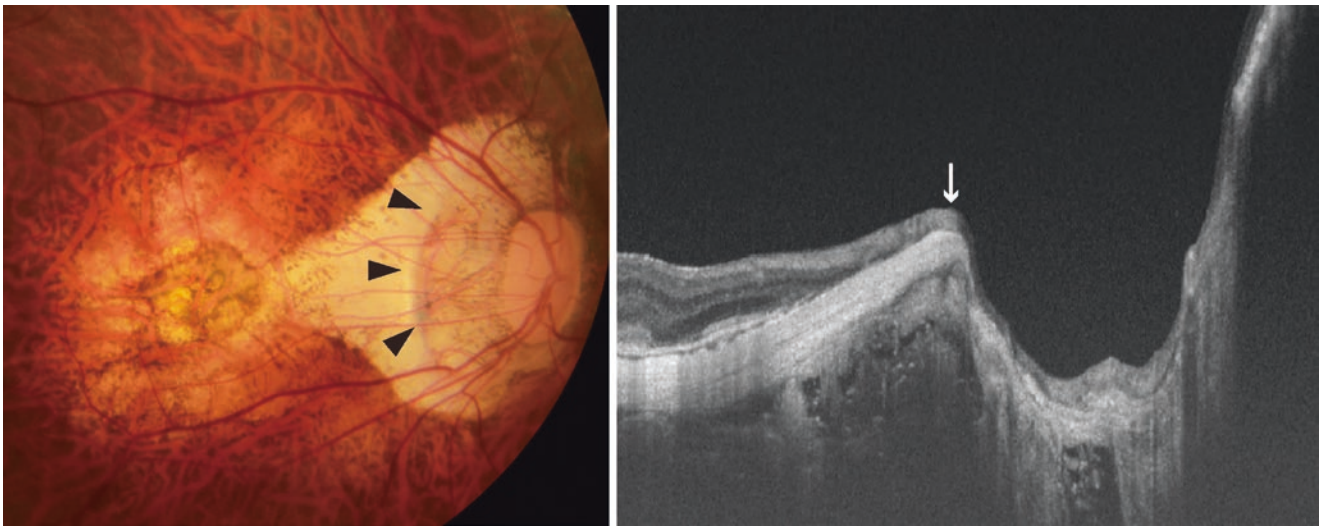

Fig. 23.5 Scleral ridge formation temporal to the optic disc. (Left) Right fundus of a 70-year-old woman with an axial length of 31.1 mm shows scleral ridge (arrowheads) temporal to the optic disc. (Right) A horizontal OCT section across the optic disc shows an acutely protruded scleral ridge (arrow). Retina is severely thinned at and nasal to the scleral ridge. Subarachnoid space is also seen in this image

associated with a progression of the visual field defects. Akagi et al. reported that the angle of scleral bending at the site of the scleral ridge correlated significantly with retinal nerve fiber layer thickness above the ridge and the visual field defect severity, suggesting that a compression and the thinning of retinal nerve fiber at the scleral ridge may be a cause of visual field defects [16]. Based on these studies, periodical visual field examinations (especially Goldmann perimetry) is strongly recommended for the eyes with scleral ridge.

23.6 Peripapillary Intrachoroidal Cavitation (ICC)

Intrachoroidal cavitation (ICC) is a crescent-shaped yellow-orange lesion around the inferior region of the peripapillary myopic conus (Fig. 23.6). In OCT images, ICC is observed as an intrachoroidal hypo-reflective space (Fig. 23.6) [17, 18]. However, swept-source OCT shows that some ICC was suprachoroidal separation [18]. In its early development, ICC is just observed as the thickening of peripapillary choroid. ICC most commonly develops lower to the optic disc, but it can also be seen temporal to the optic disc or all around the optic disc. Shimada et al. examined an assessment with the Goldmann visual field test and found glaucomatous visual field defects in 71.0% of eyes with peripapillary ICC [4]. Spaide et al. reported that the thinning or the disruption of the retina at the ICC border area, which may contribute to visual field defects [18]. When the overlying inner retina is defected at the ICC border area, visual field defects similar to glaucoma are found (Fig. 23.7). In eyes with temporal ICC, a central scotoma is seen [19]. As a cause of ICC, a defect of the border tissue of Jacoby between the choroid and the optic nerve has been suggested [18].

23.7 Optic Disc Pit and Conus Pit

Optic disc pit (Fig. 23.8) and conus pit (Fig. 23.9) are pit-like clefts present near the outer border of the optic disc or within the adjacent scleral crescent in eyes with PM. Ohno-Matsui et al. showed such pit-like clefts were found in 16.2% of highly myopic eyes [1]. These pits occur in eyes with PM due to mechanical expansion of peripapillary region [1]. OCT revealed that the optic disc pits frequently existed in the superior or inferior pole of the optic disc (Fig. 23.8). OCT also demonstrated the presence of conus pits in peripapillary gamma zone (Fig. 23.9), and the invagination of the retinal veins sometimes occurs at the site of conus pits [20]. In addition, the retinal nerve fibers are thinned or completely lost overlying these pits, which causes visual field defects that are similar to glaucoma. Therefore, it is necessary to check the presence of these pits using OCT when we see patients glaucomatous visual field defects in PM.

Fig. 23.6 Peripapillary intrachoroidal cavitation (ICC) or suprachoroidal separation without cavity formation. (Top row) Left fundus of a 47-year-old man with an axial length of 28.1 mm. Yellowish lesion (arrowheads) is seen around the peripapillary atrophy (PPA). Retinal vein is herniated at around the border of the PPA and ICC. A vertical OCT section across the optic disc shows that the choroid is thickened toward the optic nerve. Sclera is dislocated posteriorly in that area. A disruption of bordering tissue of Jacoby is observed (arrow). (Middle Row) Right fundus of a 60-year-old woman with an axial length of 27.7 mm. Yellowish ICC is seen upper and lower to the PPA. A vertical OCT section across the optic disc shows that the choroid is thickened toward the optic nerve. Sclera is dislocated posteriorly in that area. Choroidal tissue seems to attach the RPE-Bruch's membrane, suggesting that this is more like a suprachoroidal separation. (Bottom Row) Right fundus of a 41-year-old woman with an axial length of 27.8 mm. Yellowish lesion is seen lower to the PPA (arrowheads). A vertical OCT section across the optic disc shows that the choroid is thickened toward the optic nerve. Sclera is dislocated posteriorly in that area. Choroidal tissue seems to attach the RPE-Bruch's membrane, suggesting that this is more like a suprachoroidal separation

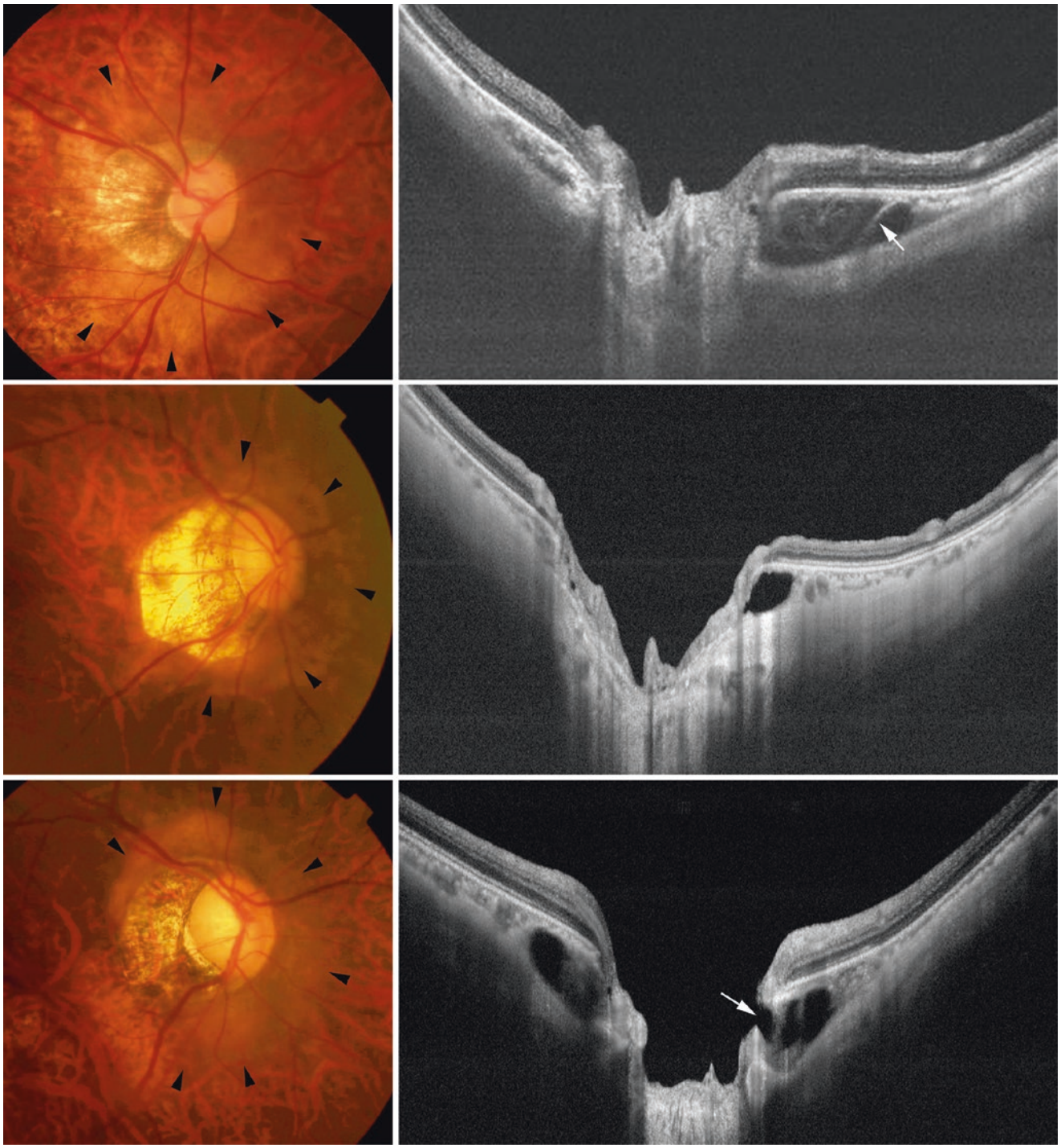

Fig. 23.7 Peripapillary intrachoroidal cavitation (ICC) or suprachoroidal separation with cavity formation. (Top Row) Right fundus of a 54-year-old woman with a refractive error of -14.0 diopters. Yellowish lesion is widely observed around the optic disc and the peripapillary atrophy (PPA). A vertical OCT section across the optic disc shows that the choroid is thickened toward the optic nerve. Sclera is dislocated posteriorly in that area. ICC area shows hypo-reflectance and some strands are seen to course the ICC space (arrow). (Second Row) Right fundus of a 53-year-old man with a refractive error of -10.0 diopters. A yellowish ICC is seen widely around the optic disc and PPA (arrowheads). A vertical OCT section across the optic disc shows that the choroid is thickened toward the optic nerve. Sclera is dislocated posteriorly in that area. Fluid space is seen within the area of ICC. (Third Row) Right fundus of a 57-year-old man with axial length of 29.3 mm. Yellowish lesion is widely observed around the optic disc and the peripapillary atrophy (PPA) (arrowheads). A vertical OCT section across the optic disc shows deep ICCs upper and lower to the optic nerve. Fluid space occupies most of the ICC, and the sclera is dislocated posteriorly. A full thickness defect of the retina is observed at the margin of ICC (arrow) and a direct connection between vitreous cavity and ICC space is seen. (Bottom Row) Right fundus of a 76-year-old woman with axial length of 31.4 mm. Yellowish ICC is observed lower nasal to the optic disc (arrowheads). A vertical OCT section across the optic disc shows very deep ICC lower to the optic nerve. A large defect of full thickness of the retina is observed at the margin of ICC (arrow). A direct communication between vitreous and ICC is seen. Some strands are seen within the ICC (arrowheads)

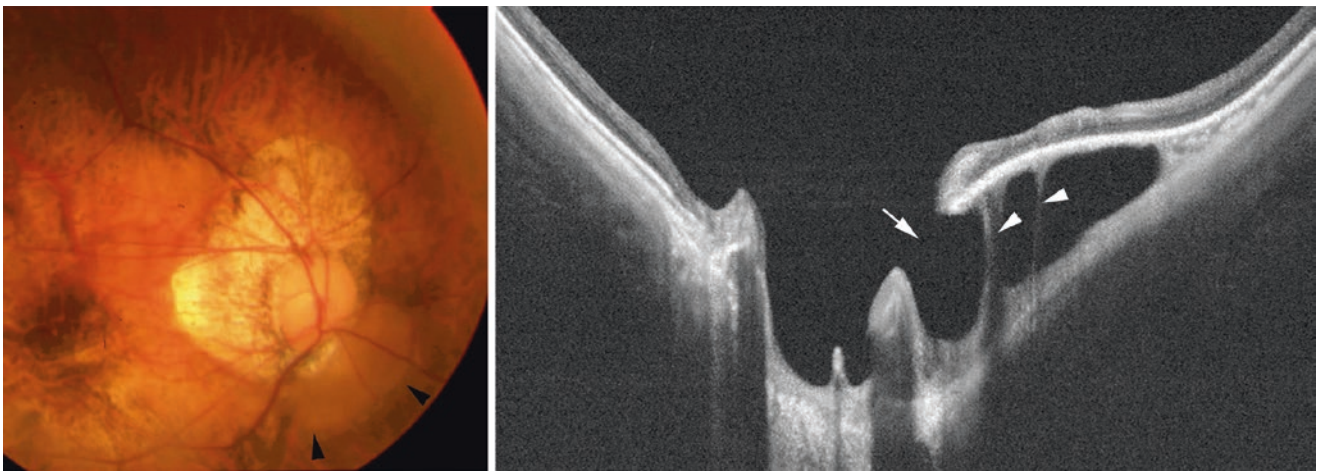

Fig. 23.7 (continued)

Fig. 23.8 Optic disc pits. Right fundus of a 51-year-old woman with axial length of 32.8 mm. Multiple disc pits (equivalent to lamina cribrosa defects) are seen along the upper border of a large optic disc (arrowheads). A horizontal OCT section across the upper edge of the optic disc shows a defect of lamina cribrosa (between arrows). The retina overlying disc pits is lost

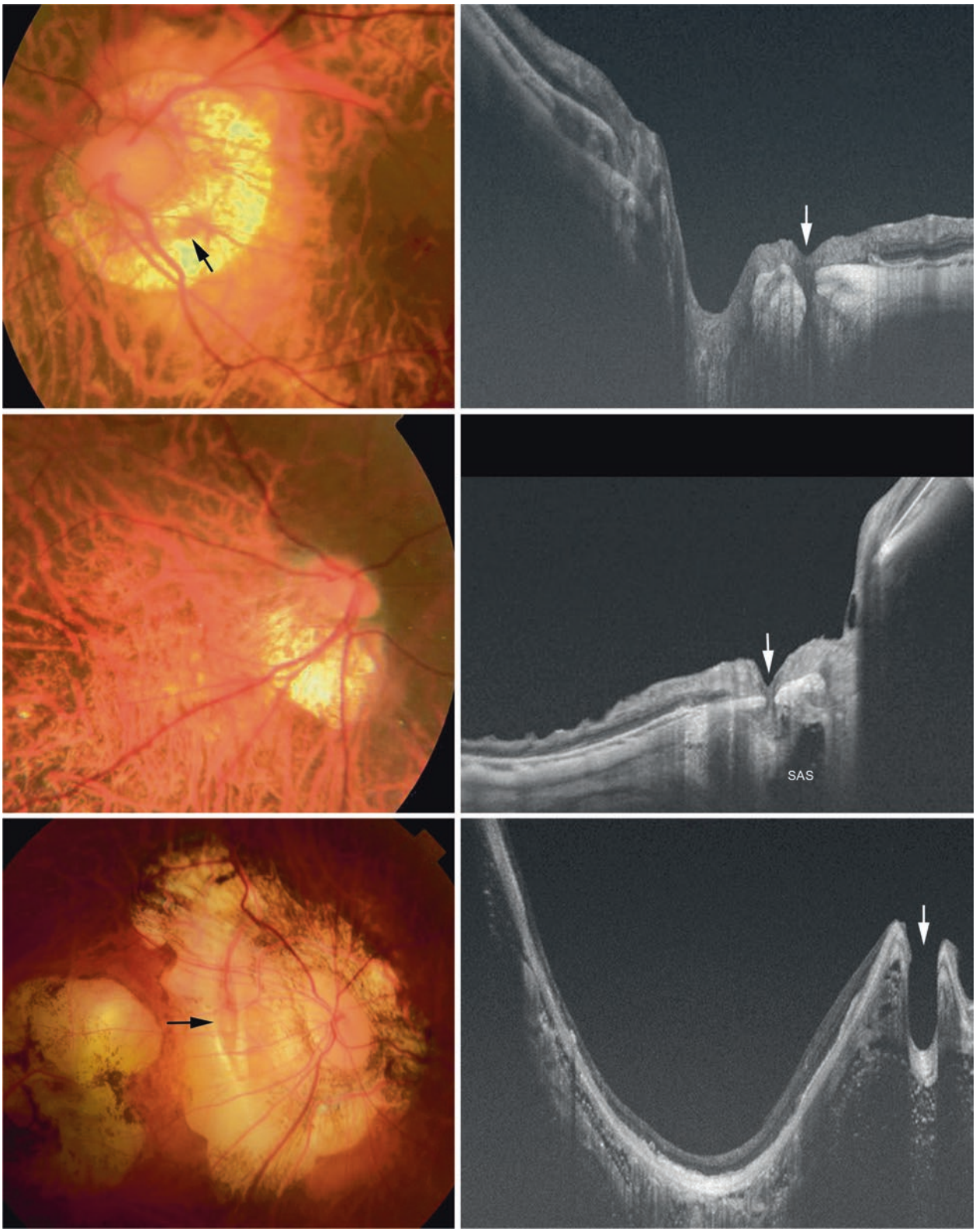

Fig. 23.9 Conus pits in pathologic myopia. (Top Row) Left fundus of a 36-year-old woman with axial length of 32.6 mm. An orange-colored pit (arrow) is seen within a large area of peripapillary atrophy (PPA). An oblique OCT scan across the optic disc shows a conus pit, as a full-thickness defect of sclera (arrow). Overlying retina is herniated into the conus pit. (Middle Row) Right fundus of a 70-year-old woman with axial length of 33.2 mm. Conus pit is not obvious in the fundus image. An oblique OCT scan across the optic disc shows a conus pit, as a full-thickness defect of the sclera at the site pointed by an arrow. Overlying retina is herniated into the conus pit. Subarachnoid space (SAS) is seen close to the bottom of the conus pit. (Bottom Row) Right fundus of a 51-year-old woman with axial length of 32.8 mm. A vertically oval-shaped pit (arrow) is observed within a very large PPA. A branch of Zinn-Haller arterial ring is seen to emerge from the upper end of the pit. A horizontal OCT section across the optic disc shows a very deep conus pit (pointed by arrow) nasal to the scleral ridge. Retina is almost absent over the pit

23.8 Focal Lamina Cribrosa Defects

Focal lamina cribrosa defects are synonyms of optic disc pits, and acquired optic disc pits are considered an extreme form of focal lamina cribrosa defects. In PM eyes, focal lamina cribrosa defects can be better-detected more than non-highly myopic eyes (Fig. 23.10) due to the thinning of the prelaminar tissue overlying the lamina cribrosa. In addition, lamina cribrosa is more superficially located in myopic eyes with megalodisc. In PM eyes, focal laminar defects tend to occur at the temporal edge of the optic disc, which may damage papillomacular nerve fiber bundle resulting in the central visual field defect (Fig. 23.10). Focal laminar defects were also found in POAG eyes with high myopia [21, 22]. Jong et al. showed that focal laminar defects in myopic eyes were associated with axial length, maximal length of peripapillary atrophy, and disc tilt angle in multivariate logistic regression analysis [21, 23].

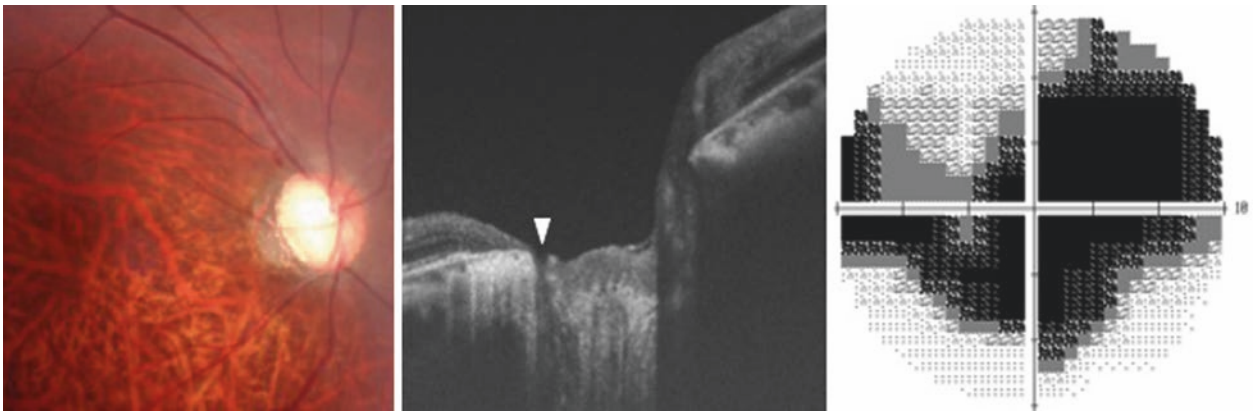

Fig. 23.10 Focal lamina cribrosa defect in an axial myopia. Right fundus of a 46-year-old woman with axial length of 31.3 mm. A horizontal OCT image shows the focal laminar defect at the temporal border of the optic disc. Arrowhead points prelaminar tissue dimpling at the site of the focal laminar defect. Visual field examination using the central 10° visual field (Humphrey Field Analyzer) shows a central scotoma corresponding to the site of the laminar defects

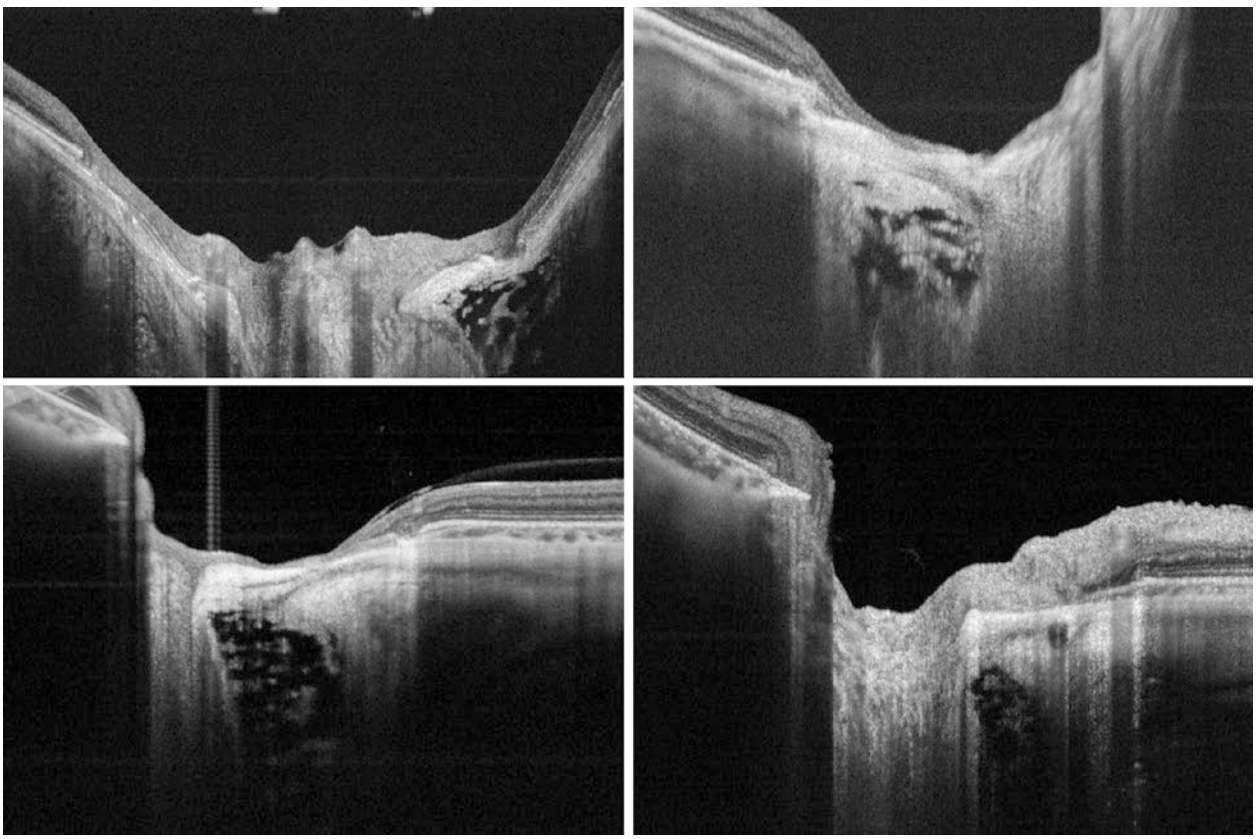

Fig. 23.11 Subarachnoid space (SAS) observed in eyes with pathologic myopia. OCT images show the SAS as a hypo-reflective space, which is triangular with the base toward the eye. The peripapillary sclera is continuous with the pia mater along the inner boundary of the SAS and also continuous with the dura mater along the outer boundary of the SAS. Arachnoid trabeculae is also observed within SAS

23.9 Enlargement of Subarachnoid Space (SAS)

Subarachnoid space (SAS) is barely visible in non-highly myopic eyes; however, by using EDI-OCT or swept-source OCT, the SAS is visible in eyes with PM through large conus [14, 24] (Fig. 23.11). The SAS is enlarged especially near its anterior surface based on histological study as well as clinical study using OCT [25]. Thus, the SAS in eyes with PM tends to be triangular, with the base toward the eye. Such an increased area exposed to the cerebrospinal pressure and the thinning of the lamina cribrosa and the peripapillary sclera may play a role for the optic nerve damage even within a range of normal intraocular pressure.

The sclera overlying the SAS is very thin in some cases, with a short distance between SAS and vitreous cavity. In extreme cases, there is a direct communication between SAS and vitreous [14]. Arachnoid trabeculae, the pia mater, and the dura mater are also visible in some cases.

23.10 Increased Distance of Zinn–Haller Arterial Circle (ZHAC) from the Optic Disc

Zinn–Haller arterial circle (ZHAC) is an intrascleral arteriolar anastomosis derived from the paraoptic medial and lateral short posterior ciliary arteries (SPCA). The ZHAC is the main blood supply to the optic nerve head at the level of the lamina cribrosa. Because of its intrascleral location, it was difficult to observe in situ.

However, in PM eyes, the ZHAC is visible through a large conus by using ICG angiography and EDI-OCT/swept-source OCT [26, 27]. OCT shows an entire course of ZHAC from the SPCA emissary to branches toward the optic nerve (Fig. 23.12). The ZHAC is observed by OCT angiography in some cases (Fig. 23.13) [28].

In eyes with PM, the ZHAC tends to be away from the optic nerve (Fig. 23.14). The most distant point is the emissary of SPCA into the ZHAC, and thus the ZHAC is some-

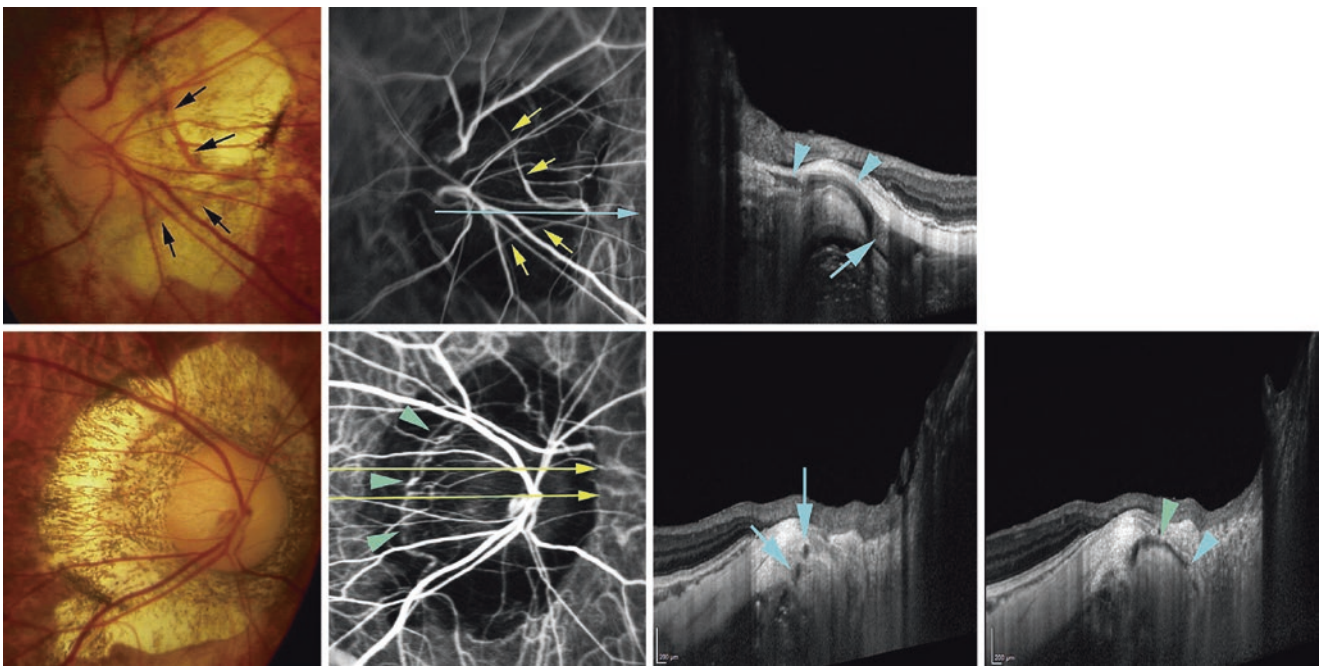

Fig. 23.12 Detection of the path from the retrobulbar short posterior ciliary artery to the Zinn-Haller arterial circle (ZHAC) by OCT and the detection of centripetal branches running toward the optic nerve from the ZHAC both by indocyanine green (ICG) angiography and OCT (Cited with permission from [26]). (Top Left) Fundus photograph of the left eye of a 55-year-old man with an axial length of 31.2 mm. A large temporal conus is observed. Blood vessels suggesting the ZHAC are seen within the conus (arrows). (Top Middle) ICG angiographic finding at 1 min after dye injection showing the temporal part of the ZHAC with a triangular shape (arrows). A lateral short posterior ciliary artery enters the ZHAC at its most horizontally distant point. A blue line shows the scanned line by OCT. (Top Right) Horizontal OCT scan shows that the short posterior ciliary artery enters the sclera (arrow) and courses toward the ZHAC intrasclerally (along the arrowheads). (Bottom Left) Fundus photograph of right eye of a 68-year-old man with an axial length of 29.7 mm. An annular conus is seen. (Bottom second from the left) ICG angiographic finding at 1 min after dye injection showing multiple vessels consisting of the ZHAC (arrowheads) located temporal to the optic disc within the area of the conus. The scanned lines by OCT are shown as yellow lines. (Bottom third from the left) Upper horizontal OCT scan shows two hypo-reflective circular areas (arrows) corresponding to vessels of the ZHAC. (Bottom Right) In the lower section, the centripetal branch (arrowheads) toward the optic nerve can be seen

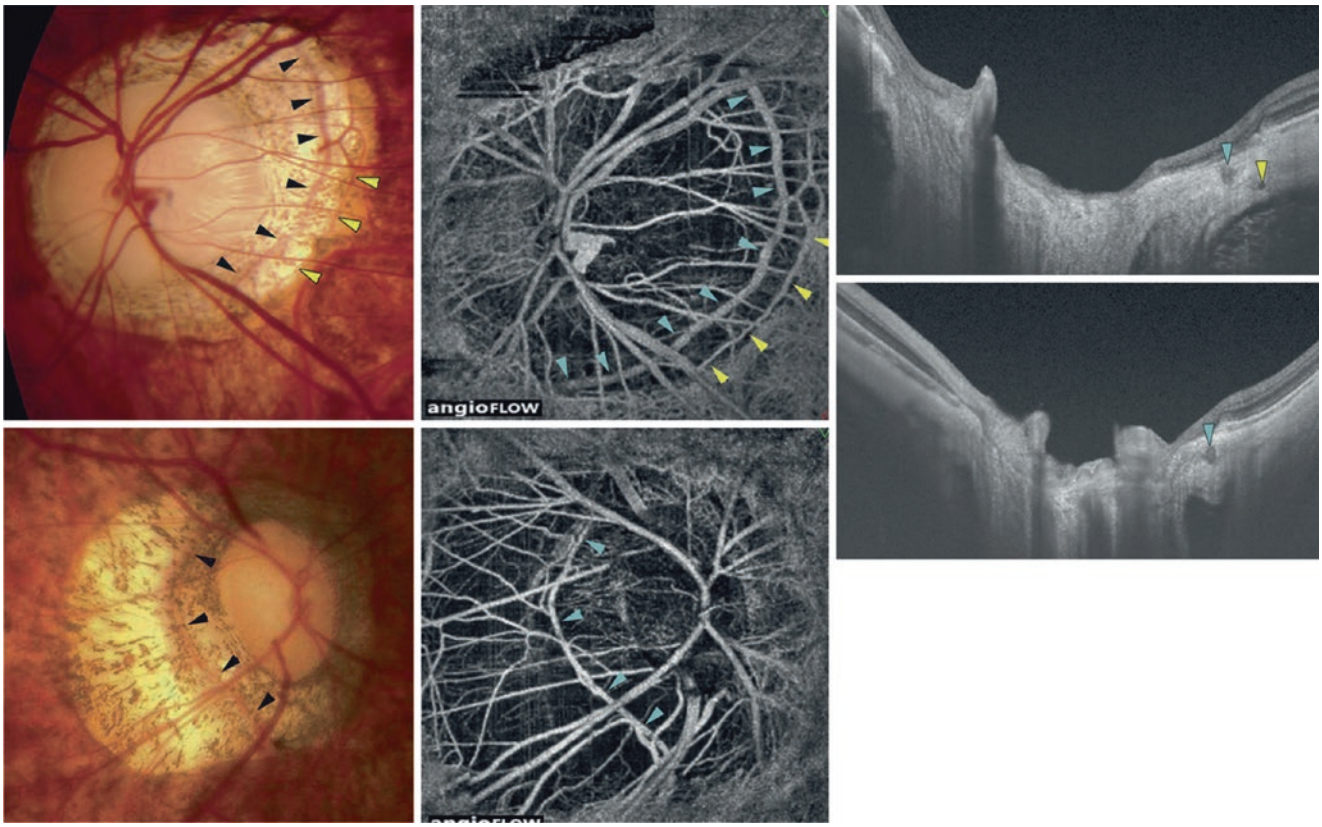

Fig. 23.13 (Cited with permission from [28]). The Zinn-Haller arterial circle (ZHAC) as imaged by optical coherence tomography angiography (OCT-A). (Top Left) In the left fundus, ZHAC (black arrowheads) is detected in the region of the peripapillary conus (gamma zone). Outside of the main arterial circle (black arrowheads), a second arterial circle is present (yellow arrowheads). (Top Middle) On OCT-A image, a double ring of ZHAC consisting of a wider ring (blue arrowheads) and a narrower ring (yellow arrowheads) can be seen. In particular inferior to the optic disc, the wider ring is observed to a wider extent than on the fundus photo. (Top Right, upper image) In a horizontal section of the swept-source OCT image, cross sections of the inner (wider) artery of the ZHAC (blue arrowhead) and the outer (narrower) artery of the ZHAC (yellow arrowhead) are visible within the peripapillary sclera in the region of the parapapillary gamma zone. The outer artery of the ZHAC as compared to the inner artery is located deeper in the sclera. (Top Right, lower image) In a vertical section of swept-source OCT image, a cross section of the inner artery of the ZHAC is visible within the scleral stroma (arrowhead). (Bottom Left) In the right fundus, the ZHAC (arrowheads) is visible in the region of the peripapillary conus (parapapillary gamma zone). (Bottom Right) On the OCT-A image, the ZHAC (arrowheads), in particular its small branches, are more clearly seen than on the fundus photo

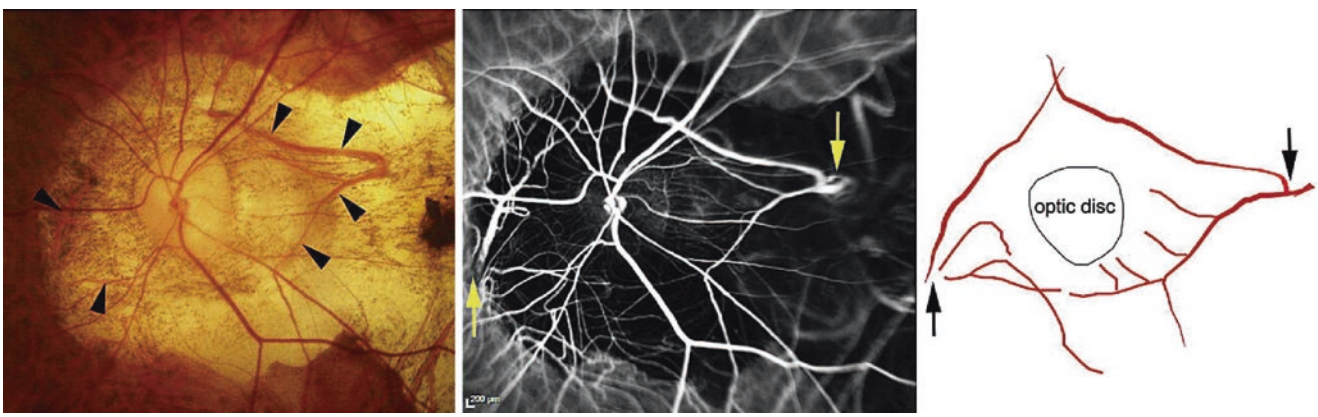

Fig. 23.14 (Cited with permission from [26]). A rhomboid shape of the Zinn-Haller arterial circle (ZHAC) in pathologic myopia observed by indocyanine green (ICG) angiography. (Left) Left fundus of an 84-year-old woman with an axial length of 30.0 mm. A large annular conus is observed. Blood vessels suggesting the ZHAC are seen within the conus (arrowheads). (Middle) ICG angiographic finding at 1 min after the dye injection showing a rhomboid-shaped ZHAC surrounding the optic disc. Medial and lateral short posterior ciliary arteries enter the ZHAC at the points shown by arrows. (Right) Schematic drawing of ICG angiographic finding. The ZHAC is drawn in red and has a horizontally long rhomboid shape. The medial and lateral short posterior ciliary arteries enter the ZHAC at the most horizontally protruded point (arrows). Centripetal branches running toward the optic nerve from the ZHAC are shown

times rhomboid or triangular in shape. In histological study, Jonas et al. reported that the distance between the ZHAC and the optic disc margin reached nearly 3000 μm in extremely myopic eyes [29]. Such an increased distance of the ZHAC away from the optic disc may cause an ischemic insult to the optic nerve.

References

1. Ohno-Matsui K, Akiba M, Moriyama M, Shimada N, Ishibashi T, Tokoro T, et al. Acquired optic nerve and peripapillary pits in pathologic myopia. Ophthalmology. 2012;119(8):1685–92.
2. Sawada Y, Hangai M, Ishikawa M, Yoshitomi T. Association of myopic deformation of optic disc with visual field progression in paired eyes with open-angle glaucoma. PLoS One. 2017;12(1):e0170733.
3. Toranzo J, Cohen SY, Erginay A, Gaudric A. Peripapillary intrachoroidal cavitation in myopia. Am J Ophthalmol. 2005;140(4):731–2.
4. Shimada N, Ohno-Matsui K, Yoshida T, Yasuzumi K, Kojima A, Kobayashi K, et al. Characteristics of peripapillary detachment in pathologic myopia. Arch Ophthalmol (Chicago, Ill: 1960). 2006;124(1):46–52.
5. Fan YY, Jonas JB, Wang YX, Chen CX, Wei WB. Horizontal and vertical optic disc rotation. The Beijing eye study. PLoS One. 2017;12(5):e0175749.
6. Sawada Y, Hangai M, Ishikawa M, Yoshitomi T. Association of myopic optic disc deformation with visual field defects in paired eyes with open-angle glaucoma: a cross-sectional study. PLoS One. 2016;11(8):e0161961.
7. Nagaoka N, Jonas JB, Morohoshi K, Moriyama M, Shimada N, Yoshida T, et al. Glaucomatous-type optic discs in high myopia. PLoS One. 2015;10(10):e0138825.
8. Jonas JB. Optic disk size correlated with refractive error. Am J Ophthalmol. 2005;139(2):346–8.
9. Wang Y, Xu L, Zhang L, Yang H, Ma Y, Jonas JB. Optic disc size in a population based study in northern China: the Beijing eye study. Br J Ophthalmol. 2006;90(3):353–6.
10. Jonas JB, Jonas SB, Jonas RA, Holbach L, Dai Y, Sun X, et al. Parapapillary atrophy: histological gamma zone and delta zone. PLoS One. 2012;7(10):e47237.
11. Jonas JB, Fang Y, Weber P, Ohno-Matsui K. Parapapillary gamma and delta zones in high myopia. Retina (Philadelphia, Pa). 2018;38(5):931–8.
12. Jonas JB, Xu L. Histological changes of high axial myopia. Eye (Lond). 2014 ;28(2):113–7.
13. Curtin BJ. The posterior staphyloma of pathologic myopia. Trans Am Ophthalmol Soc. 1977;75:67–86.
14. Ohno-Matsui K, Akiba M, Moriyama M, Ishibashi T, Tokoro T, Spaide RF. Imaging retrobulbar subarachnoid space around optic nerve by swept-source optical coherence tomography in eyes with pathologic myopia. Invest Ophthalmol Vis Sci. 2011;52(13):9644–50.
15. Ohno-Matsui K, Shimada N, Yasuzumi K, Hayashi K, Yoshida T, Kojima A, et al. Long-term development of significant visual field defects in highly myopic eyes. Am J Ophthalmol. 2011;152(2):256–65.
16. Akagi T, Hangai M, Kimura Y, Ikeda HO, Nonaka A, Matsumoto A, et al. Peripapillary scleral deformation and retinal nerve fiber damage in high myopia assessed with swept-source optical coherence tomography. Am J Ophthalmol. 2013;155(5):927–36.
17. Freund KB, Ciardella AP, Yannuzzi LA, Pece A, Goldbaum M, Kokame GT, et al. Peripapillary detachment in pathologic myopia. Arch Ophthalmol (Chicago, Ill: 1960). 2003;121(2):197–204.
18. Spaide RF, Akiba M, Ohno-Matsui K. Evaluation of peripapillary intrachoroidal cavitation with swept source and enhanced depth imaging optical coherence tomography. Retina (Philadelphia, Pa). 2012;32(6):1037–44.
19. Ohno-Matsui K, Shimada N, Akiba M, Moriyama M, Ishibashi T, Tokoro T. Characteristics of intrachoroidal cavitation located temporal to optic disc in highly myopic eyes. Eye (London). 2013;27(5):630–8.
20. Ohno-Matsui K. Invagination of retinal vein into conus pit in a case with pathologic myopia. Nippon Ganka Gakkai Zasshi. 2017;121(2):146–9.
21. Kimura Y, Akagi T, Hangai M, Takayama K, Hasegawa T, Suda K, et al. Lamina cribrosa defects and optic disc morphology in primary open angle glaucoma with high myopia. PLoS One. 2014;9(12):e115313.
22. Miki A, Ikuno Y, Asai T, Usui S, Nishida K. Defects of the lamina cribrosa in high myopia and glaucoma. PLoS One. 2015;10(9):e0137909.
23. Han JC, Cho SH, Sohn DY, Kee C. The characteristics of lamina cribrosa defects in myopic eyes with and without open-angle glaucoma. Invest Ophthalmol Vis Sci. 2016;57(2):486–94.
24. Park SC, De Moraes CG, Teng CC, Tello C, Liebmann JM, Ritch R. Enhanced depth imaging optical coherence tomography of deep optic nerve complex structures in glaucoma. Ophthalmology. 2012;119(1):3–9.
25. Jonas JB, Jonas SB, Jonas RA, Holbach L, Panda-Jonas S. Histology of the parapapillary region in high myopia. Am J Ophthalmol. 2011;152(6):1021–9.
26. Ohno-Matsui K, Kasahara K, Moriyama M. Detection of Zinn-Haller arterial ring in highly myopic eyes by simultaneous indocyanine green angiography and optical coherence tomography. Am J Ophthalmol. 2013;155(5):920–6.
27. Ohno-Matsui K, Futagami S, Yamashita S, Tokoro T. Zinn-Haller arterial ring observed by ICG angiography in high myopia. Br J Ophthalmol. 1998;82(12):1357–62.
28. Ishida T, Jonas JB, Ishii M, Shinohara K, Ikegaya Y, Ohno-Matsui K. Peripapillary arterial ring of Zinn-Haller in highly myopic eyes as detected by optical coherence tomography angiography. Retina (Philadelphia, Pa). 2017;37(2):299–304.
29. Jonas JB, Holbach L, Panda-Jonas S. Peripapillary arterial circle of Zinn-Haller: location and spatial relationships with myopia. PLoS One. 2013;8(11):e78867.

Part VIII

Long-Term Progression

Long-Term Progression of Fundus Changes; Summary and Flow Charts

24

Yuxin Fang

Abstract

The progression pattern of myopic maculopathy based on META-PM classification is shown. Frequent natural progression patterns include a progression from peripapillary diffuse atrophy to macular diffuse atrophy, development of patchy atrophy in the area of macular diffuse atrophy, enlargement of lesions of patchy atrophy, enlargement of macular atrophy, progression to patchy atrophy from lacquer cracks, and development of MNV-related macular atrophy around myopic macular neovascularization (MNV).

Keywords

Long-term progression · META-PM classification · Diffuse atrophy · Patchy atrophy · MNV-related macular atrophy

In 2015, the Meta-Analysis of Pathologic Myopia (META-PM) study group proposed an International photographic classification system for myopic maculopathy [1]. This META-PM classification has been consistently used in many studies investigating the long-term natural course of myopic maculopathy [2–7]. In two population-based longitudinal studies, the 10-year progression rate of myopic maculopathy was 35.5% in the elderly Chinese (aged 40+) (the Beijing Eye study) [3] and the 5-year progression rate was 35.3% in rural Chinese adult population (aged 30+) (the Handan Eye Study) [4]. In a large highly myopic Chinese cohort (Zhongshan Ophthalmic Center-Brien Holden Vision Institute High Myopia Cohort Study), myopic maculopathy progressed in approximately 15% of 657 highly myopic eyes over 2 years [6].

Y. Fang (✉)
Department of Ophthalmology and Visual Science, Tokyo Medical and Dental University, Tokyo, Japan

In this chapter, we aim to illuminate the progression pattern of myopic maculopathy mainly based on META-PM classification. The data are from a retrospective case series study including 810 eyes of 432 highly myopic patients who had been followed for ≥10 years in the High Myopia Clinic at Tokyo Medical and Dental University [2]. In the mean follow-up of 18 years, the progression of myopic maculopathy was observed in 58.6% for all and in 74.3% in eyes with pathologic myopia at baseline.

24.1 Progression Patterns and Clinical Characteristics of Each Lesion of Myopic Maculopathy at Baseline (Table 24.1)

24.1.1 From High Myopia to Pathologic Myopia

Pathologic myopia (PM) is defined as myopic maculopathy equal to or more severe than diffuse choroidal atrophy (category 2), or by a presence of "plus lesions" such as myopic macular neovascularization (MNV) or lacquer cracks, or by a presence of a posterior staphyloma [1, 8]. During a mean follow-up of 19.5 years, 27% of 289 highly myopic (HM) eyes without PM at baseline progressed to PM [2]. Within those 78 eyes with progression, 59 eyes (75.6%) progressed to diffuse choroidal atrophy, 16 eyes (20.5%) progressed to patchy atrophy, and the remaining 3 eyes (3.8%) progressed to MNV-related macular atrophy.

In 10-year follow-up in the Beijing Eye study [3], the progression from HM to PM was observed in 15 of 79 eyes (19%) with tessellated fundus at baseline. Twelve of the 15 eyes showed the progression to diffuse atrophy, 1 eye showed the progression to lacquer cracks, 1 eye with the progression to patchy atrophy and 1 eye with the progression to macular atrophy. Fang et al. [2] reported that the patients with progression were significantly older (40.6 ± 17.0 years vs.

K. Ohno-Matsui (ed.), *Atlas of Pathologic Myopia*, https://doi.org/10.1007/978-981-15-4261-9_24

Table 24.1 The progression patterns and clinical characteristics at baseline and at last visit according to each lesion of myopic maculopathy

Lesion of myopic maculopathy at baseline	Progression and its patterns	No. of eyes (%)	Age at baseline (yrs.)	Age at last visit (yrs.)	Axial length at baseline (mm)	Axial length at last visit (mm)	Follow-up (yrs.)
No maculopathy (22 eyes)	Total	14/22 (63.6%)	21.8±18.9	41.1±20.3	26.3±1.2	28.3±11.7	20.2±15.9
	Development of tessellated fundus	**10/14 (71.4%)**	17.4±17.4	36.6± 19.1	26.2±1.2	28.2±1.8	20.0±16.6
	Development of diffuse choroidal atrophy	4/14 (28.6%)	32.8±20.4	52.5±21.3	26.4±1.2	28.7±1.5	20.8±4.5
Tessellated fundus (266 eyes)	Total	74/266 (27.9%)	39.4 ± 16.8	60.3 ± 17.2	28.3 ± 1.4	29.9 ± 1.7	20.9 ± 6.3
	Development of diffuse choroidal atrophy	**55/74 (74.3%)**	38.6 ± 17.6	59.4 ± 18.2	28.2 ± 1.5	29.7 ± 1.7	20.8 ± 6.6
	Development of patchy choroidal atrophy	16/74 (21.6%)	39.3 ± 14.3	61.0 ± 14.0	28.8 ± 1.2	30.8 ± 1.2	21.7 ± 5.4
	Development of myopic MNV (including MNV-related macular atrophy)	5/74 (6.8%)	53.8 ± 13.3	72.0 ± 11.6	28.6 ± 1.6	30.2 ± 1.6	18.2 ± 4.0
	Development of new lacquer cracks	8/74 (10.8%)	43.5 ± 9.0	61.5 ± 8.1	29.4 ± 0.9	30.7 ± 0.7	18.0 ± 2.8
Peripapillary diffuse choroidal atrophy without plus lesions (158 eyes)	Total	82/158 (51.9%)	43.5 ± 15.8	65.2 ± 14.0	29.0 ± 1.7	30.4 ± 1.8	21.7 ± 7.5
	Development of macular diffuse choroidal atrophy	**64/82 (78.0%)**	42.8 ± 16.2	64.6 ± 14.7	29.1 ± 1.7	30.6 ± 1.9	21.8 ± 7.7
	Development of patchy choroidal atrophy	27/82 (32.9%)	42.0 ± 16.7	63.7 ± 14.2	28.5 ± 1.5	30.3 ± 1.6	21.7 ± 8.1
	Development of myopic MNV (including MNV-related macular atrophy)	13/82 (15.9%)	47.3 ± 16.8	68.0 ± 46.6	28.6 ± 1.7	29.6 ± 1.5	20.7 ± 5.5
	Development of new lacquer cracks	8/82 (9.8%)	26.9 ± 18.4	50.3 ± 9.8	28.1 ± 1.4	30.9 ± 2.1	23.4 ± 9.2
	Development of patchy-related macular atrophy	3/82 (3.7%)	53.7 ± 4.5	80.0 ± 4.6	31.0 ± 2.3	31.5 ± 2.2	26.3 ± 4.0
Macular diffuse choroidal atrophy without plus lesions (59 eyes)	Total	29/59 (49.2%)	53.4 ± 13.1	72.1 ± 11.7	29.9 ± 1.7	30.9 ± 1.9	18.6 ± 5.8
	Development of patchy choroidal atrophy	**23/29 (79.3%)**	53.6 ± 12.6	72.1 ± 12.2	29.8 ± 1.6	30.9 ± 1.8	18.6 ± 5.4
	Development of myopic MNV (including MNV-related macular atrophy)	5/29 (17.2%)	58.4 ± 10.7	75.0 ± 7.9	29.9 ± 2.3	30.1 ± 1.4	16.6 ± 5.9
	Development of new lacquer cracks	1/29 (3.4%)	26	56	31.4	35	30
	Development of patchy-related macular atrophy	0	–	–	–	–	–
Patchy atrophy without plus lesions (63 eyes)	Total	60/63 (95.2%)	49.3 ± 13.7	68.9 ± 12.6	31.1 + 1.4	31.9 ± 1.6	19.6 ± 7.8
	Enlargement of the original patchy atrophy	**59/60 (98.3%)**	49.6 ± 13.5	69.1 ± 12.7	31.1 ± 1.4	31.9 ± 1.6	19.4 ± 7.7
	Development of new patchy choroidal atrophy	29/60 (48.3%)	49.8 ± 13.9	71.4 ± 12.3	31.1 ± 1.5	31.9 ± 1.6	21.7 ± 8.3
	Development of myopic MNV (including MNV-related macular atrophy)	13/60 (21.7%)	47.1 ± 8.2	69.8 ± 8.2	31.0 ± 1.3	31.3 ± 1.6	22.7 ± 7.6
	Development of patchy-related macular atrophy	5/60 (8.3%)	50.8 ± 17.5	73.8 ± 12.4	30.7 ± 1.7	31.5 ± 2.0	23.0 ± 7.0
Macular atrophy without plus lesions (35 eyes)	**Enlargement of macular atrophy**	**35/35 (100%)**	51.1 ± 12.7	68.1 ± 13.0	29.7 ± 1.8	30.2 ± 1.5	17.2 ± 7.7
Lacquer cracks (66 eyes)	Total	43/66 (65.2%)	42.8 ± 10.4	62.1 ± 11.5	30.1 ± 1.5	31.5 ± 2.0	19.1 ± 7.4
	Development of new lacquer cracks	7/43 (16.3%)	35.3 ± 14.2	51.7 ± 12.5	30.3 ± 0.7	31.0 ± 0.7	16.7 ± 6.6
	Development of new patchy atrophy	**38/43 (88.4%)**	43.7 ± 9.2	63.3 ± 10.7	30.0 ± 1.6	31.6 ± 2.1	19.4 ± 7.3
Myopic MNV (109 eyes with active or scar phase without macular atrophy)	**Development of MNV-related macular atrophy**	**101/109 (92.7%)**	54.2 ± 12.2	69.5 ± 11.6	28.6 ± 1.6	29.5 ± 1.7	15.8 ± 6.1

Yrs. years, *med* median, *MNV* macular neovascularization, *PDCA* Peripapillary diffuse choroidal atrophy, *MDCA* macular diffuse choroidal atrophy; Reproduced and modified with permission from [2]

29.4 ± 15.3 years) and had longer axial length at baseline (28.3 ± 1.5 vs. 27.3 ± 1.3 mm) than those without progression. The progression from HM to PM was significantly associated with older age, longer axial length at baseline, greater axial elongation during a follow-up and the development or enlargement of parapapillary atrophy after adjusting for gender, myopic maculopathy at baseline, and a duration of follow-up [2].

Diffuse atrophy usually begins at around the age 40. Li et al. confirmed that myopic maculopathy developed or progressed disproportionally more commonly among people aged 40 years and older [6]. This findings was compatible with that no subjects progressed to diffuse atrophy in 44 highly myopic Chinese adolescents aged 12-16 at baseline who had been followed up for 10 years in Singapore Cohort Study of Risk Factors for Myopia (SCORM) [5]. Fang et al. [2] reported that the strongest risk factor associated with the progression from HM to PM was the development or enlargement of parapapillary atrophy. A longer term observation is required to assess if those eyes with enlargement of parapapillary atrophy will eventually become PM in the future and if there are any other parameters for a higher risk of the development of myopic maculopathy.

It is important and challenging to determine whether or not simple childhood myopia will become eventual PM in adulthood. A retrospective case series study conducted in the High Myopia Clinic at Tokyo Medical and Dental University included 56 eyes of 29 children and adolescents aged 15 years or younger who were followed up for over 20 years [9]. At the last visit, 35 eyes (63%) showed PM in adulthood, of which 29 eyes (83%) showed pre-existing peripapillary diffuse choroidal atrophy during childhood or adolescence, and the remaining 6 (17%) eyes showed tessellation only. This suggested that the presence of peripapillary diffuse choroidal atrophy in children with high axial myopia may be an indicator for the eventual development of advanced myopic choroidal atrophy in later life. In addition, peripapillary diffuse choroidal atrophy was significantly associated with an abrupt and extreme thinning of the peripapillary choroid in OCT images [10], thus the measurement of nasal choroidal thickness in high myopic children using 56.5 μm at 3 mm nasal to fovea as a cut-off value for predicting the occurrence of myopic choroidal atrophy is warranted [11].

24.2 Progression of Diffuse Choroidal Atrophy (Myopic Maculopathy Category 2)

24.2.1 Peripapillary Diffuse Choroidal Atrophy (PDCA)

Diffuse choroidal atrophy develops initially around the optic disc, i.e., peripapillary diffuse choroidal atrophy (PDCA). Approximately half of the eyes with PDCA without plus lesions at baseline progressed, most frequently showed an enlargement of PDCA to macular diffuse choroidal atrophy (MDCA) (Table 24.1).

In the progression from PDCA to MDCA, the mean choroidal thickness was reduced by almost a half at all locations except nasal part (subfoveal choroidal thickness: from 85 μm to 50 μm; temporal choroidal thickness: from 112 μm to 62 μm; superior choroidal thickness from 112 μm to 66 μm; inferior choroidal thickness from 93 μm to 57 μm, vs. nasal choroidal thickness: from 32 μm to 21 μm). The cut-off value to differentiate the eyes with MDCA from PDCA was 62 μm at the subfovea [11]. (See Chap. 17).

24.2.2 Macular Diffuse Choroidal Atrophy (MDCA)

Approximately a half of the eyes with MDCA without plus lesions at baseline progressed, in which almost 80% of eyes developed patchy atrophies and 17% developed myopic macular neovascularization (MNV) (Table 24.1).

There was no significant difference in the subfoveal choroidal thickness between the eyes with MDCA (50 μm) and patchy atrophy (49 μm). Swept-source OCT showed that patchy atrophy was not simply an atrophy but were holes of Bruch's membrane [12, 13]. It suggested that the progression from diffuse atrophy to patchy atrophy was not due to a progressive choroidal thinning but was due to a new development of Bruch's membrane hole in the area of already thinned choroid. It was also possible that the Bruch's membrane was fragile in eyes with extremely thin choroid such as in the eyes with MDCA. Therefore, MDCA may be a prerequisite or precursor for developing Bruch's membrane holes by making Bruch's membrane more fragile in the first place. However, this is speculative and needs to be proven.

It has to be considered that approximately the remaining half of eyes with diffuse atrophy did not develop Bruch's membrane defects after a mean follow-up of 19 years [2]. This may indicate that approximately one-half of the eyes with diffuse atrophy may remain stable for a relatively long period.

24.3 Progression of Patchy Atrophy

Almost all eyes (95%) with patchy atrophy progressed, in which an enlargement of the original patchy atrophy was found predominantly in 98%, and new patchy atrophy was found in 47% followed by the development of myopic MNV in 21.7% and patchy-related macular atrophy in 8.3% (Table 24.1). Such high percentages of progression of eyes with patchy atrophy could be explained by biomechanical properties of Bruch's membrane. Once its defect is created, the Bruch's membrane defect tends to enlarge over time.

24.4 Progression of Myopic MNV

Patients with myopic MNV tend to be older (mean age, 53 years) and have relatively short axial lengths (mean, 28.9 mm) as compared to the patients with other lesions due to PM [2]. In this study population, 93% of the eyes with myopic MNV, either in the active stage or the scar phase, progressed to MNV-related macular atrophy without any treatment. Currently, anti-VEGF treatment is the first-line therapy for myopic MNV. Onishi et al. [14] reported that the incidence of MNV-related macular atrophy was lower (73.9%) in treated eyes with the intravitreal injection of ranibizumab at 5 years after MNV onset than the natural course. Chhablani et al. [15] described the 5-year outcomes after intravitreal bevacizumab monotherapy in 33 eyes with myopic MNV. In their study, the foveal atrophy was found at baseline in 5 eyes (15.2%) and in 14 eyes (42.4%) at the final visit.

24.5 Progression of Lacquer Cracks

The common progression pattern of lacquer cracks (which are linear defects of Bruch's membrane) is a progression to patchy atrophy and an increase of the number of lacquer cracks [2, 16]. Multimodal imaging is needed for the precise detection of lacquer cracks. A progression of lacquer cracks was found in 53.7% of the eyes with a mean follow-up period of 3.5 years [16]. In this study, an increase in the number of lacquer cracks was the most frequent pattern followed by a progression to patchy atrophy and an elongation of existing lacquer cracks (See more details in Chap. 13).

24.6 A Scheme Depicting the Progression Patterns of Myopic Maculopathy Suggested by OCT Findings (Fig. 24.1)

First, the progression from category 0 (no myopic maculopathy) to category 1 (fundus tessellation) is not associated with a decline of the best-corrected visual acuity. Although the tessellation is not considered as PM, a remarkable thinning of the choroid begins with the appearance of tessellation, which is the first sign of the progression of myopic maculopathy. Second, diffuse atrophy (category 2) primarily occurs in the peripapillary region (peripapillary diffuse choroidal atrophy; PDCA) and eventually extends into the macula (macular diffuse choroidal atrophy; MDCA). Third, the eyes with patchy atrophy have a hole in the macular Bruch's membrane that either forms by an enlargement of lacquer cracks or develops in the regions of advanced diffuse atrophy with a more vulnerable Bruch's membrane. Fourth, both patchy atrophy and macular atrophy (MNV-related and patchy-related) tend to enlarge with time. Fifth, macular atrophy is almost always MNV-related, although patchy-related MA can occasionally occur.

24.7 Risk Factors for Progression of Myopic Maculopathy

Risk factors for progression of myopic maculopathy include older age, longer axial length, greater increase in axial length, a presence or enlargement of parapapillary diffuse choroidal atrophy (PDCA) [2], and eyes with diffuse atrophy or a greater category of baseline myopic maculopathy [6] (Fig. 24.2).

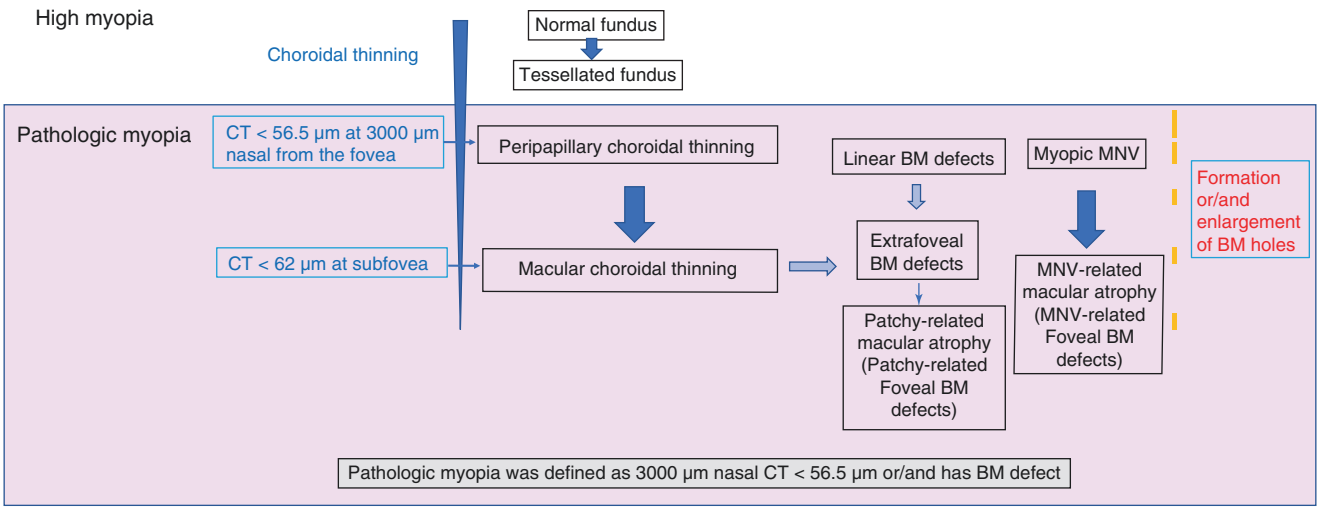

Fig. 24.1 A scheme depicting the progression patterns of myopic maculopathy and corresponding characteristics of OCT findings. *BM* Bruch's membrane, *MNV* macular neovascularization, *CT* choroidal thickness

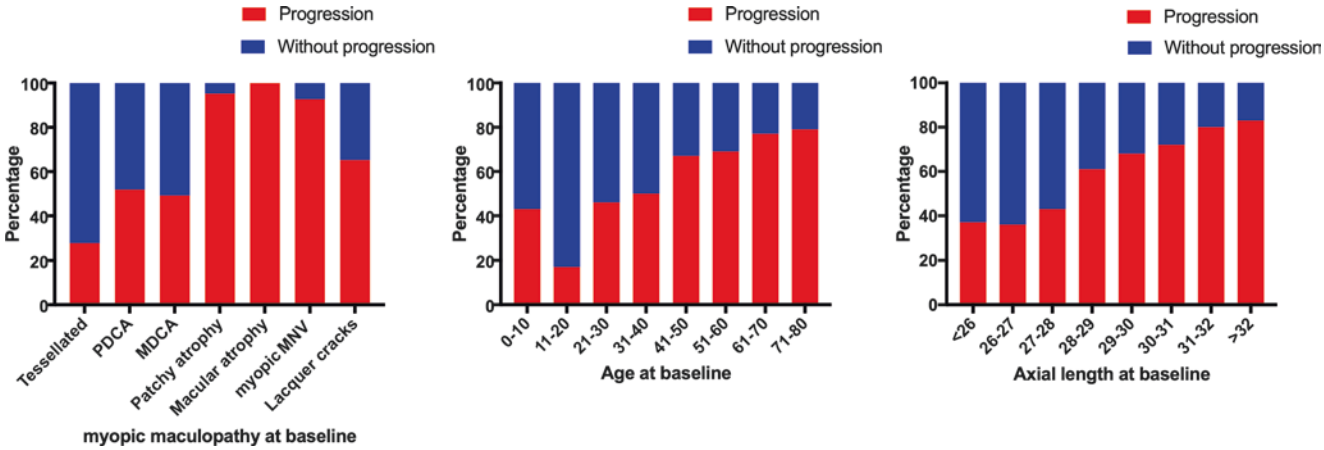

Fig. 24.2 Proportion of progression of myopic maculopathy by myopic maculopathy lesion, age and axial length at baseline. *PDCA* peripapillary diffuse choroidal atrophy, *MDCA* macular diffuse choroidal atrophy, *MNV* macular neovascularization

References

1. Ohno-Matsui K, Kawasaki R, Jonas JB, Cheung CM, Saw SM, Verhoeven VJ, et al. International photographic classification and grading system for myopic maculopathy. Am J Ophthalmol. 2015;159(5):877–83.
2. Fang Y, Yokoi T, Nagaoka N, Shinohara K, Onishi Y, Ishida T, et al. Progression of myopic maculopathy during 18-year follow-up. Ophthalmology. 2018;125(6):863–77.
3. Yan YN, Wang YX, Yang Y, Xu L, Xu J, Wang Q, et al. Ten-year progression of myopic maculopathy: the Beijing eye study 2001-2011. Ophthalmology. 2018;125(8):1253–63.
4. Lin C, Li SM, Ohno-Matsui K, Wang BS, Fang YX, Cao K, et al. Five-year incidence and progression of myopic maculopathy in a rural Chinese adult population: the Handan eye study. Ophthalmic Physiol Opt. 2018;38(3):337–45.
5. Wong YL, Ding Y, Sabanayagam C, Wong CW, Verkicharla P, Ohno-Matsui K, et al. Longitudinal changes in disc and retinal lesions among highly myopic adolescents in Singapore over a 10-year period. Eye Contact Lens. 2018;44(5):286–91.
6. Li Z, Liu R, Xiao O, Guo X, Wang D, Zhang J, et al. Progression of myopic maculopathy in highly myopic Chinese eyes. Invest Ophthalmol Vis Sci. 2019;60(4):1096–104.
7. Ueda E, Yasuda M, Fujiwara K, Hashimoto S, Ohno-Matsui K, Hata J, et al. Trends in the prevalence of myopia and myopic maculopathy in a Japanese population: the Hisayama study. Invest Ophthalmol Vis Sci. 2019;60(8):2781–6.
8. Ohno-Matsui K, Lai TY, Lai CC, Cheung CM. Updates of pathologic myopia. Prog Retin Eye Res. 2016;52:156–87.
9. Yokoi T, Jonas JB, Shimada N, Nagaoka N, Moriyama M, Yoshida T, et al. Peripapillary diffuse chorioretinal atrophy in children as a sign of eventual pathologic myopia in adults. Ophthalmology. 2016;123(8):1783–7.
10. Yokoi T, Zhu D, Bi HS, Jonas JB, Jonas RA, Nagaoka N, et al. Parapapillary diffuse choroidal atrophy in children is associated with extreme thinning of parapapillary choroid. Invest Ophthalmol Vis Sci. 2017;58(2):901–6.
11. Fang Y, Du R, Nagaoka N, Yokoi T, Shinohara K, Xu X, et al. OCT-based diagnostic criteria for different stages of myopic maculopathy. Ophthalmology. 2019;126(7):1018–32.
12. Ohno-Matsui K, Jonas JB, Spaide RF. Macular Bruch membrane holes in highly myopic patchy chorioretinal atrophy. Am J Ophthalmol. 2016;166:22–8.
13. Du R, Fang Y, Jonas JB, Yokoi T, Takahashi H, Uramoto K, et al. Clinical features of patchy chorioretinal atrophy in pathologic myopia. Retina. 2020;40(5):951–59.
14. Onishi Y, Yokoi T, Kasahara K, Yoshida T, Nagaoka N, Shinohara K, et al. Five-year outcomes of intravitreal ranibizumab for choroidal neovascularization in patients with pathologic myopia. Retina. 2019;39(7):1289–98.
15. Chhablani J, Paulose RM, Lasave AF, Wu L, Carpentier C, Maia M, et al. Intravitreal bevacizumab monotherapy in myopic choroidal neovascularisation: 5-year outcomes for the PAN-American collaborative retina study group. Br J Ophthalmol. 2018;102(4):455–9.
16. Xu X, Fang Y, Uramoto K, Nagaoka N, Shinohara K, Yokoi T, et al. Clinical features of lacquer cracks in eyes with pathologic myopia. Retina. 2019;39(7):1265–77.

Long-Term Progression of Fundus Changes; from Children to Adults

25

Tae Igarashi-Yokoi and Yuxin Fang

Abstract

Two cases with the long-term progression in fundus and the optic disc appearance from childhood to adulthood are shown.

In children with high myopia, the optic disc appearance is generally normal or slightly tilted, however, about 30% of the cases have noticeable morphological changes in the optic disc appearance already in their early teens to 30s. Peripapillary diffuse choroidal atrophy which is observed as disproportionate choroidal thinning temporal to the optic disc by swept-source OCT is an important sign to identify children who will become pathologic myopia in adulthood. In addition to the development of peripapillary diffuse choroidal atrophy, the optic disc shows a marked change in its appearance and in size from childhood to adulthood.

Keywords

Long-term progression · Childhood myopia · Peripapillary diffuse choroidal atrophy

T. Igarashi-Yokoi · Y. Fang (✉)
Department of Ophthalmology and Visual Science, Tokyo Medical and Dental University, Tokyo, Japan
e-mail: yokooph@tmd.ac.jp

K. Ohno-Matsui (ed.), *Atlas of Pathologic Myopia*, https://doi.org/10.1007/978-981-15-4261-9_25

25.1 Case 1-Progression From Peripapillary Diffuse Choroidal Atrophy (PDCA) in Childhood to Macular Diffuse Choroidal Atrophy (MDCA), Accompanying with a Marked Enlargement of the Optic Disc (Fig. 25.1)

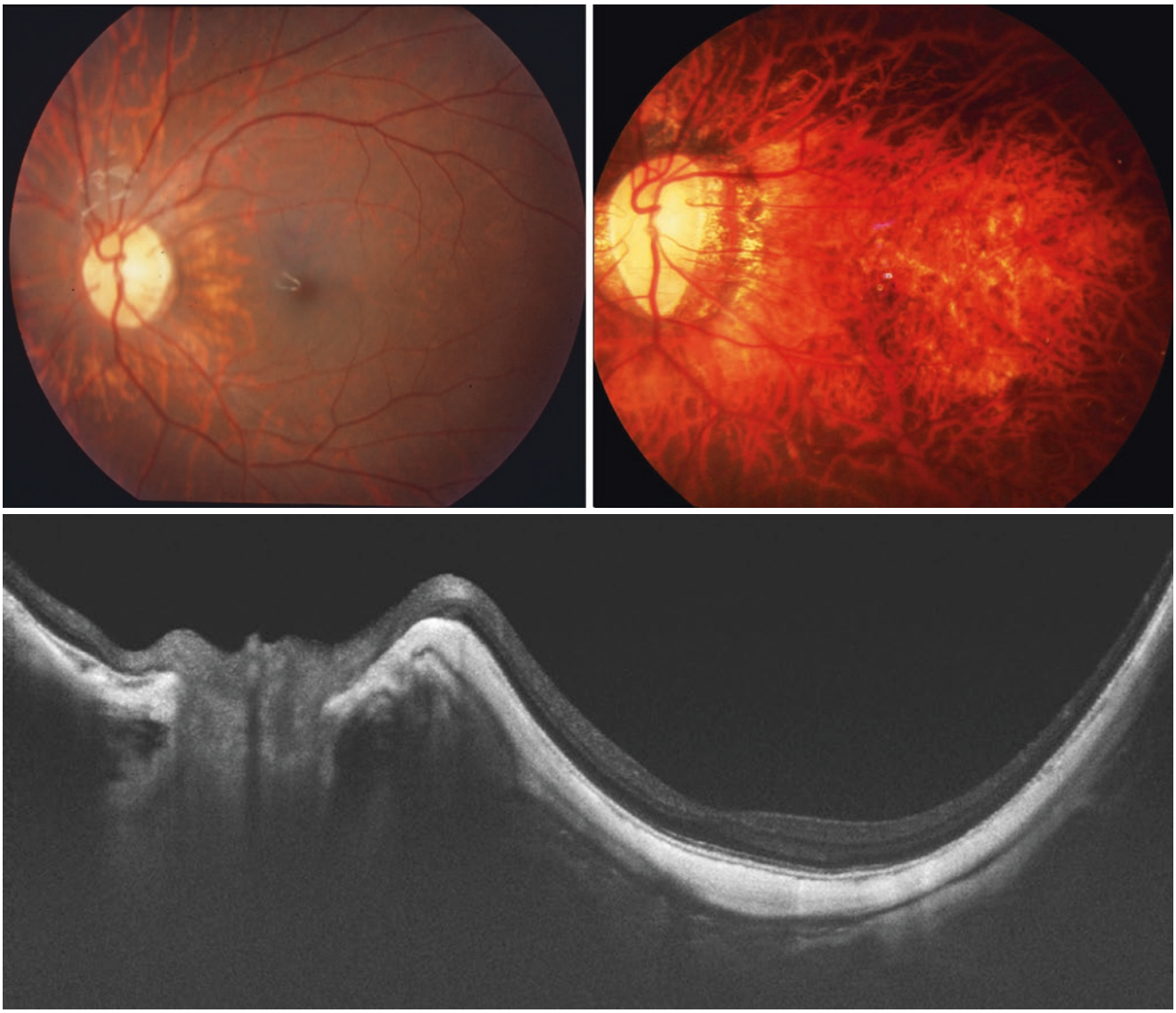

Fig. 25.1 (Top Left) Left fundus of an 8-year-old boy shows peripapillary diffuse choroidal atrophy (PDCA). Optic disc appearance is nearly normal. Refractive error is -10.2D and an axial length is 28.0 mm. (Top Right) Left fundus at the age of 41 shows a development of macular diffuse atrophy covering the entire area of the posterior fundus. Several lacquer cracks are also seen. Optic disc has enlarged, especially a lower part of the optic disc is elongated, showing a bizarre shape of the optic disc. Parapapillary gamma and delta zone have developed. Refractive error is -24.5D and axial length is 33.6 mm. (Bottom) Horizontal section of swept-source OCT image across the optic disc at the age of 41 shows a marked thinning of the choroid in the entire posterior fundus as well as a formation of ridge-like protrusion temporal to the optic disc

25.2 Case 2-A Marked Change in Optic Disc Appearance From Childhood to Adulthood (Fig. 25.2)

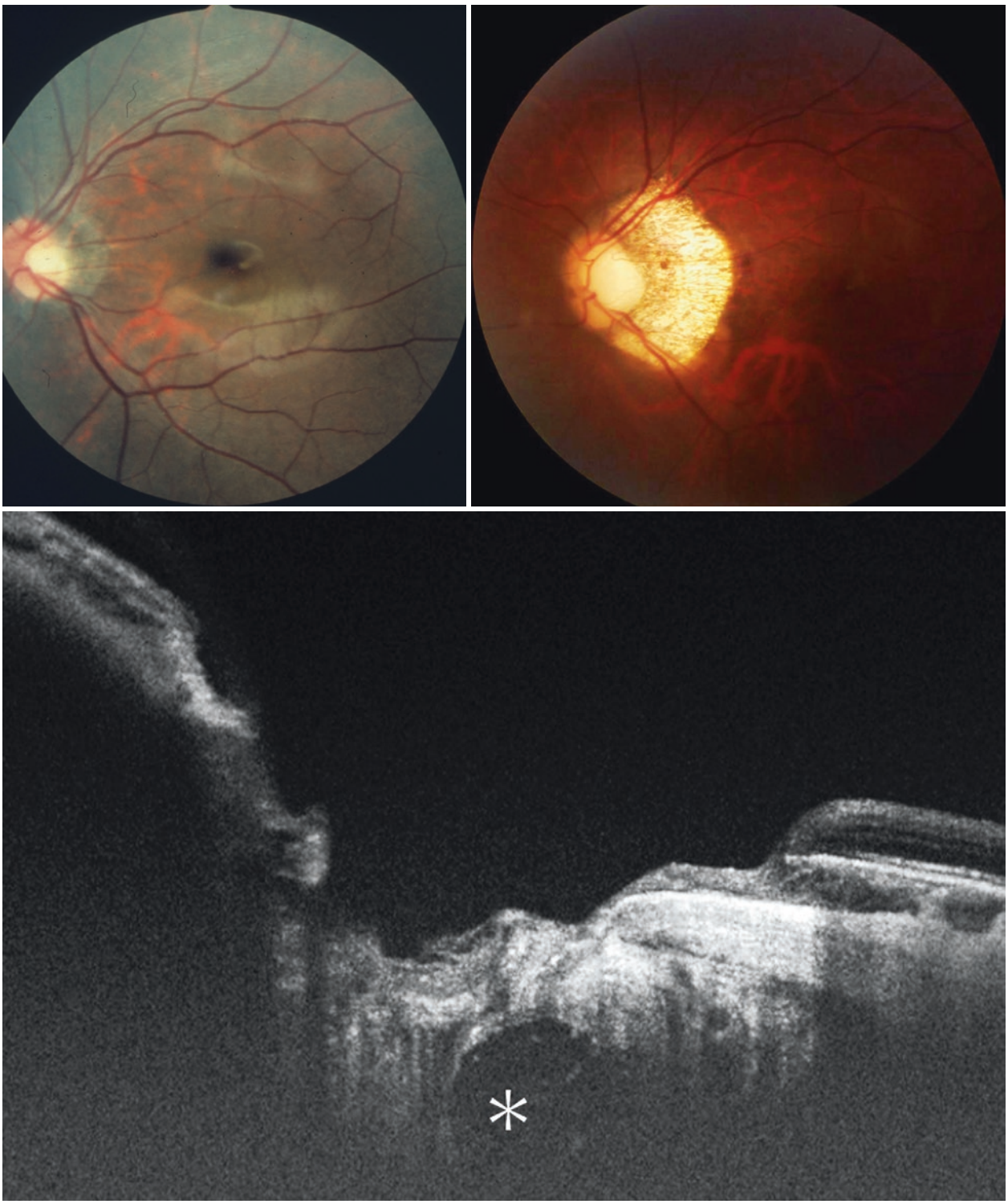

Fig. 25.2 (Top Left) Left fundus of a 12-year-old boy shows mild tilting of the optic nerve with a parapapillary beta zone. No visual field defects are detected with Goldmann perimetry. Refractive error is -8.5D an and axial length is 28.9 mm. (Top Right) Left fundus at the age of 47 shows that the optic disc is deformed and its temporal margin is protruded toward the macula. Parapapillary gamma and delta zone have developed temporally. Humphrey visual field analyzer shows an arcuate scotoma in the superior hemifield. The Refractive error is -14.0D and an axial length is 31.0 mm. (Bottom) Horizontal section of swept-source OCT image across the optic nerve shows an intrachoroidal cavitation (ICC) accompanying with a herniation of retinal tissue into ICC space. Subarachnoid space (∗) around the optic nerve is enlarged

Long-Term Progression of Fundus changes in Adults (1)

26

Takashi Watanabe and Yuxin Fang

Abstract

To understand the progression patterns of myopic maculopathy, a long-term observation of highly myopic adult patients is essential. In this chapter, several cases with multiple progression patterns of myopic maculopathy are shown.

Keywords

Long-term progression · Myopic maculopathy · Diffuse atrophy · Patchy atrophy · Lacquer cracks

In eyes with pathologic myopia (PM), different kinds of lesions of myopic maculopathy as well as peripapillary lesions (including peripapillary intrachoroidal cavitation and peripapillary atrophy) are observed simultaneously. The lesions of myopic maculopathy progress with time, enlarge, and fuse with each other. A fusion with peripapillary atrophy and myopic maculopathy (especially patchy atrophy and myopic macular neovascularization (MNV)-related macular atrophy) is also seen. To understand complicated patterns of progression seen in the posterior fundus of PM eyes, several cases with multiple progression patterns are shown in this chapter. In some cases, a progression needs to be differentiated from inflammatory lesions like punctate inner choroidopathy. This differentiation requires a lot more case series study.

T. Watanabe · Y. Fang (✉)
Department of Ophthalmology and Visual Science, Tokyo Medical and Dental University, Tokyo, Japan

K. Ohno-Matsui (ed.), *Atlas of Pathologic Myopia*, https://doi.org/10.1007/978-981-15-4261-9_26

26.1 Case 1-Progression From Lacquer Cracks to Patchy Atrophy, an Enlargement and Fusion of Lesions with Patchy Atrophy (Figs. 26.1, 26.2, 26.3, 26.4, 26.5, 26.6, 26.7 and 26.8)

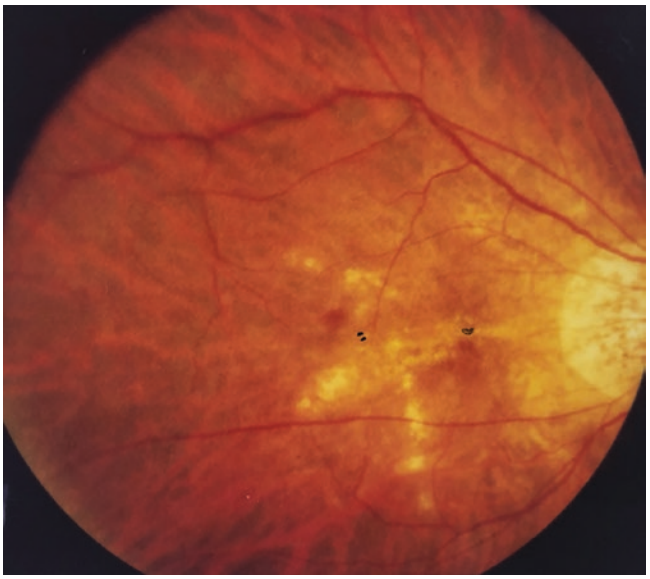

Fig. 26.1 Right fundus at the initial visit (February 1998) of a 45-year-old man with a refractive error of -12.0 diopters and an axial length of 28.7 mm. Several lacquer cracks are seen to run horizontally, vertically, and obliquely in the macula. Yellowish diffuse atrophy is found around the optic disc. The best-corrected visual acuity is 1.0

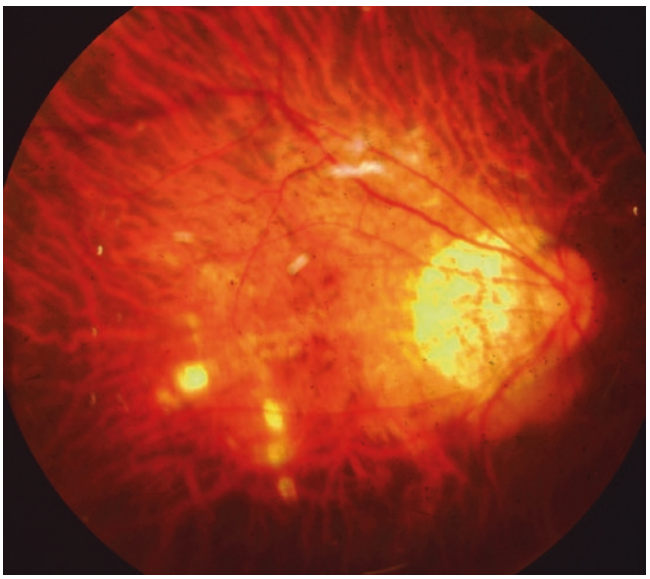

Fig. 26.2 One year later (September 1999), several lesions of patchy atrophy have occurred along the lacquer cracks

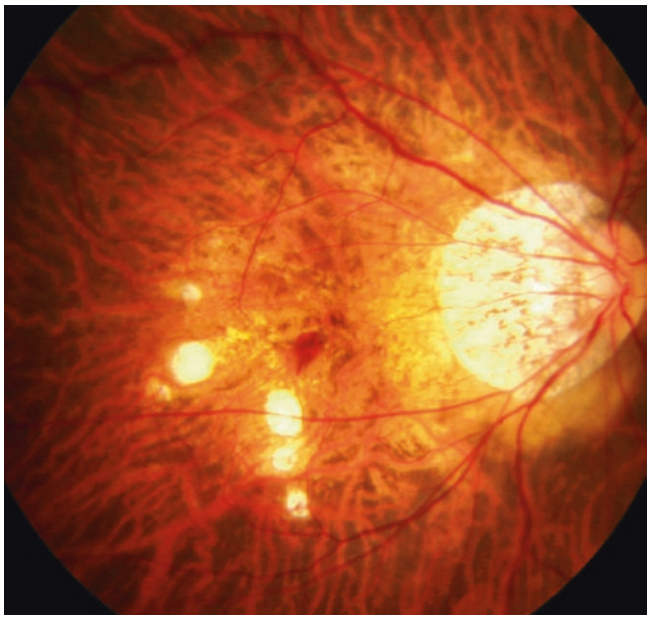

Fig. 26.3 Two years later (September 2001), the lesions of patchy atrophy have enlarged and new lesion of patchy atrophy has occurred along the upper temporal lacquer crack. Simple hemorrhage suggesting a formation of new lacquer crack has appeared in the macula. Peripapillary intrachoroidal cavitation can be seen lower to the optic disc

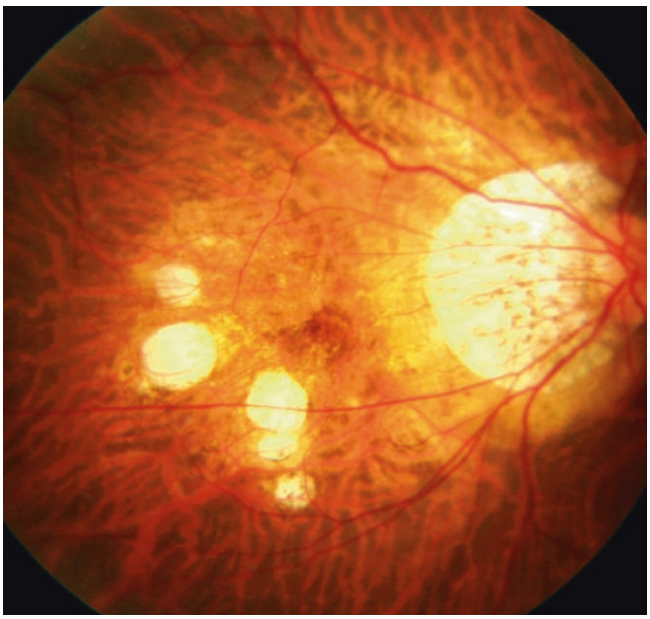

Fig. 26.4 Eight years later (September 2006), all lesions of patchy atrophy have further enlarged. Yellowish diffuse choroidal atrophy has covered the whole macular area

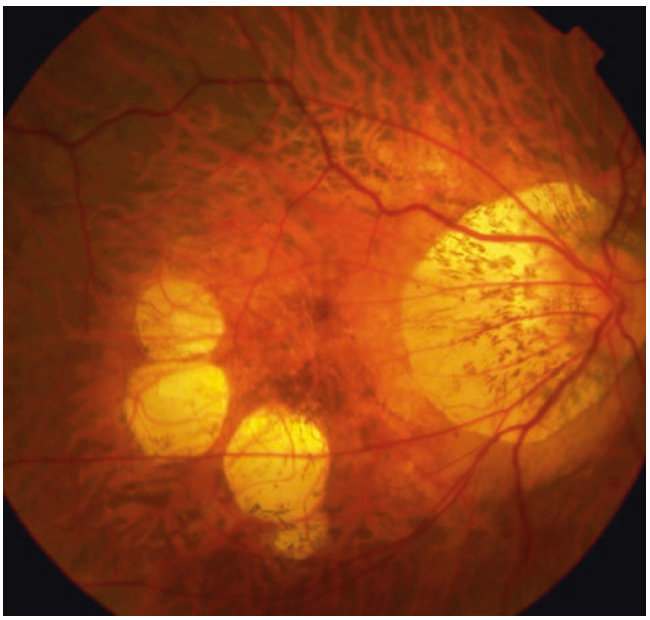

Fig. 26.5 Fourteen years later (September 2012), all lesions of patchy atrophy have continued to enlarge and have fused with each other. Note that a course of upper temporal major retinal vein has become irregular. The best-corrected visual acuity is 1.0. The refractive error is -16.0 diopter. The axial length is 29.8 mm

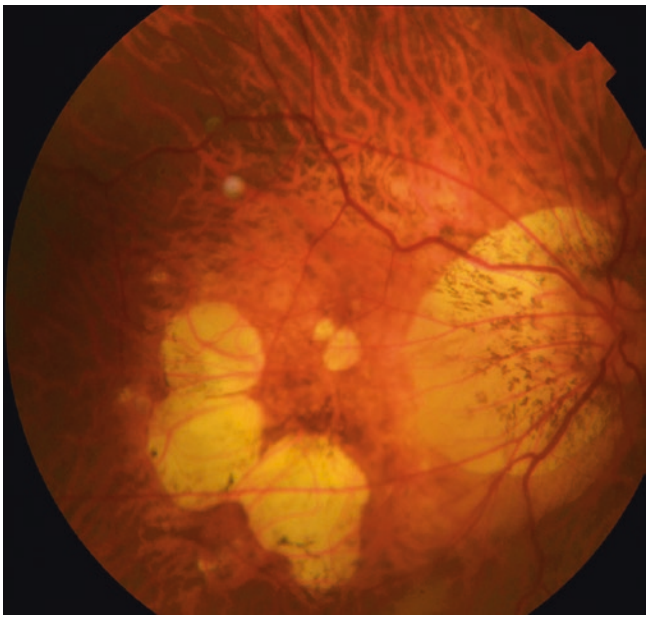

Fig. 26.6 Eighteen years later (September 2016), two new lesions of patchy atrophies have appeared (upper to the fovea). The original patchy atrophies have further enlarged and tended to coalesce

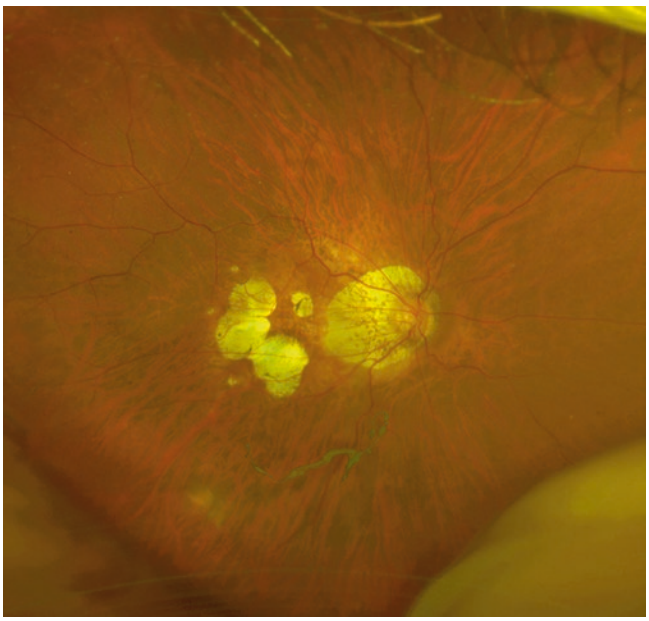

Fig. 26.7 Twenty-one years later (April 2019), the patchy atrophy has enlarged within the area of the posterior staphyloma. The fovea itself has been spared and the best-corrected visual acuity is 0.6

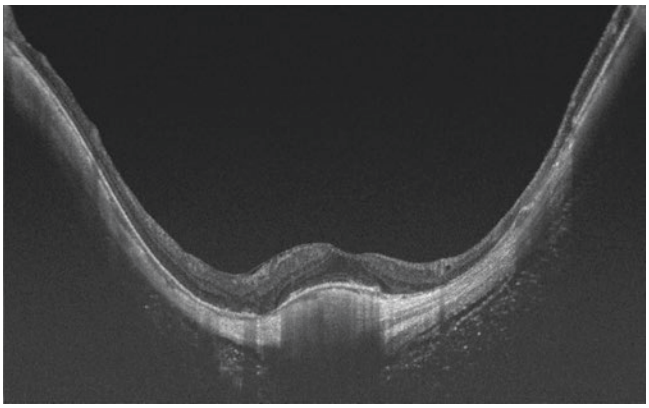

Fig. 26.8 A vertical section of swept source OCT (April 2019) shows a defect of retinal pigment epithelium (RPE) and Bruch's membrane in the area of patchy atrophy. Choroid is also absent in the area of patchy atrophy. Thin choroid still remains in the area without patchy atrophy. Dome-shaped macula is also observed

26.2 Case 2-Progression From Lacquer Cracks to Patchy Atrophy, an Increase and Enlargement and Fusion of Lesions with Patchy Atrophy, and Fusion with Patchy Atrophy and Peripapillary Atrophy (Figs. 26.9, 26.10, 26.11, 26.12, 26.13, 26.14 and 26.15)

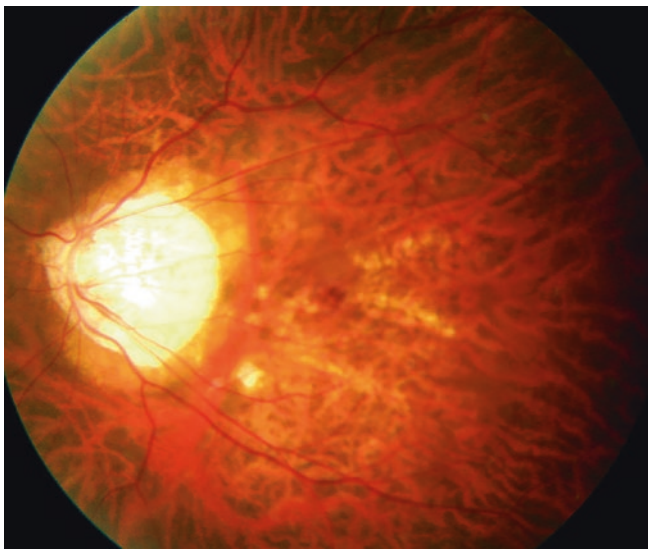

Fig. 26.9 Left fundus at the initial visit (September 2006) of a 46-year-old man shows lacquer cracks running obliquely and a small lesion of patchy atrophy lower temporal to the optic disc. The optic disc is severely tilted and a large temporally peripapillary atrophy is seen. Peripapillary intrachoroidal cavitation is observed superior and inferior to the optic disc. The refractive error is -19.0D and the axial length measurements are 30.6 mm. The best-corrected visual acuity is 1.2

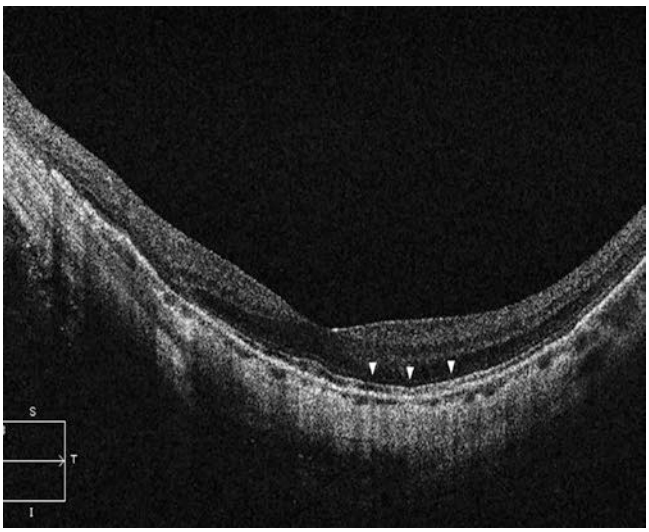

Fig. 26.11 Horizontal OCT section (February 2008) across the lacquer cracks shows an increased light penetrance into the deeper tissues (arrowheads)

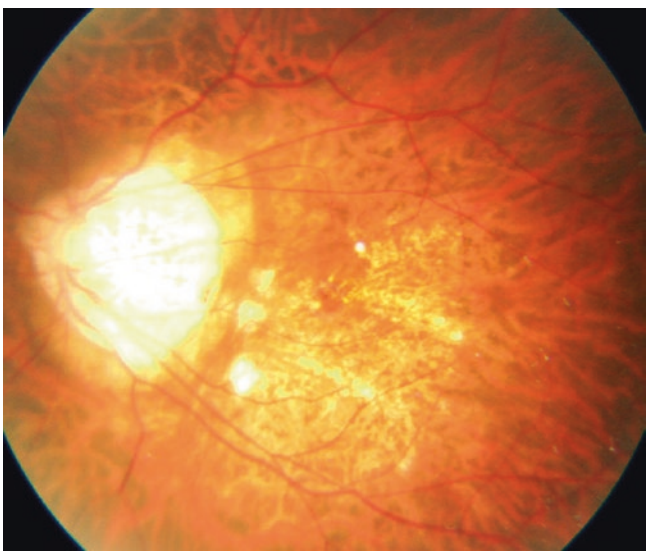

Fig. 26.10 Two years later (February 2008), the lesion of patchy atrophy lower temporal to the optic disc has enlarged and two new lesions of patchy atrophy have occurred temporal to the optic disc

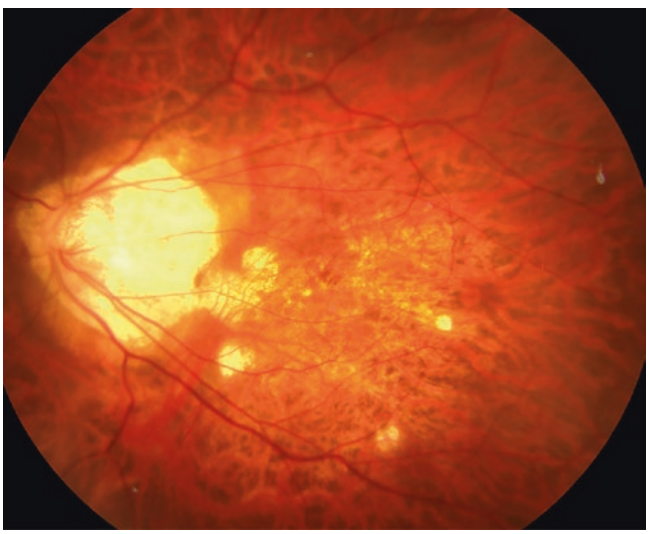

Fig. 26.12 Four years later (May 2010), lacquer cracks have become less obvious in the background of macular diffuse choroidal atrophy. The two lesions of patchy atrophy temporal to the optic disc have enlarged and they have fused with peripapillary atrophy. One new lesion of patchy atrophy has appeared temporal to the fovea

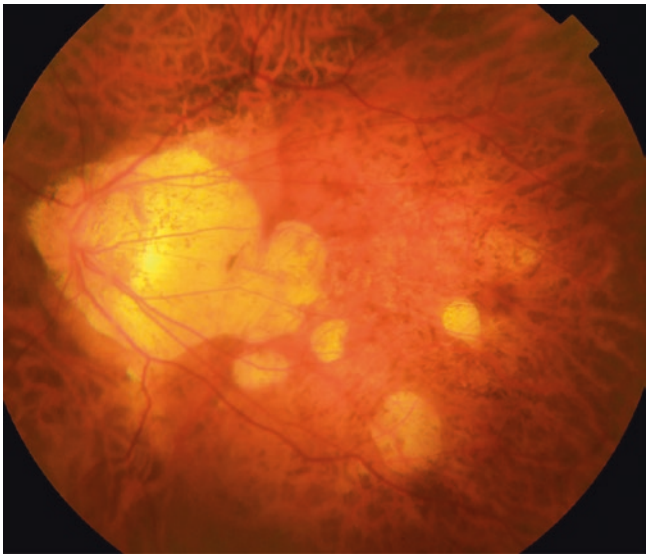

Fig. 26.13 Ten years later (April 2016), all lesions of patchy atrophy have further enlarged and diffuse atrophy has covered the entire posterior pole. Original lacquer cracks are no longer obvious. The two lesions of patchy atrophy temporal to the optic disc have coalesced with peripapillary atrophy, and have formed one big atrophic lesion

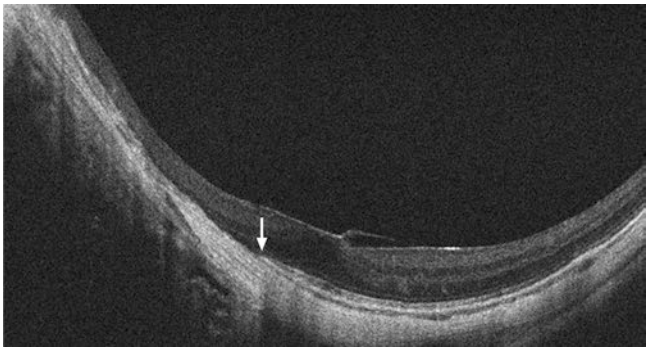

Fig. 26.15 Horizontal OCT image (November 2018) shows a defect of RPE and Bruch's membrane in the area of patchy atrophy. The choroid is absent and the inner retina is in a direct contact with the sclera. The end of the RPE is shown by an arrow

26.3 Case 3-Development of Multiple Lesions Along the Retinal Vessels and Patchy Atrophies, and Fusion with Large Peripapillary Atrophy (Figs. 26.16, 26.17, 26.18, 26.19, 26.20, 26.21 and 26.22)

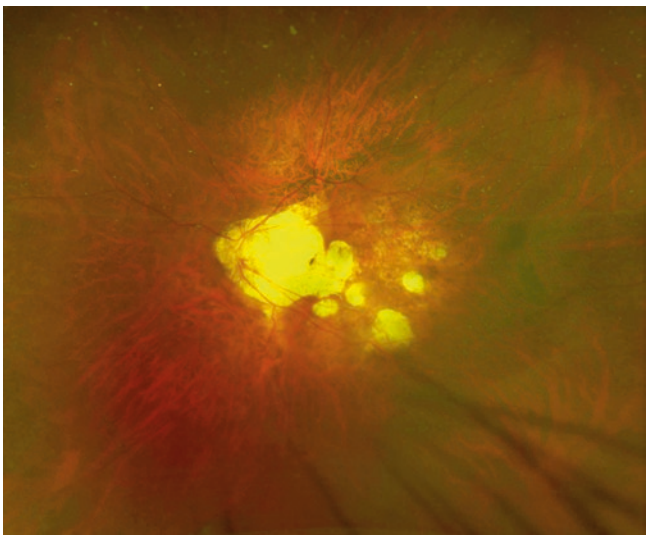

Fig. 26.14 Twelve years later (November 2018), all lesions of patchy atrophy have further enlarged. However, the fovea is spared between the lesions of patchy atrophy. The axial length is 31.5 mm. The best-corrected visual acuity is still 1.2

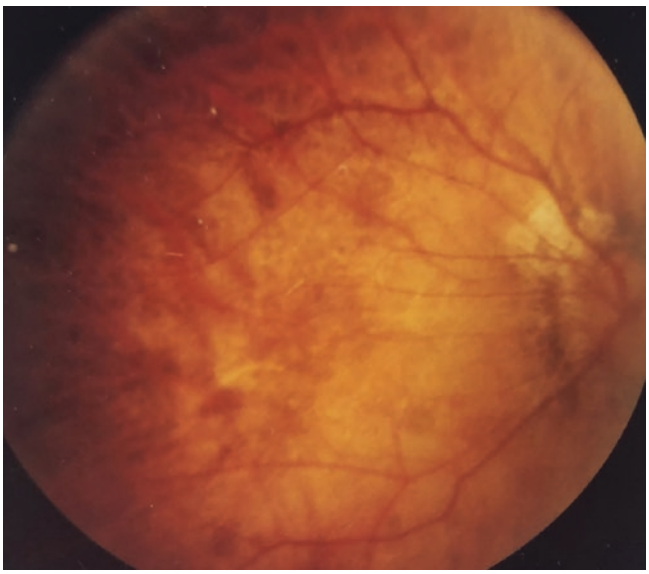

Fig. 26.16 Right fundus at the initial visit (December 1995) of a 50-year-old woman shows yellowish diffuse atrophy covering the entire posterior fundus. The optic disc is tilted and temporal peripapillary atrophy is seen. Refractive error is -24.0 diopters and an axial length is 32.4 mm. The best-corrected visual acuity is 0.9

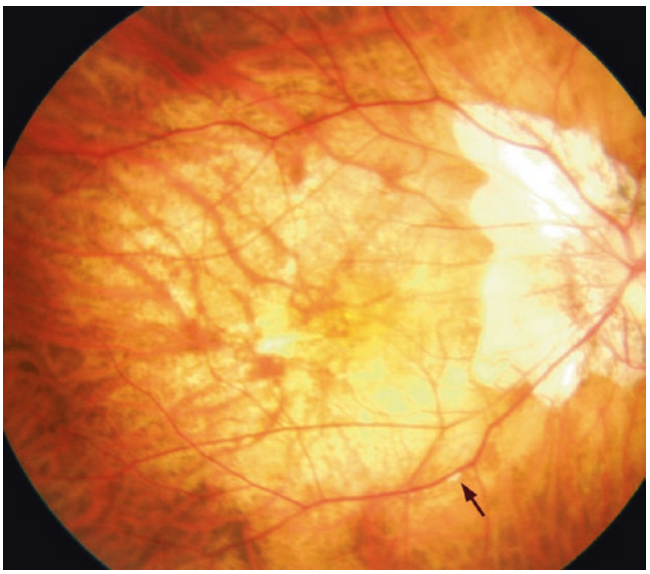

Fig. 26.17 Eleven years later (July 2006), a tiny new patchy atrophy has appeared along the lower temporal retinal vein (arrow)

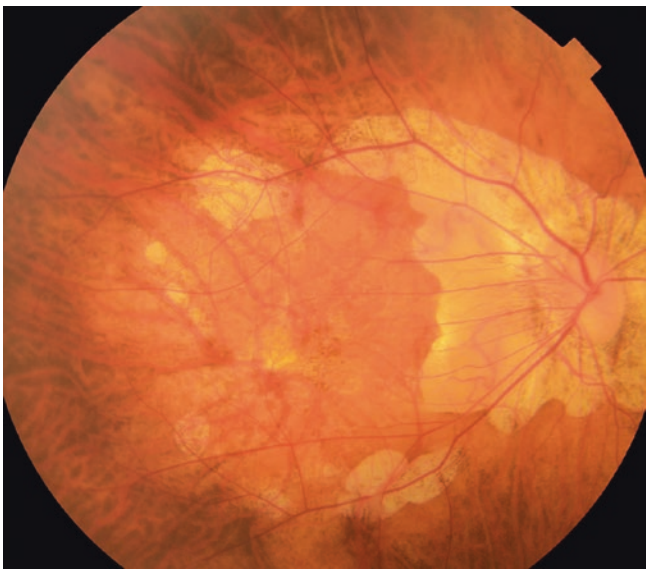

Fig. 26.19 Twenty-one years later (May 2016), patchy atrophies have further enlarged along the staphyloma edges and have coalesced with each other. Some lesions have fused with peripapillary atrophy

Fig. 26.18 Fifteen years later (November 2010), the number of patchy atrophies has increased along upper temporal and lower temporal retinal veins at staphyloma edges (arrows)

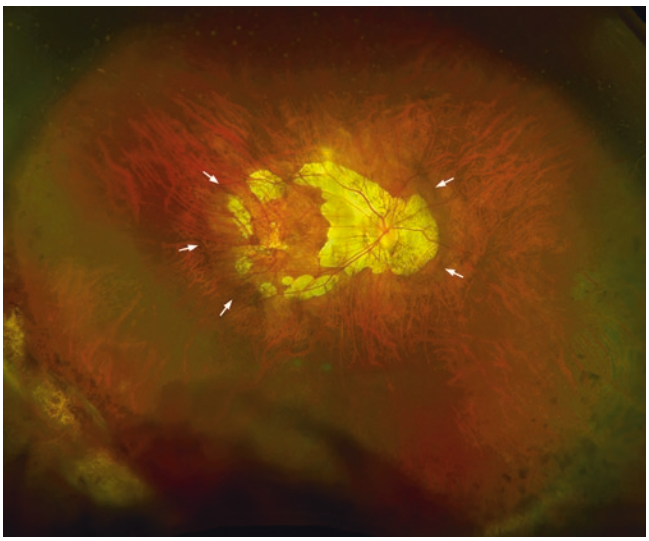

Fig. 26.20 Twenty-two years later (September 2017), a wide-field fundus image shows a pigmented border of wide macular staphyloma (arrows). Please note that most of patchy atrophies as well as peripapillary atrophy have enlarged along the upper and lower major retinal veins within the staphyloma. The best-corrected visual acuity is 0.7 and the axial length is 33.5 mm

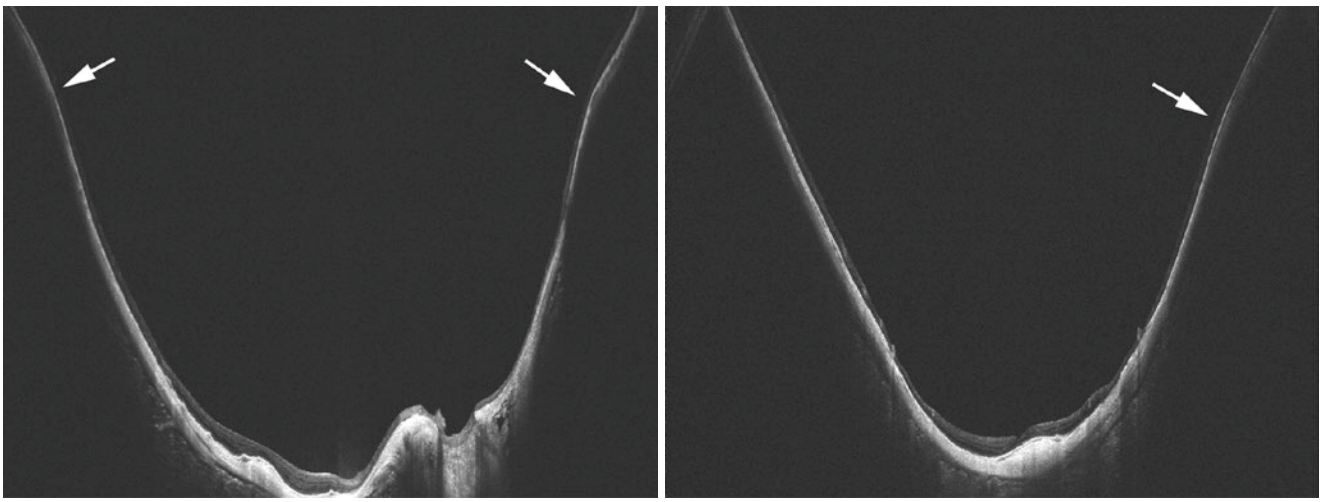

Fig. 26.21 Ultra-widefield OCT images show staphyloma edges (arrows). Scleral ridge temporal to the optic disc is seen in a horizontal section (Left). Dome-shaped macula can be seen both in horizontal (Left) and vertical (Right) sections

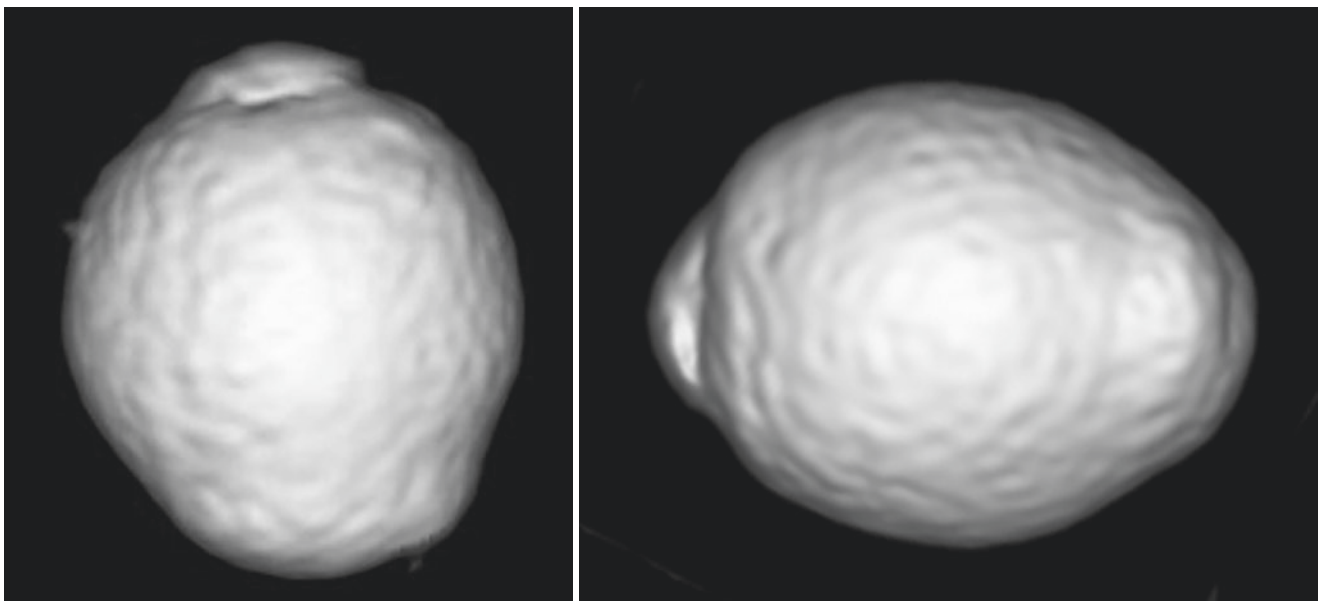

Fig. 26.22 Three-dimensional MRI scan shows a wide area of posterior outpouching due to a staphyloma

Long-Term Progression of Fundus Changes in Adults (2)

27

Reina Saito and Yuxin Fang

Abstract

Three cases with multiple progression patterns of myopic maculopathy in a long-term follow-up are presented.

Keywords

Long-term follow-up · Progression · Myopic maculopathy · Diffuse atrophy · Patchy atrophy · MNV

R. Saito · Y. Fang (✉)
Department of Ophthalmology and Visual Science, Tokyo Medical and Dental University, Tokyo, Japan

K. Ohno-Matsui (ed.), *Atlas of Pathologic Myopia*, https://doi.org/10.1007/978-981-15-4261-9_27

27.1 Case 1-Maintaining Good Vision Despite a Marked Enlargement of Diffuse Atrophy and Development of Myopic MNV (Figs. 27.1, 27.2, 27.3, 27.4, 27.5 and 27.6)

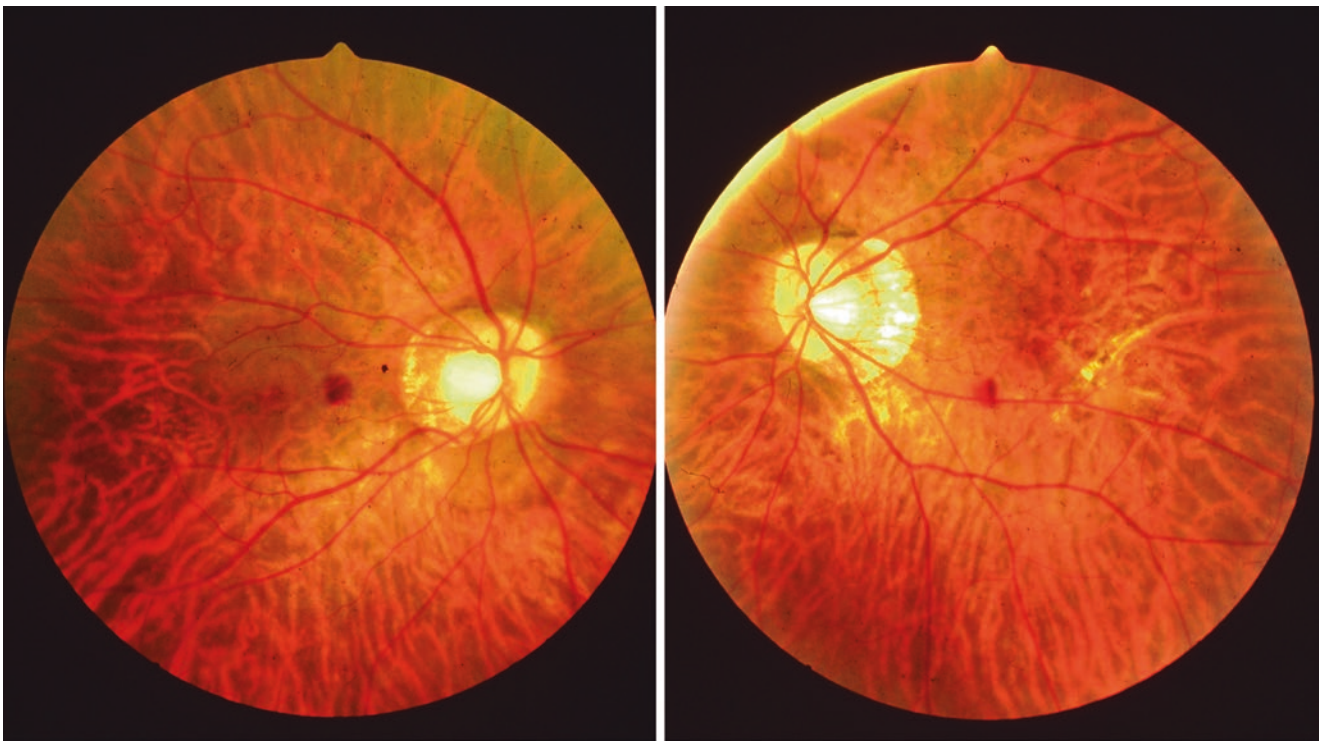

Fig. 27.1 Right and left fundus at the initial visit (1986) of a 31-year-old man show a small area of yellowish diffuse atrophy around the optic disc. The best-corrected acuity is 1.0 in the right eye and 0.7 in the left. Refractive error is -15.0D in the right eye and -17.5D in the left. Axial length is 29.4 mm in the right eye and 29.9 mm in the left

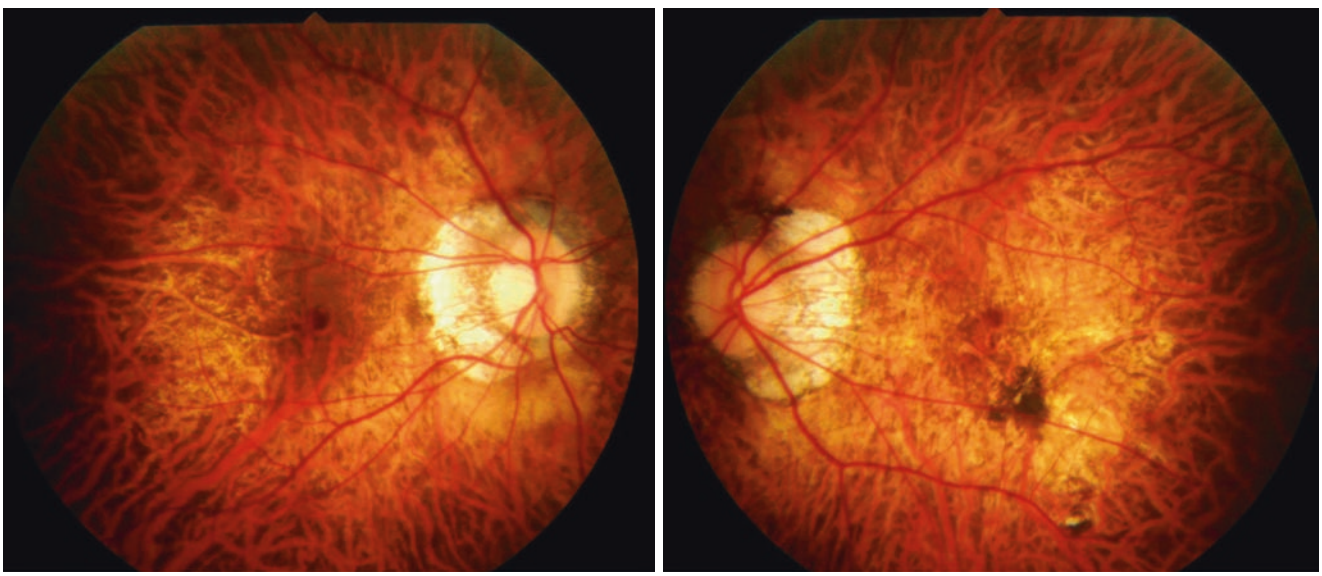

Fig. 27.2 Fifteen years later (September 2001), the area of diffuse atrophy and peripapillary atrophy have enlarged. Peripapillary intrachoroidal cavitation is seen lower to the optic disc in the right eye. Two lesions with pigmentation are seen lower to the macula in the left eye. The best-corrected visual acuity is 1.0 in both eyes. Axial length is 30.1 mm in the right eye and 31.3 mm in the left

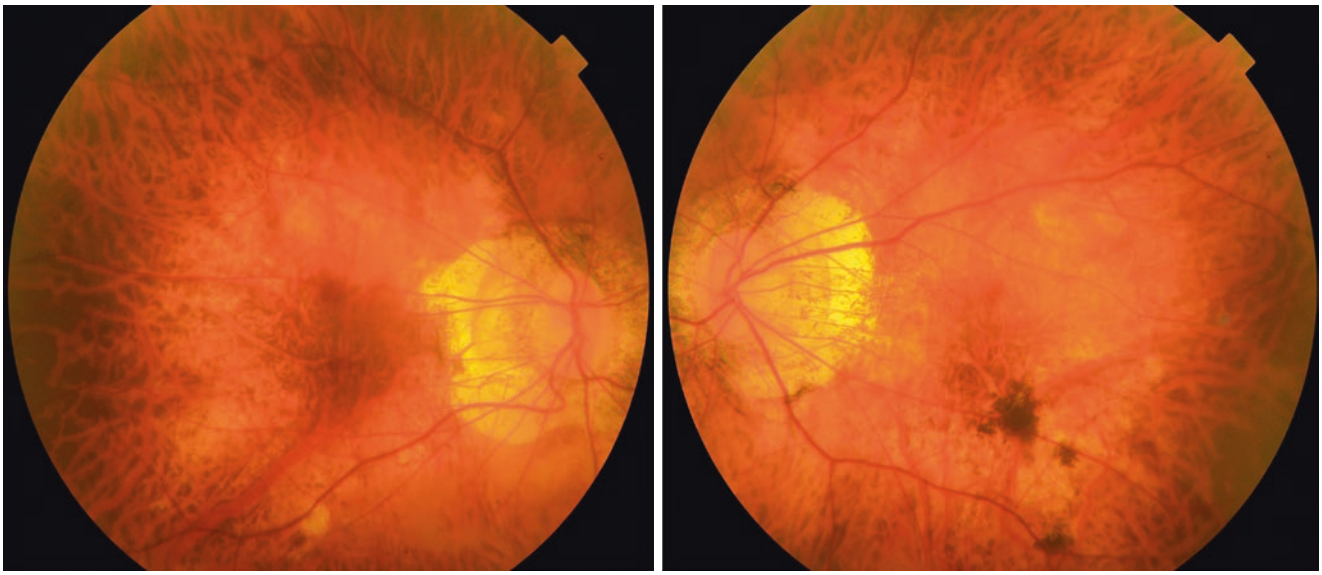

Fig. 27.3 Thirty years later (February 2016), diffuse atrophy has extended to cover the entire posterior pole in both eyes. Right fundus shows mild pigmentation in the macula and a small patchy atrophy has appeared lower to the macula. The peripapillary atrophy has further enlarged and extended around the optic disc in both eyes

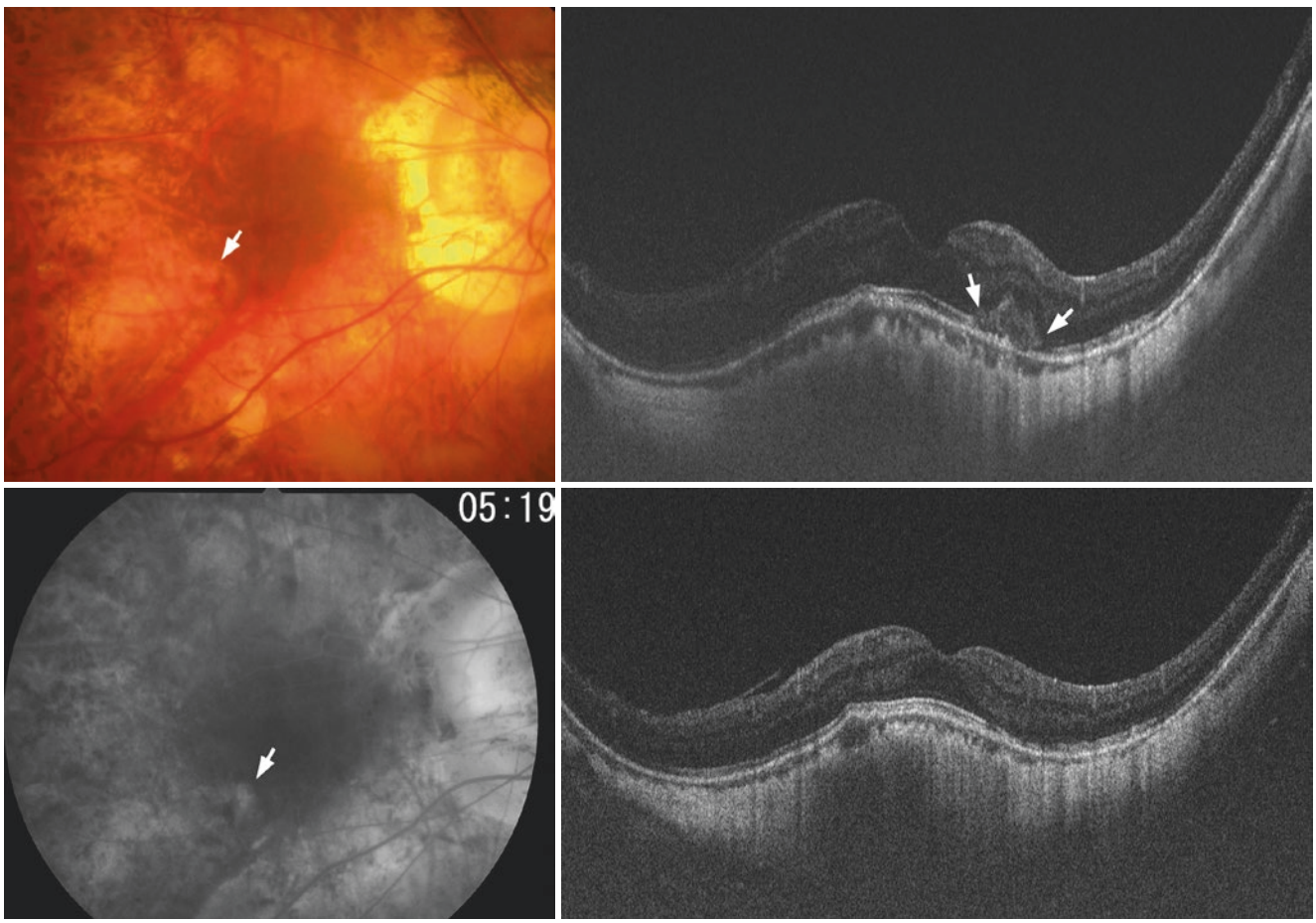

Fig. 27.4 Thirty-one years later (May 2017), he complained the sudden blind spot in his right eye. Oblique OCT scan across the fovea shows subretinal hyper-reflective tissue (arrows), which represents a myopic macular neovascularization (MNV). The MNV shows hyperfluorescence (arrow) in the fluorescein angiogram. After 1 month following intravitreal injection of ranibizumab, OCT shows a complete disappearance of the myopic MNV

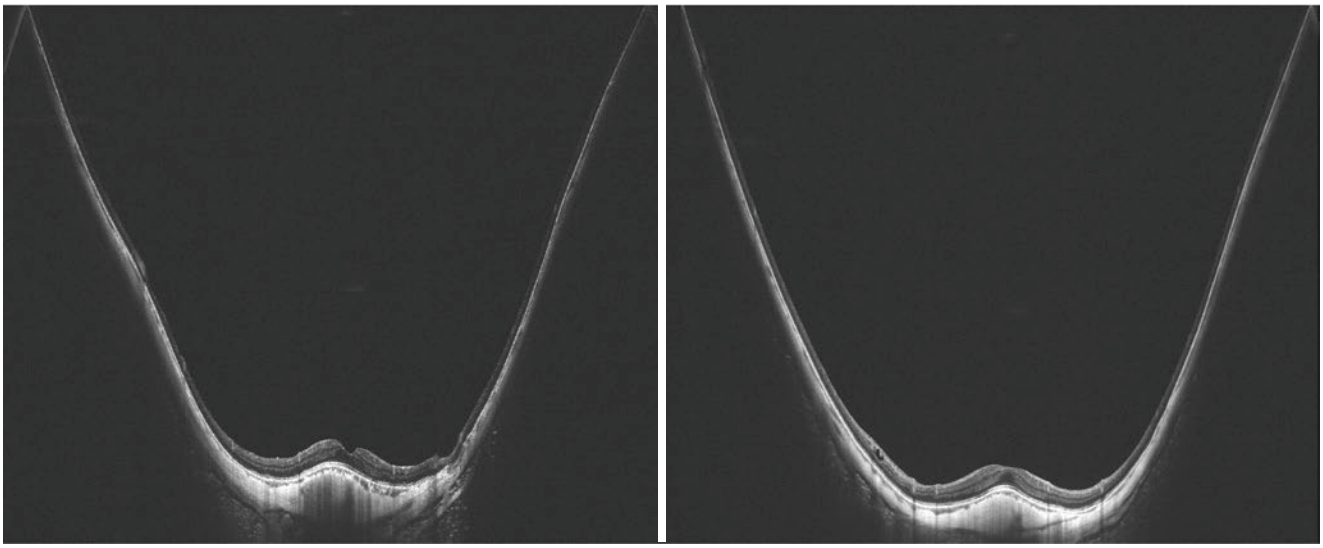

Fig. 27.5 Ultra wide-field OCT images of the right eye (Left) and the left eye (Right) (July 2018) show the dome-shaped macula in vertical scans bilaterally. No evident OCT features suggesting staphyloma edges (e.g., gradual choroidal thinning toward the staphyloma edge as well as scleral inward protrusion) are seen, which means that there is no obvious staphyloma despite the dome-shaped macula in those axially elongated eyes. A defect of the retinal pigment epithelium (RPE) and Bruch's membrane are seen in the area of patchy atrophy in the right eye

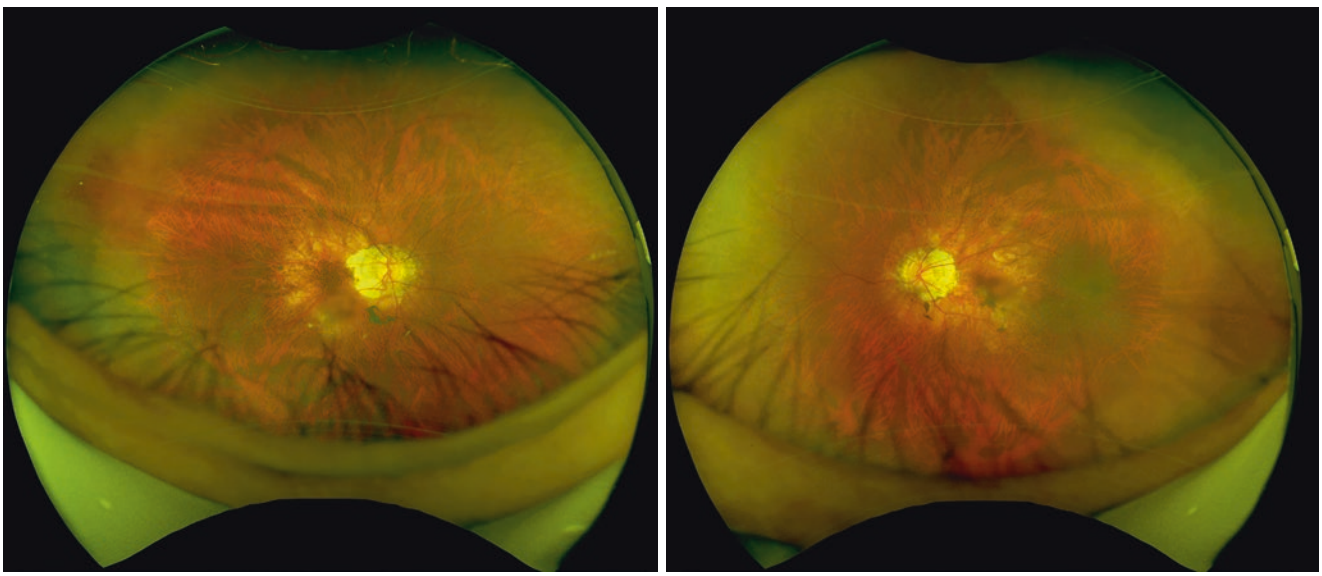

Fig. 27.6 Wide-field fundus images at the last visit (February 2019). The best-corrected visual acuity is 1.0 in both eyes. Axial length is 32.3 mm in the right eye and 32.3 mm in the left

27.2 Case 2-Development of Patchy Atrophy, Followed by MNV Development Along The Foveal Edge of Patchy Atrophy, and Finally a Formation of Large Macular Atrophy by Fusion of MNV-Related Macular Atrophy and Patchy Atrophies

(Figs. 27.7, 27.8, 27.9, 27.10, 27.11, 27.12, 27.13, 27.14, 27.15, 27.16 and 27.17)

Fig. 27.7 Right fundus at the initial visit (August 1996) of a 41-year-old woman shows diffuse choroidal atrophy around the optic disc. An ill-defined pigmented lesion is seen lower temporal to the macula. A temporal peripapillary crescent is also seen. The best-corrected visual acuity is 1.0. Refractive error is -15.8 D and an axial length is 29.5 mm

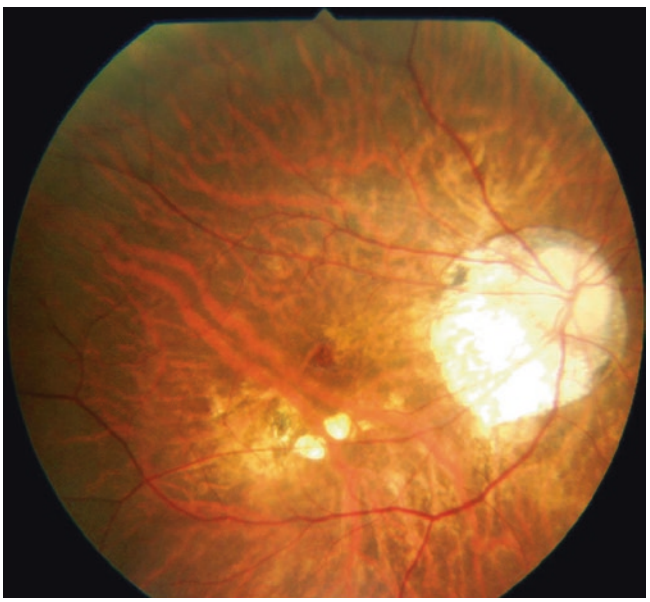

Fig. 27.8 Seven years later (November 2003), two lesions of patchy atrophy have appeared lower to the macula. These two lesions appear separated by a large choroidal vein

Fig. 27.9 Eleven years later (November 2007), myopic macular neovascularization (MNV) has developed along the foveal edge of a fused patchy atrophy (arrow). Fluorescein angiogram shows dye leakage from the MNV (arrow). The best-corrected visual acuity has decreased to 0.6. She received a total of three injections of intravitreal bevacizumab

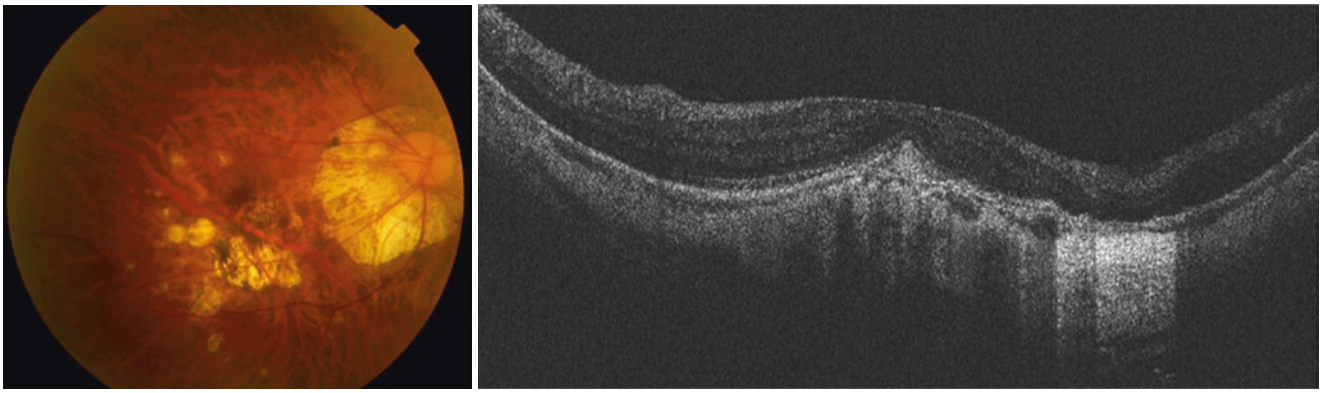

Fig. 27.10 Seventeen years later (October 2013), the right fundus shows a pigmentation of scarred MNV, an enlargement of original patchy atrophy and a development of multiple new lesions of patchy atrophy. Vertical OCT shows the well-defined subfoveal hyperreflectivity compatible with a scarred MNV. In the area of patchy atrophy, an increased penetration of the light into deep tissues is seen due to the RPE defect. Dome-shaped macula is also seen. The best-corrected visual acuity is 0.2

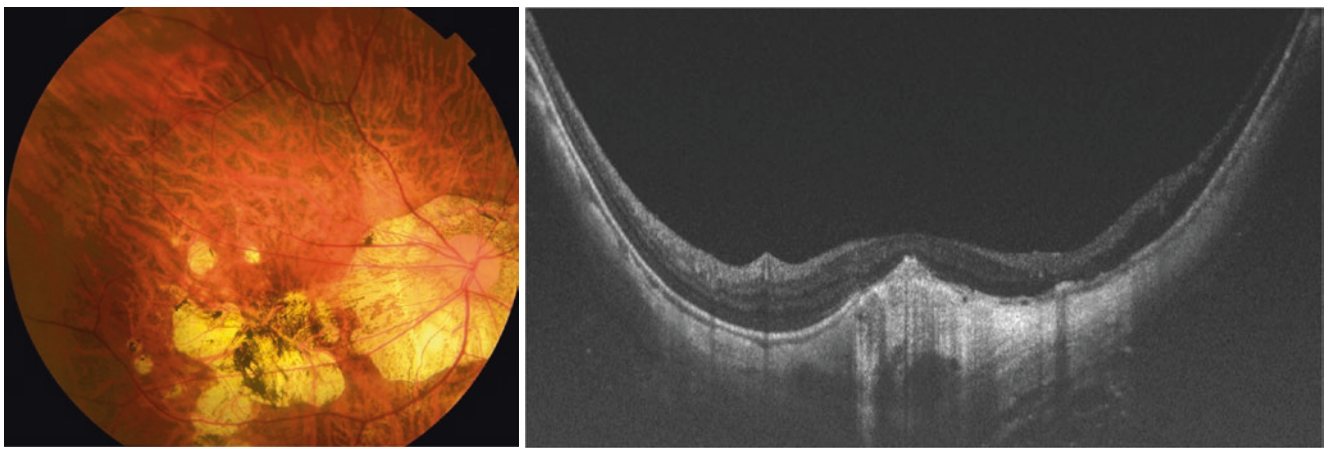

Fig. 27.11 Twenty-three years later (July 2019), the right fundus shows a large macular atrophy which is formed by an enlargement and fusion of MNV-related macula atrophy and patchy atrophy. OCT shows a large area of RPE defect. However, the best-corrected visual acuity is still 0.6. The axial length is 32.1 mm

Fig. 27.12 Left fundus at the first visit (August 1996) shows diffuse atrophy around the optic disc and a temporal peripapillary crescent. The best-corrected acuity is 1.0. The refractive error is -17.3 D and the axial length is 29.8 mm

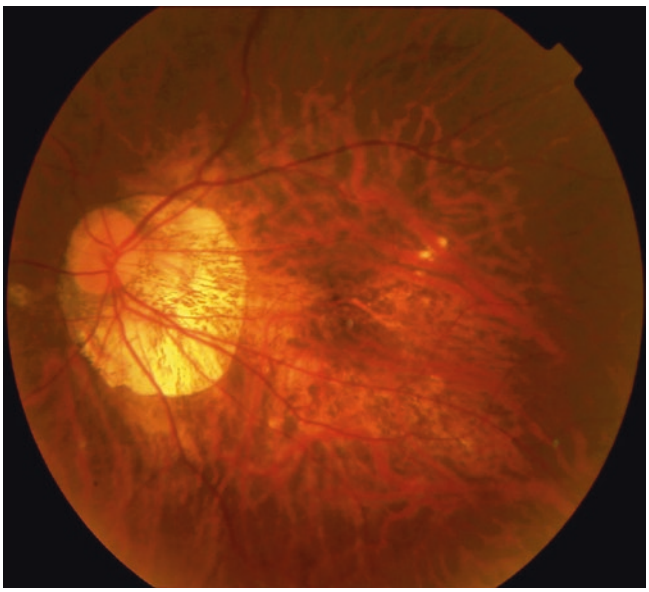

Fig. 27.13 Eleven years later (December 2007), two small lesions of patchy atrophy have appeared upper temporal to the macula. These two lesions appear separated by a large choroidal vein

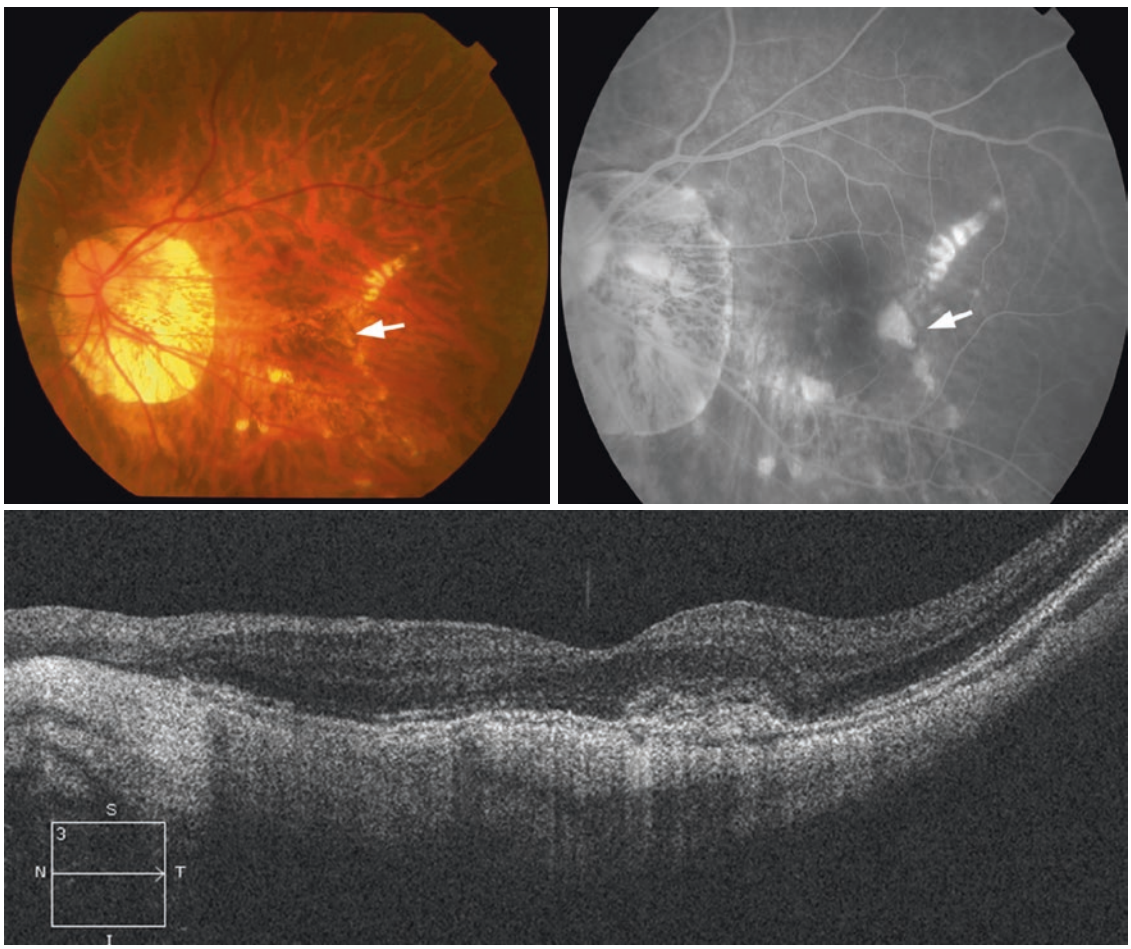

Fig. 27.14 Twelve years later (July 2008), the left fundus shows myopic MNV temporal to the fovea (arrow). Multiple lacquer cracks accompanying with a development and enlargement of patchy atrophy along the course of lacquer cracks are seen in the macula area. Fluorescein angiogram shows dye leakage from the MNV (arrow). OCT shows a subretinal hyper-reflective lesion with slight serous retinal detachment. The visual acuity has decreased to 0.5. This eye was treated with intravitreal injections of bevacizumab

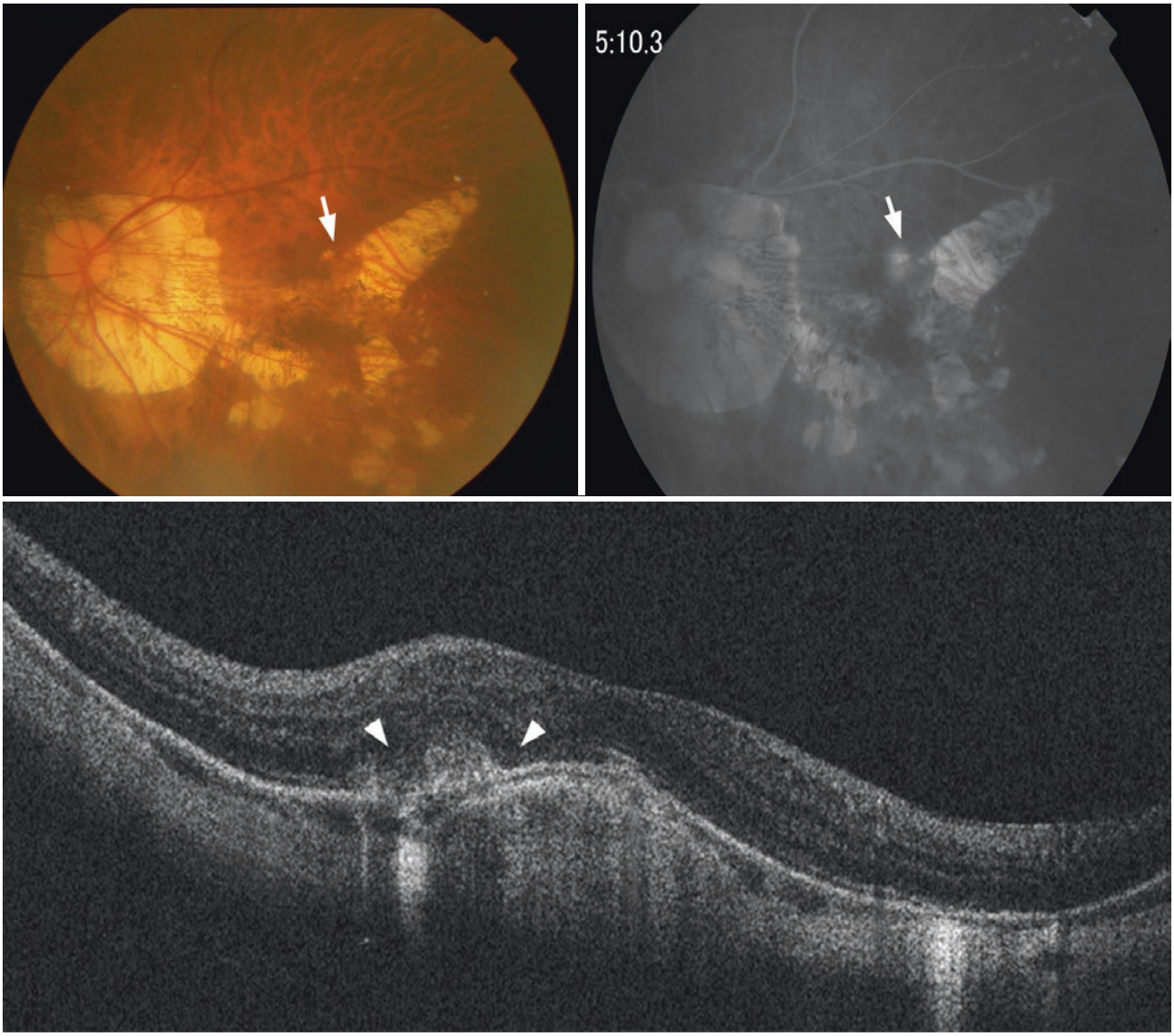

Fig. 27.15 Eighteen years later (February 2014), the patient complained of a new metamorphopsia. A new myopic MNV is observed (arrow). An enlargement of patchy atrophy is seen. This eye was treated with intravitreal injections of ranibizumab

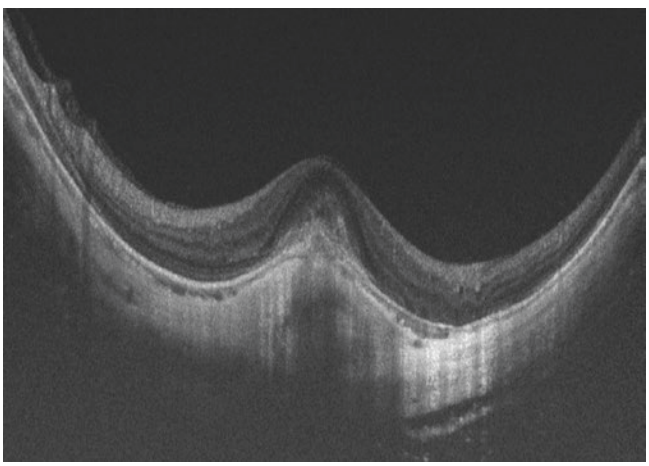

Fig. 27.16 Twenty years later (September 2016), the patient complained of a decreased vision. The visual acuity has decreased to 0.3. OCT shows that a myopic MNV has appeared in the fovea

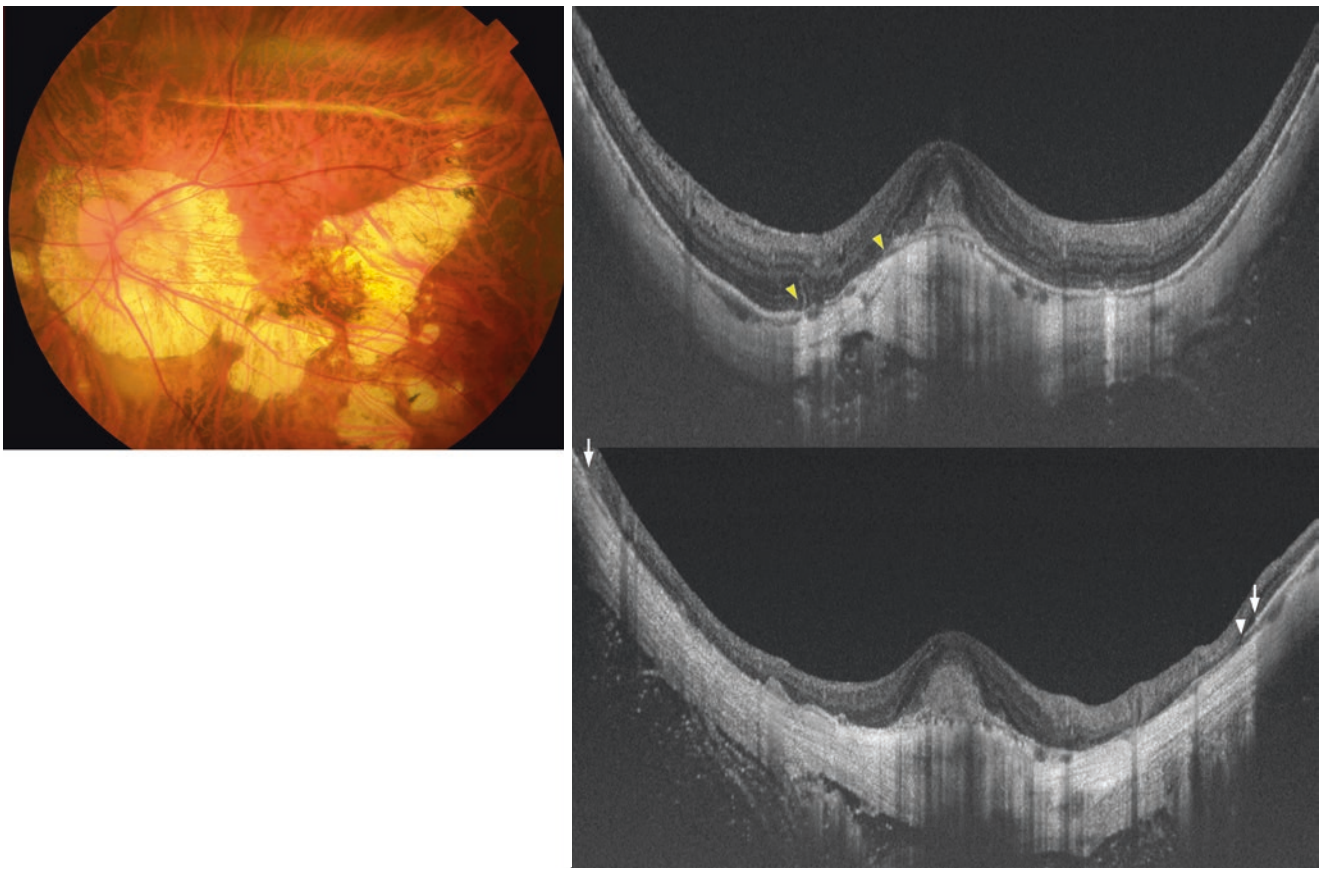

Fig. 27.17 Left fundus at 23 years after the initial visit shows a further enlargement of patchy atrophies and a fusion with MNV-related macular atrophy. (Top Right) Vertical OCT section shows the subfoveal hyperreflectivity and MNV-related macular atrophy (arrowheads). (Bottom) Oblique OCT scan shows a large area of RPE defect and Bruch's membrane defect corresponding to two areas of patchy atrophy. The ends of the RPE and Bruch's membrane are indicated by arrows and an arrowhead, respectively. The best-corrected visual acuity is 0.5. The axial length is 32.4 mm

27.3 Case 3-Enlargement of Diffuse Choroidal Atrophy and a Development of Patchy Atrophy Within an Area of Diffuse Atrophy

(Figs. 27.18, 27.19, 27.20, 27.21, 27.22, 27.23, 27.24, 27.25, 27.26, 27.27 and 27.28)

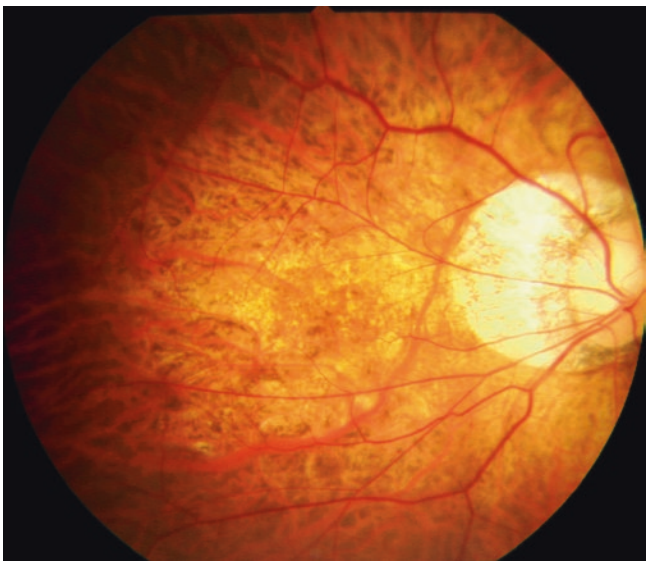

Fig. 27.18 Right fundus at the initial visit (May 2004) of a 53-year-old man shows diffuse choroidal atrophy covering the entire posterior fundus. A temporal peripapillary atrophy is also seen. The best-corrected acuity is 1.0. The axial length is 29.0 mm and the refractive error is -13.4 D

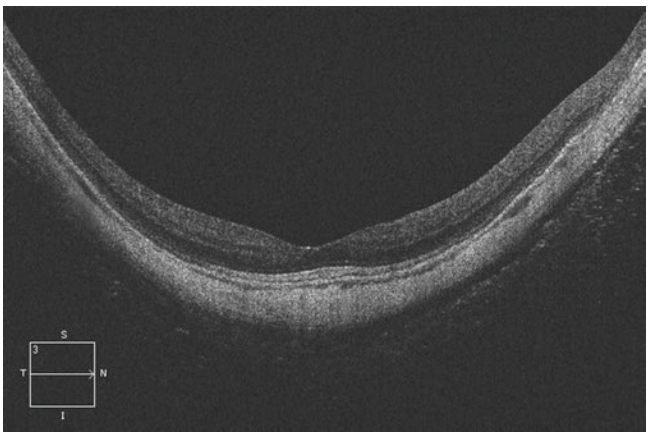

Fig. 27.20 Four years later (October 2008), horizontal OCT image shows an extreme thinning of the choroid. Subfoveal choroidal thickness is 28 μm

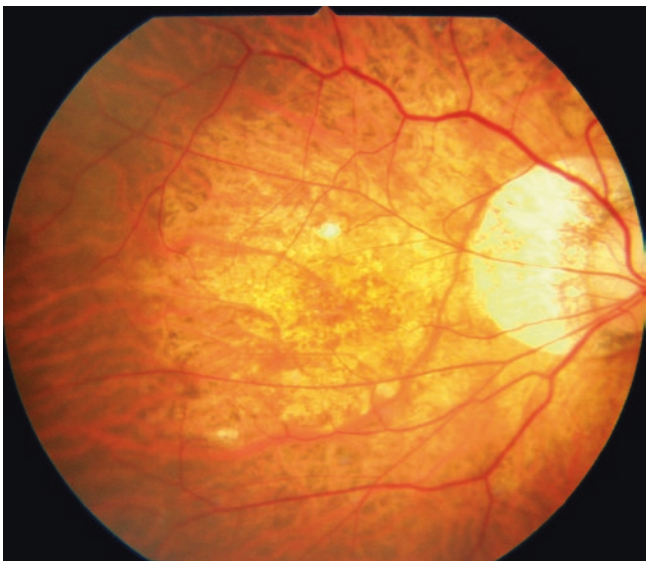

Fig. 27.19 One year later (June 2005), two small lesions of patchy atrophy have appeared upper and lower to the macula

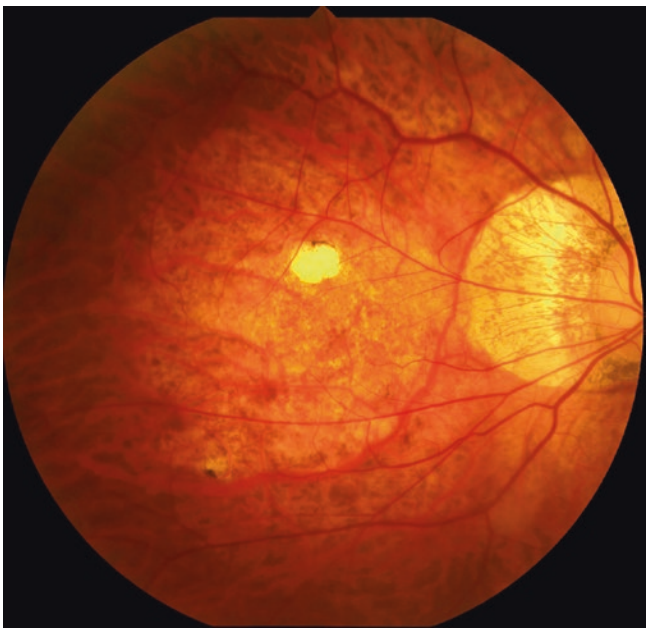

Fig. 27.21 Six years later (October 2010), the upper lesion of patchy atrophy has enlarged. Peripapillary atrophy has also enlarged

Fig. 27.22 Twelve years later (December 2016), the upper lesion of patchy atrophy has further enlarged. New lesions of patchy atrophy have appeared in the lower fundus. Swept-source OCT image across the two lesions of patchy atrophy shows a defect of RPE and Bruch's membrane. The subfoveal choroidal thickness is still 28 μm

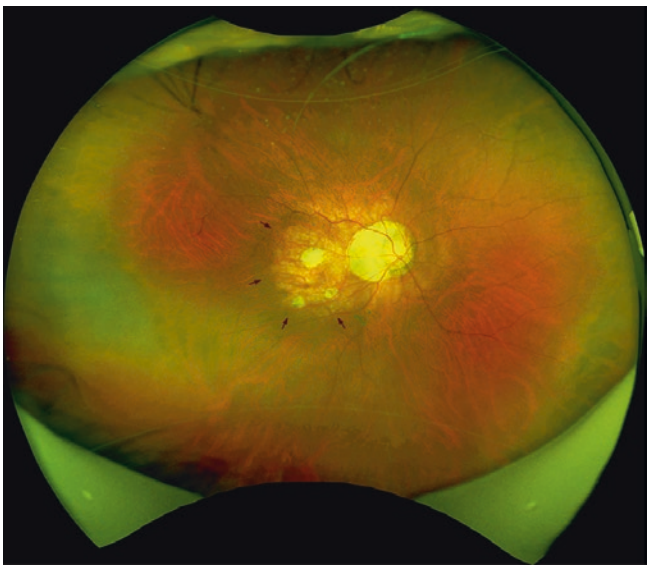

Fig. 27.23 Wide-field fundus image at 15 years after the first visit (January 2019) shows slightly pigmented temporal border of posterior staphyloma (arrows). Diffuse atrophy is seen only within the staphyloma. The axial length is 31.5 mm and the refractive error is -13.3 D. The best-corrected acuity is 1.0

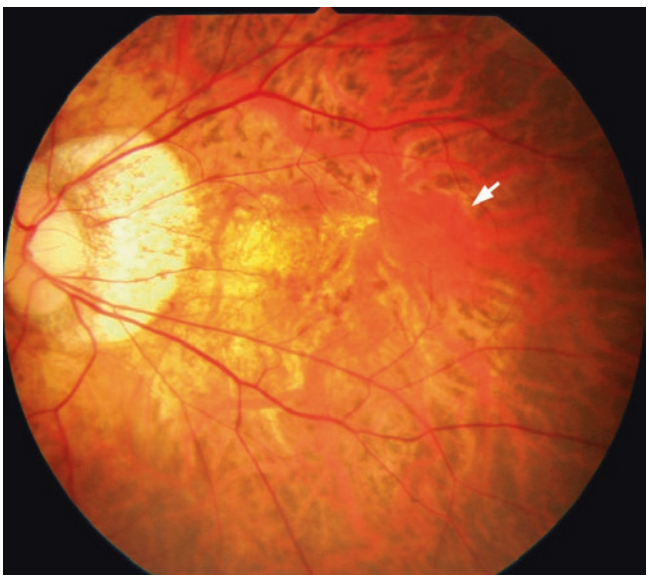

Fig. 27.24 Left fundus at the first visit (June 2005) shows macular diffuse choroidal atrophy and a temporal peripapillary atrophy. Please note a large macular vortex vein with ampulla (arrow). The best-corrected visual acuity is 1.2. Axial length is 29.2 mm and the refractive error is -12.3 D

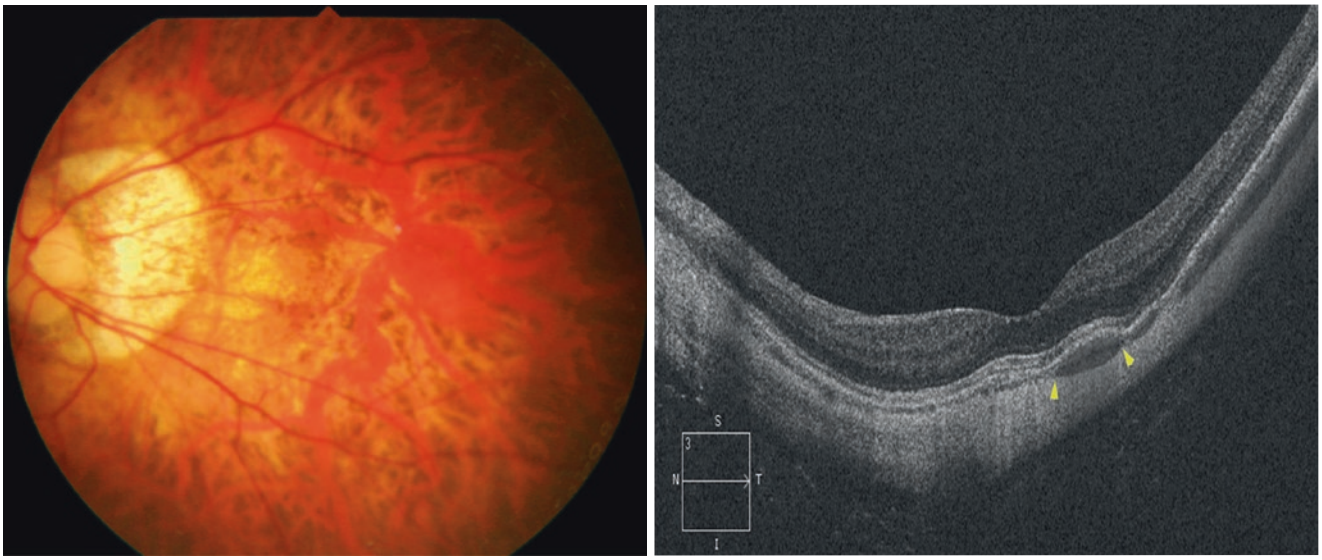

Fig. 27.25 Three years later (October 2008), there is no obvious change in the left fundus. Horizontal OCT image shows the extreme thinning of choroid. Subfoveal choroidal thickness is 24 μm. Branches of macular vortex vein (between arrowheads) are seen

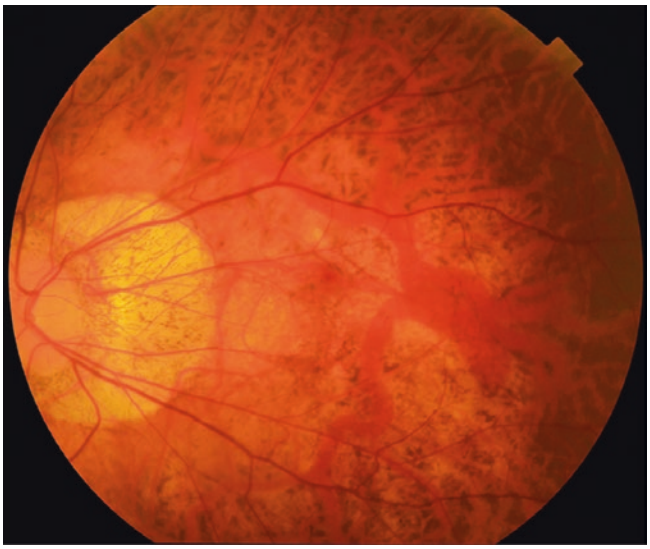

Fig. 27.26 Twelve years later (December 2017), the area of diffuse atrophy and peripapillary atrophy have further enlarged. A close observation of the fundus photo shows that some branches of macular vortex vein have disappeared especially in the area nasal to the fovea

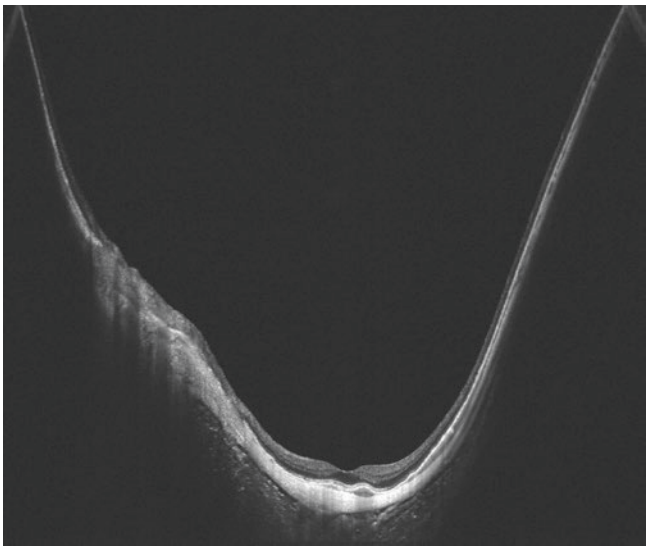

Fig. 27.27 Wide-field OCT image shows branches of macular vortex vein. In the area outside macular vortex vein, the choroid is extremely thin. Subfoveal choroidal thickness is 23 μm

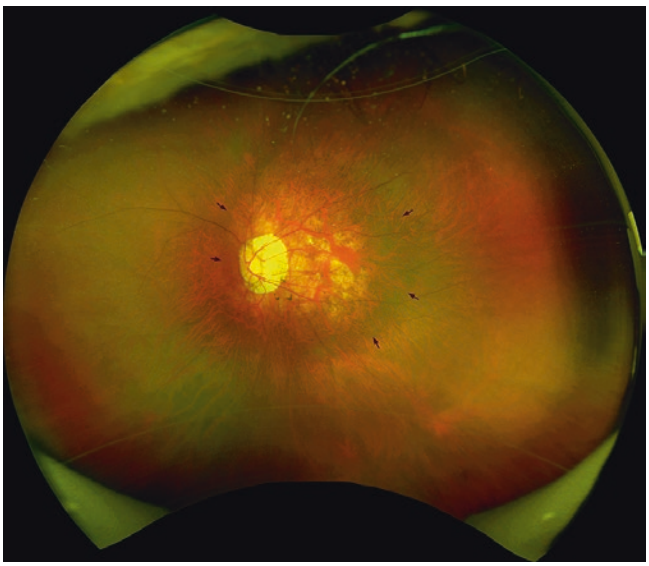

Fig. 27.28 Fifteen years later (January 2019), a wide-field fundus image shows the depigmented and pigmented changes at the edge of staphyloma (arrows). Diffuse atrophy is restricted within the staphylomatous area. The axial length is 31.1 mm and the refractive error is -12.3 D. The best-corrected visual acuity is 1.2

Long-Term Progression of Fundus Changes in Adults (3)

28

Takeshi Azuma and Yuxin Fang

Abstract

Three cases with a long-term follow-up of myopic macular neovascularization (MNV) and MNV-related macular atrophy are shown. The progression of other lesions of myopic maculopathy is also demonstrated.

Keywords

Long-term follow-up · Myopic maculopathy · MNV · MNV-related macular atrophy

T. Azuma · Y. Fang (✉)
Department of Ophthalmology and Visual Science, Tokyo Medical and Dental University, Tokyo, Japan

K. Ohno-Matsui (ed.), *Atlas of Pathologic Myopia*, https://doi.org/10.1007/978-981-15-4261-9_28

28.1 Case 1-Development and Enlargement of MNV-Related Macular Atrophy Accompanying with a Development of Multiple Lesions of Patchy Atrophy (Figs. 28.1, 28.2, 28.3, 28.4, 28.5, 28.6, 28.7, 28.8, 28.9, 28.10 and 28.11)

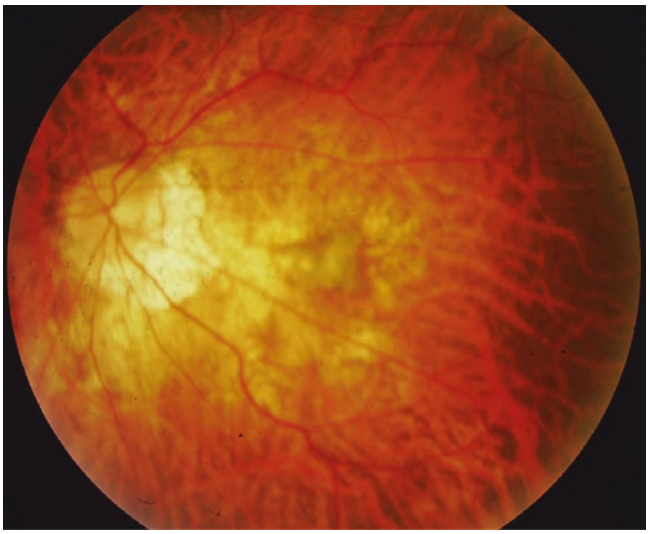

Fig. 28.1 Left fundus at the first visit (August 1988) of a 53-year-old woman shows grayish myopic MNV accompanying with bleeding in the background of diffuse choroidal atrophy. The best-corrected visual acuity (BCVA) is 0.1. The refractive error is -20.0D and the axial length is 29.9 mm. Because there was no treatment available at that time, she was followed without PDT or anti-VEGF therapies

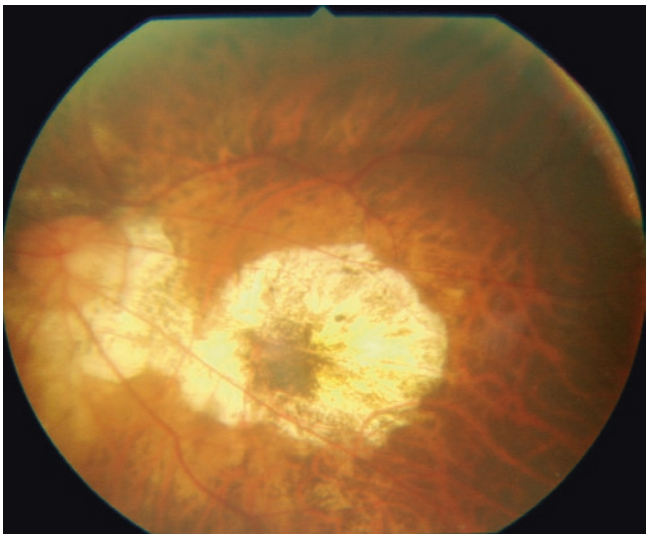

Fig. 28.2 Fifteen years later (October 2003), left fundus shows a large, well-defined MNV-related macular atrophy with pigmented MNV in its center. The BCVA is 0.02

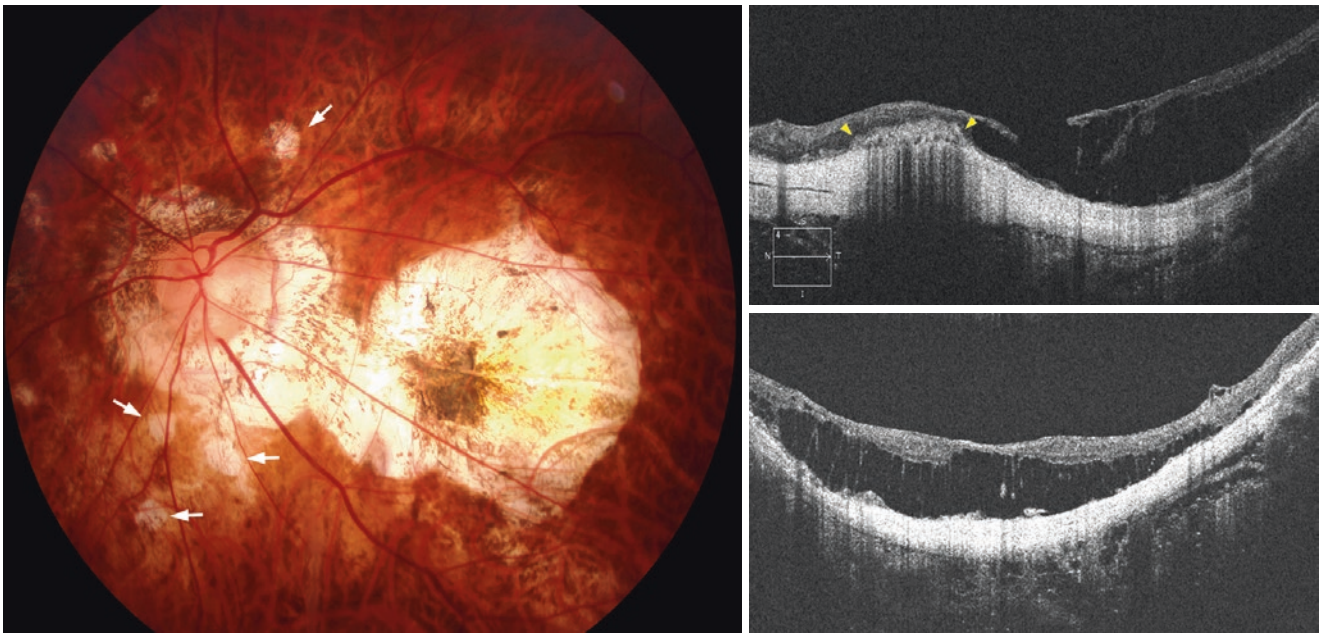

Fig. 28.3 Twenty-two years later (May 2010), MNV-related macular atrophy has further enlarged especially in its lower part and has fused with peripapillary atrophy in the nasal part. Several new patchy atrophies have appeared (arrows) around the optic disc. Horizontal OCT scan (Top Right) shows subretinal scarred MNV (arrowheads). Outer retinoschisis is observed both in horizontal (Top Right) and vertical (Bottom Right) OCT scans. Inner lamellar macular hole is also noted in horizontal scan. Axial length is 31.1 mm

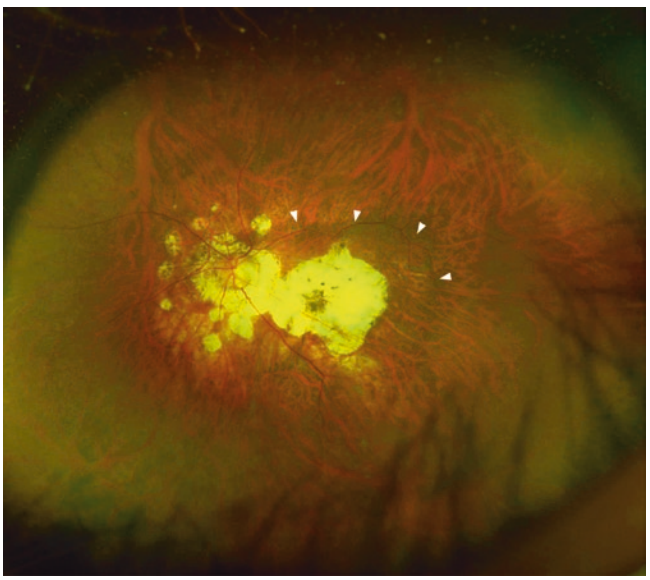

Fig. 28.4 Twenty-nine years later (March 2017), a wide-field fundus image shows a very large atrophy which is formed by a fusion of MNV-related macular atrophy and peripapillary atrophy. Multiple lesions of patchy atrophy around the optic disc have further enlarged. The upper edge of wide macular staphyloma shows slight pigmentation (arrowheads). The BCVA is 0.01

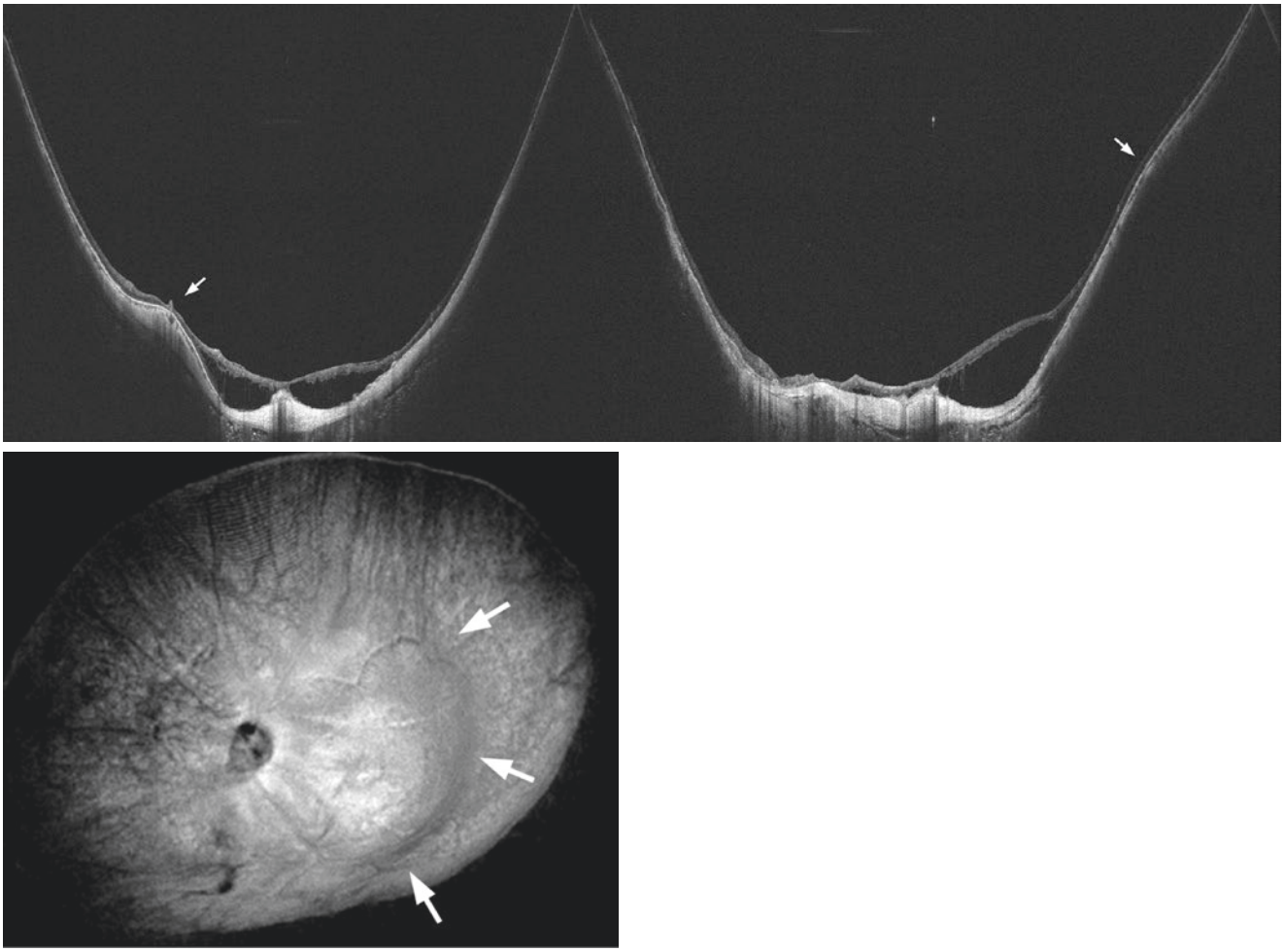

Fig. 28.5 Ultra wide-field OCT images at 29 years after the initial visit (September 2017) show a wide macular staphyloma. The upper edge of the staphyloma (arrow) is seen as scleral inward protrusion in a vertical OCT scan (Left) and the temporal edge of the staphyloma (arrow) is seen in a horizontal scan (Right). Three-dimensional reconstructed image shows an en face view of wide staphyloma (Bottom). The staphyloma edges are indicated by arrows. The extent of outer retinoschisis is localized within the staphylomatous area. The fovea is spared because of the dome-shaped macula and partly because of MNV. An outer retinoschisis surrounds a dome-shaped macula. The BCVA is 0.01

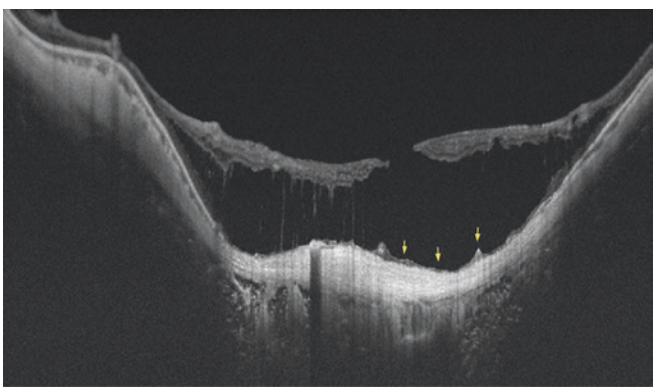

Fig. 28.6 Swept-source OCT image at 30 years after the first visit (September 2018). Although this image looks like retinal detachment associated with full thickness macular hole, it should be diagnosed as severe outer retinoschisis with inner lamellar macular hole. The outer retinal tissue still remains on the retinal pigment epithelium (RPE) (arrows). The axial length is 31.3 mm. The BCVA is 0.02

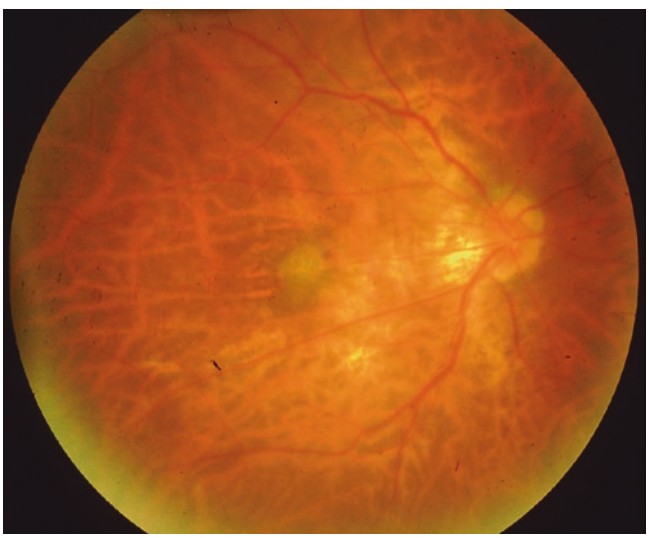

Fig. 28.7 Right fundus at the first visit (July 1989) shows grayish myopic MNV in the background of tessellated fundus. The best-corrected visual acuity (BCVA) is 0.6. The refractive error is -17.0 D and the axial length is 28.5 mm

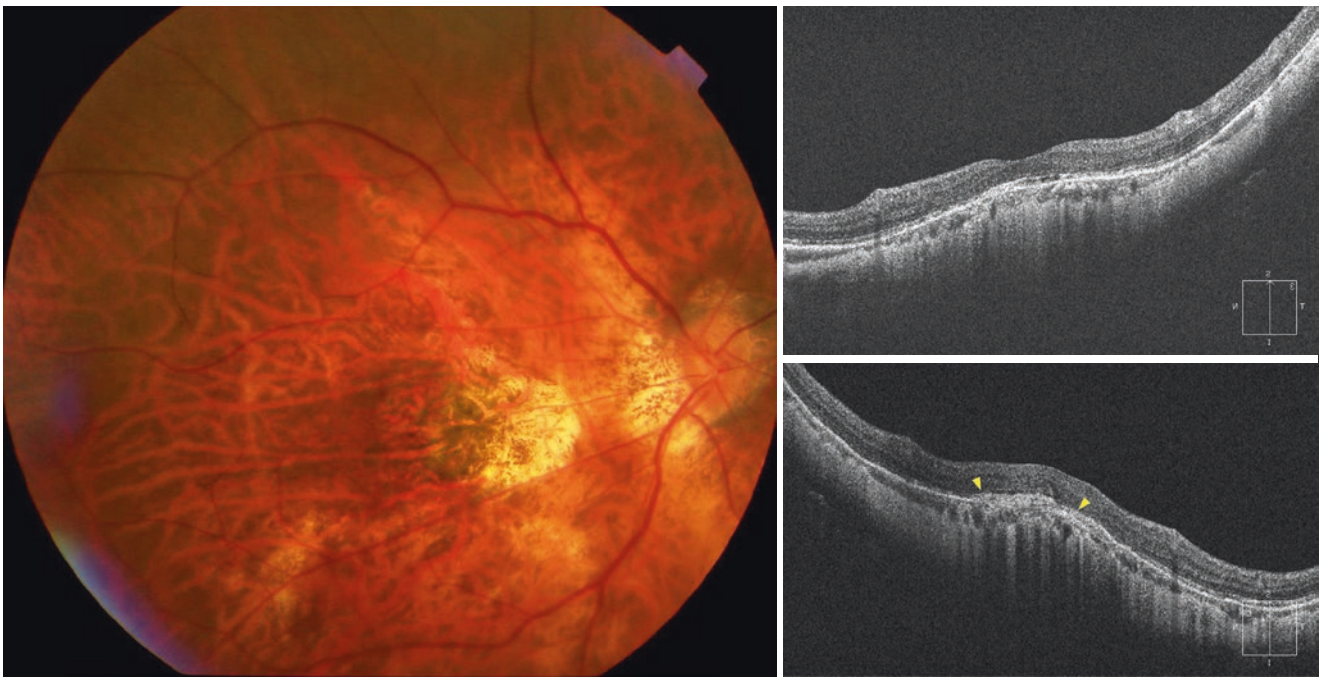

Fig. 28.8 Twenty-one years later (May 2010), MNV-related macular atrophy is formed especially nasal to the scarred MNV. OCT shows a hyperreflective tissue above the RPE suggestive of regressed myopic MNV (arrowheads). The axial length is 29.3 mm and the BCVA is 0.2

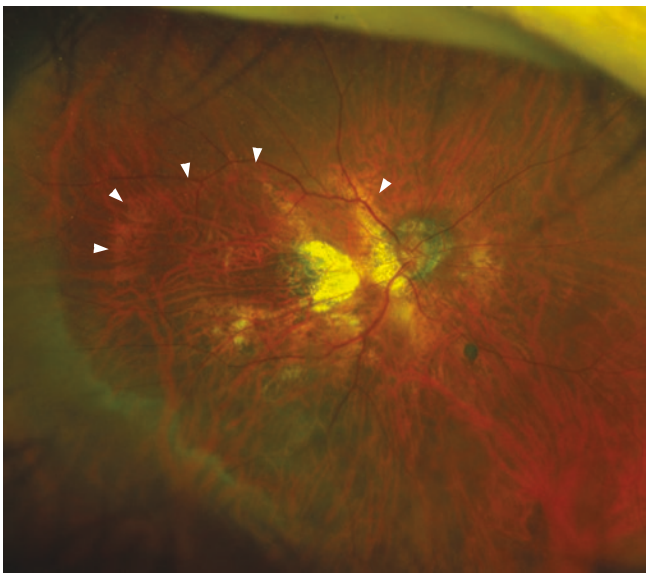

Fig. 28.9 Twenty-nine years later (March 2017), a wide-field fundus image shows that the MNV-related macular atrophy has further enlarged. The edges of the staphyloma are also observed (arrowheads)

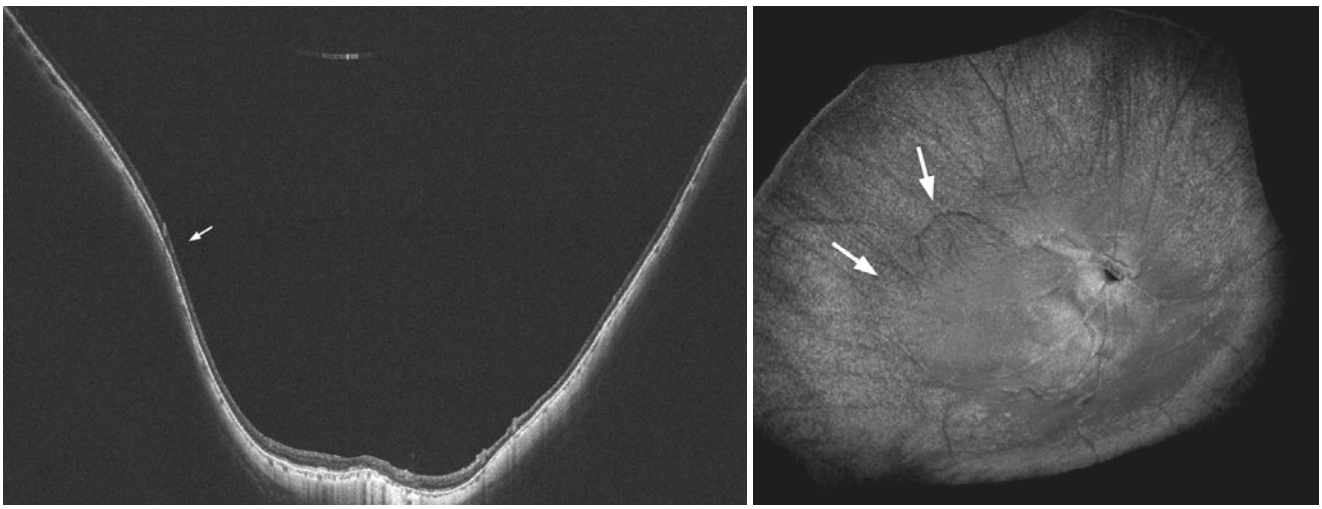

Fig. 28.10 Ultra wide-field OCT image at 29 years after the first visit (September 2017) shows a wide macular staphyloma. Scleral curvature alteration is seen at the site pointed by an arrow in a vertical OCT scan across the fovea (Left). Three-dimensional reconstructed OCT image (Right) viewed from the front shows a margin of wide macular staphyloma (arrows)

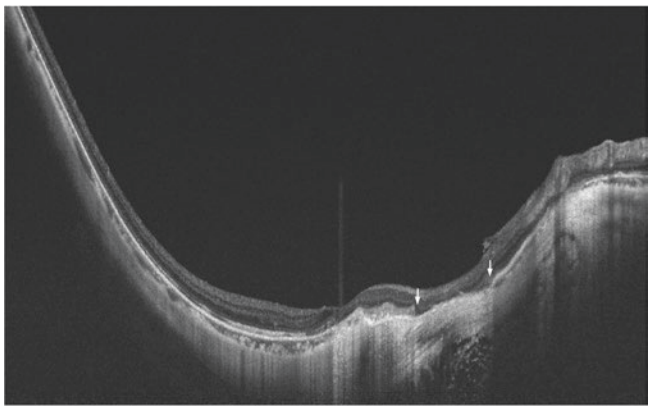

Fig. 28.11 Horizontal swept-source OCT image at 30 years after first visit. In the area of nasal parafoveal macular atrophy (arrows), the outer retina, RPE, Bruch's membrane and choroid are completely absent. The axial length is 29.4 mm and the BCVA is 0.2

28.2 Case 2-Development and Recurrence of Myopic MNV and Progression to MNV-Related Macular Atrophy (Figs. 28.12, 28.13, 28.14, 28.15, 28.16, 28.17, 28.18, 28.19 and 28.20)

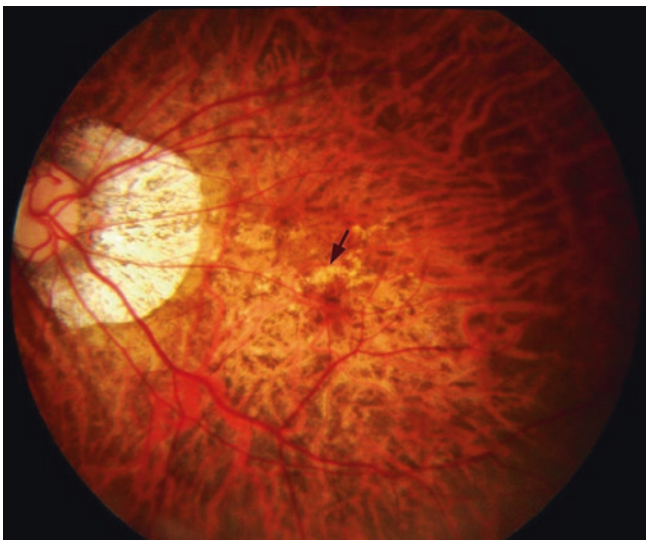

Fig. 28.12 Left fundus of a 42-year-old woman at the initial visit (November 2005) shows diffuse choroidal atrophy and multiple lacquer cracks. The lacquer crack near the fovea seems slightly wide (arrow). The best-corrected visual acuity is 1.2. The refractive error is -15.5 D and the axial length is 29.1 mm

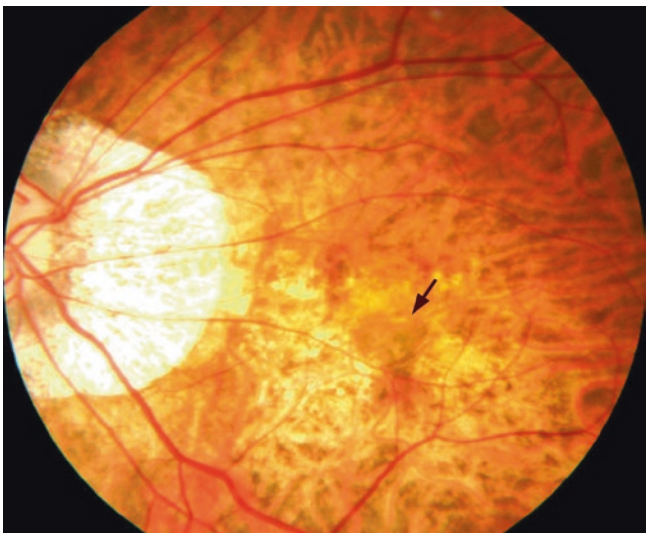

Fig. 28.14 One year later (August 2006), grayish myopic MNV (arrow) has developed lower to the fovea. The BCVA is still 1.2

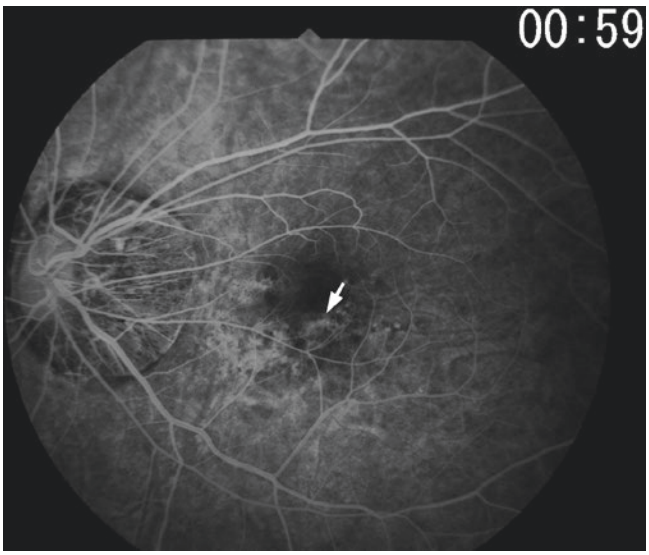

Fig. 28.13 Early phase fluorescein angiogram at the initial visit shows linear hyperfluorescence corresponding to the lacquer crack (arrow). There is no dye leakage in the late phase. The possibility that this slightly wide lacquer crack is linearly-shrunken MNV is not completely denied

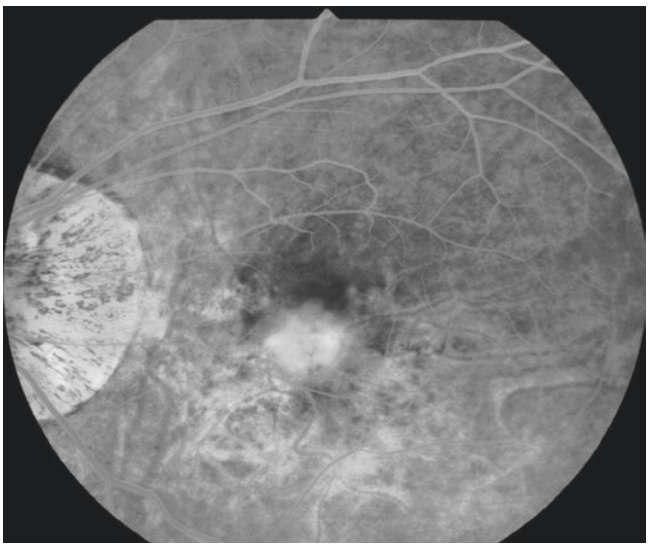

Fig. 28.15 Late phase fluorescein angiogram shows hyperfluorescent lesion corresponding to the MNV accompanied by active leakage with less distinct margins. She was treated with sub-tenon triamcinolone acetonide

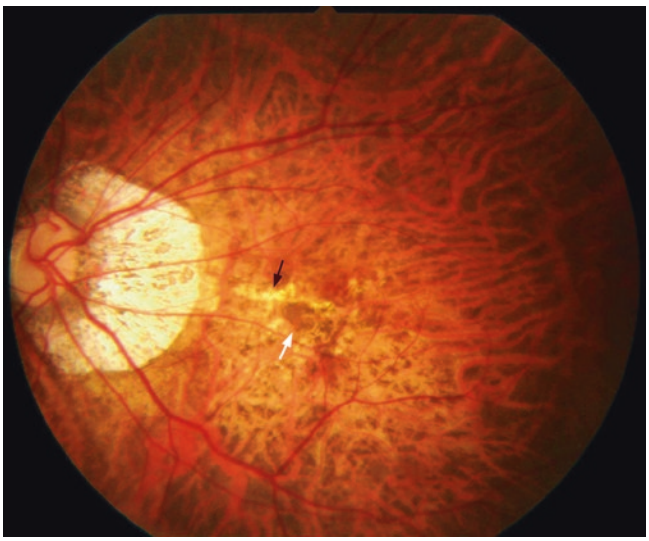

Fig. 28.16 Two years later (April 2007), the MNV has become a pigmented scar (white arrow). The lacquer crack upper to the MNV has become clearer and slightly widened (black arrow)

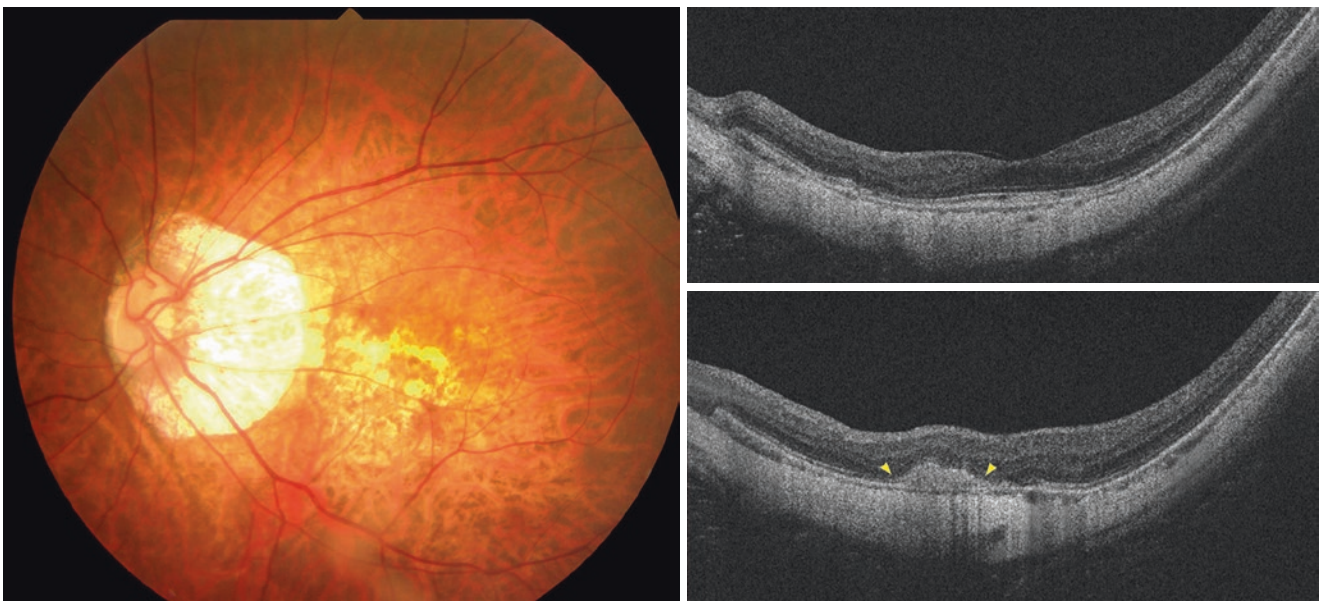

Fig. 28.17 Three years later (October 2008), the left fundus shows the choroidal atrophy around the regressed MNV (MNV-related macular atrophy). Horizontal OCT scan shows that the central fovea is not involved (Top Right). Another horizontal OCT scan across the lesion (Bottom Right) shows a hyper-reflective area above the RPE suggestive of regressed myopic MNV (arrowheads) lower to the fovea. There is no subretinal or intraretinal fluid. The BCVA is still 1.5. The axial length is 30.9 mm

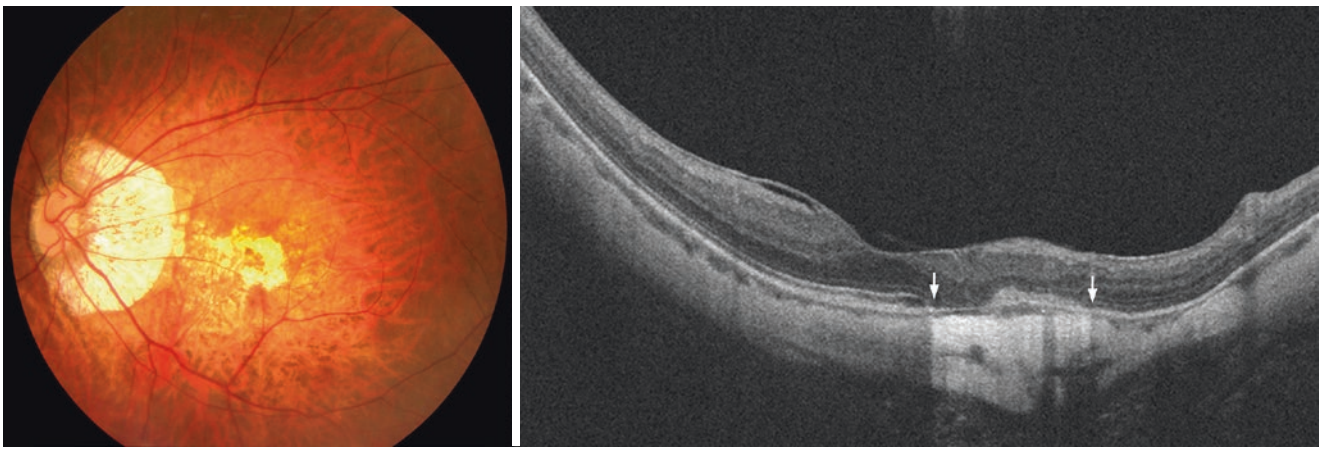

Fig. 28.18 Five years later (December 2010), MNV-related macular atrophy has enlarged. Vertical OCT section across the fovea shows scarred MNV lower to the fovea and an increased light penetration through the RPE defect (between arrows) in the area of MNV-related macular atrophy

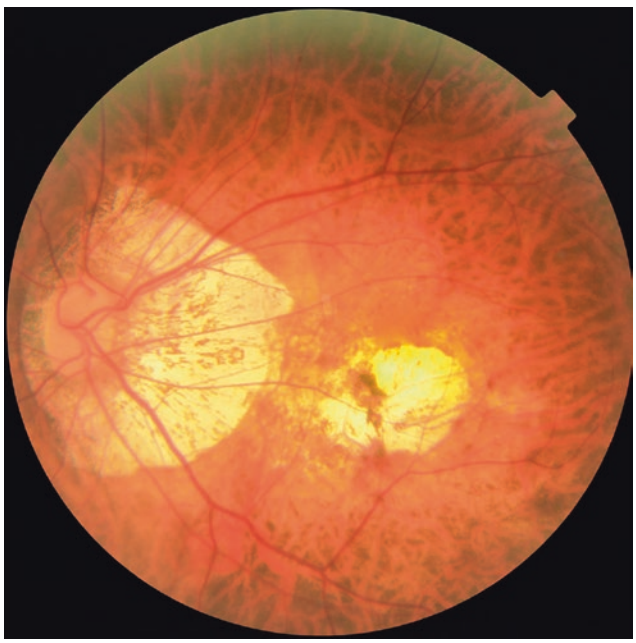

Fig. 28.19 Fourteen years later (March 2019), a well-defined macular atrophy has further enlarged. Although Goldmann perimetry demonstrates superior central absolute scotoma, the BCVA is still 1.5. Axial length is 31.4 mm

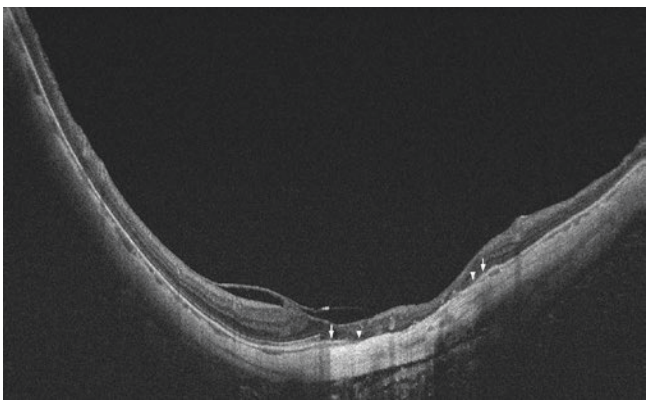

Fig. 28.20 A vertical section of swept-source OCT taken at the same time as (March 2019) shows the end of the RPE (arrows) in the area of MNV-related macular atrophy. The ends of Bruch's membrane (arrowheads) are located inside the area without RPE. In the area of Bruch's membrane defect, the inner retina directly sits on the sclera because almost the entire choroid and outer retina are absent

28.3 Case 3-Development and Enlargement of MNV-Related Macular Atrophy and Fusion with Multiple Lesions of Patchy Atrophy Accompanied with Progression of Myopic Traction Maculopathy (Figs. 28.21, 28.22, 28.23, 28.24, 28.25, 28.26 and 28.27)

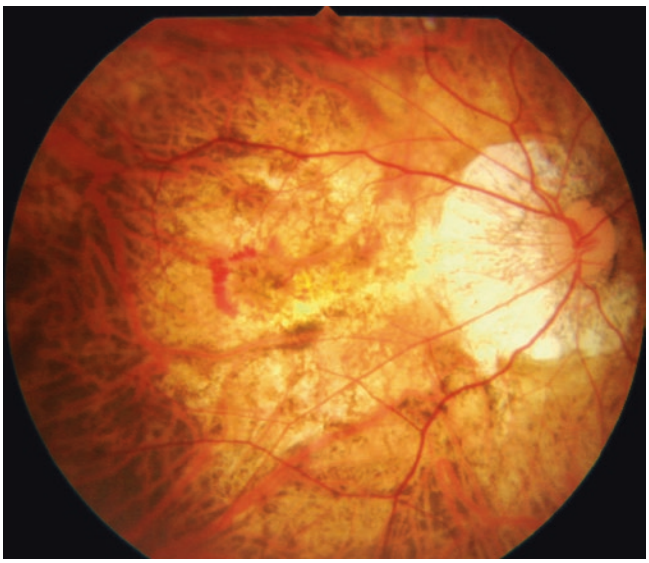

Fig. 28.21 Right fundus of a 65-year-old woman (June 2007) shows grayish MNV surrounded by subretinal bleeding in the macula. The best-corrected visual acuity (BCVA) is 0.1. The refractive error is -5.3 D (pseudophakic) and the axial length is 31.1 mm

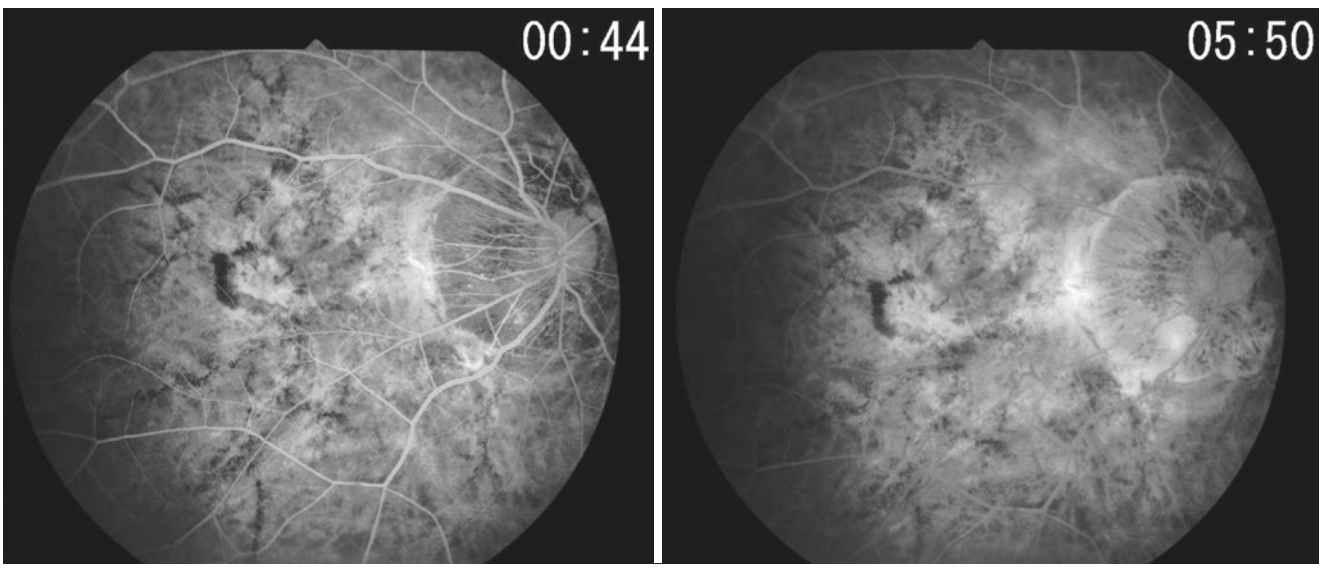

Fig. 28.22 Fluorescein angiogram in the early phase (Left) shows a well-demarcated hyperfluorescent lesion surrounded by a ring of blocked hypofluorescence. In the late phase (Right), a mild dye leakage from the MNV is seen. Multiple linear hypofluorescent lesions are seen in the background diffuse atrophy are considered to be myopic stretch lines

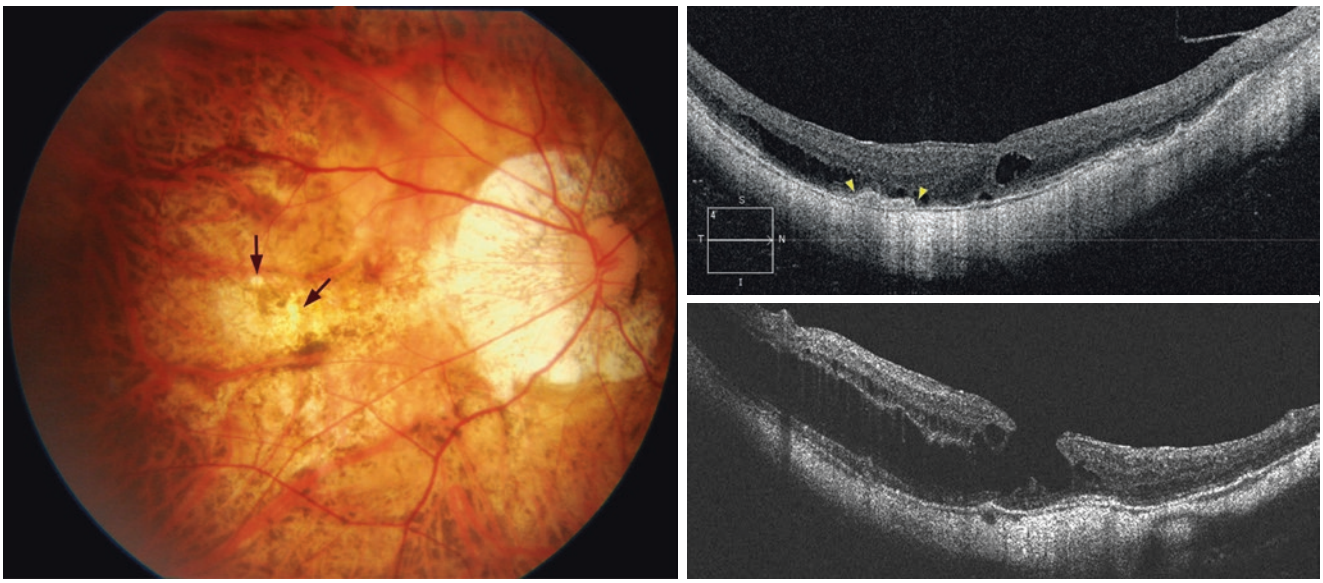

Fig. 28.23 Ten months after the intravitreal injection of bevacizumab (April 2008), a small MNV-related macular atrophy is formed around the regressed MNV (arrows). A horizontal OCT section (Top Right) shows a hyper-reflective area above the RPE without subretinal or intraretinal fluid, suggesting the scarred MNV. Myopic traction maculopathy is also observed both in a horizontal and vertical OCT (Bottom Right) scans including macular outer retinoschisis and inner lamellar macular hole. The BCVA is 0.5

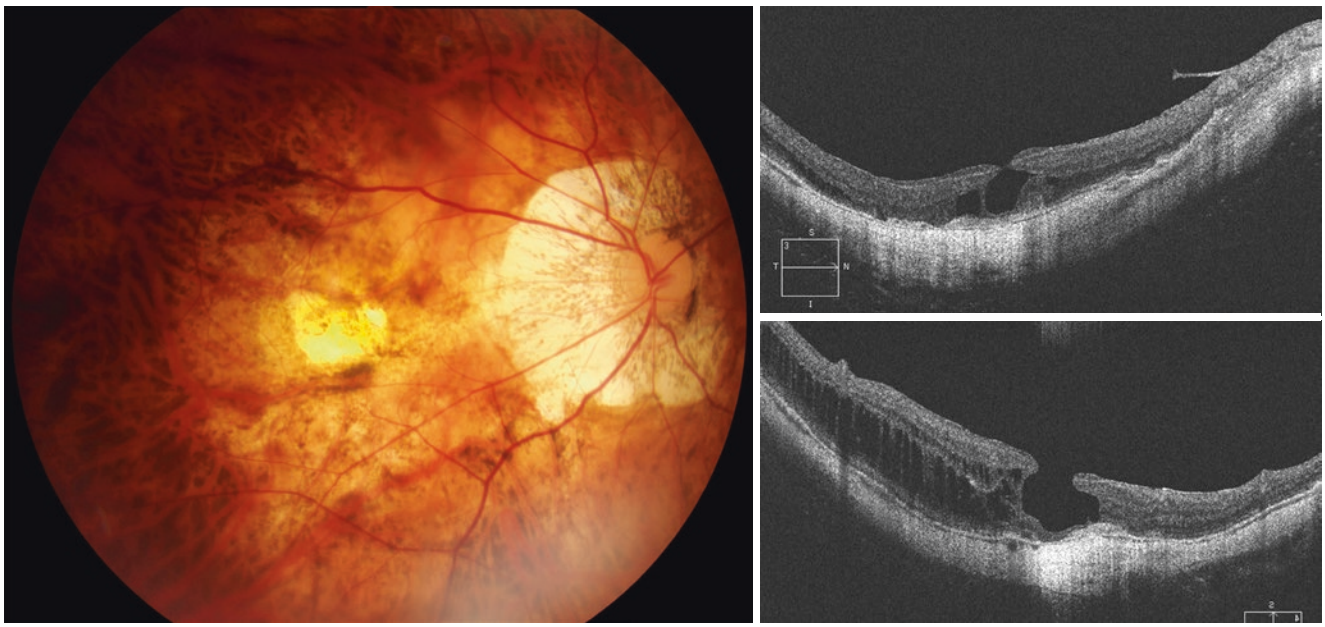

Fig. 28.24 Three years after anti-VEGF therapy (October 2010), macular atrophy has enlarged around the regressed MNV (MNV-related macular atrophy). Both horizontal (Top Right) and vertical OCT (Bottom Right) scans show the RPE defect in the area of macular atrophy with an increased light penetration into the deep tissue. The axial length is 32.0 mm and the BCVA is 0.1

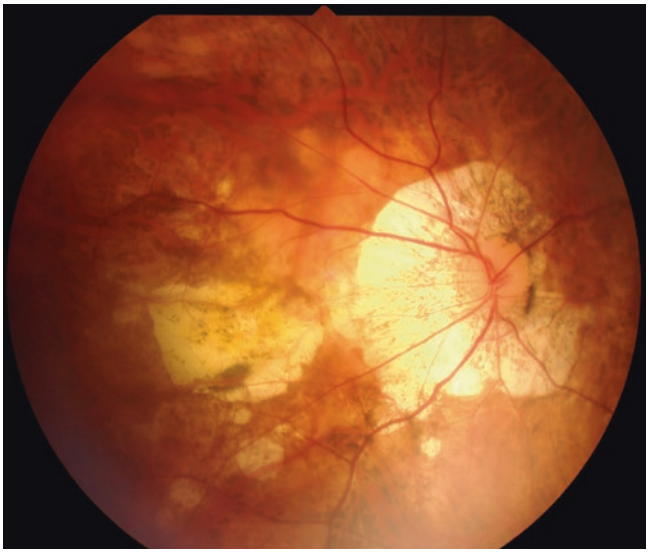

Fig. 28.25 Six years after the anti-VEGF therapies (November 2013), macular atrophy has further enlarged. Multiple new patchy atrophies have developed around the macular atrophy in the background of the diffuse atrophy. Because of severe outer retinoschisis, the retina in the macular area seems a little blurred

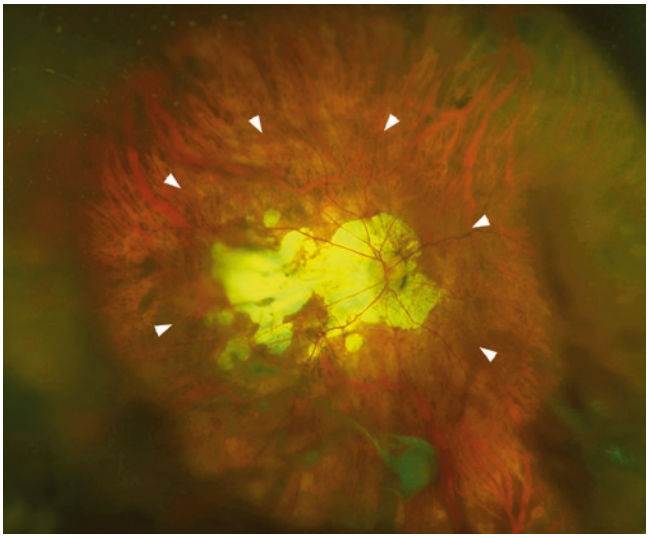

Fig. 28.26 Ten years after the anti-VEGF therapies (September 2017), a wide-field fundus image shows an enlarged macular atrophy fused with surrounding patchy atrophy and peripapillary atrophy. The edges of the staphyloma are also observed (arrowheads). The axial length is 32.0 mm and the BCVA is 0.07

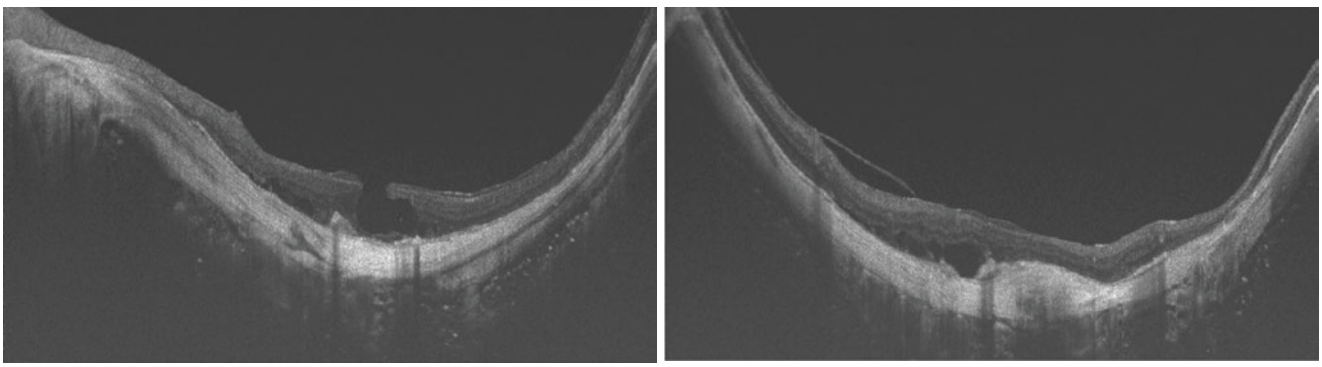

Fig. 28.27 Swept-source OCT in horizontal (Left) and vertical (Right) sections show a large area lacking outer retina, RPE, Bruch's membrane and the choroid at the corresponding area of the macular atrophy and patchy atrophy. The inner retina directly sits on the sclera. The height of macular schisis seems has reduced, however an inner lamellar hole is still observed. In the vertical OCT section (Right), the dome-shaped macula is more obvious than the images taken earlier, accompanying with an increase of the height and the abruptness of the scleral inward protrusion